NUMERICAL SEAKEEPING PREDICTIONS OF SHALLOW WATER EFFECT ON TWO SHIP INTERACTIONS IN WAVES

by

Lin Li

Submitted

in partial fulfillment of the requirements

for the degree of

DOCTOR OF PHILOSOPHY

Major Subject: Naval Architecture

at

DALHOUSIE UNIVERSITY

Halifax, Nova Scotia June, 2001

Contents

List of Tables

List of Figures

Nomenclature

A_w^a	waterplane area of ship_a
A_w^b	waterplane area of ship_b
B	beam of ship
B_a	beam of ship_a
B_b	beam of ship_b
C_b	block coefficient
C_b^a	block coefficient of ship_a
C_b^b	block coefficient of ship_b
C_{jk}^a	restoring force coefficient matrix of ship_a
C_{jk}^b	restoring force coefficient matrix of ship_b
dx	longitudinal separation distance of two ships
dy	lateral separation distance between the centerlines of two ships
d_{a1}	radius of inertia of the waterplane of ship_a around the $o_a y_a$-axis
d_{a3}	radius of inertia of the waterplane of ship_a around the $o_a x_a$-axis
d_{b1}	radius of inertia of the waterplane of ship_b around the $o_b y_b$-axis
d_{b3}	radius of inertia of the waterplane of ship_b around the $o_b x_b$-axis

f_j^{Raa}	time independent radiated force on ship_a due to the oscillation of ship_a itself while ship_b is at rest
f_j^{Rab}	time independent radiated force on ship_a due to the oscillation of ship_b while ship_a is at rest
f_j^{Rbb}	time independent radiated force on ship_b due to the oscillation of ship_b itself while ship_a is at rest
f_j^{Rba}	time independent radiated force on ship_b due to the oscillation of ship_a while ship_b is at rest
F_j^a	time dependent hydrodynamic force acting on ship_a
F_j^b	time dependent hydrodynamic force acting on ship_b
F_j^{aS}	hydrostatic force acting on ship_a
F_j^{bS}	hydrostatic force acting on ship_b
f_j^{Ra}	time independent radiated force on ship_a, $f_j^{Ra} = f_j^{Raa} + f_j^{Rba}$
f_j^{Rb}	time independent radiated force on ship_b, $f_j^{Ra} = f_j^{Rab} + f_j^{Rbb}$
f_j^{Da}	time independent diffracted force on ship_a
f_j^{Db}	time independent diffracted force on ship_b
f_j^{Ia}	time independent incident wave force on ship_a
f_j^{Ib}	time independent incident wave force on ship_b
F_j^{Ra}	time dependent radiated force on ship_a, $F_j^{Ra} = F_j^{Raa} + F_j^{Rba}$
F_j^{Rb}	time dependent radiated force on ship_b, $F_j^{Ra} = F_j^{Rab} + F_j^{Rbb}$
F_j^{Da}	time dependent diffracted force on ship_a
F_j^{Db}	time dependent diffracted force on ship_b
F_j^{Ia}	time dependent incident wave force on ship_a
F_j^{Ib}	time dependent incident wave force on ship_b
F_j^{Wa}	time dependent wave exciting force on ship_a, $F_j^{Wa} = F_j^{Ia} + F_j^{Da}$

F_j^{Wb}	time dependent wave exciting force on ship_b, $F_j^{Wb} = F_j^{Ib} + F_j^{Db}$
F_1	surge force amplitude
F_2	sway force amplitude
F_3	heave force amplitude
h	water depth
$G, \overline{G}, \hat{G}$	Green's Functions
g	gravitational acceleration
Gy	lateral separation gap of two ships, $Gy = dy - 1/2(B_a + B_b)$
I_{jk}^a	moments of inertia of ship_a, j,k=1,2,3
I_{jk}^b	moments of inertia of ship_b, j,k=1,2,3
k	wave number
K	$K = \omega^2/g$
L	ship length between perpendiculars
L_a	ship_a length between perpendiculars
L_b	ship_b length between perpendiculars
m_j	m-terms, j=1,2,3,....6
m_j^a	m-terms of ship_a, j=1,2,3,...,6
m_j^b	m-terms of ship_b, j=1,2,3,...,6
m_{jk}^a	generalized mass matrix of ship_a, j,k=1,2,3,...,6
m_{jk}^b	generalized mass matrix of ship_b, j,k=1,2,3,...,6
M^a	mass of ship_a
M^b	mass of ship_b
M^{aa}	submatrix of the equation of motion representing ship_a's contribution
M^{bb}	submatrix of the equation of motion representing ship_b's

	contribution
M^{ab}	submatrix of the equation of motion representing interactions
M^{ba}	submatrix of the equation of motion representing interactions
M_4	roll force amplitude
M_5	pitch force amplitude
M_6	yaw force amplitude
$\vec{n}^a$	unit normal vector on wetted surface of ship_a
	pointing into the fluid
$\vec{n}^b$	unit normal vector on wetted surface of ship_b
	pointing into the fluid
n_j^a	generalized unit normal on wetted surface of
	ship_a, j=1,2,3,...,6
n_j^b	generalized unit normal on wetted surface of
	ship_b, j=1,2,3,...,6
$oxyz$	steady moving coordinate system
$o_a x_a y_a z_a$	ship-fixed coordinate system of ship_a
$o_b x_b y_b z_b$	ship-fixed coordinate system of ship_b
p	pressure
$p(x, y, z)$	field point
$q(\xi, \eta, \zeta)$	source point
R_{xx}	roll radius of gyration of the ship
	for ship_a in $o_a x_a y_a z_a$ coordinate system
	for ship_b in $o_b x_b y_b z_b$ coordinate system
R_{yy}	pitch radius of gyration of the ship
	for ship_a in $o_a x_a y_a z_a$ coordinate system

	for ship_b in $o_b x_b y_b z_b$ coordinate system
R_{zz}	yaw radius of gyration of the ship
	for ship_a in $o_a x_a y_a z_a$ coordinate system
	for ship_b in $o_b x_b y_b z_b$ coordinate system
$\vec{r}_a$	position vector from the centre of gravity of ship_a
	to a point $p(x_a, y_a, z_a)$ on the ship hull surface
$\vec{r}_b$	position vector from the centre of gravity of ship_b
	to a point $p(x_b, y_b, z_b)$ on the ship hull surface
$\vec{r}_g$	position vector from the centre of gravity of a ship
	to a point $p(x, y, z)$ on the ship hull surface
S_a	mean wetted surface of ship_a
S_b	mean wetted surface of ship_b
T	draft of a ship
T_a	draft of ship_a
T_b	draft of ship_b
t	time
U	steady forward speed of a ship
W	steady flow velocity, $W = \nabla(-Ux + \phi_s)$
x_1^a, x_1^b	surge motion of ship_a and ship_b
x_2^a, x_2^b	sway motion of ship_a and ship_b
x_3^a, x_3^b	heave motion of ship_a and ship_b
x_4^a, x_4^b	roll motion of ship_a and ship_b
x_5^a, x_5^b	pitch motion of ship_a and ship_b
x_6^a, x_6^b	yaw motion of ship_a and ship_b
(x_g^a, y_g^a, z_g^a)	coordinate of centre of gravity of ship_a in $o_a x_a y_a z_a$

(x_g^b, y_g^b, z_g^b)	coordinate of centre of gravity of ship_b in $o_b x_b y_b z_b$
$\bar{x}_k^a, \bar{x}_k^b$	time independent motion amplitudes of ship_a and ship_b, k=1,2,...,6
$\bar{x}_f^a$	x-coordinate of the centre of the flotation of ship_a
$\bar{x}_f^b$	x-coordinate of the centre of the flotation of ship_b
$\dot{x}_k^a$	velocity of ship_a, k=1,2,3 translation; k=4,5,6 rotation
$\dot{x}_k^b$	velocity of ship_b, k=1,2,3 translation; k=4,5,6 rotation
$\ddot{x}_k^a$	acceleration of ship_a, k=1,2,3 translation; k=4,5,6 rotation
$\ddot{x}_k^b$	acceleration of ship_b, k=1,2,3 translation; k=4,5,6 rotation
z_B^a	z-coordinate of the centre of bouyancy of ship_a in $o_a x_a y_a z_a$
z_B^b	z-coordinate of the centre of bouyancy of ship_b in $o_b x_b y_b z_b$
β	angle between the wave propagation direction and the x-axis $\beta = 180°$ for head seas
$\triangle$	volume displacement of a ship
$\triangle^a$	volume displacement of ship_a
$\triangle^b$	volume displacement of ship_b
∇	weight displacement of a ship
∇_a	weight displacement of ship_a
∇_a	weight displacement of a ship_b
δ	h/T, the ratio of water depth to the draft of a ship
δ_a	h/T_a, the ratio of water depth to the draft of ship_a
δ_b	h/T_b, the ratio of water depth to the draft of ship_b
ζ_a	incident wave amplitude
ζ_1	surge motion amplitude
ζ_2	sway motion amplitude

ζ_3	heave motion amplitude
ζ_4	roll motion amplitude
ζ_5	pitch motion amplitude
ζ_6	yaw motion amplitude
λ	incident wave length
λ_{jk}^{aa}	damping coefficient of ship_a due to the motion of ship_a while ship_b is at rest
λ_{jk}^{ab}	damping coefficient of ship_a due to the motion of ship_b. while ship_a is at rest
λ_{jk}^{bb}	damping coefficient of ship_b due to the motion of ship_b while ship_a is at rest
λ_{jk}^{ba}	damping coefficient of ship_b due to the motion of ship_a while ship_b is at rest
μ_{jk}^{aa}	added mass of ship_a due to the motion of ship_a while ship_b is at rest
μ_{jk}^{ab}	added mass of ship_a due to the motion of ship_b while ship_a is at rest
μ_{jk}^{bb}	added mass of ship_b due to the motion of ship_b while ship_a is at rest
μ_{jk}^{ba}	added mass of ship_b due to the motion of ship_a while ship_b is at rest
ρ	water density
σ_S^a	steady flow source density on ship_a
σ_S^b	steady flow source density on ship_b
σ_D^a	diffraction source density on ship_a

σ_D^b	diffraction source density on ship_b
σ_k^{aa}	radiation source density on ship_a due to the motion of ship_a while ship_b is at rest
σ_k^{ab}	radiation source density on ship_a due to the motion of ship_b while ship_a is at rest
σ_k^{ba}	radiation source density on ship_b due to the motion of ship_a while ship_b is at rest
σ_k^{bb}	radiation source density on ship_b due to the motion of ship_b while ship_b is at rest
Φ	time dependent unsteady velocity potential
Φ_S	steady velocity potential,$\Phi_S = -Ux + \phi_s$
Φ_D	time dependent diffracted wave velocity potential
ϕ_D	time independent diffracted wave velocity potential
Φ_I	time dependent incident wave velocity potential
ϕ_I	time independent incident wave velocity potential
ϕ_k	canonical radiated wave velocity potential
ϕ_k^a	the radiated wave potential of k^{th} direction, $k = 1, 2, ..., 6$ due to the oscillation of ship_a while ship_b is at rest
ϕ_k^b	the radiated wave potential of k^{th} direction, $k = 1, 2, ..., 6$ due to the oscillation of ship_b while ship_a is at rest
Φ_R^a	time dependent radiated wave velocity potential of ship_a
Φ_R^b	time dependent radiated wave velocity potential of ship_b
ϕ_R	time independent radiated wave velocity potential
Φ_R	time dependent radiated wave velocity potential
Φ_T	time dependent total wave velocity potential

ϕ_s	steady disturbance velocity potential
Φ_R^a	time dependent radiated wave velocity potential of ship_a
ω	incident wave frequency
ω_e	frequency of wave encounter

Acknowledgements

I would like to express my sincere gratitude to my supervisor, Professor C. C. Hsiung, for his support, encouragement and guidance throughout my studies. His critical attitude and rigorous scholarship in research has had a great influence on me, and I believe this influence will accompany me for the rest of my life. Without him, this thesis would possibly never have been completed.

I would also like to thank my thesis committee members, Professor J. Militzer of the Mechanical Engineering Department, Professor M. Rahman of the Engineering Mathematics Department, and Dr. K. McTaggart of the Defence Research Establishment Atlantic, for their valuable advice on my course work, as well as insightful suggestions and comments on my thesis work.

I have learned a lot through the course work at Dalhousie University. I am indebted to all faculty members from whom I have taken courses. I am especially grateful to Professor C. C. Hsiung, Professor M. Rahman and Professor J. Militzer who offer courses on Hydrodynamics, Partial Differential Equations and Numerical Computations which have been very useful for my academic background and thesis research.

My thanks are also due to the financial support from the Natural Science and Engineering Research Council of Canada and the Centre for Marine Vessel Develop-

ment and Research (1996-2000), Faculty of Graduate Studies Scholarship (1997-2000) and Bruce and Dorothy Rosetti Engineering Research Scholarship(1998-1999).

Finally, I would like to express gratitude to my parents, who have been giving me the invaluable and endless encouragement, support and love in my life. I also would like to thank my husband, Feng Li, and my son, William Li, for their patience, care and sacrifice during my study. I could not have finished the study without the support from all of them.

Abstract

The main objective of this study is to numerically predict the shallow water effect on two ship interactions in waves. An algorithm has been developed to solve the free-surface Green function of zero forward speed in water of finite depth and in shallow water. The improper integral containing a singularity in the integral form of the Green function was solved by the Gauss-Laguerre quadrature. John's Conventional Expansion (i.e. the series form of the Green function) was found more effective than the integral form of the Green function when $R/h > 1/2$, where R is the horizontal distance between the source point and the field point and h is the depth of water. Therefore, a numerical scheme which combined both the integral form and the series form of the Green function was applied to compute the free-surface Green function with the water depth effect. The $1/r$ term in the potential function is treated by the Hess-Smith method. The interactions due to the coupled motions and hydrodynamic forces of two ships with forward speed in waves were then computed by the three-dimensional panel method based on the zero forward speed free-surface Green function with a forward speed correction. The effect of water depth on double-body flow and m-terms which have been used to compute the steady flow effect on the wave field were also considered. The m-terms were computed by the integral equation method based on the double-body flow of two ship interactions. The viscous rolling damping coefficient had been determined by the method of Schmitke for Ship_a and Ship_b separately.

To verify this code, two numerical test cases were provided: two identical cylinders interact in water of finite depth and in shallow water. Furthermore, two ship interactions in shallow water, in water of finite depth and in deep water were carried out in regular waves with headings of 120^o, 150^o and 180^o for forward speeds of 12 knots and 0 knots. Also a lateral separation distance of $dy = 52.705m$ (gap distance $Gy = 30.0m$) and a longitudinal separation distance $dx = 45m$ were considered in the computations.

Chapter 1

Introduction

1.1 Two Ship Interactions in Shallow Water and Waves

The subject of hydrodynamic interaction between bodies moving in close proximity has received much attention not only by hydrodynamicists but also by ship designers and even ship operators. The determination of interaction forces and moments plays a significant role in many practical situations, such as proximity manoeuvres of naval vessels, collision-course encounters of ships in shallow regions, congested vessel traffic in harbors and even the passing of two ships in canals. The interaction phenomenon is generally exacerbated by the effects of shallow water. This is particularly true in the case of the super-tankers such as VLCC (Very Large Crude Oil Carrier) where consideration of these effects is imperative.

The problem of ship-ship interaction has long been a subject for investigation and argument. In deep water, the major stimulus for systematic study of the phenomenon arose from the needs of the warship replenishing while underway at sea. It has already been pointed out that merchant ships are most likely to be in close quarters situations in shallow water where interaction effects may be larger and cause loss of control.

Some of the most notable investigations of ship-ship interactions have been conducted by Dand (1975). The collisions and stranding of the vessels occurred in shallow water which featured prominently in the determination of hydrodynamic forces and moments. Usually, ship motions in shallow water are not only changed by the shallow water effect but are also affected by the additional forces which are induced by the interaction with other ships. The interaction forces are usually larger and decrease more slowly with distance in shallow water as compared to deep water. Therefore in deep water hydrodynamic effects, such as ship-ship interaction, rudder effectiveness and propeller bias may not contribute significantly to the occurrence of a collision situation. But, tug-ship interaction is a typical example of collision in shallow water. Therefore, the accurate prediction of interaction hydrodynamic forces and moments and ship motions in shallow water will have important significance for avoiding ship collisions in shallow water regions.

The general problem of interaction of ships in restricted water had been investigated by several people. e.g. Fujino (1976), King (1977), Newman (1969), Tuck (1978), Tuck & Newman (1974), Yeung (1977,1978) and Hsiung & Gui (1988). But, most of them were only based on two-dimensional flow in shallow water, i.e., using an aerodynamic equivalence principle, which essentially models the flow in the far

field as the flow past a two-dimensional airfoil. In the near field, a two-dimensional problem in a plane containing a cross-section of the ship is obtained by neglecting changes along the length of the ship. After solving these two boundary-value problems, the concept of the inner and outer asymptotic expansion is used to match the solutions to these two problems and thus provide an approximate solution valid over the most of the flow field. This method is very classical and of limited appplication. Davis (1982) started to use the source distributed method, but was still limited by the slender-body theory, rigid free-surface assumption and by no incident wave.

Usually, in the past, most numerical computations for the three-dimensional two ship interactions were performed in deep water, such as Lin (1974), Fang (1986), Kashiwagi (1993), Li, He & Hsiung (1999, 2000). The main reason is the limitation of complexity of shallow water theory, in other words, the lack of a method to solve the free-surface Green function in finite depth or shallow water. The current study will solve the three-dimensional two ships interaction in finite depth or shallow water in waves.

1.2 Shallow Water Theory

Most work on ship seakeeping prediction assumes that the water is infinitely deep. However, there are a number of practical situations where the water depth may be an important factor in the ship motion problem. Published work on the effect of water depth includes Kim (1969), Tuck (1970,1974), Beck & Tuck (1972), Van Oort-

merssen (1976) and Andersen (1979). Most of them were based on the slender body assumption and no consideration of free-surface involved by solving a two-dimensional problem. Endo (1987) produced a more accurate seakeeping prediction in shallow water, but some parts of his method still needed to be improved.

The influence of limited water depth on the ship motions becomes obvious when the water depth is less than about 4 times the draft of the ship (Van Oortmerssen, 1976). When the ratio of water depth to draft is less than 2, the effect of the bottom becomes significant (Van Oortemerssen, 1976). The motions of a ship are directly affected in two ways by the restricted water depth: (i) the incident waves are changed and as a result, the wave exciting forces exerted on the ship differ from those in deep water; and (ii) the hydrodynamic coefficients of the ship (i.e. radiation forces) are changed by the nearness of the sea bottom. These two factors will directly affect the ship motions.

Very few studies have been presented on the motions of a ship in shallow water. The application of strip theory has limited potential. Because of the nearness of the sea bottom, three-dimensional effects become more important. Therefore, the three-dimensional panel method with the free-surface Green function in finite depth or shallow water has been chosen in the current study.

1.3 The Free-Surface Green's Function Method

During the past three decades, several numerical methods have been applied to the study of hydrodynamics of floating bodies at the free surface. These numerical meth-

ods fall into three groups, namely, multipole expansion, finite element(variational principle), and surface source distribution.

The theory of multipole expansion has been used to express the velocity potentials in terms of an infinite series of Legendre polynomials or Chebyshev polynomials with unknown coefficients which are obtained by imposing the body surface condition. The multipole expansion was developed by Ursell (1949) and some detailed discussions of it were given by Thorne (1957). Newman (1961,1992), Wu (1991), Williams & Abul-Azm (1988,1989) successfully applied it to various siutations including circular cylinders, spheres and spheroids floating on or submerged beneath a free surface. However, the multipole expansion theory is rarely used to compute the ship hydrodynamic characteristics because of the complex body surface conditions.

Some people have used the finite element method, boundary element method or hybrid element method to analyze the water wave diffraction and radiation problems associated with floating structures, including Kagemoto & Yue (1986). These methods are limited by expensive and time-consuming computer requirements for solving the three-dimensional problems.

Among the previously mentioned methods, the surface source distribution method (the Green function method, also known as the boundary integral equation method (BIEM)), is preferred for analysis of a three-dimensional body of an arbitrary shape in a uniform depth of water. In this method, the source potential, or the Green function, is the fundamental element in the analysis of wave-induced motions and forces

acting on floating or submerged vessels. In the case of most practical importance, a numerical model is based on the distributions of sources which are located on the submerged portion of the body surface. This procedure, which can be justified by Green's theorem, requires the solution of an integral equation in the domain of the body surface, either for the source strength or for the velocity potential. In practice, the body surface is discretized in an appropriate manner, and the integral equation is reduced to a finite system of linear equations.

Two distinct numerical problems must be overcome to implement this approach successfully for a fully three-dimensional body geometry. First, the body surface must be described with a reasonable degree of fidelity and a large number of discrete "panel" elements must be utilized to accomplish this, typically between 100 and 1000. The corresponding linear system of equations is characterized by a square matrix of complex coefficients with the same dimension and the equation system must be solved by a suitable application of linear algebra.

The second numerical problem, peculiar to the field of free-surface hydrodynamics, is the evaluation of the source potential and its derivatives. These are complicated mathematical functions, which must be evaluated successively for each combination of panels. This is regarded as the main difficulty in performing three-dimensional computations of hydrodynamic parameters, such as the body motions in waves, or the pressure forces exerted on the body in the environment. Wehausen and Laitone (1960), Sarpkaya & Isaacson (1981), Susbielles & Bratu (1981) and Newman (1985, 1992) gave the mathematical expressions for the oscillatory source potential for infinite and finite (constant) depth of the fluid.

In the frequency domain, the three-dimensional panel methods, such as the free-surface Green function method (Hsiung & Huang, 1991 and Papanikolaou & Schellin, 1992) and the Rankine source method (Bertram & Söding, 1991), have been applied to solve the ship motion problems. The Rankine source method requires a large number of panels, more than 1000 typically, and the computation could only be conducted for $\omega_e U/g > 0.25$, Where ω_e is the frequency of encounter, U is forward speed and g is the acceleration of gravity. Also the hull surface boundary condition was not satisfied in the steady flow. Therefore, the free-surface Green function method has been adopted to calculate the hydrodynamic forces and motions of two ship interaction in waves with a forward speed correction in the current study.

In the case of finite depth, Wehausen and Laitone's expression (1960) for the source potential is in terms of a contour integral form. John's expression (1950) is in the form of a discrete eigenfunction expansion. However, the evaluation of the principal-value integral in the integral form of the Green function presents a difficulty because of an improper integral containing a singularity and it is also time-consuming in computation. There is a logarithmic singularity which involves each term of the infinite-series expansion form as well. Therefore, very few studies have been presented on ship motions in waves in finite depth or shallow water with the free-surface Green function method based on solving the Green function in finite depth or shallow water. This makes the current study more of a challenge and more significant.

Monacella (1966) has proposed a technique by which the integrand of the principal-

value integral tends to vanish because of its symmetry. This singularity removal method has been employed by Faltinsen & Michelsen (1975) with additional refinement. This method consumes a large amount of computing time. Newman (1984) has introduced new alternative forms of the principal-value integral in the Green function for infinite water depth, but they lack generality in applications.

Later, Newman (1985) developed new algorithms for the computation of the Green function in both infinite and finite water cases. He started from the premise that numerical integration should be avoided in all cases and uses series expansions and polynomial approximations to gain computational efficiency. Endo (1983)introduced a technique which calculated the singular integral in the Green function for finite water depth directly by Gauss-Laguerre quadratures. This technique consumes much less time than that of Monacella. When $0 < R/h < 1/2$ where R is the horizontal distance between the source point and field point and h is the depth of water, this technique gives very effective results. However, when $R/h > 1/2$, the results are not reasonable. This has been proven by the current study. John (1950) gave the Green function in the form of the infinite-series expansion for finite water depth. But, this series is practically useless for small values of R/h. Each term of series expansion contains a logarithmic singularity when $R/h = 0$. Numerical computation confirms these estimates, and $6h/R$ has been found to be an appropriate number of terms in the series to achieve 6 places of decimals accuracy in the domain for $R/h > 1/2$.

Based on the above analysis, a new algorithm has been developed for solving the Green function and its derivatives in finite depth of water or in shallow water in current study. When $0 < R/h < 1/2$, the Gauss-Laguerre quadrature is adopted

to solve the integral form the Green function. When $R/h > 1/2$, John's series form of Green function is applied. This algorithm has been proven to be very efficient in examples in the current study.

1.4 Forward Speed Correction Theory

The Green function with forward speed was first studied by Chang (1977), and subsequently continued by many other people(i.e. Inglis & Price (1981), Wu & Eatock-Taylor (1988)). However, using the forward speed Green function to calculate the body motions in waves has been less successful. It was found that the accurate and converged results were more difficult to obtain than in the case with zero forward speed.

Hsiung & Huang (1990). further proved above conclusions by comparing both the three-dimensional Green function with forward speed and without forward speed. There are two aspects of difficulty in applying the forward-speed three-dimensional Green function to the computation of ship motions:

- The oscillatory integrand in Green's function gives considerable difficulties. The trapezoidal rule, applied to approximate the integration, needs a very long computing time, since the discretized interval had to be sufficiently small in order to obtain a meaningful result.
- The potential function in terms of the forward-speed Green function includes

an integral along the waterline. It takes much computing time to calculate the Green function $G(p, q, \omega_e)$ as the source point p and the field point q are on the free surface, and $G(p, q, \omega_e)$ converges very slowly.

Since the zero-speed free-surface Green function is simpler than the Green function with forward speed, difficulties in computation can be avoided and much computing time is saved. And, so far, the published numerical results of ship motion based on the Green function with forward speed are not as good as the results based on the zero-speed Green function with forward speed correction. Therefore, the zero speed of free-surface Green function with the simple forward speed correction is adopted and has been proven to be very effective.

1.5 Roll Damping Correction

The roll motion of ships has a great impact on ship operations particularly in shallow water regions. However, the numerical prediction of ship motion based on pure theoretical analysis usually produces significant errors in roll prediction. The wave-making damping predicted by the potential flow around most hull forms is only a small fraction of the total roll damping which is experienced in reality. According to many studies such as Schimitke (1978), additional important contributions to rolling damping come from bilge keel vortices, effects of dynamic lift on appendages and hull circulatory. The hull form with relatively sharp corners at the bilge and/or at the keel will shed eddies which absorb a good deal of energy and represent a significant source of additional roll damping. Skin friction forces on the surface of the rolling

hull may also be significant and any appendages will generate forces which oppose the rolling motion. Eddy shedding, skin friction and appendage forces were all found to have greater influence on rolling damping at low forward speed. To correct this problem, Schmitke's method is adopted when calculating the viscous rolling damping of the two ships separately in present study.

1.6 Objective and Scope of the Present Work

The main objective of the work presented in this thesis is to study the shallow water effect on the seakeeping of two ship interactions in waves.

The study of two ship interactions in shallow water and waves will investigate not only the interactions of two ships but also the effect of water depth. Unlike the single ship case, the two ship case is more complex because the motion has 12 degrees of freedom and takes much more time for computation. Furthermore, hydrodynamic terms such as added mass, damping, and wave diffraction force must take into account for the presence of two ships in waves. In addition, the parameter h (depth of water) involved in the two ship interaction case makes the problem much more complicated than the two ship case in deep water. The incident wave, m-terms (the effect of steady flow to unsteady flow), diffracted wave, radiated wave and coupled motions for ship_a and ship_b will be affected directly. Particularly, the parameter h makes solving of the free-surface Green function much more difficult.

First, the water depth effects on incident waves for ship_a and ship_b have been solved separately. The double-body flow Green function and m-terms have been taken into account for the finite depth and shallow water cases. An algorithm has been developed to solve the free-surface Green function with zero-forward speed in water of finite depth and in shallow water. The improper integral containing a singularity in the integral form of the Green function was solved by using Gauss-Laguerre quadrature. John's conventional expansion (i.e. the series form of the Green function) was found more effective than the intergral form of the Green function when $R/h > 1/2$. Therefore, a numerical scheme which combined both the integral form and the series form of the Green function has been applied to compute the Green function in water of finite depth and shallow. Then, the Green function would be used for solving the added mass, damping coefficients and diffraction force for ship_a and ship_b. The $1/r$ term in the potential function was treated by the Hess-Smith Method (1964).

The 12×12 systems of equations were built up to solve for the coupled motions of 12 degrees of freedom of ship_a and ship_b. The interaction due to coupled motions and hydrodynamic forces of two ships in waves with forward speed was computed by the three-dimensional panel method based on zero forward speed free-surface Green's function with a forward speed correction. The m-terms were performed by the integral equation method based on double-body flow of two ship interaction. Schmitke's method was adopted to calculate the viscous rolling damping for ship_a and ship_b separately.

To verify the code, two numerical test cases were considered:

- Two identical cylinders interacting in water of finite depth.

- Two identical cylinders interacting in shallow water.

Finally, two ship interactions in shallow water, in water of finite depth and in deep water interactions were preformed in regular waves with headings of 120^o. 150^o and 180^o for forward speeds of 12 knots and 0 knots. Also a lateral separation distance between the centerlines of two ships $dy = 52.705m$ (i.e. lateral separation gap $Gy = 30.0m$), and a longitudinal separation distance between the lateral axes of two ships $dx = 45.0m$ were considered in computations.

Chapter 2

Formulation of the Problem

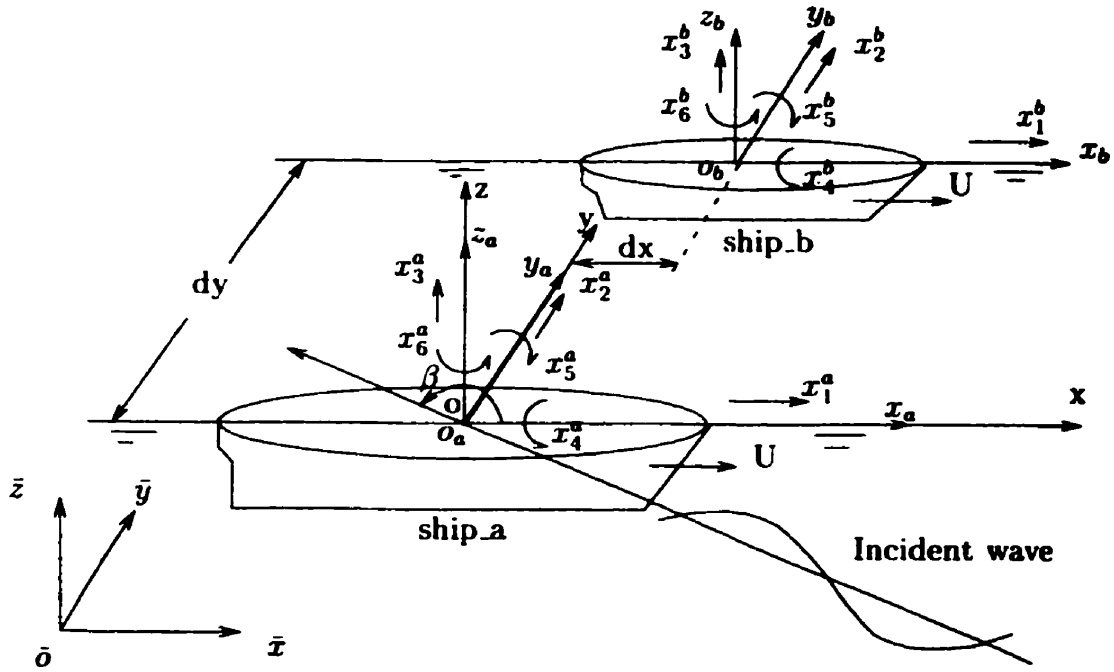

Figure 2.1: Coordinate systems

In order to predict coupled motions of two ships denoted as ship_a and ship_b in

waves, each ship is regarded as an unrestrained rigid body with its own six degrees of freedom as defined in Figure 2.1. Three components of of translation are surge parallel to the longitudinal axis (x_1^a and x_1^b), sway in the lateral direction orthogonal to surge (x_2^a and x_2^b) and heave in the vertical direction (x_3^a and x_3^b). Rotational motions about the respective axes are roll(x_4^a and x_4^b), pitch(x_5^a and x_5^b) and yaw (x_6^a and x_6^b).

Four coordinate systems are employed as follows:

- Space coordinate system $\bar{o}\bar{x}\bar{y}\bar{z}$;
- Moving coordinate system $oxyz$;
- Ship_a coordinate system $o_a x_a y_a z_a$; and
- Ship_b coordinate system $o_b x_b y_b z_b$.

In Figure 2.1, $\bar{o}\bar{x}\bar{y}\bar{z}$ is the space-fixed coordinate system with $\bar{o}\bar{x}\bar{y}$ plane on the calm water surface and the $\bar{o}\bar{z}$ axis being positive upwards. The coordinate system $oxyz$ is a moving system which moves in the $\bar{o}\bar{x}$ direction with a steady forward speed U with respect to the $\bar{o}\bar{x}\bar{y}\bar{z}$ system and the oxy plane coincides with the $\bar{o}\bar{x}\bar{y}$ plane, and the ox axis is in the same direction as the $\bar{o}\bar{x}$ axis. The systems $o_a x_a y_a z_a$ and $o_b x_b y_b z_b$ are fixed on ship_a and ship_b, respectively. The $o_a x_a y_a$ plane and the $o_b x_b y_b$ plane coincide with the oxy plane when ship_a and ship_b at their static equilibrium positions. The $o_a z_a$ and $o_b z_b$ axes are positive upwards, and they move with ship_a and ship_b with a steady forward speed U as well. The origins o_a and o_b are located at the midship section of ship_a and ship_b, respectively. The regular incident wave is propagating in the direction with a heading angle β which is the angle between the positive ox direction and incident wave direction. dx is longitudinal separation

distance between two ships' lateral axes. dy is lateral separation distance between the centerlines of two ships.

In the computation, the motions and forces of ship_a and ship_b were converted to the local coordinate system in which the origin is at the centre of gravity of each ship. The phase angles for motions and forces are also given relative to the wave crest at the centre of gravity for each ship.

2.1 Fundamental Equations

2.1.1 Velocity Potentials

It is assumed that the fluid is inviscid and incompressible, and the flow is irrotational, so that the flow around the two ships can be described by the potential theory. The resultant velocity potential Φ_T in the flow field is in the following form:

$$\Phi_T(x, y, z, t) = -Ux + \phi_s(x, y, z) + \Phi(x, y, z, t) \tag{2.1}$$

where, on the right hand side, the first term is the velocity potential of uniform flow and U is the steady forward speed of the ships; the second term, $\phi_s(x, y, z)$, is the steady disturbance potential. The sum of the first and second terms is called the steady flow potential. The third term is the wave velocity potential which can be written as:

$$\Phi(x, y, z, t) = \Phi_I + \Phi_D + \Phi_R = Re[(\phi_I(x, y, z) + \phi_D(x, y, z) + \phi_R(x, y, z))e^{-i\omega_e t}] \tag{2.2}$$

where Φ_I, Φ_D and Φ_R are velocity potentials of incident wave, diffracted wave and radiated wave, respectively.

2.1.2 Hydrodynamic Forces

The hydrodynamic force acting on ship_a and ship_b can be expressed as:

$$F_j^a = \int\int_{S_a} P n_j^a dS, \qquad j = 1, 2, ..., 6 \qquad on \;\; S_a \tag{2.3}$$

$$F_j^b = \int\int_{S_b} P n_j^b dS, \qquad j = 1, 2, ..., 6 \qquad on \;\; S_b \tag{2.4}$$

where S_a and S_b are the mean wetted hull surfaces of ship_a and ship_b, respectively. n_j^a is the generalized unit normal of ship_a,

$$n_j^a = \begin{cases} \vec{n}^a & \text{if j=1,2,3} \\ \vec{r}_a \times \vec{n}^a & \text{if j=4,5,6} \end{cases} \tag{2.5}$$

n_j^b is the generalized unit normal of ship_b,

$$n_j^b = \begin{cases} \vec{n}^b & \text{if j=1,2,3} \\ \vec{r}_b \times \vec{n}^b & \text{if j=4,5,6} \end{cases} \tag{2.6}$$

where $\vec{n}^a$ and $\vec{n}^b$ are unit normal pointing towards the hull surface of ship_a and ship_b hull. respectively. $\vec{r}_a$ is the position vector from the centre of gravity of ship_a to a point $p(x_a, y_a, z_a)$ on the ship. $\vec{r}_b$ is the position vector from the centre of gravity of ship_b to a point $p(x_b, y_b, z_b)$ on the ship. The hydrodynamic pressure of the fluid is

$$p = -\rho(\frac{\partial \Phi}{\partial t} + W \cdot \nabla \Phi) \tag{2.7}$$

where

$$W = \nabla(-Ux + \phi_s) \tag{2.8}$$

is the steady flow velocity vector. Substituting Equation(2.7) and Equation(2.8) into Equation(2.3) and Equation(2.4), the hydrodynamic force on the two ships can be expressed as:

$$F_j^a = \int\int_{S_a} -\rho[\frac{\partial \Phi}{\partial t} + \nabla(-Ux + \phi_s) \cdot \nabla \Phi] n_j^a dS, \qquad j = 1, 2, ..., 6 \tag{2.9}$$

$$F_j^b = \int\int_{S_b} -\rho[\frac{\partial \Phi}{\partial t} + \nabla(-Ux + \phi_s) \cdot \nabla \Phi] n_j^b dS, \qquad j = 1, 2, ..., 6 \tag{2.10}$$

Depending on the value of Φ (Φ could be Φ_I, Φ_D, Φ_R or the combination of all components), one can compute any components of wave forces or the total hydrodynamic force from Equations (2.9) and (2.10). The steady flow effects are considered in computations.

2.1.3 Hydrostatic Forces

The hydrostatic forces acting on ship_a and ship_b can be expressed as:

$$F_j^{aS} = -C_{jk}^a \cdot x_k^a \tag{2.11}$$

$$F_j^{bS} = -C_{jk}^b \cdot x_k^b \tag{2.12}$$

where x_k^a, $k = 1, 2, ..., 6$, are the generalized motion displacements of ship_a.

$$x_k^a = Re[\bar{x}_k^a e^{-i\omega_e t}] \tag{2.13}$$

and x_k^b, $k = 1, 2, ..., 6$, are the generalized motion displacements of ship_b,

$$x_k^b = Re[\bar{x}_k^b e^{-i\omega_e t}] \tag{2.14}$$

As shown in Equations(2.13) and (2.14) $\bar{x}_k^a$ and $\bar{x}_k^b$ are the time independent complex amplitudes of motions corresponding to ship_a and ship_b. ω_e is the frequency of encounter. For $k = 1, 2, 3$, x_k^a and x_k^b represent the translational displacements of ship_a and ship_b, respectively. For $k = 4, 5, 6$, x_k^a and x_k^b represent the angular displacements of ship_a and ship_b, respectively. In Equation(2.11) and Equation(2.12), C_{jk}^a is the restoring force coefficient matrix of ship_a:

$$C_{jk}^a = \begin{pmatrix} 0 & 0 & 0 & 0 & 0 & 0 \\ 0 & 0 & 0 & 0 & 0 & 0 \\ 0 & 0 & \rho g A_w^a & 0 & \rho g A_w^a \bar{x}_f^a & 0 \\ 0 & 0 & 0 & \rho g (A_w^a d_{a3}^2 + z_B^a \triangle^a) & 0 & 0 \\ 0 & 0 & \rho g A_w^a \bar{x}_f^a & 0 & \rho g (A_w^a d_{a1}^2 + z_B^a \triangle^a) & 0 \\ 0 & 0 & 0 & 0 & 0 & 0 \end{pmatrix} \tag{2.15}$$

and C^b_{jk} is the restoring force coefficient matrix of ship_b:

$$C^b_{jk} = \begin{pmatrix} 0 & 0 & 0 & 0 & 0 & 0 \\ 0 & 0 & 0 & 0 & 0 & 0 \\ 0 & 0 & \rho g A^b_w & 0 & \rho g A^b_w \bar{x}^b_f & 0 \\ 0 & 0 & 0 & \rho g (A^b_w d^2_{b3} + z^b_B \triangle^b) & 0 & 0 \\ 0 & 0 & \rho g A^b_w \bar{x}^b_f & 0 & \rho g (A^b_w d^2_{b1} + z^b_B \triangle^b) & 0 \\ 0 & 0 & 0 & 0 & 0 & 0 \end{pmatrix} \tag{2.16}$$

where A^a_w and A^b_w are the waterplane areas of ship_a and ship_b. $\bar{x}^a_f$ and $\bar{x}^b_f$ are the x-coordinates of the centre of flotation of ship_a and ship_b. $\triangle^a$ and $\triangle^b$ are the volume displacements of ship_a and ship_b. d_{a1}, d_{b1}, d_{a3} and d_{b3} are the radii of gyration of waterplanes about oy-and ox-axes. z^a_B and z^b_B are the z-coordinates of the centre of buoyancy of ship_a and ship_b.

2.1.4 Ship Motions

As we assumed that the ships are rigid bodies, their motions must satisfy the Laws of Momentum Conservation. Therefore, the equations of motion of two ships can be described by Newton's Law as :

$$m^a_{jk} \ddot{x}^a_k = F^a_j + F^{aS}_j \tag{2.17}$$

$$m^b_{jk} \ddot{x}^b_k = F^b_j + F^{bS}_j \tag{2.18}$$

where m^a_{jk} is the generalized mass matrix of ship_a:

$$m^a_{jk} = \begin{pmatrix} M^a & 0 & 0 & 0 & 0 & 0 \\ 0 & M^a & 0 & 0 & 0 & 0 \\ 0 & 0 & M^a & 0 & 0 & 0 \\ 0 & 0 & 0 & I^a_{11} & I^a_{12} & I^a_{13} \\ 0 & 0 & 0 & I^a_{21} & I^a_{22} & I^a_{23} \\ 0 & 0 & 0 & I^a_{31} & I^a_{32} & I^a_{33} \end{pmatrix} \tag{2.19}$$

and m^b_{jk} is the generalized mass matrix of ship_b:

$$m^b_{jk} = \begin{pmatrix} M^b & 0 & 0 & 0 & 0 & 0 \\ 0 & M^b & 0 & 0 & 0 & 0 \\ 0 & 0 & M^b & 0 & 0 & 0 \\ 0 & 0 & 0 & I^b_{11} & I^b_{12} & I^b_{13} \\ 0 & 0 & 0 & I^b_{21} & I^b_{22} & I^b_{23} \\ 0 & 0 & 0 & I^b_{31} & I^b_{32} & I^b_{33} \end{pmatrix} \tag{2.20}$$

where M^a is the mass of ship_a and M^b is the mass of ship_b; I^a_{jk} are the moments of inertia of ship_a and I^b_{jk} are the moments of inertia of ship_b. According to the definition of x^a_k and x^b_k (see Equations(2.13) and (2.14)), when $k = 1, 2$ or 3, $\ddot{x}^a_k$ represents the translational acceleration of ship_a and $\ddot{x}^b_k$ represents the translational acceleration of ship_b: when $k = 4, 5$ or 6, $\ddot{x}^a_k$ represents the angular acceleration of ship_a and $\ddot{x}^b_k$ represents the angular acceleration of ship_b. In order to solve the ship motion problem, we need to know the hydrostatic forces F^{aS}_j and F^{bS}_j which have been given in the previous section in Equations (2.11) to (2.16), and the hydrodynamic forces F^a_j and F^b_j which will be discussed in the following sections.

2.2 Steady Flow

2.2.1 Double-Body Flow Velocity Potential

A ship moving in the water with a steady forward speed U will generate water waves and produce the wave-making resistance. Since the wave-making resistance is balanced by the propulsion force, it will not be considered here. However, the steady forward speed will also affect the radiated wave of a moving ship and the radiated wave forces. This effect is called the steady flow effect. To approximate the steady flow effect in ship motion analysis, we will treat the disturbance potential by using the double-body flow method. The double-body velocity potential for steady flow can be expressed as:

$$\Phi_S(x, y, z) = -Ux + \phi_s(x, y, z) \tag{2.21}$$

the steady disturbance potential ϕ_s can be defined by

$$\nabla^2 \phi_s = 0$$

$$\frac{\partial \phi_s}{\partial z} = 0 \qquad (z = 0)$$

$$\frac{\partial \phi_s}{\partial z} = 0 \qquad (z = -h)$$

$$\frac{\partial \phi_s}{\partial n} |_{S_a} = U \cdot n_1^a \tag{2.22}$$

$$\frac{\partial \phi_s}{\partial n} |_{S_b} = U \cdot n_1^b$$

$$\nabla\phi_s = 0 \qquad (\ at\ infinity)$$

Applying the Green's function method, ϕ_s can be expressed as follows:

$$\phi_s(p) = \frac{1}{4\pi}\int\int_{S_a} \sigma_S^a(q)\hat{G}(p;q)dS(q) + \frac{1}{4\pi}\int\int_{S_b} \sigma_S^b(q)\hat{G}(p;q)dS(q) \tag{2.23}$$

where $p = p(x, y, z)$ is the field point, $q = q(\xi, \eta, \zeta)$ is the source point, $\sigma_S^a(q)$ is the steady flow source density on ship_a and $\sigma_S^b(q)$ is the steady flow source density on ship_b. $\hat{G}(p;q)$ is Green's function of the steady disturbance problem which can be expressed in terms of the Rankine source distribution for a double body,

$$\begin{aligned}\hat{G}(p;q) &= \sum_{i=1}^{\infty}\frac{1}{r_{1i}} + \frac{1}{r_{2i}} \\ &= \frac{1}{r_{11}} + \frac{1}{r_{21}} + \frac{1}{r_{12}} + \frac{1}{r_{22}} + \frac{1}{r_{13}} + \frac{1}{r_{23}} + \cdots\end{aligned} \tag{2.24}$$

where

$$\begin{aligned}r_{11} &= [(x-\xi)^2 + (y-\eta)^2 + (z-\zeta)^2]^{\frac{1}{2}} \\ r_{21} &= [(x-\xi)^2 + (y-\eta)^2 + (z+\zeta)^2]^{\frac{1}{2}} \\ r_{12} &= [(x-\xi)^2 + (y-\eta)^2 + (z-\zeta+2h)^2]^{\frac{1}{2}} \\ r_{22} &= [(x-\xi)^2 + (y-\eta)^2 + (z+\zeta+2h)^2]^{\frac{1}{2}} \\ r_{13} &= [(x-\xi)^2 + (y-\eta)^2 + (z-\zeta-2h)^2]^{\frac{1}{2}} \\ r_{23} &= [(x-\xi)^2 + (y-\eta)^2 + (z+\zeta-2h)^2]^{\frac{1}{2}} \\ &\cdots\cdots\cdots\cdots\cdots\end{aligned}$$

If the field point p falls on the surface of S_a, we obtain the disturbance potential on ship_a from Equation(2.23):

$$\phi_s^a(p) = \frac{1}{4\pi}\int\int_{S_a} \sigma_S^a(q)\hat{G}^{aa}(p;q)dS(q) + \frac{1}{4\pi}\int\int_{S_b} \sigma_S^b(q)\hat{G}^{ab}(p;q)dS(q) \qquad (2.25)$$

If the field point p falls on the surface of S_b, we obtain the disturbance potential on ship_b from Equation(2.23):

$$\phi_s^b(p) = \frac{1}{4\pi}\int\int_{S_a} \sigma_S^a(q)\hat{G}^{ba}(p;q)dS(q) + \frac{1}{4\pi}\int\int_{S_b} \sigma_S^b(q)\hat{G}^{bb}(p;q)dS(q) \qquad (2.26)$$

Applying the body surface boundary conditions of the disturbance potential ϕ_s in Equation(2.22) we have:

$$2\pi\sigma_S^a(p) + \int\int_{S_a} \sigma_S^a(q)\frac{\partial\hat{G}^{aa}(p;q)}{\partial n}\,|_{S_a}\, dS(q) + \int\int_{S_b} \sigma_S^b(q)\frac{\partial\hat{G}^{ab}(p;q)}{\partial n}\,|_{S_a}\, dS(q) = U\cdot n_1^a \qquad (2.27)$$

$$2\pi\sigma_S^b(p) + \int\int_{S_a} \sigma_S^a(q)\frac{\partial\hat{G}^{ba}(p;q)}{\partial n}\,|_{S_b}\, dS(q) + \int\int_{S_b} \sigma_S^b(q)\frac{\partial\hat{G}^{bb}(p;q)}{\partial n}\,|_{S_b}\, dS(q) = U\cdot n_1^b \qquad (2.28)$$

Equations (2.27) and (2.28) can be solved simultaneously for the source densities σ_S^a and σ_S^b. Then Equations (2.25) and (2.26) can be used to calculate the disturbance potentials $\phi_s^a(p)$ and $\phi_s^b(p)$.

2.2.2 Steady Flow Effect : m-terms

The steady flow effect to the radiation body boundary condition can be represented by m-terms. The m-terms are defined by Newman (1978):

$$(m_1, m_2, m_3) = -(\vec{n} \cdot \nabla)\vec{W} \tag{2.29}$$

$$(m_4, m_5, m_6) = -(\vec{n} \cdot \nabla)(\vec{r}_g \times \vec{W}) \tag{2.30}$$

where $r_g = (x_g, y_g, z_g)$ is the position vector from the centre of gravity of the ship to a point (x, y, z) on the hull surface. For a single ship, we know that the m-terms can be solved from the following integral equations:

$$\frac{\partial \phi_s(p)}{\partial x}|_{p\epsilon S} = \frac{1}{4\pi}\int\int_S [\phi_{s\xi}(q)\frac{\partial \hat{G}(p,q)}{\partial n(q)}|_{p\epsilon S} - \hat{G}(p,q)|_{p\epsilon S} m_1(q)]dS \tag{2.31}$$

$$\frac{\partial \phi_s(p)}{\partial y}|_{p\epsilon S} = \frac{1}{4\pi}\int\int_S [\phi_{s\eta}(q)\frac{\partial \hat{G}(p,q)}{\partial n(q)}|_{p\epsilon S} - \hat{G}(p,q)|_{p\epsilon S} m_2(q)]dS \tag{2.32}$$

$$\frac{\partial \phi_s(p)}{\partial z}|_{p\epsilon S} = \frac{1}{4\pi}\int\int_S [\phi_{s\zeta}(q)\frac{\partial \hat{G}(p,q)}{\partial n(q)}|_{p\epsilon S} - \hat{G}(p,q)|_{p\epsilon S} m_3(q)]dS \tag{2.33}$$

where $\phi_{s\xi}(q)$, $\phi_{s\eta}(q)$ and $\phi_{s\zeta}(q)$ are the partial derivatives of steady disturbance potential ϕ_s with respective to ξ, η and ζ. In the case of two ships, we assume $S = S_a + S_b$, and we have to consider two cases when the field point falls on ship_a and ship_b separately, then the integral Equation (2.31) becomes two integral equations:

$$\begin{aligned}\frac{\partial \phi_s(p)}{\partial x}|_{p\epsilon S_a} = &\frac{1}{4\pi}\int\int_{S_a} [\phi_{s\xi}(q)\frac{\partial \hat{G}(p,q)}{\partial n(q)}|_{p\epsilon S_a} - \hat{G}(p,q)|_{p\epsilon S_a} m_1^a(q)]dS + \\ &\frac{1}{4\pi}\int\int_{S_b} [\phi_{s\xi}(q)\frac{\partial \hat{G}(p,q)}{\partial n(q)}|_{p\epsilon S_a} - \hat{G}(p,q)|_{p\epsilon S_a} m_1^b(q)]dS \\ \frac{\partial \phi_s(p)}{\partial x}|_{p\epsilon S_b} = &\frac{1}{4\pi}\int\int_{S_a} [\phi_{s\xi}(p)\frac{\partial \hat{G}(p,q)}{\partial n(q)}|_{p\epsilon S_b} - \hat{G}(p,q)|_{p\epsilon S_b} m_1^a(q)]dS + \end{aligned} \tag{2.34}$$

$$\frac{1}{4\pi}\int\int_{S_b}[\phi_{s\xi}(q)\frac{\partial \hat{G}(p,q)}{\partial n(q)}|_{p\epsilon S_b} - \hat{G}(p,q)|_{p\epsilon S_b} m_1^b(q)]dS$$

where m_1^a and m_1^b are the m_1 terms of ship_a and ship_b, respectively. Similarly, we can derive the integral equations of m_2 for ship_a and ship_b as follows:

$$\begin{aligned}
\frac{\partial \phi_s(p)}{\partial y}|_{p\epsilon S_a} &= \frac{1}{4\pi}\int\int_{S_a}[\phi_{s\eta}(q)\frac{\partial \hat{G}(p,q)}{\partial n(q)}|_{p\epsilon S_a} - \hat{G}(p,q)|_{p\epsilon S_a} m_2^a(q)]dS + \\
&\quad \frac{1}{4\pi}\int\int_{S_b}[\phi_{s\eta}(q)\frac{\partial \hat{G}(p,q)}{\partial n(q)}|_{\bar{x}\epsilon S_a} - \hat{G}(p,q)|_{p\epsilon S_a} m_2^b(q)]dS \\
\frac{\partial \phi_s(p)}{\partial y}|_{p\epsilon S_b} &= \frac{1}{4\pi}\int\int_{S_a}[\phi_{s\eta}(q)\frac{\partial \hat{G}(p,q)}{\partial n(q)}|_{p\epsilon S_b} - \hat{G}(p,q)|_{p\epsilon S_b} m_2^a(q)]dS + \\
&\quad \frac{1}{4\pi}\int\int_{S_b}[\phi_{s\eta}(q)\frac{\partial \hat{G}(p,q)}{\partial n(q)}|_{p\epsilon S_b} - \hat{G}(p,q)|_{p\epsilon S_b} m_2^b(q)]dS
\end{aligned} \tag{2.35}$$

and the integral equations of m_3 for ship_a and ship_b as follows:

$$\begin{aligned}
\frac{\partial \phi_s(p)}{\partial z}|_{p\epsilon S_a} &= \frac{1}{4\pi}\int\int_{S_a}[\phi_{s\zeta}(q)\frac{\partial \hat{G}(p,q)}{\partial n(q)}|_{p\epsilon S_a} - \hat{G}(p,q)|_{p\epsilon S_a} m_3^a(q)]dS + \\
&\quad \frac{1}{4\pi}\int\int_{S_b}[\phi_{s\zeta}(q)\frac{\partial \hat{G}(p,q)}{\partial n(q)}|_{p\epsilon S_a} - \hat{G}(p,q)|_{p\epsilon S_a} m_3^b(q)]dS \\
\frac{\partial \phi_s(p)}{\partial z}|_{p\epsilon S_b} &= \frac{1}{4\pi}\int\int_{S_a}[\phi_{s\zeta}(q)\frac{\partial \hat{G}(p,q)}{\partial n(q)}|_{p\epsilon S_b} - \hat{G}(p,q)|_{p\epsilon S_b} m_3^a(q)]dS + \\
&\quad \frac{1}{4\pi}\int\int_{S_b}[\phi_{s\zeta}(q)\frac{\partial \hat{G}(p,q)}{\partial n(q)}|_{p\epsilon S_b} - \hat{G}(p,q)|_{p\epsilon S_b} m_3^b(q)]dS
\end{aligned} \tag{2.36}$$

Equations (2.34), (2.35) and (2.36) are coupled motion equations which can be solved as linear equation systems. $\hat{G}(p,q)$ is the double-body Green's function. For m_1 and m_2 terms of ship_a and ship_b,

$$\hat{G}(p;q) = \sum_{i=1}^{\infty}\frac{1}{r_{1i}} + \frac{1}{r_{2i}} \tag{2.37}$$

for m_3 terms of ship_a and ship_b,

$$\hat{G}(p;q) = \sum_{i=1}^{\infty} \frac{1}{r_{1i}} - \frac{1}{r_{2i}} \tag{2.38}$$

$$m_4^a = n_2^a w_3 - n_3^a w_2 + y_g^a m_3^a - z_g^a m_2^a \tag{2.39}$$

$$m_5^a = n_3^a w_1 - n_1^a w_3 + z_g^a m_1^a - x_g^a m_3^a \tag{2.40}$$

$$m_6^a = n_1^a w_2 - n_2^a w_1 + x_g^a m_2^a - y_g^a m_1^a \tag{2.41}$$

m_4^b, m_5^b and m_6^b can be computed from the following equations:

$$m_4^b = n_2^b w_3 - n_3^b w_2 + y_g^b m_3^b - z_g^b m_2^b \tag{2.42}$$

$$m_5^b = n_3^b w_1 - n_1^b w_3 + z_g^b m_1^b - x_g^b m_3^b \tag{2.43}$$

$$m_6^b = n_1^b w_2 - n_2^b w_1 + x_g^b m_2^b - y_g^b m_1^b \tag{2.44}$$

where w_1, w_2 and w_3 are the components of the steady flow velocity; n_j^a, j=1,2,3, are the unit normals of ship_a, n_j^b, j=1,2,3, are the unit normals of ship_b; (x_g^a, y_g^a, z_g^a) and (x_g^b, y_g^b, z_g^b) are the centres of gravity of ship_a and ship_b.

2.3 Incident Wave

According to the linear wave theory, the regular incident wave potential function in the finite depth of water can be obtained by solving the first-order boundary value

problem with the perturbation method as the following form:

$$\Phi_I(x, y, z, t) = Re[\phi_I(x, y, z)e^{-i\omega_e t}] \tag{2.45}$$

with

$$\phi_I(x, y, z) = \frac{g\zeta_a}{i\omega} \cdot \frac{\cosh(k(z+h))}{\cosh(kh)} \cdot e^{ik(x\cos\beta + y\sin\beta)} \tag{2.46}$$

where $\phi_I(x, y, z)$ is called the spatial potential function of the incident wave which is independent of time t; h is the depth of the water; ζ_a is the incident wave amplitude; $\omega_e = \omega - k \cdot Ucos\beta$ is wave encounter frequency; $\omega^2/g = k \cdot \tanh(kh)$; ω is the wave frequency; $k = 2\pi/\lambda$ is the wave number; g is the acceleration of gravity; β is the wave heading angle (the angle between the wave propagation direction and the positive ox axis direction as shown in Figure 2.1.

$$Re[\phi_I(x, y, z)] = \frac{\zeta_a g}{\omega} \cdot \frac{\cosh(k(z+h))}{\cosh(kh)} \cdot \sin(k(x\cos\beta + y\sin\beta)) \tag{2.47}$$

$$Im[\phi_I(x, y, z)] = -\frac{\zeta_a g}{\omega} \cdot \frac{\cosh(k(z+h))}{\cosh(kh)} \cdot \cos(k(x\cos\beta + y\sin\beta)) \tag{2.48}$$

$$\frac{\partial Re(\phi_I(x, y, z))}{\partial x} = \frac{\zeta_a gk}{\omega} \cdot \frac{\cosh(k(z+h))}{\cosh(kh)} \cdot \cos\beta \cdot \cos(k(x\cos\beta + y\sin\beta)) \tag{2.49}$$

$$\frac{\partial Re(\phi_I(x, y, z))}{\partial y} = \frac{\zeta_a gk}{\omega} \cdot \frac{\cosh(k(z+h))}{\cosh(kh)} \cdot \sin\beta \cdot \cos(k(x\cos\beta + y\sin\beta)) \tag{2.50}$$

$$\frac{\partial Re(\phi_I(x,y,z))}{\partial z} = \frac{\zeta_a g k}{\omega} \cdot \frac{\sinh(k(z+h))}{\cosh(kh)} \cdot \sin(k(x\cos\beta + y\sin\beta)) \tag{2.51}$$

$$\frac{\partial Im(\phi_I(x,y,z))}{\partial x} = \frac{\zeta_a g k}{\omega} \cdot \frac{\cosh(k(z+h))}{\cosh(kh)} \cdot \cos\beta \cdot \sin(k(x\cos\beta + y\sin\beta)) \tag{2.52}$$

$$\frac{\partial Im(\phi_I(x,y,z))}{\partial y} = \frac{\zeta_a g k}{\omega} \cdot \frac{\cosh(k(z+h))}{\cosh(kh)} \cdot \sin\beta \cdot \sin(k(x\cos\beta + y\sin\beta)) \tag{2.53}$$

$$\frac{\partial Re(\phi_I(x,y,z))}{\partial z} = -\frac{\zeta_a g k}{\omega} \cdot \frac{\sinh(k(z+h))}{\cosh(kh)} \cdot \cos(k(x\cos\beta + y\sin\beta)) \tag{2.54}$$

2.3.1 Incident Wave Force (Froude-Krylov Force)

If we simply neglect the contribution of diffracted wave and radiated wave forces on the hull and only consider the contribution of ϕ_I as if the hull does not exist, the wave force will be only the incident wave force, or Froude-Krylov force. Substituting the incident wave potential ϕ_I Equation(2.46) into Equation(2.9), the Froude-Krylov force acting on ship_a can be expressed as:

$$F_j^{Ia} = Re[f_j^{Ia} e^{-i\omega_e t}] \tag{2.55}$$

with

$$f_j^{Ia} = -\rho\omega \int\int_{S_a} Im[\phi_I] n_j^a dS - \rho \int\int_{S_a} Re[\nabla\phi_I \cdot \nabla\phi_s] n_j^a dS$$
$$+i\Big\{\rho\omega \int\int_{S_a} Re[\phi_I] n_j^a dS - \rho \int\int_{S_a} Im[\nabla\phi_I \cdot \nabla\phi_s] n_j^a dS\Big\} \quad (2.56)$$

Similarly, the Froude-Krylov force acting on ship_b can be obtained by substituting Equation(2.46) into Equation (2.10).

$$F_j^{Ib} = Re[f_j^{Ib} e^{-i\omega_e t}] \quad (2.57)$$

where

$$f_j^{Ib} = -\rho\omega \int\int_{S_b} Im[\phi_I] n_j^b dS - \rho \int\int_{S_b} Re[\nabla\phi_I \cdot \nabla\phi_s] n_j^b dS$$
$$+i\Big\{\rho\omega \int\int_{S_b} Re[\phi_I] n_j^b dS - \rho \int\int_{S_b} Im[\nabla\phi_I \cdot \nabla\phi_s] n_j^b dS\Big\} \quad (2.58)$$

2.4 Diffracted Waves

The existence of a fixed ship hull in waves will affect the incident wave and generate a wave system called the diffracted wave. In the case of two ships moving in waves, we evaluate the diffracted wave by assuming that two ships are fixed in incident waves.

2.4.1 Diffracted Wave Velocity Potential

The diffracted wave is also assumed to be a periodical wave with the velocity potential

$$\Phi_D(x, y, z, t) = Re[\phi_D(x, y, z) e^{-i\omega_e t}] \quad (2.59)$$

The diffracted wave potential can be found by solving the following boundary value equations

$$\nabla^2\phi_D = 0$$

$$(g\frac{\partial}{\partial z} + U^2\frac{\partial^2}{\partial x^2} + 2i\omega_e U\frac{\partial}{\partial x} - \omega_e^2)\phi_D = 0 \quad (z = 0)$$

$$\frac{\partial\phi_D}{\partial n}\,|_{S_a} = -\frac{\partial\phi_I}{\partial n}\,|_{S_a} \tag{2.60}$$

$$\frac{\partial\phi_D}{\partial n}\,|_{S_b} = -\frac{\partial\phi_I}{\partial n}\,|_{S_b}$$

$$\frac{\partial\phi_D}{\partial n}\,|_{z\to -h} = 0$$

radiation condition : outgoing wave

Again, Green's function method is applied to obtain the diffracted wave potential which is expressed as

$$\phi_D(p) = \frac{1}{4\pi}\int\int_{S_a}\sigma_D^a(q)G(p;q)dS(q) + \frac{1}{4\pi}\int\int_{S_b}\sigma_D^b(q)G(p;q)dS(q) \tag{2.61}$$

where $\sigma_D^a(q)$ is the source density on ship_a and $\sigma_D^b(q)$ is the source density on ship_b. The Green function $G(p;q)$ is given by Wehausen & Laitone(1960),

$$\begin{aligned} G(p;q) &= \frac{1}{r} + \frac{1}{r^*} \\ &+ 2P\nu\int_0^\infty \frac{(\mu+K)\exp(-\mu h)\cosh(\mu(\zeta+h))\cosh(\mu(z+h))}{\mu\cdot\sinh(\mu h) - K\cdot\cosh(\mu h)}J_0(\mu R)d\mu \\ &+ i\frac{2\pi(k+K)\exp(-kh)\sinh(kh)\cosh(k(\zeta+h))\cosh(k(z+h))}{K\cdot h + \sinh^2(kh)}J_0(kR) \end{aligned} \tag{2.62}$$

where

$$K = \frac{\omega^2}{g} = k \cdot \tanh(kh) \tag{2.63}$$

$$r = [(x-\xi)^2 + (y-\eta)^2 + (z-\zeta)^2]^{\frac{1}{2}} \tag{2.64}$$

$$r^* = [(x-\xi)^2 + (y-\eta)^2 + (z+2h+\zeta)^2]^{\frac{1}{2}} \tag{2.65}$$

$$R = [(x-\xi)^2 + (y-\eta)^2]^{\frac{1}{2}} \tag{2.66}$$

$p = p(x, y, z)$ is the field point; $q = q(\xi, \eta, \zeta)$ is the source point; h is the water depth; $-\frac{1}{r^*}$ is the potential of the image source; $k = 2\pi/\lambda$ is the wave number; PV indicates the Cauchy principal value of the integral which has a singularity at $\mu = k$; and J_0 denotes the Bessel function of the first kind of zero order.

By applying the body surface boundary conditions to Equation(2.61), we have:

$$\begin{cases} 2\pi\sigma_D^a(p) + \int\int_{S_a} \sigma_D^a(q) \frac{\partial G(p;q)}{\partial n} \mid_{S_a} dS(q) + \int\int_{S_b} \sigma_D^b(q) \frac{\partial G(p;q)}{\partial n} \mid_{S_a} dS(q) = -\frac{\partial \phi_I}{\partial n} \mid_{S_a} \\ 2\pi\sigma_D^b(p) + \int\int_{S_a} \sigma_D^a(q) \frac{\partial G(p;q)}{\partial n} \mid_{S_b} dS(q) + \int\int_{S_b} \sigma_D^b(q) \frac{\partial G(p;q)}{\partial n} \mid_{S_b} dS(q) = -\frac{\partial \phi_I}{\partial n} \mid_{S_b} \end{cases} \tag{2.67}$$

The source densities σ_D^a and σ_D^b can be solved numerically from this set of equations. Then the diffracted wave potential $\phi_D(p)$ can be obtained from Equation(2.61).

2.4.2 Diffracted Wave Force

The diffracted wave force of the jth mode of motion on the ship hulls can be expressed as

$$F_j^D(x, y, z, t) = Re[f_j^D(x, y, z)e^{-i\omega t}] \tag{2.68}$$

with

$$f_j^D = f_j^{Da} + f_j^{Db} \tag{2.69}$$

where f_j^{Da} is the diffracted wave force acting on ship_a and f_j^{Db} is the diffracted wave force acting on ship_b. Substituting the diffracted wave potential obtained from Equation(2.61) into Equation(2.9) we have the diffracted wave force acting on ship_a:

$$f_j^{Da} = -\rho\omega_e \int\int_{S_a} Im[\phi_D]n_j^a dS + \rho U \int\int_{S_a} Re[\frac{\partial \phi_D}{\partial x}]n_j^a dS - \rho \int\int_{S_a} Re[\nabla\phi_D \cdot \nabla\phi_s]n_j^a dS$$

$$+i\Big\{\rho\omega_e \int\int_{S_a} Re[\phi_D]n_j^a dS + \rho U \int\int_{S_a} Im[\frac{\partial \phi_D}{\partial x}]n_j^a dS - \rho \int\int_{S_a} Im[\nabla\phi_D \cdot \nabla\phi_s]n_j^a dS\Big\} \tag{2.70}$$

Likewise, the diffracted wave force acting on ship_b can be obtained by substituting diffracted wave potential into Equation(2.10):

$$f_j^{Db} = -\rho\omega_e \int\int_{S_b} Im[\phi_D]n_j^b dS + \rho U \int\int_{S_b} Re[\frac{\partial \phi_D}{\partial x}]n_j^b dS - \rho \int\int_{S_b} Re[\nabla\phi_D \cdot \nabla\phi_s]n_j^b dS$$

$$+i\Big\{\rho\omega_e \int\int_{S_a} Re[\phi_D]n_j^b dS + \rho U \int\int_{S_b} Im[\frac{\partial \phi_D}{\partial x}]n_j^b dS - \rho \int\int_{S_b} Im[\nabla\phi_D \cdot \nabla\phi_s]n_j^b dS\Big\} \tag{2.71}$$

2.5 Radiated Wave

The major difference between the one ship motion and the two ship motion problems is the radiated wave. In the case where two ships are in forced motion with six degrees of freedom, separately, the radiated wave is generated by the oscillation of both ships. The radiated wave force of a ship is not only due to its own oscillation but also due to the oscillation of the other ship.

2.5.1 Radiated Wave Potential

The radiated wave potential can be expressed as:

$$\Phi_R(x, y, z, t) = Re[\phi_R(x, y, z)e^{-i\omega_e t}] \tag{2.72}$$

For two ships freely floating in calm water, the radiated wave potential can be determined by satisfying the body surface condition with two separation settings: 1) ship_a is in motion and ship_b is at rest; and 2) ship_b is in motion and ship_a is at rest. Then we can express the radiated wave potential in the following form:

$$\Phi_R(x, y, z, t) = \Phi_R^a + \Phi_R^b = Re[(\phi_k^a + \phi_k^b)e^{-i\omega_e t}] \tag{2.73}$$

where $\phi_k^a = \phi_k^a(x, y, z)$, $k = 1, 2, ..., 6$, is the radiated wave potential per unit velocity of the k^{th} mode of motion due to the oscillation of ship_a while ship_b is at rest, and $\phi_k^b = \phi_k^b(x, y, z)$, $k = 1, 2, ..., 6$, is the radiated wave potential per unit velocity of the k^{th} mode of motion due to the oscillation of ship_b while ship_a is at rest.

Ship-a in Motion and Ship-b at Rest

The radiated wave potential per unit velocity of the k^{th} mode of motion can be found by solving the following boundary value equations:

$$\begin{gathered}
\nabla^2\phi_k^a = 0 \\
(g\frac{\partial}{\partial z} + U^2\frac{\partial^2}{\partial x^2} + 2i\omega_e U\frac{\partial}{\partial x} - \omega_e^2)\phi_k^a = 0 \quad (z = 0) \\
\frac{\partial\phi_k^a}{\partial n}\,|_{S_a} = n_k^a - \frac{m_k^a}{i\omega_e} \\
\frac{\partial\phi_k^a}{\partial n}\,|_{S_b} = 0
\end{gathered} \tag{2.74}$$

$$\frac{\partial \phi_k^a}{\partial n} |_{z \to -h} = 0$$

radiation condition : outgoing wave

where n_k^a is the generalized unit normal of ship_a (see Equation(2.5)) pointing towards the wetted hull surface of ship_a; U is the ship steady forward speed; g the gravitational acceleration; and m_k^a is the m-term of ship_a of the k^{th} mode of motion due to the influence of the forward speed.

Ship-b in Motion and Ship-a at Rest

Similarly, the radiated wave potential per unit velocity of the k^{th} mode of motion can be found by solving the following boundary value equations:

$$\nabla^2 \phi_k^b = 0$$

$$(g\frac{\partial}{\partial z} + U^2 \frac{\partial^2}{\partial x^2} + 2i\omega_e U \frac{\partial}{\partial x} - \omega_e^2)\phi_k^b = 0 \quad (z = 0)$$

$$\frac{\partial \phi_k^b}{\partial n} |_{S_b} = n_k^b - \frac{m_k^b}{i\omega_e} \tag{2.75}$$

$$\frac{\partial \phi_k^b}{\partial n} |_{S_a} = 0$$

$$\frac{\partial \phi_k^b}{\partial n} |_{z \to -h} = 0$$

radiation condition : outgoing wave

where n_k^b is the generalized unit normal of ship_b pointing towards from the wetted hull surface of ship_b (see Equation(2.6)); and m_k^b is the m-term of ship_b of the k^{th} direction due to the influence of the forward speed.

By applying Green's function method to Equations (2.74) and (2.75), and ignoring

the waterline integral term, we can obtain the radiated wave potential of ship_a and ship_b (Liu & Miao(1986)):

$$\phi_k^a(p) = \frac{1}{4\pi}\int\int_{S_a} \sigma_k^{aa}(q)G(p;q)dS(q) + \frac{1}{4\pi}\int\int_{S_b} \sigma_k^{ab}(q)G(p;q)dS(q) \qquad (2.76)$$

$$\phi_k^b(p) = \frac{1}{4\pi}\int\int_{S_a} \sigma_k^{ba}(q)G(p;q)dS(q) + \frac{1}{4\pi}\int\int_{S_b} \sigma_k^{bb}(q)G(p;q)dS(q) \qquad (2.77)$$

where σ_k^{aa} is the source density on ship_a due to the motion of ship_a while ship_b is at rest, and σ_k^{ab} is the source density on ship_b due to the motion of ship_a while ship_b is at rest. Also σ_k^{bb} is the source density on ship_b due to the motion of ship_b while ship_a is at rest, and σ_k^{ba} is the source density on ship_a due to the motion of ship_b while ship_a is at rest. $G(p;q)$ is Green's function of zero forward speed as Equation(2.62).

Applying boundary conditions of ϕ_k^a and ϕ_k^b to Equations(2.76) and (2.77), we have the following two sets of integral equations:

$$\begin{cases} 2\pi\sigma_k^{aa}(p) + \int\int_{S_a} \sigma_k^{aa}(q)\frac{\partial G(p;q)}{\partial n}|_{S_a}dS(q) + \int\int_{S_b} \sigma_k^{ab}(q)\frac{\partial G(p;q)}{\partial n}|_{S_a}dS(q) &= \frac{\partial \phi_k^a(p)}{\partial n}|_{S_a} \\ & = n_k^a - \frac{m_k^a}{i\omega_e} \\ 2\pi\sigma_k^{ab}(p) + \int\int_{S_a} \sigma_k^{aa}(q)\frac{\partial G(p;q)}{\partial n}|_{S_b}dS(q) + \int\int_{S_b} \sigma_k^{ab}(q)\frac{\partial G(p;q)}{\partial n}|_{S_b}dS(q) &= \frac{\partial \phi_k^a(p)}{\partial n}|_{S_b} = 0 \end{cases} \qquad (2.78)$$

$$\begin{cases} 2\pi\sigma_k^{bb}(p) + \int\int_{S_a} \sigma_k^{ba}(q)\frac{\partial G(p;q)}{\partial n}|_{S_b}dS(q) + \int\int_{S_b} \sigma_k^{bb}(q)\frac{\partial G(p;q)}{\partial n}|_{S_b}dS(q) &= \frac{\partial \phi_k^b(p)}{\partial n}|_{S_b} \\ & = n_k^b - \frac{m_k^b}{i\omega_e} \\ 2\pi\sigma_k^{ba}(p)\int\int_{S_a} \sigma_k^{ba}(q)\frac{\partial G(p;q)}{\partial n}|_{S_a}dS(q) + \int\int_{S_b} \sigma_k^{bb}(q)\frac{\partial G(p;q)}{\partial n}|_{S_a}dS(q) &= \frac{\partial \phi_k^b(p)}{\partial n}|_{S_a} = 0 \end{cases} \qquad (2.79)$$

The source densities $\sigma_k^{aa}(q)$, $\sigma_k^{ab}(q)$ can be obtained by solving the first set of equa-

tions, and $\sigma_k^{ba}(q)$ and $\sigma_k^{bb}(q)$ can be obtained by solving the second set of equations. Once the source densities and Green's function are known, the radiation potentials of ship_a and ship_b can be obtained by solving Equations(2.76) and (2.77).

2.5.2 Radiated Wave Force

Radiated Wave Forces on Ship-a

The radiated wave force of the jth mode of motion acting on ship_a is:

$$F_j^{Ra}(x,y,z,t) = Re[f_j^{Ra}e^{-i\omega_e t}] \tag{2.80}$$

where $f_j^{Ra} = f_j^{Ra}(x,y,z)$ is the time independent spatial radiated wave force on ship_a.

$$f_j^{Ra} = f_j^{Raa} + f_j^{Rab} \tag{2.81}$$

where f_j^{Raa} is the radiated wave force on ship_a due to the oscillation of ship_a itself while ship_b is at rest, and f_j^{Rab}, the interaction term, is the radiated wave force on ship_a due to the oscillation of ship_b while ship_a is at rest. By substituting the radiated wave potential of ship_a Equations(2.76) and (2.77) into Equations(2.7) and (2.3) we can obtain the radiated wave force for ship_a as follows,

$$\begin{aligned} f_j^{Raa} &= \rho\omega_e^2 \sum_{k=1}^{6} \bar{x}_k^a \Big\{ \int\int_{S_a} Re[\phi_k^a] n_j^a dS + \frac{U}{\omega_e} \int\int_{S_a} Im[\frac{\partial \phi_k^a}{\partial x}] n_j^a dS \\ &- \frac{1}{\omega_e} \int\int_{S_a} Im[\nabla\phi_k^a \cdot \nabla\phi_s] n_j^a dS \Big\} \end{aligned}$$

$$+ \quad i\rho\omega_e \sum_{k=1}^{6} \bar{x}_k^a \Big\{ \omega_e \int\int_{S_a} Im[\phi_k^a] n_j^a dS - U \int\int_{S_a} Re[\frac{\partial \phi_k^a}{\partial x}] n_j^a dS$$
$$+ \quad \int\int_{S_a} Re[\nabla \phi_k^a \cdot \nabla \phi_s] n_j^a dS \Big\} \tag{2.82}$$

$$\begin{aligned} f_j^{Rab} &= \rho\omega_e^2 \sum_{k=1}^{6} \bar{x}_k^b \Big\{ \int\int_{S_a} Re[\phi_k^b] n_j^a dS + \frac{U}{\omega_e} \int\int_{S_a} Im[\frac{\partial \phi_k^b}{\partial x}] n_j^a dS \\ &- \frac{1}{\omega_e} \int\int_{S_a} Im[\nabla \phi_k^b \cdot \nabla \phi_s] n_j^a dS \Big\} \\ &+ i\rho\omega_e \sum_{k=1}^{6} \bar{x}_k^b \Big\{ \omega_e \int\int_{S_a} Im[\phi_k^b] n_j^a dS - U \int\int_{S_a} Re[\frac{\partial \phi_k^b}{\partial x}] n_j^a dS \\ &+ \int\int_{S_a} Re[\nabla \phi_k^b \cdot \nabla \phi_s] n_j^a dS \Big\} \end{aligned} \tag{2.83}$$

where $\bar{x}_k^a$ is the complex amplitude of the k^{th} mode of motion of ship_a.

$$x_k^a = Re[\bar{x}_k^a e^{-i\omega_e t}] \tag{2.84}$$

and $\bar{x}_k^b$ is the complex amplitude of the k^{th} mode of motion of ship_b.

$$x_k^b = Re[\bar{x}_k^b e^{-i\omega_e t}] \tag{2.85}$$

Radiated Wave Forces on Ship-b

Similarly, the radiated wave force of the jth mode of motion acting on ship_b is:

$$F_j^{Rb}(x, y, z, t) = Re[f_j^{Rb} e^{-i\omega_e t}] \tag{2.86}$$

Here $f_j^{Rb} = f_j^{Rb}(x, y, z)$ is the time independent spatial radiated wave force on ship_b.

$$f_j^{Rb} = f_j^{Rba} + f_j^{Rbb} \tag{2.87}$$

where f_j^{Rbb} is the radiated wave force on ship_b due to the oscillation of ship_b while ship_a is at rest. f_j^{Rba} is the radiated wave force on ship_b due to the oscillation of ship_a while ship_b is at rest. By substituting the radiated wave potential of ship_a Equations(2.76) and (2.77) into Equations (2.7) and (2.4), respectively, we can obtain:

$$\begin{aligned} f_j^{Rbb} &= \rho\omega_e^2 \sum_{k=1}^{6} \bar{x}_k^b \Big\{ \int\int_{S_b} Re[\phi_k^b] n_j^b dS + \frac{U}{\omega_e} \int\int_{S_b} Im[\frac{\partial \phi_k^b}{\partial x}] n_j^b dS \\ &- \frac{1}{\omega_e} \int\int_{S_b} Im[\nabla \phi_k^b \cdot \nabla \phi_s] n_j^b dS \Big\} \\ &+ i\rho\omega_e \sum_{k=1}^{6} \bar{x}_k^b \Big\{ \omega_e \int\int_{S_b} Im[\phi_k^b] n_j^b dS - U \int\int_{S_b} Re[\frac{\partial \phi_k^b}{\partial x}] n_j^b dS \\ &+ \int\int_{S_b} Re[\nabla \phi_k^b \cdot \nabla \phi_s] n_j^b dS \Big\} \end{aligned} \tag{2.88}$$

$$\begin{aligned} f_j^{Rba} &= \rho\omega_e^2 \sum_{k=1}^{6} \bar{x}_k^a \Big\{ \int\int_{S_b} Re[\phi_k^a] n_j^b dS + \frac{U}{\omega_e} \int\int_{S_b} Im[\frac{\partial \phi_k^a}{\partial x}] n_j^b dS \\ &- \frac{1}{\omega_e} \int\int_{S_b} Im[\nabla \phi_k^a \cdot \nabla \phi_s] n_j^b dS \Big\} \\ &+ i\rho\omega_e \sum_{k=1}^{6} \bar{x}_k^a \Big\{ \omega_e \int\int_{S_b} Im[\phi_k^a] n_j^b dS - U \int\int_{S_b} Re[\frac{\partial \phi_k^a}{\partial x}] n_j^b dS \\ &+ \int\int_{S_b} Re[\nabla \phi_k^a \cdot \nabla \phi_s] n_j^b dS \Big\} \end{aligned} \tag{2.89}$$

Added Mass and Damping Coefficients

According to Equations (2.84) and (2.85), the body motion of two ships can be expressed respectively as:

$$\begin{aligned} \dot{x}_k^a &= Re[-i\omega_e \bar{x}_k^a e^{-i\omega_e t}] \\ \ddot{x}_k^a &= Re[-\omega_e^2 \bar{x}_k^a e^{-i\omega_e t}] \end{aligned} \tag{2.90}$$

and

$$\dot{x}_k^b = Re[-i\omega_e \bar{x}_k^b e^{-i\omega_e t}]$$
$$\ddot{x}_k^b = Re[-\omega_e^2 \bar{x}_k^b e^{-i\omega_e t}] \tag{2.91}$$

Substituting Equations(2.90) and (2.91) into Equations(2.82) and (2.83), the radiated wave force on ship_a can be written as:

$$f_j^{Raa} = -\ddot{x}_k^a \mu_{jk}^{aa} - \dot{x}_k^a \lambda_{jk}^{aa}$$
$$f_j^{Rab} = -\ddot{x}_k^b \mu_{jk}^{ab} - \dot{x}_k^b \lambda_{jk}^{ab} \tag{2.92}$$

where μ_{jk}^{aa} is the added mass of ship_a due to the motion of ship_a; μ_{jk}^{ab} is the added mass of ship_a due to the motion of ship_b; λ_{jk}^{aa} is the damping coefficient of ship_a due to the motion of ship_a: and λ_{jk}^{ab} is the damping coefficient of ship_a due to the motion of ship_b.

$$\mu_{jk}^{aa} = \rho\Big\{ \int\int_{S_a} Re[\phi_k^a] n_j^a dS + \frac{U}{\omega_e} \int\int_{S_a} Im[\frac{\partial \phi_k^a}{\partial x}] n_j^a dS - \frac{1}{\omega_e} \int\int_{S_a} Im[\nabla \phi_k^a \cdot \nabla \phi_s] n_j^a dS \Big\} \tag{2.93}$$

$$\mu_{jk}^{ab} = \rho\Big\{ \int\int_{S_a} Re[\phi_k^b] n_j^a dS + \frac{U}{\omega_e} \int\int_{S_a} Im[\frac{\partial \phi_k^b}{\partial x}] n_j^a dS - \frac{1}{\omega_e} \int\int_{S_a} Im[\nabla \phi_k^b \cdot \nabla \phi_s] n_j^a dS \Big\} \tag{2.94}$$

$$\lambda_{jk}^{aa} = \rho\Big\{ \omega_e \int\int_{S_a} Im[\phi_k^a] n_j^a dS - U \int\int_{S_a} Re[\frac{\partial \phi_k^a}{\partial x}] n_j^a dS + \int\int_{S_a} Re[\nabla \phi_k^a \cdot \nabla \phi_s] n_j^a dS \Big\} \tag{2.95}$$

$$\lambda_{jk}^{ab} = \rho\Big\{ \omega_e \int\int_{S_a} Im[\phi_k^b] n_j^a dS - U \int\int_{S_a} Re[\frac{\partial \phi_k^b}{\partial x}] n_j^a dS + \int\int_{S_a} Re[\nabla \phi_k^b \cdot \nabla \phi_s] n_j^a dS \Big\} \tag{2.96}$$

where $Im[...]$ represents the imaginary part of a complex function and $Re[...]$ represents the real part of a complex function.

Similarly, by substituting Equations(2.90) and (2.91) into Equations(2.88) and (2.89), the added mass and damping coefficients of ship_b can be expressed as:

$$\mu_{jk}^{bb} = \rho\Big\{ \int\int_{S_b} Re[\phi_k^b] n_j^b dS + \frac{U}{\omega_e} \int\int_{S_b} Im[\frac{\partial \phi_k^b}{\partial x}] n_j^b dS - \frac{1}{\omega_e} \int\int_{S_b} Im[\nabla \phi_k^b \cdot \nabla \phi_s] n_j^b dS \Big\} \tag{2.97}$$

$$\mu_{jk}^{ba} = \rho\Big\{ \int\int_{S_b} Re[\phi_k^a] n_j^b dS + \frac{U}{\omega_e} \int\int_{S_b} Im[\frac{\partial \phi_k^a}{\partial x}] n_j^b dS - \frac{1}{\omega_e} \int\int_{S_b} Im[\nabla \phi_k^a \cdot \nabla \phi_s] n_j^b dS \Big\} \tag{2.98}$$

$$\lambda_{jk}^{bb} = \rho\Big\{ \omega_e \int\int_{S_b} Im[\phi_k^b] n_j^b dS - U \int\int_{S_b} Re[\frac{\partial \phi_k^b}{\partial x}] n_j^b dS + \int\int_{S_b} Re[\nabla \phi_k^b \cdot \nabla \phi_s] n_j^b dS \Big\} \tag{2.99}$$

$$\lambda_{jk}^{ba} = \rho\Big\{ \omega_e \int\int_{S_b} Im[\phi_k^a] n_j^b dS - U \int\int_{S_b} Re[\frac{\partial \phi_k^a}{\partial x}] n_j^b dS + \int\int_{S_b} Re[\nabla \phi_k^a \cdot \nabla \phi_s] n_j^b dS \Big\} \tag{2.100}$$

where μ_{jk}^{bb} is the added mass of ship_b due to the motion of ship_b, μ_{jk}^{ba} is the added mass of ship_b due to the motion of ship_a, λ_{jk}^{bb} is the damping coefficient of ship_b due to the motion of ship_b, and λ_{jk}^{ba} is the damping coefficient of ship_b due to the motion of ship_a.

2.6 Wave Exciting Force

The wave exciting forces on ship_a and ship_b for the jth mode of motion can be expressed by the sum of the Froude-Krylov force and diffracted wave force as:

$$F_j^{Wa} = F_j^{Ia} + F_j^{Da} \tag{2.101}$$

$$F_j^{Wb} = F_j^{Ib} + F_j^{Db} \tag{2.102}$$

The wave exciting force on ship_a can be written as:

$$F_j^{Wa} = Re[f_j^{Wa} e^{-i\omega_e t}] \tag{2.103}$$

where

$$f_j^{Wa} = f_j^{Ia} + f_j^{Da} \tag{2.104}$$

f_j^{Ia} and f_j^{Da} are time-independent and have already been given in Equations (2.56) and (2.70), respectively. Similarly, the wave exciting force on ship_b can be shown as:

$$F_j^{Wb} = Re[f_j^{Wb} e^{-i\omega_e t}] \tag{2.105}$$

where

$$f_j^{Wb} = f_j^{Ib} + f_j^{Db} \tag{2.106}$$

f_j^{Ib} and f_j^{Db} are time-independent and have already been expressed in Equations (2.58) and (2.71), respectively.

2.7 Coupled Motion Equations

Finally, we are ready to write the equations of motion of two ships advancing in waves. Substituting Equations(2.101), (2.102), (2.11), (2.12) into Equations(2.17) and (2.18), after moving the terms of radiated wave forces to the left-hand side of the equations and with the definition of added mass and damping coefficients in Equation(2.93) to Equation(2.100), we are able to derive the coupled motion equations of ship_a and ship_b in the following forms:

$$\sum_{k=1}^{6}\{[-\omega_e^2(m_{jk}^a+\mu_{jk}^{aa})-i\omega_e\lambda_{jk}^{aa}+C_{jk}^a]\bar{x}_k^a+[-\omega_e^2\mu_{jk}^{ab}-i\omega_e\lambda_{jk}^{ab}]\bar{x}_k^b\}=f_j^{Wa} \quad (2.107)$$

$$\sum_{k=1}^{6}\{[-\omega_e^2\mu_{jk}^{ba}-i\omega_e\lambda_{jk}^{ba}]\bar{x}_k^a+[-\omega_e^2(m_{jk}^b+\mu_{jk}^{bb})-i\omega_e\lambda_{jk}^{bb}+C_{jk}^b]\bar{x}_k^b\}=f_j^{Wb} \quad (2.108)$$

where $j = 1, 2, ..., 6$ and

m_{jk}^a = mass matrix of ship_a

m_{jk}^b = mass matrix of ship_b

C_{jk}^a = restoring force coefficient matrix of ship_a

C_{jk}^b = restoring force coefficient matrix of ship_b

$\bar{x}_k^a$ = complex motion amplitudes of ship_a

$\bar{x}_k^b$ = complex motion amplitudes of ship_b

We can see that in the case of two ship motions, there are two sets of coupled motion equations. Compared to the motion equation of single ship motion, there are two more terms that appear in each set of equations which take into account the radiated wave effect from the other ship. By solving coupled motion Equations (2.107) and (2.108) we can obtain the motions of ship_a and ship_b. To numerically implement this, Equation(2.107) and Equation(2.108) must be discretized and written in a matrix form. This will be discussed in the Chapter 4.

2.8 Viscous Roll Damping

The roll motion of ships has a great impact on ship operations. However, theoretical prediction using the aforementioned potential theory cannot give satisfactory roll motion results comparing with the experimental results. For most ship hull forms,

the radiation damping predicted for the potential flow around the hull forms is only a fraction of the total roll damping which is experienced in reality. The discrepancies, according to many studies, are mainly caused by the viscous roll damping. Hull forms with relatively sharp corners at the bilges and/or at the keel will shed eddies as the ship rolls. This absorbs a good deal of energy and is a significant source of additional roll damping. Skin friction forces on the surface of the rolling hull may also be significant and any appendages will generate forces which oppose the roll motion. The effect of eddy shedding, skin friction, bilge keel and other appendages such as rudders, fins on the roll damping experienced at low forward speed will arise because of the influence of viscosity which is neglected in theoretical computation. To correct this problem, Schmitke's method (1978) is adopted to calculate the viscous roll damping of the two ships separately.

The viscous roll damping coefficient can be expressed as follows:

$$B_{44}^{V} = B_{BK} + B_E + B_H + B_F \tag{2.109}$$

where B_{BK}, B_E and B_H denote contributions from bilge keels, eddy-making resistance of the hull. and hull friction. respectively. B_F represents the viscous effect of appendages other than bilge keels(rudders, fins, etc.) at zero speed. Each component can be computed from the following empirical equations:

Bilge Keel

$$B_{BK} = \frac{1}{\pi^3}\rho l b_k r^3 \omega_e \eta_4 C_0 C_a C_k C_n B F^{-a} \tag{2.110}$$

where l is the bilge keel length, b_k bilge keel breadth, r the distance from the centre of the bilge keel to the centre of gravity of the ship, ω_e the frequency of encounter,

η_4 the roll amplitude, and α the foil angle of attack. C_0, C_a, C_k, C_n, B, and F are coefficients depending on the ship form and Reynolds number. They are given by Schmitke (1978).

Eddy-making

$$B_E = \frac{4}{3\pi}\rho\omega_e\eta_4 r^3 SC \tag{2.111}$$

where S is the wetted surface area of the hull section, and C is a drag coefficient depending on the hull form.

Hull friction

$$B_H = \frac{4}{3\pi}\rho\omega_e\eta_4 C_{DF}\int_L dx \int_{C_x} r(yn_2 + zn_3)^2 dl \tag{2.112}$$

where C_{DF} is the skin friction drag coefficient, C_x is the hull cross section, dl is the girthwise length element.

Other appendages(rudders, fins, ...)

$$B_F = \frac{4}{3\pi}\rho\omega_e\eta_4 \sum (y^2 + z^2)^{3/2} SC_n \tag{2.113}$$

where C_n is the normal force coefficient for a flat plate inclined at a large angle to the flow.

Viscous roll damping is a nonlinear function of roll amplitude. It is computed by an iterative scheme. The computation of viscous roll damping is initialized from the computed motion responses based on the potential theory, and the linear roll damping coefficient is replaced with the viscous roll damping coefficient in the equations of motion. The computed roll motion amplitude is then used to compute the viscous damping again. The iteration will continue until a given criterion is satisfied.

In our computation, the criterion for iteration is set to be

$$\frac{|b_{44}^{(k+1)} - b_{44}^{(k)}|}{b_{44}^{(k)}} < 0.05 \tag{2.114}$$

where k is the iteration index number. When $k = 1$, $b_{44}^{(1)} = b_{44}$ which is the same as the non-viscous roll damping coefficient calculated from the radiated wave potential.

Chapter 3

Green's Functions and Their Numerical Analysis

3.1 The Integral Form of Green's Function in Finite Depth of Water

For a fluid of constant finite depth h with vanishing normal velocity on the bottom, the Green function: which is Equation(2.62), can be expressed in terms of integral as follows (Wehausen & Laitone, 1960):

$$\begin{aligned} G(p;q) &= \frac{1}{r} + \frac{1}{r'} \\ &+ 2PV\int_0^\infty \frac{(\mu+K)\exp(-\mu h)\cosh(\mu(\zeta+h))\cosh(\mu(z+h))}{\mu\cdot\sinh(\mu h) - K\cdot\cosh(\mu h)} J_0(\mu R)d\mu \\ &+ i\frac{2\pi(k+K)\exp(-kh)\sinh(kh)\cosh(k(\zeta+h))\cosh(k(z+h))}{K\cdot h + \sinh^2(kh)} J_0(kR) \end{aligned} \tag{3.1}$$

where

$$K = \frac{\omega^2}{g} = k \cdot \tanh(kh) \tag{3.2}$$

$$r = [(x-\xi)^2 + (y-\eta)^2 + (z-\zeta)^2]^{\frac{1}{2}} \tag{3.3}$$

$$r^* = [(x-\xi)^2 + (y-\eta)^2 + (z+2h+\zeta)^2]^{\frac{1}{2}} \tag{3.4}$$

$$R = [(x-\xi)^2 + (y-\eta)^2]^{\frac{1}{2}} \tag{3.5}$$

and μ is an integral variable, $p = p(x, y, z)$ is the field point; $q = q(\xi, \eta, \zeta)$ is the source point; h is the water depth; r^* is the distance between field point and image source point and $k = 2\pi/\lambda$ is the wave number. PV indicates the Cauchy principal value of the integral which has a singularity at $\mu = k$, whereas J_0 denotes the Bessel function of the first kind of zero order.

3.1.1 Method to Solve Cauchy Principal-Value Integral

There is a principal-value integral with a pole at $\mu = k$ in the integrand of Equation(3.1). The contour of integration passes above the pole to satisfy the radiation condition of outgoing waves at infinity. Consider the principal value integral of the form.

$$PV \int_0^\infty \exp(-x) \cdot \frac{f(x)}{g(x)} dx = PV \int_0^\infty \exp(-x) \cdot F(x) dx \tag{3.6}$$

where

$$F(x) = \frac{f(x)}{g(x)} \tag{3.7}$$

When $g(x)$ has a pole of one degree at $x = a$, $F(x)$ is no longer bounded. In the vicinity of the singular point, $F(x)$ is approximated by:

$$F(x) \simeq F_1(x) = \frac{f(a)}{(x-a)g'(a)} \tag{3.8}$$

Then, Equation(3.6) can be rewritten in terms of the sum of I_1 and I_2 as follows:

$$\begin{aligned} PV\int_0^\infty \exp(-x)F(x)dx &= \int_0^\infty \exp(-x)[F(x) - F_1(x)]dx \\ &+ PV\int_0^\infty \exp(-x)F_1(x)dx \\ &= I_1 + I_2 \end{aligned} \tag{3.9}$$

3.1.2 Basic Theory to Evaluate the Cauchy Principal-Value Integral by Gauss-Laguerre Quadrature

The Gauss-Laguerre quadrature is used to approximate the integral in the following form:

$$\int_0^\infty x^r \exp(-x)f(x)dx \simeq \sum_{j=1}^{N} w_j f(x_j) \tag{3.10}$$

where w_j is a weight factor; x_j is the ith zero of the nth Laguerre Polynomial $Ln(x)$; and the integrand $f(x)$ is bounded. Substituting Equation(3.8) into Equation(3.9), we obtain

$$\begin{aligned} I_1 &= \int_0^\infty \exp(-x)[F(x) - F_1(x)]dx \\ &= \int_0^\infty \exp(-x)\cdot\{\frac{f(x)}{g(x)} - \frac{f(a)}{(x-a)g'(a)}\}dx \end{aligned} \tag{3.11}$$

$$\begin{aligned} I_2 &= PV\int_0^\infty \exp(-x)F_1(x)dx \\ &= PV\int_0^\infty \frac{\exp(-x)}{(x-a)}dx \cdot \frac{f(a)}{g'(a)} \\ &= H \cdot \frac{f(a)}{g'(a)} \end{aligned} \tag{3.12}$$

Letting $x - a = t$, $x = a + t$, then

$$\begin{aligned} H &= PV\int_0^\infty \frac{\exp(-x)}{x-a}dx \\ &= PV\int_{-a}^\infty \frac{\exp(-a-t)}{t}dt \\ &= PV\int_{-a}^\infty \exp(-a)\frac{\exp(-t)}{t}dt \\ &= \exp(-a)\cdot PV\int_{-a}^\infty \frac{\exp(-t)}{t}dt \\ &= -\exp(-a)E_i(a) \end{aligned} \tag{3.13}$$

Therefore,

$$I_2 = -\exp(-a)E_i(a)\cdot\frac{f(a)}{g'(a)} \tag{3.14}$$

and,

$$\begin{aligned} PV\int_0^\infty \exp(-x)\cdot\frac{f(x)}{g(x)}dx &= I_1 + I_2 \\ &= \int_0^\infty \exp(-x)\{\frac{f(x)}{g(x)} - \frac{f(a)}{(x-a)g'(a)}\}dx \\ &- \exp(-a)E_i(a)\frac{f(a)}{g'(a)} \end{aligned} \tag{3.15}$$

The integral in Equation(3.15) can be solved by Gauss-Laguerre quadrature which is shown in Equation(3.10), where $\tau = 0$.

3.1.3 Treatment of the Integral Form of Green's Function

From Equation(3.1),

$$G(p;q) = G_{IR1} + G_{IR2} + G_{II} \tag{3.16}$$

where

$$G_{IR1} = \frac{1}{r} + \frac{1}{r^*} \tag{3.17}$$

$$G_{IR2} = 2PV \int_0^\infty \frac{(\mu + K) \cdot \exp(-\mu h) \cdot \cosh(\mu(\zeta + h)) \cdot \cosh(\mu(z + h))}{\mu \cdot \sinh(\mu h) - K \cdot \cosh(\mu h)} J_0(\mu R) d\mu \tag{3.18}$$

$$G_{II} = i2\pi \cdot \frac{(k + K) \exp(-kh) \sinh(kh) \cdot \cosh(k(\zeta + h)) \cdot \cosh(k(z + h)) \cdot J_0(kR)}{Kh + \sinh^2(kh)} \tag{3.19}$$

Non-dimensionalized Integral Form of Green's Function in Finite Depth of Water

Because of the depth h involved in the Green's function in finite depth of water, we made the Green function dimensionless by multiplying the depth h. Then, the product $G \cdot h$ is regarded as a function of non-dimensional parameters. We introduce the non-dimensional parameters as follows:

$$\sigma = K \cdot h, \qquad \nu_0 = k \cdot h, \qquad \nu = \mu \cdot h$$

$$r_1 = \frac{R}{h} = \frac{\sqrt{(x - \xi)^2 + (y - \eta)^2}}{h}, \qquad r_2 = \frac{c}{h}, \qquad r_3 = \frac{z}{h}$$

Then,

$$K = \frac{\sigma}{h}, \qquad k = \frac{\nu_0}{h}, \qquad \mu = \frac{\nu}{h}$$

$$R = r_1 \cdot h, \qquad c = r_2 \cdot h, \qquad z = r_3 \cdot h$$

Substituting K, k, μ, R, c, and z into Equation(3.18) and Equation(3.19), we obtain:

$$G_{IR2}h = 2PV \int_0^\infty \exp(-\nu) \frac{(\nu+\sigma)\cosh(\nu(r_2+1))\cosh(\nu(r_3+1))}{\nu\sinh\nu - \sigma\cosh\nu} \cdot J_0(\nu r_1) d\nu \quad (3.20)$$

There is a singularity at $\nu = \nu_0$ in the principal value of the integral in Equation(3.20). Upon defining in Equation(3.15),

$$f(\nu) = (\nu+\sigma)\cosh(\nu(r_2+1))\cosh(\nu(r_3+1))J_0(\nu r_1) \quad (3.21)$$

$$g(\nu) = \nu\sinh\nu - \sigma\cosh\nu \quad (3.22)$$

$$g'(\nu) = \sinh\nu + \nu\cosh\nu - \sigma\sinh\nu \quad (3.23)$$

Then Equation(3.20) becomes,

$$\begin{aligned} G_{IR2}h &= 2\int_0^\infty \exp(-\nu)\Big[\frac{(\nu+\sigma)\cosh(\nu(r_2+1))\cosh(\nu(r_3+1))}{\nu\sinh\nu - \sigma\cosh\nu} J_0(\nu r_1) \\ &- \frac{(\nu_0+\sigma)\cosh(\nu_0(r_2+1))\cosh(\nu_0(r_3+1))J_0(\nu_0 r_1)}{(\nu-\nu_0)(\sinh\nu_0 + \nu_0\cosh\nu_0 - \sigma\sinh\nu_0)}\Big] d\nu \\ &- 2\exp(-\nu_0)E_i(\nu_0)\frac{(\nu_0+\sigma)\cosh(\nu_0(r_2+1))\cosh(\nu_0(r_3+1))J_0(\nu_0 r_1)}{\sinh\nu_0 + \nu_0\cosh\nu_0 - \sigma\sinh\nu_0} \end{aligned} \quad (3.24)$$

The integral in Equation(3.24) will be solved by using Gauss-Laguerre quadrature. According to Equation(3.19),

$$G_{II}h = i2\pi \frac{(\nu_0+\sigma)e^{-\nu_0}\sinh\nu_0\cosh(\nu_0(r_2+1))\cosh(\nu_0(r_3+1))J_0(\nu_0 r_1)}{\sigma + \sinh^2\nu_0} \quad (3.25)$$

G_{II} can be computed directly from Equation(3.25).

Analytical Expressions for the Derivatives of the Integral Form of Green's Function

According to Equation(3.24) and Equation(3.25), the derivatives of G_{IR2} and G_{II} can be expressed as follows:

$$\begin{aligned}\frac{\partial G_{IR2}}{\partial x} &= -\frac{2}{h^3}\int_0^\infty e^{-\nu}[\frac{(\nu+\sigma)\cosh(\nu(r_2+1))\cosh(\nu(r_3+1))J_1(\nu r_1)\nu}{\nu\sinh\nu-\sigma\cosh\nu}\cdot\frac{(x-\xi)}{r_1} \\ &+ \frac{(\nu_0+\sigma)\cosh(\nu_0(r_2+1))\ cosh(\nu_0(r_3+1))J_1(\nu_0 r_1)\nu_0}{(\nu-\nu_0)(\sinh\nu_0+\nu_0\cosh\nu_0-\sigma\sinh\nu_0)}\cdot\frac{(x-\xi)}{r_1}]d\nu \\ &+ \frac{2}{h^3}e^{-\nu_0}E_i(\nu_0)\frac{(\nu_0+\sigma)\cosh(\nu_0(r_2+1))\cosh(\nu_0(r_3+1))J_1(\nu_0 r_1)\nu_0}{\sinh\nu_0+\nu_0\cosh\nu_0-\sigma\sinh\nu_0} \\ &\times \frac{(x-\xi)}{r_1} \end{aligned} \tag{3.26}$$

$$\begin{aligned}\frac{\partial G_{IR2}}{\partial y} &= -\frac{2}{h^3}\int_0^\infty e^{-\nu}[\frac{(\nu+\sigma)\cosh(\nu(r_2+1))\cosh(\nu(r_3+1))J_1(\nu r_1)\cdot\nu}{\nu\sinh\nu-\sigma\cosh\nu}\cdot\frac{(y-\eta)}{r_1} \\ &+ \frac{(\nu_0+\sigma)\cosh(\nu_0(r_2+1))\ cosh(\nu_0(r_3+1))\cdot J_1(\nu_0 r_1)\cdot\nu_0}{(\nu-\nu_0)(\sinh\nu_0+\nu_0\cosh\nu_0-\sigma\sinh\nu_0)}\cdot\frac{(y-\eta)}{r_1}]d\nu \\ &+ \frac{2}{h^3}e^{-\nu_0}E_i(\nu_0)\frac{(\nu_0+\sigma)\cosh(\nu_0(r_2+1))\ \cosh(\nu_0(r_3+1))J_1(\nu_0 r_1)\cdot\nu_0}{\sinh\nu_0+\nu_0\cosh\nu_0-\sigma\sinh\nu_0} \\ &\times \frac{(y-\eta)}{r_1} \end{aligned} \tag{3.27}$$

$$\begin{aligned}\frac{\partial G_{IR2}}{\partial z} &= \frac{2}{h^2}\int_0^\infty e^{-\nu}[\frac{(\nu+\sigma)\cosh(\nu(r_2+1))\sinh(\nu(r_3+1))J_0(\nu r_1)\cdot\nu}{\nu\sinh\nu-\sigma\cosh\nu} \\ &- \frac{(\nu_0+\sigma)\cosh(\nu_0(r_2+1))\ sinh(\nu_0(r_3+1))\cdot J_0(\nu_0 r_1)\cdot\nu_0}{(\nu-\nu_0)(\sinh\nu_0+\nu_0\cosh\nu_0-\sigma\sinh\nu_0)}]d\nu \\ &- \frac{2}{h^2}e^{-\nu_0}E_i(\nu_0)\frac{(\nu_0+\sigma)\cosh(\nu_0(r_2+1))\sinh(\nu_0(r_3+1))J_0(\nu_0 r_1)\nu_0}{\sinh\nu_0+\nu_0\cosh\nu_0-\sigma\sinh\nu_0} \end{aligned} \tag{3.28}$$

And,

$$\frac{\partial G_{II}}{\partial x} = -i\frac{2\pi}{h^3}\cdot\frac{(\nu_0+\sigma)e^{-\nu_0}\sinh\nu_0\cosh(\nu_0(r_2+1))\cosh(\nu_0(r_3+1))J_1(\nu_0 r_1)\nu_0}{\sigma+\sinh^2\nu_0} \times \frac{(x-\xi)}{r_1} \tag{3.29}$$

$$\frac{\partial G_{II}}{\partial y} = -i\frac{2\pi}{h^3}\cdot\frac{(\nu_0+\sigma)e^{-\nu_0}\sinh\nu_0\cosh(\nu_0(r_2+1))\cosh(\nu_0(r_3+1))J_1(\nu_0 r_1)\nu_0}{\sigma+\sinh^2\nu_0} \times \frac{(y-\eta)}{r_1} \tag{3.30}$$

$$\frac{\partial G_{II}}{\partial x} = i\frac{2\pi}{h^2}\cdot\frac{(\nu_0+\sigma)e^{-\nu_0}\sinh\nu_0\cosh(\nu_0(r_2+1))\sinh(\nu_0(r_3+1))J_0(\nu_0 r_1)\cdot\nu_0}{\sigma+\sinh^2\nu_0} \tag{3.31}$$

3.1.4 Verification and Comparison of the Integral Form of Green's Function

To verify this method, Green's function $G(x,y,-h;\xi,0,0)$ in Equation(3.1) is calculated under the condition $k\cdot h = 5.000454$ and $K\cdot h = 5.0$, where k and K both satisfy the equation $K = k\cdot tanh(kh)$. At the field point $p = p(x,y,-h)$ and the source point $q = q(\xi,0,0)$:

$$\begin{aligned} G(x,y,-h;\xi,0,0) &= 2[(x-\xi)^2+y^2+h^2]^{-\frac{1}{2}} \\ &+ 2PV\int_0^\infty \frac{(\mu+K)\cdot\exp(-\mu h)\cdot\cosh(\mu h)}{\mu\cdot\sinh(\mu h)-K\cdot\cosh(\mu h)}J_0(\mu R)d\mu \\ &+ i\frac{2\pi(k+K)\cdot\exp(-kh)\cdot\sinh(kh)\cdot\cosh(kh))}{K\cdot h+\sinh^2(kh)}J_0(kR) \end{aligned}$$

(3.32)

where

$$R = [(x-\xi)^2 + y^2]^{\frac{1}{2}} \tag{3.33}$$

The Non-dimensionalized Form

Nondimensionlized Equation(3.32) can be rewritten as:

$$\begin{aligned} G \cdot h(r_1, \sigma, \nu_0) &= \frac{2}{(r_1^2+1)^{\frac{1}{2}}} + 2PV \int_0^\infty \frac{(\nu+\sigma)\exp(-\nu)\cosh(\nu)}{\nu \cdot \sinh\nu - \sigma\cosh(\nu)} J_0(r_1\nu)d\nu \\ &\quad + i2\pi \frac{(\nu_0+\sigma)\exp(-\nu_0)\sinh(\nu_0)\cosh(\nu_0)J_0(\nu_0 r_1)}{\sigma + \sinh^2(\nu_0)} \end{aligned} \tag{3.34}$$

where $r_1 = R/h = [(x-\xi)^2 + y^2]^{\frac{1}{2}}/h$; $\sigma = K \cdot h$; $\nu_0 = k \cdot h$; and $\nu = \mu \cdot h$, which is the positive real root of $\nu \cdot \tanh(\nu) - \sigma = 0$. The imaginary part of Equation(3.34) could be obtained directly. The real part of $G \cdot h$ in Equation(3.34):

$$Re\{G \cdot h\} = \frac{2}{(r_1^2+1)^{\frac{1}{2}}} + Q \tag{3.35}$$

$$Q = 2PV \int_0^\infty \frac{(\nu+\sigma)\exp(-\nu)\cosh(\nu)}{\nu \cdot \sinh\nu - \sigma\cosh(\nu)} J_0(r_1\nu)d\nu \tag{3.36}$$

Upon defining

$$F(\nu) \equiv \frac{f(\nu)}{g(\nu)} \tag{3.37}$$

where

$$f(\nu) = (\nu+\sigma)\cosh(\nu)J_0(\nu r_1) \tag{3.38}$$

$$g(\nu) = \nu\sinh(\nu) - \sigma\cosh(\nu) \tag{3.39}$$

$$g'(\nu) = \sinh(\nu) + \nu\cosh(\nu) - \sigma\sinh(\nu) \tag{3.40}$$

and using Equation(3.8), for ν at vicinity of ν_0, $F(\nu)$ becomes

$$\begin{aligned} F(\nu) &\simeq F_1(\nu) \\ &= \frac{f(\nu_0)}{(\nu-\nu_0)g'(\nu_0)} \\ &= \frac{(\nu_0+\sigma)\cosh(\nu_0)J_0(\nu_0 r_1)}{(\nu-\nu_0)\{\sinh(\nu_0)+\nu_0\cosh(\nu_0)-\sigma\sinh(\nu_0)\}} \end{aligned} \tag{3.41}$$

Finally, Q becomes

$$\begin{aligned} Q &= \int_0^\infty e^{-\nu}\{\frac{(\nu+\sigma)\cosh(\nu)J_0(\nu r_1)}{\nu\sinh(\nu)-\sigma\cosh(\nu)} \\ &- \frac{(\nu_0+\sigma)\cosh(\nu_0)J_0(\nu r_1)}{(\nu-\nu_0)[\sinh(\nu_0)+\nu_0\cosh(\nu_0)-\sigma\sinh(\nu_0)]}\}d\nu \\ &- e^{-\nu_0}E_i(\nu_0)\frac{(\nu_0+\sigma)\cosh(\nu_0)J_0(\nu_0 r_1)}{\sinh(\nu_0)+\nu_0\cosh(\nu_0)-\sigma\sinh(\nu_0)} \end{aligned} \tag{3.42}$$

In this example, $\nu_0 = k\cdot h = 5.000454$, $\sigma = K\cdot h = 5.0$, The integral in Equation(3.42) will be solved by using Gauss-Laguerre quadrature.

The Computed Results for Integral Form Green Function

A comparison is made in Figure 3.1 under the condition of $k \cdot h = 5.000454$ and $K \cdot h = 5.0$, k and K satisfying Equation(3.2). The real part of the $G \cdot h$ obtained by the present method with Gauss-Laguerre quadrature ($n = 64$) is compared with that obtained by the method of Monacella(1966). The results are virtually identical which shows that the Gauss-Laguerre quadrature method is very efficient for solving the integral form of Green's function.

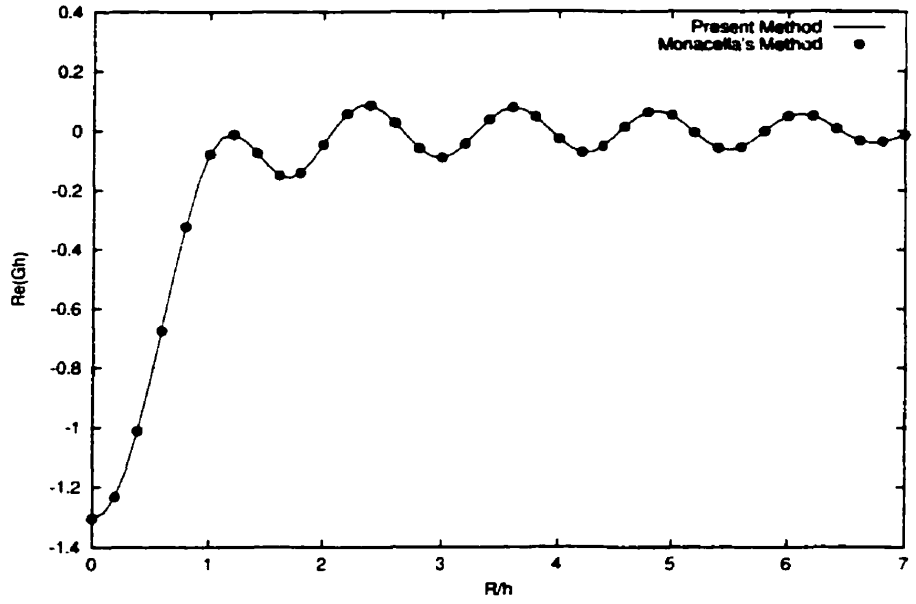

Figure 3.1: The real part of Gh with the integral form when $K'h = 5.0$, $kh = 5.000454$, and $0<R/h<7$

3.2 The Series Form of Green's Function in Finite Depth of Water

John (1949;1950) has derived the following infinite-series expansion form for Green's function in finite depth of water.

$$G(p;q) = 2\pi \cdot \frac{K'^2 - k^2}{k^2h - K'^2h + K'} \cdot \cosh(k(z+h)) \cdot \cosh(k(\zeta+h)) \cdot [Y_0'(kR) - iJ_0(kR)]$$
$$+4\sum_{n=1}^{\infty} \frac{k_n^2 + K'^2}{k_n^2h + K'^2h - K'} \cdot \cos(k_n(z+h))\cos(k_n(\zeta+h)) \cdot K(k_nR) \qquad (3.43)$$

where, $p = p(x,y,z)$ is the field point; $q = q(\xi,\eta,\zeta)$ is the source point; h is water depth; J_0 is Bessel function of the first kind; Y_0' is Bessel function of the second kind; and K_0 is the modified Bessel function of the second kind; and $R = [(x-\xi)^2+(y-\eta)^2]^{\frac{1}{2}}$.

k is positive real root of the transcendental equation:

$$K = \frac{\omega^2}{g} = k \cdot \tanh(kh) \tag{3.44}$$

And k_n denotes the set of corresponding positive real roots of equation:

$$k_n \cdot \tan(k_n h) = -K \tag{3.45}$$

From Equation(3.43)

$$G(p;q) = Re\{G\} + Im\{G\} = G_{SR} + G_{SI} \tag{3.46}$$

where,

$$\begin{aligned} G_{SR} &= 2\pi \cdot \frac{K^2 - k^2}{k^2 h - K^2 h + K} \cdot \cosh(k(z+h)) \cdot \cosh(k(\zeta+h)) \cdot Y_0(kR) \\ &\quad +4 \sum_{n=1}^{\infty} \frac{k_n^2 + K^2}{k_n^2 h + K^2 h - K} \cdot \cos(k_n(z+h)) \cos(k_n(\zeta+h)) \cdot K_0(k_n R) \end{aligned} \tag{3.47}$$

$$G_{SI} = -i2\pi \cdot \frac{K^2 - k^2}{k^2 h - K^2 h + K} \cdot \cosh(k(z+h)) \cdot \cosh(k(\zeta+h)) \cdot J_0(kR) \tag{3.48}$$

3.2.1 Non-dimensionalized Series Form of Green's Function

Similar to the integral form, we choose non-dimensional parameters as follows:

$$\sigma = K \cdot h, \qquad \nu_0 = k \cdot h, \qquad \alpha_n = k_n \cdot h$$

$$r_1 = \frac{R}{h} = \frac{\sqrt{(x-\xi)^2 + (y-\eta)^2}}{h}, \qquad r_2 = \frac{c}{h}, \qquad r_3 = \frac{z}{h}$$

Then,

$$K = \frac{\sigma}{h}, \qquad k = \frac{\nu_0}{h}, \qquad k_n = \frac{\alpha_n}{h}$$

$$R = r_1 \cdot h, \qquad c = r_2 \cdot h, \qquad z = r_3 \cdot h$$

And substituting K, k, k_n, R, c, z into Equation(3.47), we obtain:

$$\begin{aligned} G_{SR}h &= 2\pi \cdot \frac{\sigma^2 - \nu_0^2}{\nu_0^2 - \sigma^2 + \sigma} \cdot \cosh(\nu_0(r_2+1)) \cosh(\nu_0(r_3+1)) Y_0(\nu_0 r_1) \\ &\quad +4 \sum_{n=1}^{\infty} \frac{\alpha_n^2 + \sigma^2}{\alpha_n^2 + \sigma^2 - \sigma} \cdot \cos(\alpha_n(r_2+1)) \cos(\alpha_n(r_3+1)) K_0(\alpha_n r_1) \quad (3.49) \end{aligned}$$

The rate of convergence of Equation(3.49) depends primarily on the ratio of R/h, and the number of terms required for a given accuracy is proportional to h/R. Equation(3.49) is not applicable for small values of R/h, since each term of series contains a logarithmic singularity when $R/h = 0$. Numerical results confirm these estimates, and $6h/R$ is found to be an appropriate number of terms in the series to achieve enough accuracy in the domain for $R/h > 1/2$. Wehausen and Laitone(1960) gave the following equations:

$$\frac{\exp(-kh)\sinh(kh)}{Kh + \sinh^2(kh)} = \frac{2\exp(-kh)\cosh(kh)}{2kh + \sinh 2(kh)} = \frac{k-K}{k^2h - K^2h + K} \qquad (3.50)$$

Then, from Equation(3.48)

$$\frac{K^2 - k^2}{k^2 - K^2h + K} = -(k+K) \cdot \frac{k-K}{k^2 - K^2h + K} = -(k+K) \cdot \frac{\exp(-kh)\sinh(kh)}{Kh + \sinh^2(kh)} \quad (3.51)$$

So.

$$G_{SI} = i2\pi \cdot \frac{(k+K)\exp(-kh)\sinh(kh)\cdot\cosh(k(z+h))\cdot\cosh(k(c+h))\cdot J_0(kR)}{Kh+\sinh^2(kh)} \tag{3.52}$$

Equation(3.52) is as same as Equation(3.19), i.e. the imaginary parts of integral form and series form of Green function in finite depth of water have the same expression, i.e. $G_{SI} = G_{II}$. Therefore, they have the same non-dimensional form $G_{SI}h = G_{II}h$.

3.2.2 Analytical Expressions for Derivatives of the Series Form of Green's Function

Based on the above derivations, it is possible to find the derivatives of G_{SR} and G_{SI} as follows:

$$\begin{aligned}\frac{\partial G_{SR}}{\partial x} &= -\frac{2\pi}{h^3}\cdot\frac{\sigma^2-\nu_0^2}{\nu_0^2-\sigma^2+\sigma}\cosh(\nu_0(r_2+1))\cosh(\nu_0(r_3+1))Y_1(\nu_0 r_1)\nu_0\frac{(x-\xi)}{r_1} \\ &- \frac{4}{h^3}\sum_{n=1}^{\infty}\frac{\alpha_n^2+\sigma^2}{\alpha_n^2+\sigma^2-\sigma}\cos(\alpha_n(r_2+1))\cos(\alpha_n(r_3+1))K_1(\alpha_n R_1)\alpha_n\frac{(x-\xi)}{r_1}\end{aligned} \tag{3.53}$$

$$\begin{aligned}\frac{\partial G_{SR}}{\partial y} &= -\frac{2\pi}{h^3}\cdot\frac{\sigma^2-\nu_0^2}{\nu_0^2-\sigma^2+\sigma}\cosh(\nu_0(r_2+1))\cosh(\nu_0(r_3+1))Y_1(\nu_0 r_1)\nu_0\frac{(y-\eta)}{r_1} \\ &- \frac{4}{h^3}\sum_{n=1}^{\infty}\frac{\alpha_n^2+\sigma^2}{\alpha_n^2+\sigma^2-\sigma}\cos(\alpha_n(r_2+1))\cos(\alpha_n(r_3+1))K_1(\alpha_n R_1)\alpha_n\frac{(y-\eta)}{r_1}\end{aligned} \tag{3.54}$$

$$\frac{\partial G_{SR}}{\partial z} = \frac{2\pi}{h^2}\cdot\frac{\sigma^2-\nu_0^2}{\nu_0^2-\sigma^2+\sigma}\cdot\cosh(\nu_0(r_2+1))\sinh(\nu_0(r_3+1))Y_0(\nu_0 r_1)\cdot\nu_0$$
$$-\frac{4}{h^2}\sum_{n=1}^{\infty}\frac{\alpha_n^2+\sigma^2}{\alpha_n^2+\sigma^2-\sigma}\cdot\cos(\alpha_n(r_2+1))\sin(\alpha_n(r_3+1))K_0(\alpha_n R_1)\cdot\alpha_n \tag{3.55}$$

and.

$$\frac{\partial G_{SI}}{\partial x}=\frac{\partial G_{II}}{\partial x}, \qquad \frac{\partial G_{SI}}{\partial y}=\frac{\partial G_{II}}{\partial y}, \qquad \frac{\partial G_{SI}}{\partial z}=\frac{\partial G_{II}}{\partial z} \tag{3.56}$$

3.2.3 Verification of the Series Form of Green's Function

We again choose the Green's function $G(x,y,-h;\xi,0,0)$ to verify the real part of series form under the condition of $kh = 5.000454$, and $\nu h = 5.0$, by comparing its results with the integral form results. From Equation(3.47),

$$G_{SR}(x,y,-h;\xi,0,0) = 2\pi\cdot\frac{K^2-k^2}{k^2h-K^2h+K}\cdot\cosh(kh)\cdot Y_0(kR)$$
$$+4\sum_{n=1}^{\infty}\frac{k_n^2+K^2}{k_n^2h+K^2h-K}\cdot\cos(k_nh)\cdot K_0(k_nR) \tag{3.57}$$

where

$$\sigma = K\cdot h = 5.0. \qquad \nu_0 = k\cdot h = 5.000454, \qquad \alpha_n = k_n\cdot h$$

$$r_1 = \frac{R}{h} = \frac{\sqrt{(x-\xi)^2 + y^2}}{h}, \qquad r_2 = \frac{c}{h} = 0., \qquad r_3 = \frac{z}{h} = -1$$

k_n are the set of corresponding positive real roots of equation $k_n \cdot \tan k_n h = -K$.

$$k_n h \cdot \tan k_n h = -Kh \tag{3.58}$$

$$\alpha_n \cdot \tan \alpha_n = -\sigma \tag{3.59}$$

and α_n are the positive real roots of the transcendental equation

$$\alpha_n \tan \alpha_n + 5.000454 = 0 \tag{3.60}$$

Newman (1985) mentioned that $6h/R$ is an appropriate number of terms in the series to achieve 6 decimal place accuracy in the domain for $R/h > 1/2$. So, the number of series term in Equation(3.57) is determined by the following equation:

$$n_{max} = \frac{6h}{R} = \frac{6}{\frac{R}{h}} < \frac{6}{\frac{1}{2}} = 12 \tag{3.61}$$

This is the maximum number of terms = 12 when $R/h = 1/2$. By solving the transcendental Equation(3.60), the following 12 positive real roots can be found. From Equation(3.49)

Table 3.1: α values

$\alpha_1 = 0.1941111326E+01$	$\alpha_2 = 0.5549864292E+01$
$\alpha_3 = 0.8913572311E+01$	$\alpha_4 = 0.1217675018E+02$
$\alpha_5 = 0.1539391041E+02$	$\alpha_6 = 0.1858676529E+02$
$\alpha_7 = 0.2176534653E+02$	$\alpha_8 = 0.2493483925E+02$
$\alpha_9 = 0.2809822464E+02$	$\alpha_{10} = 0.3125730133E+02$
$\alpha_{11} = 0.3441323853E+02$	$\alpha_{12} = 0.3756680298E+02$

$$\begin{aligned} G_{SR} \cdot h(r_1, \sigma, \nu_0) &= 2\pi \cdot \frac{\sigma^2 - \nu_0^2}{\nu_0^2 - \sigma^2 + \sigma} \cdot \cosh(\nu_0) Y_0(\nu_0 r_1) \\ &\quad +4 \sum_{n=1}^{\infty} \frac{\alpha_n^2 + \sigma^2}{\alpha_n^2 + \sigma^2 - \sigma} \cdot \cos(\alpha_n) K_0(\alpha_n r_1) \\ &= 2\pi \cdot \frac{5.0^2 - 5.000454^2}{5.000454^2 + 5.0^2 - 5.0} \cdot \cosh(5.000454) Y_0(5.000454 r_1) \\ &\quad +4 \sum_{n=1}^{Int(6/r_1)} \frac{\alpha_n^2 + 5.0^2}{\alpha_n^2 + 5.0^2 - 5.0} \cdot \cos(\alpha_n) K_0(\alpha_n r_1) \end{aligned} \tag{3.62}$$

G_{SR} is only the function of r_1, i.e.

$$G_{SR}(x, y, -h; , a, 0, 0)h = G_{SR}(r_1) \tag{3.63}$$

3.2.4 The Computed Results and Discussions on the Series Form of Green's function

Figure 3.2 gives the comparison between the integral form and the series form. Very good agreement is observed except for the region $0 < R/h < 0.5$ and $6.5 < R/h < 7.0$. There is no convergent solution for series form of Green's function when R/h approaches to zero. Figure 3.3 gives the comparison of two forms when $0 \leq R/h \leq 20$. As we can see, the series form has the stable solution for whole region except for $0 \leq R/h \leq 0.5$, but for this region solutions can be offered by the integral form.

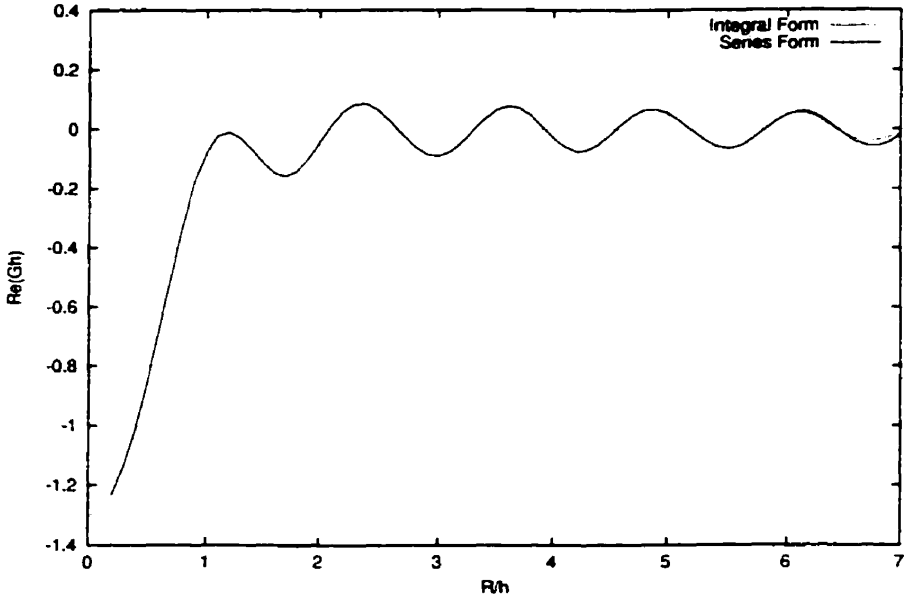

Figure 3.2: Comparison between real part of the integral and series forms of Gh when $Kh = 5.0$, $kh = 5.000454$, and $0 < R/h < 7$

The integral form does not have a stable solution when $R/h > 7.0$. Therefore, an algorithm has been proposed to solve the free-surface Green's function which is taking the integral form when $0 \leq R/h \leq 0.5$. taking the series form when $R/h > 0.5$. Figure 3.4 gives the results which are taken from the integral form when $0 \leq R/h \leq 0.5$ and from the series form of Green's function for $R/h > 0.5$. Figure 3.5 to Figure 3.12 give the results when $Kh = 0.2, 1.0, 2.0, 4.0$, individually. Figure 3.13 to Figure 3.15 give the Green's function distribution in 3-dimensions for the integral form . the series form and the combined form.

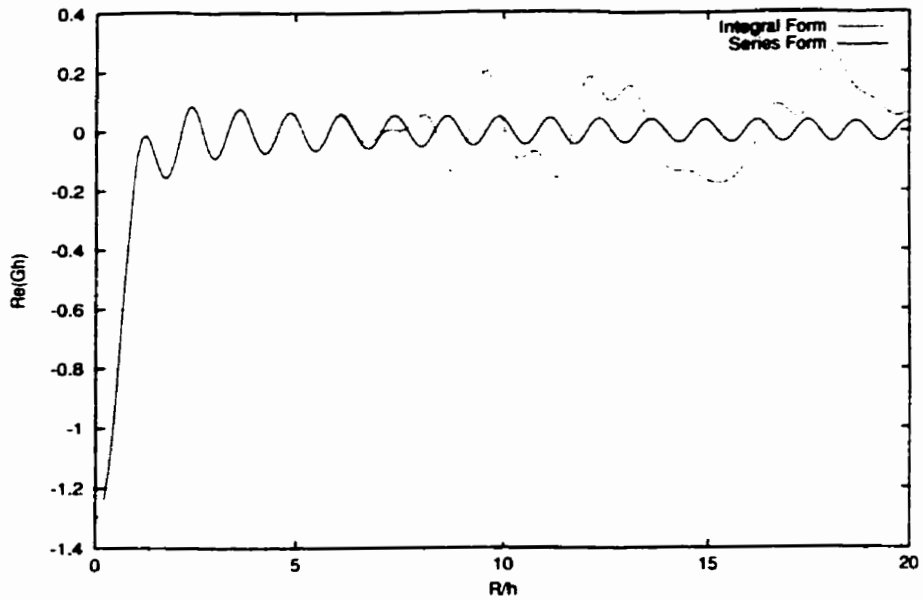

Figure 3.3: Comparison between real part of the integral and series forms of Gh when $Kh = 5.0$, $kh = 5.000454$, and $0 < R/h < 20$

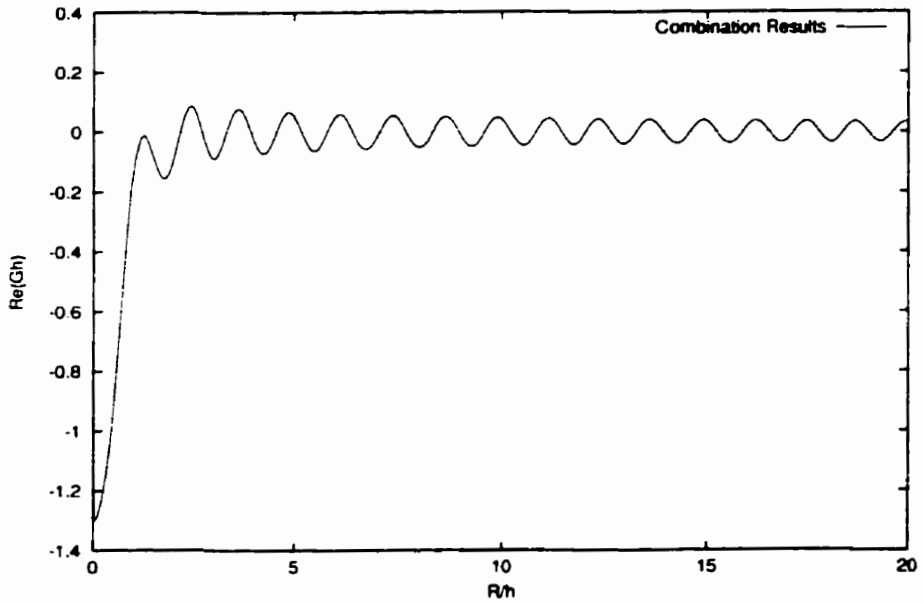

Figure 3.4: The real part of Gh combining the integral form with the series form when $Kh = 5.0$,$kh = 5.000454$, and $0 < R/h < 20$

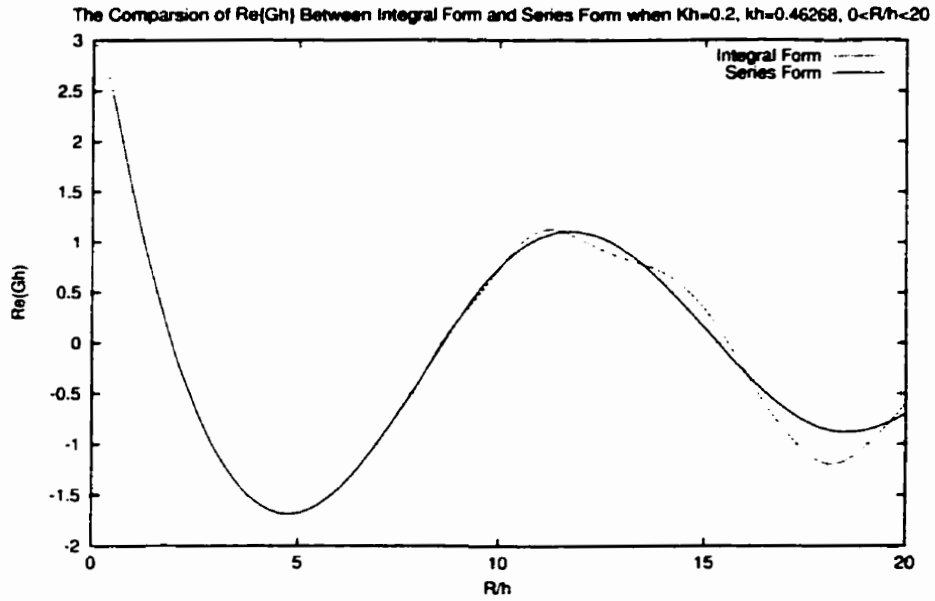

Figure 3.5: Comparison between real part of the integral and series forms of Gh when $Kh = 0.2, kh = 0.46268$, and $0 < R//h < 20$

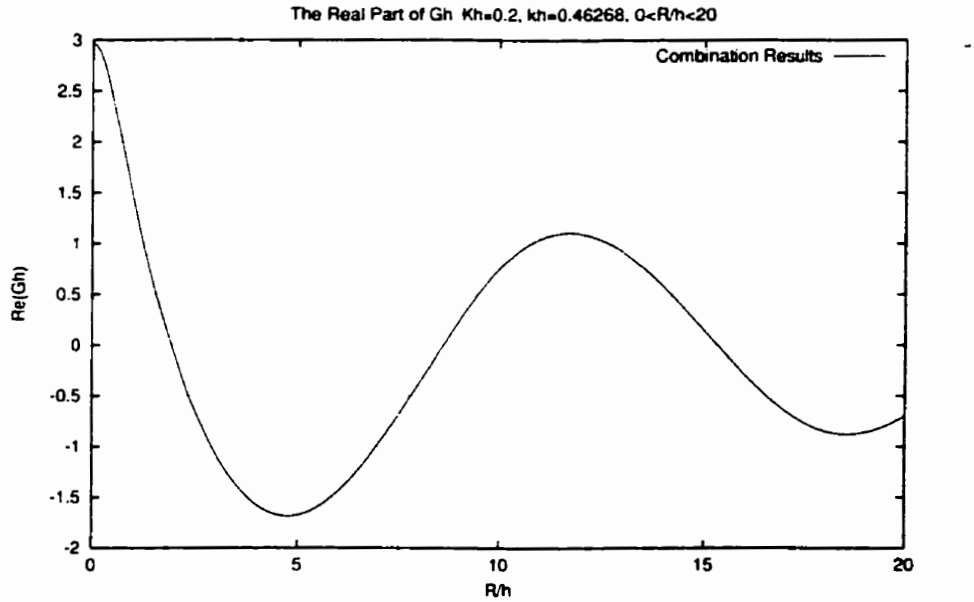

Figure 3.6: The real part of Gh combining the integral form with the series form when $Kh = 0.2, kh = 0.46268$, and $0 < R/h < 20$

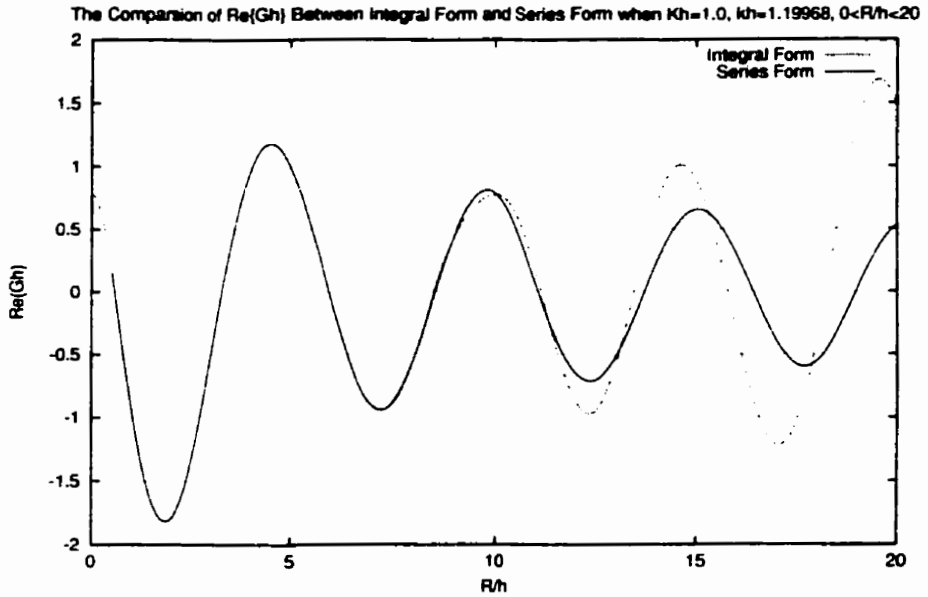

Figure 3.7: Comparison between real part of the integral and series forms of Gh When $Kh = 1.0, kh = 1.19968$, and $0 < R/h < 20$

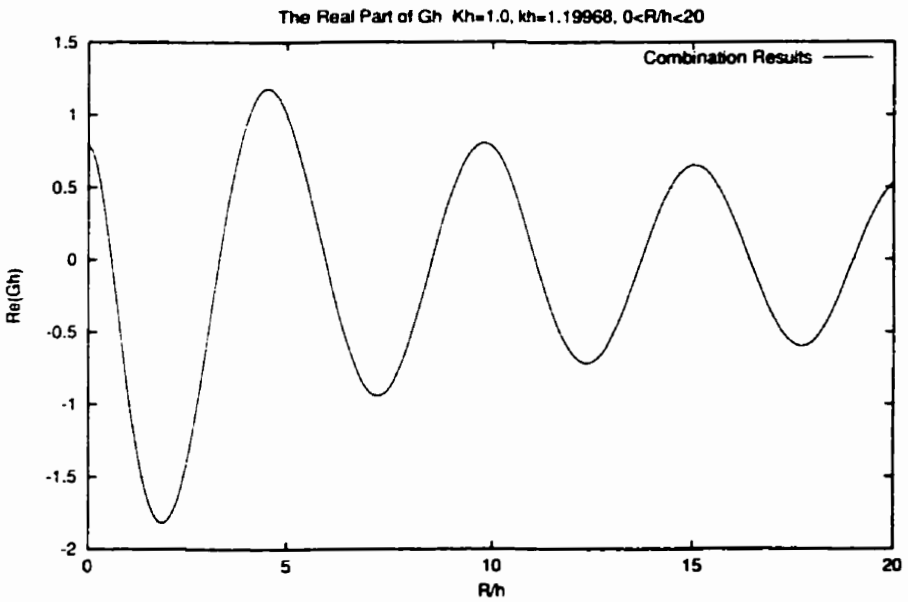

Figure 3.8: The real part of Gh combining the integral form with the series form when $Kh = 1.0, kh = 1.19968$, and $0 < R/h < 20$

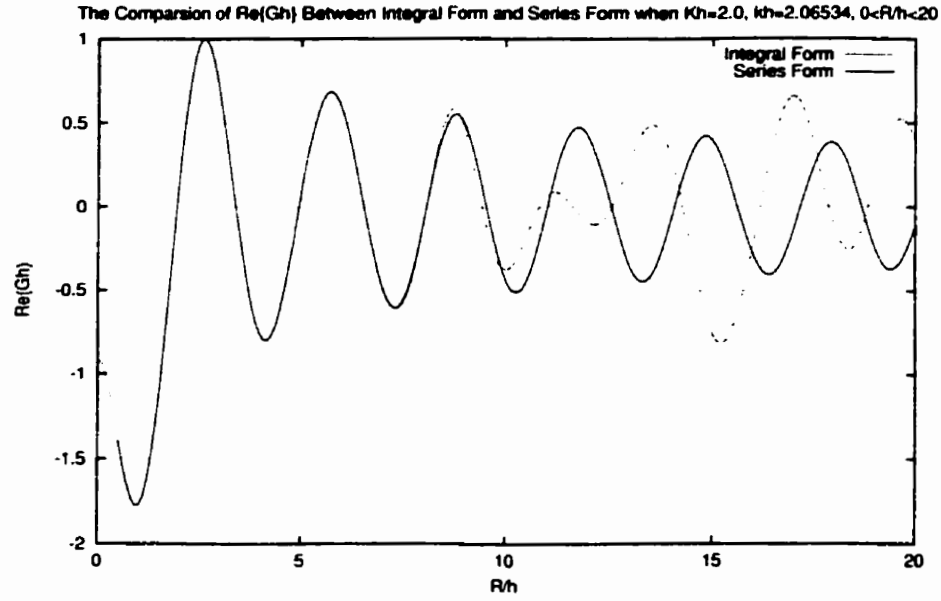

Figure 3.9: Comparison between real part of the integral and series forms of Gh when $Kh = 2.0, kh = 2.065345$, and $0 < R/h < 20$

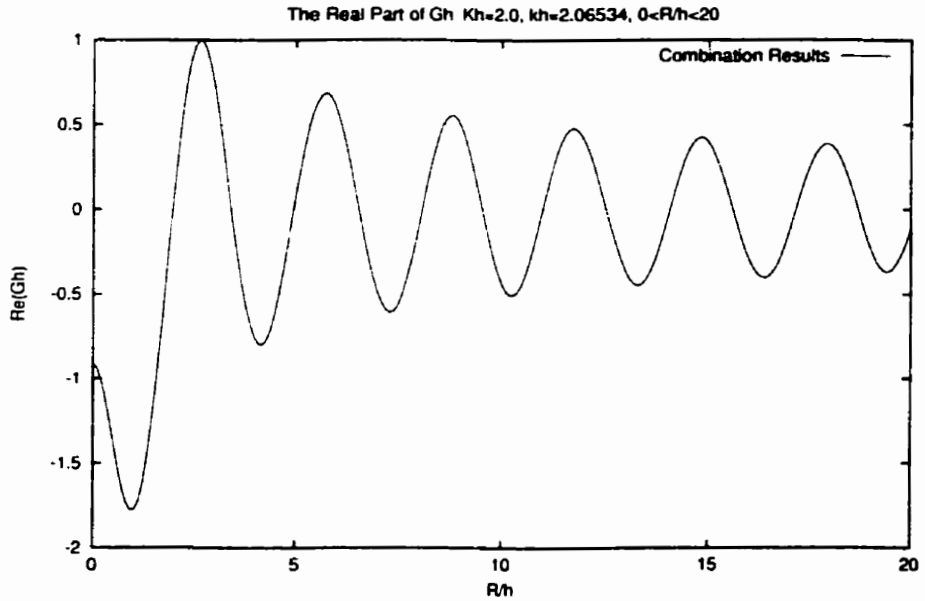

Figure 3.10: The real part of Gh combining the integral form with the series form when $Kh = 2.0, kh = 2.06534$, and $0 < R/h < 20$

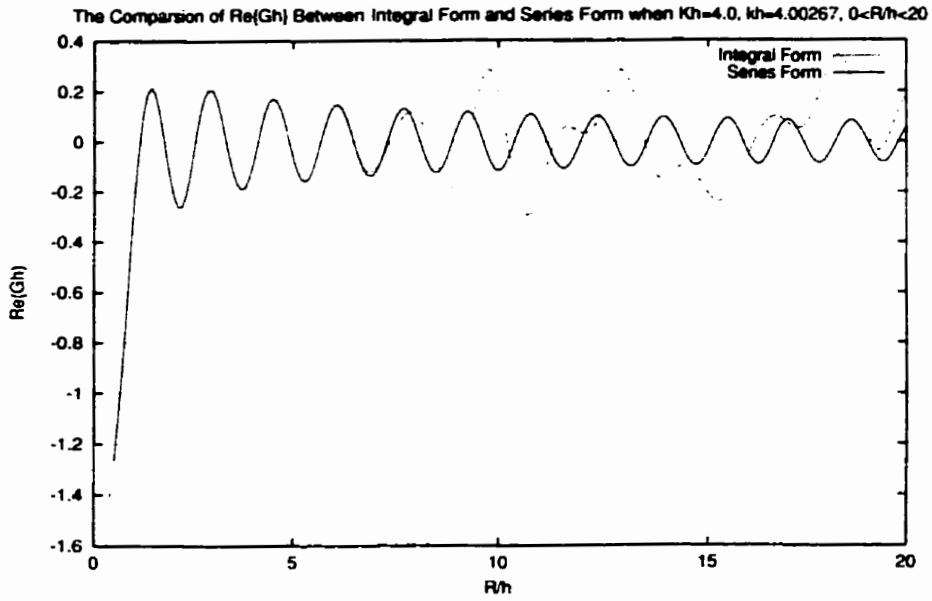

Figure 3.11: Comparison between real part of the integral and series forms of Gh when $Kh = 4.0, kh = 4.00267$, and $0 < R/h < 20$

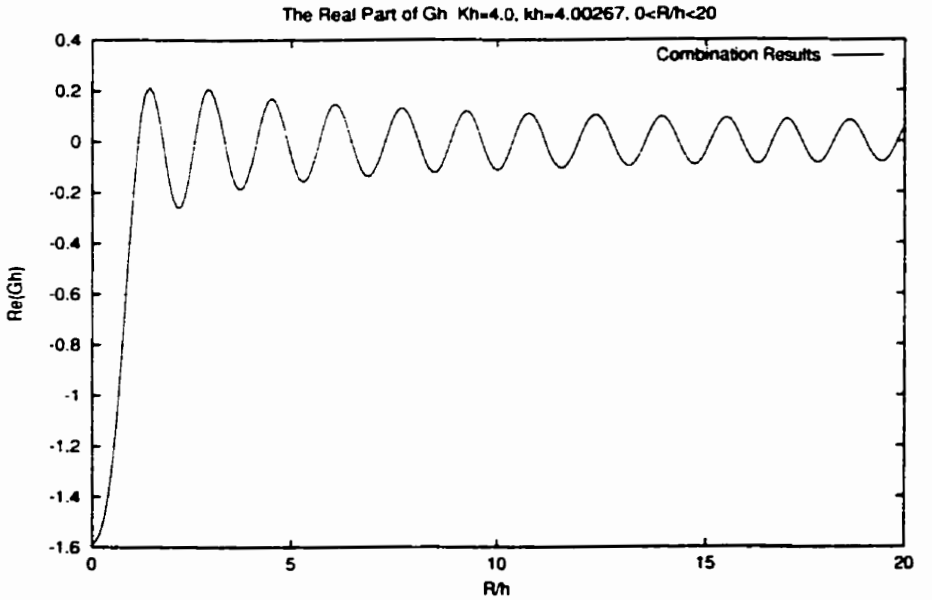

Figure 3.12: The real part of Gh combining the integral form with the series form when $Kh = 4.0, kh = 4.00267$, and $0 < R/h < 20$

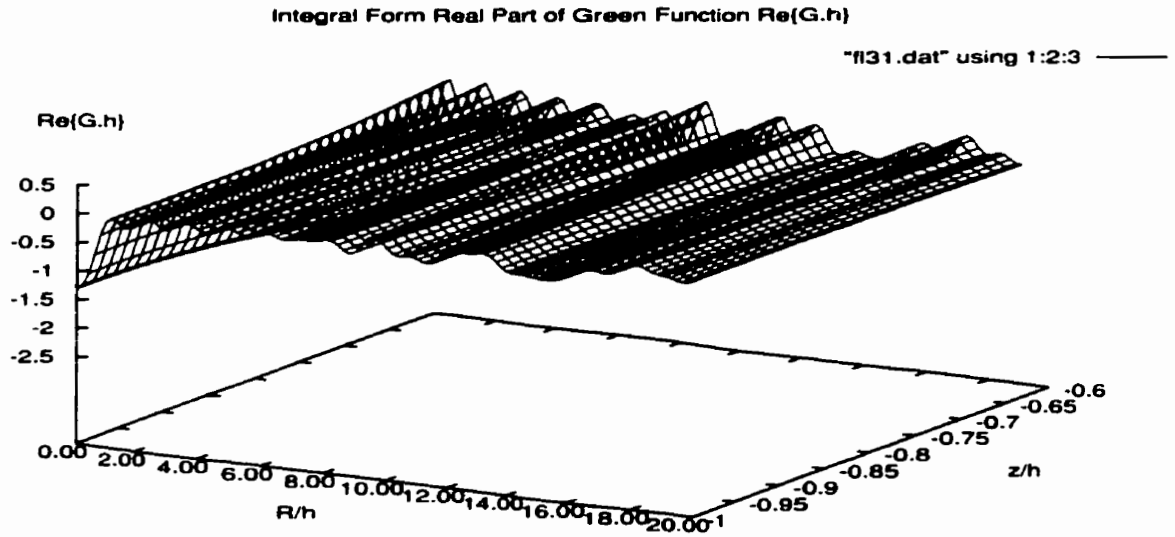

Figure 3.13: The 3-D distribution of the real part of Gh with the integral form when $Kh = 5.0, kh = 5.000454$, and $0 < R/h < 20$

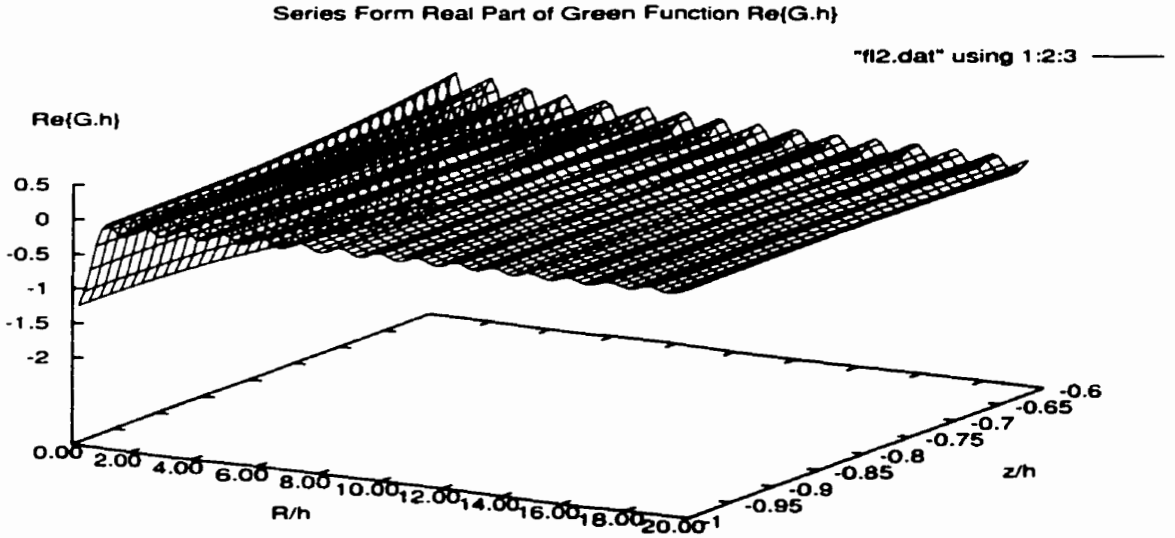

Figure 3.14: The 3-D distribution of the real part of Gh with the series form when $Kh = 5.0, kh = 5.000454$, and $0 < R/h < 20$

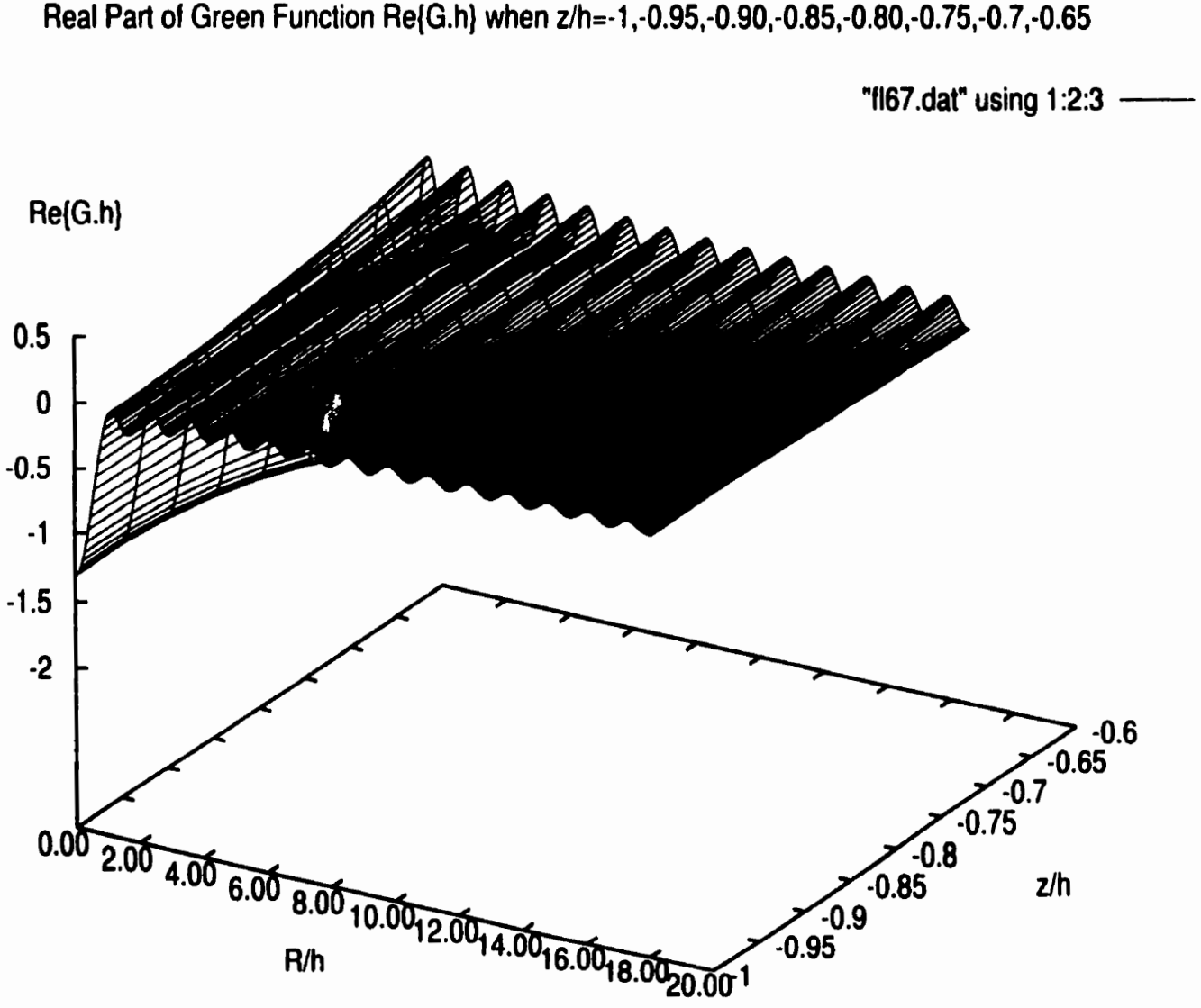

Figure 3.15: The 3-D distribution of the real part of Gh with the combined form when $Kh = 5.0, kh = 5.000454$, and $0 < R/h < 18$

3.3 Double Body Flow Disturbance Green's Function in Finite Depth of Water

The double-body velocity potential Φ_S of steady flow for zero frequency can be expressed as :

$$\Phi_S(x, y, z) = -Ux + \phi_s(x, y, z) \tag{3.64}$$

the disturbance potential ϕ_s in finite depth of water for a ship can be defined by

$$\begin{aligned}
&\nabla^2\phi_s = 0 \\
&\frac{\partial\phi_s}{\partial z} = 0 \qquad (z = 0) \\
&\frac{\partial\phi_s}{\partial z} = 0 \qquad (z = -h) \\
&\frac{\partial\phi_s}{\partial n}\,|_S = U \cdot n_1 \\
&\nabla\phi_s = 0 \qquad (\ at\ \infty)
\end{aligned} \tag{3.65}$$

where U is steady forward speed of ship. h is finite depth of water, (x, y, z) are coordinates of the field point, and n_1 is the unit normal vector pointing towards a ship surface in the $x-$direction.

In the double body flow in finite water depth, satisfying the boundary conditions on both sea bottom and rigid free surface simultaneously requires the use of an infinite row of images, at $z = 0$, $z = \pm 2h$, $\pm 4h$, $\pm 6h$, $\pm 8h$, $\cdots$, as illustrated in Figure(3.16). Therefore, the double body Green function $\hat{G}(x, y, z; \xi, \eta, \zeta)$ or $\hat{G}(p; q)$

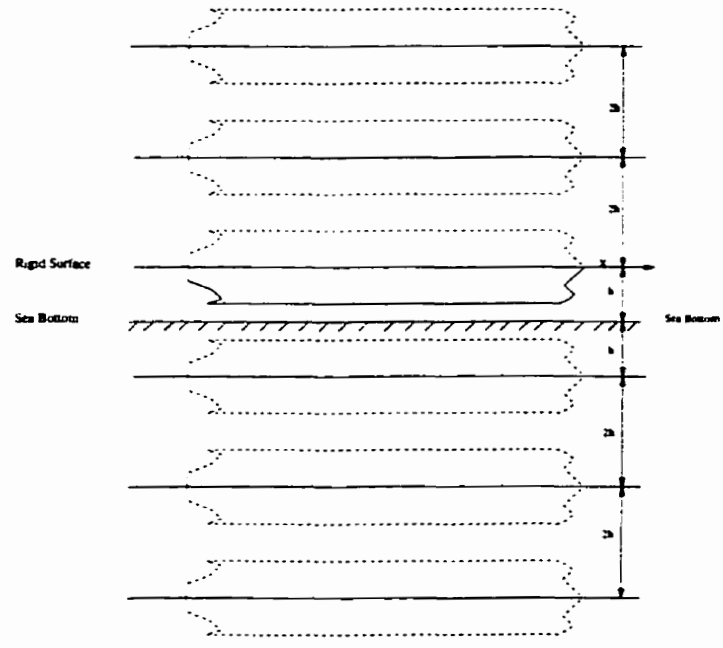

Figure 3.16: Double body images

can be expressed as:

$$\begin{aligned}\hat{G}(p;q) &= \sum_{i=1}^{\infty} \frac{1}{r_{1i}} + \frac{1}{r_{2i}} \\ &= \frac{1}{r_{11}} + \frac{1}{r_{21}} + \frac{1}{r_{12}} + \frac{1}{r_{22}} + \frac{1}{r_{13}} + \frac{1}{r_{23}} + \cdots \end{aligned} \tag{3.66}$$

where $p = p(x, y, z)$ is the field point; $q = q(x, y, z)$ is the source point, and

$$r_{11} = [(x-\xi)^2 + (y-\eta)^2 + (z-\zeta)^2]^{\frac{1}{2}}$$

$$r_{21} = [(x-\xi)^2 + (y-\eta)^2 + (z+\zeta)^2]^{\frac{1}{2}}$$

$$r_{12} = [(x-\xi)^2 + (y-\eta)^2 + (z-\zeta+2h)^2]^{\frac{1}{2}}$$

$$r_{22} = [(x-\xi)^2 + (y-\eta)^2 + (z+\zeta+2h)^2]^{\frac{1}{2}}$$

$$r_{13} = [(x-\xi)^2 + (y-\eta)^2 + (z-\zeta-2h)^2]^{\frac{1}{2}}$$

$$r_{23} = [(x-\xi)^2 + (y-\eta)^2 + (z+\zeta-2h)^2]^{\frac{1}{2}}$$

Chapter 4

Numerical Implementations

4.1 Velocity Potentials

We have described and formulated the steady flow problem, the radiated wave problem and the diffracted wave problem separately in Chapter 2. We can treat them as a generalized boundary value problem described by Laplace's equation:

$$\nabla^2\phi = 0 \tag{4.1}$$

which will be solved with the following boundary conditions:

$$\text{Free Surface Condition at z=0:} \quad B^f \tag{4.2}$$

$$\text{Body Surface Condition on Ship-a:} \quad \frac{\partial\phi}{\partial n}\,|_{S_a} = B^a \tag{4.3}$$

$$\text{Body Surface Condition on Ship-b:} \quad \frac{\partial\phi}{\partial n}\,|_{S_b} = B^b \tag{4.4}$$

$$\text{Bottom Condition} \quad : \quad \frac{\partial\phi}{\partial n}\,|_{z\to -h} = 0 \tag{4.5}$$

Radiation Condition: *Outgoing Waves* (4.6)

where ϕ is a time independent velocity potential. For steady flow, ϕ can be replaced by ϕ_s; for the radiated wave problem, ϕ can be replaced by ϕ_k^a or ϕ_k^b; and for the diffracted wave problem, ϕ can be replaced by ϕ_D. B^a and B^b are the body surface conditions on ship_a and ship_b, respectively. For steady flow, $B^a = U \cdot n_1^a$ and $B^b = U \cdot n_1^b$. For the radiated wave problem, $B^a = n_k^a - \frac{m_k^a}{i\omega_e}$, $B^b = 0$; or $B^b = n_k^b - \frac{m_k^b}{i\omega_e}$, $B^a = 0$. For the diffracted wave problem, $B^a = -\frac{\partial \phi_I}{\partial n}|_{S_a}$ and $B^b = -\frac{\partial \phi_I}{\partial n}|_{S_b}$. B^f is the free surface condition, for the wave radiation and diffraction problems

$$(g\frac{\partial}{\partial z} + U^2\frac{\partial^2}{\partial x^2} + 2i\omega_e U\frac{\partial}{\partial x} - \omega_e^2)\phi = 0\ , \quad z = 0$$

For double-body flow, B^f becomes

$$\frac{\partial \phi_s}{\partial z} = 0, \qquad z = 0$$

and it should also be noted that there is no wave radiation condition for the steady flow problem. According to Green's Theorem, the velocity potential can be expressed as:

$$\phi(p) = \frac{1}{4\pi}\int\int_{S_a} \sigma_a(q)G(p,q)dS(q) + \frac{1}{4\pi}\int\int_{S_b} \sigma_b(q)G(p,q)dS(q) \qquad (4.7)$$

where σ_a is the surface source density distribution on ship_a and σ_b is the surface source density distribution on ship_b. Corresponding to different problems, σ_a and σ_b will have different values. For example, in a wave radiation problem, σ_a could be replaced by σ_k^{aa}, σ_k^{ab} and σ_b could be replaced by σ_k^{ba}, σ_k^{bb}. In a wave diffraction problem, σ_a becomes σ_D^a and σ_b becomes σ_D^b. In a steady flow problem, σ_a becomes

σ_S^a and σ_b becomes σ_S^b. $G(p,q)$ is the generalized Green's function. The velocity potential ϕ can also be discretized as:

$$\phi(p_i) = \frac{1}{4\pi}\sum_{j=1}^{npa}[\int\int_{S_a^j} G(p_i,q_j)dS(q_j)]\sigma_1^j(q_j) + \frac{1}{4\pi}\sum_{j=1}^{npb}[\int\int_{S_b^j} G(p_i,q_j)dS(q_j)]\sigma_2^j(q_j) \tag{4.8}$$

where p_i is a field point, $i = 1, 2, 3, ...$ If p_i falls on ship_a and ship_b, we have the following coupled equations:

$$\phi^a(p_i) = \frac{1}{4\pi}\sum_{j=1}^{npa}[\int\int_{S_a^j} G(p_i,q_j)|s_a^j dS(q_j)]\sigma_1^j(q_j) + \frac{1}{4\pi}\sum_{j=1}^{npb}[\int\int_{S_b^j} G(p_i,q_j)|s_a^j dS(q_j)]\sigma_2^j(q_j) \tag{4.9}$$

$$\phi^b(p_i) = \frac{1}{4\pi}\sum_{j=1}^{npa}[\int\int_{S_a^j} G(p_i,q_j)|s_b^j dS(q_j)]\sigma_1^j(q_j) + \frac{1}{4\pi}\sum_{j=1}^{npb}[\int\int_{S_b^j} G(p_i,q_j)|s_b^j dS(q_j)]\sigma_2^j(q_j) \tag{4.10}$$

In the first equation, $i = 1, 2, ..., npa$, where npa is the total number of panels on ship_a. In the second equation, $i = 1, 2, ..., npb$, where npb is the total number of panels on ship_b.

By defining:

$$\phi_i^a = \phi^a(p_i) \qquad \phi_i^b = \phi^b(p_i) \tag{4.11}$$

$$G_{ij}^{aa} = \int\int_{S_a^j} G(p_i,q_j)|s_a^j dS(q_j) \tag{4.12}$$

$$G_{ij}^{ab} = \int\int_{S_b^j} G(p_i,q_j)|s_a^j dS(q_j) \tag{4.13}$$

$$G_{ij}^{ba} = \int\int_{S_a^j} G(p_i,q_j)|s_b^j dS(q_j) \tag{4.14}$$

$$G_{ij}^{bb} = \int\int_{S_b^j} G(p_i,q_j)|s_b^j dS(q_j) \tag{4.15}$$

Equations(4.9) and (4.10) become:

$$\phi_i^a = \frac{1}{4\pi}\sum_{j=1}^{npa} G_{ij}^{aa}{\sigma_a}^j + \frac{1}{4\pi}\sum_{j=1}^{npb} G_{ij}^{ab}{\sigma_b}^j \ , \qquad i = 1, 2, ..., npa \tag{4.16}$$

$$\phi_i^b = \frac{1}{4\pi}\sum_{j=1}^{npa} G_{ij}^{ba}{\sigma_a}^j + \frac{1}{4\pi}\sum_{j=1}^{npb} G_{ij}^{bb}{\sigma_b}^j \ , \qquad i = 1, 2, ..., npb \tag{4.17}$$

If we further define:

$$G^{aa} = \begin{pmatrix} G_{11}^{aa} & G_{12}^{aa} & ..... & G_{1,npa}^{aa} \\ G_{21}^{aa} & G_{22}^{aa} & ..... & G_{2,npa}^{aa} \\ & & ..... & \\ G_{npa,1}^{aa} & G_{npa,2}^{aa} & ..... & G_{npa,npa}^{aa} \end{pmatrix} \qquad G^{ab} = \begin{pmatrix} G_{11}^{ab} & G_{12}^{ab} & ..... & G_{1,npb}^{ab} \\ G_{21}^{ab} & G_{22}^{ab} & ..... & G_{2,npb}^{ab} \\ & & ..... & \\ G_{npa,1}^{ab} & G_{npa,2}^{ab} & ..... & G_{npa,npb}^{ab} \end{pmatrix} \tag{4.18}$$

$$G^{ba} = \begin{pmatrix} G_{11}^{ba} & G_{12}^{ba} & ..... & G_{1,npa}^{ba} \\ G_{21}^{ba} & G_{22}^{ba} & ..... & G_{2,npa}^{ba} \\ & & ..... & \\ G_{npb,1}^{ba} & G_{npb,2}^{ba} & ..... & G_{npb,npa}^{ba} \end{pmatrix} \qquad G^{bb} = \begin{pmatrix} G_{11}^{bb} & G_{12}^{bb} & ..... & G_{1,npb}^{bb} \\ G_{21}^{bb} & G_{22}^{bb} & ..... & G_{2,npb}^{bb} \\ & & ..... & \\ G_{npb,1}^{bb} & G_{npb,2}^{bb} & ..... & G_{npb,npb}^{bb} \end{pmatrix} \tag{4.19}$$

$$\phi^a = \begin{pmatrix} \phi_1^a \\ \phi_2^a \\ ... \\ \phi_{npa}^a \end{pmatrix} \qquad \phi^b = \begin{pmatrix} \phi_1^b \\ \phi_2^b \\ ... \\ \phi_{npb}^b \end{pmatrix} \tag{4.20}$$

Equations(4.16) and (4.17) can then be expressed in a matrix form as:

$$\begin{pmatrix} \phi^a \\ \phi^b \end{pmatrix} = \frac{1}{4\pi}\begin{pmatrix} G^{aa} & G^{ab} \\ G^{ba} & G^{bb} \end{pmatrix}\begin{pmatrix} \sigma_a \\ \sigma_b \end{pmatrix} \tag{4.21}$$

Equation(4.21) is the discretized linear algebra equations for velocity potentials. G^{aa}, G^{ab}, G^{ba} and G^{bb} are influence submatrices and can be obtained from the surface integration of Green's function on each panel.

4.2 Green's Function – Influence Matrices

The generalized Green's function $G(p,q)$ can be replaced by the specified Green's function to represent different problems. For the steady flow problem, the generalized Green's function becomes:

$$G(p,q) = \hat{G}(p;q) = \sum_{i=1}^{\infty} \frac{1}{r_{1i}} + \frac{1}{r_{2i}} \tag{4.22}$$

For the wave radiation and diffraction problems, the generalized Green's function becomes:

$$G(p,q) = \bar{G}(p,q) \tag{4.23}$$

where

$$\begin{aligned} \bar{G}(p;q) &= \frac{1}{r} + \frac{1}{r_1} \\ &+ 2P\mathrm{V}\cdot\int_0^{\infty} \frac{(\mu+K)exp(-\mu h)\cosh(\mu(\zeta+h))\cosh(\mu(z+h))}{\mu\cdot\sinh(\mu h) - K\cdot\cosh(\mu h)} J_0(\mu R)d\mu \\ &+ i\frac{2\pi(k+K)exp(-kh)\sinh(kh)\cosh(k(\zeta+h))\cosh(k(z+h))}{K\cdot h + \sinh^2(kh)} J_0(kR) \end{aligned} \tag{4.24}$$

The surface integrations of Green's function $\hat{G}(p,q)$ and its normal derivative $\hat{G}_n(p,q)$ are treated with the Hess and Smith method(1964). Once the hull is discretized, the potential influence matrix $[\hat{G}]$ and the normal velocity influence matrix $[\hat{G}_n]$ can be computed. The surface integrations of the wave term of Green's function $\bar{G}(p,q)$ and $\bar{G}_n(p,q)$ are computed by Gaussian quadratures for each p and q. They form the potential influence matrix and the normal velocity influence matrix of the wave term contribution, $[\bar{G}]$ and $[\bar{G}_n]$. For wave radiation and diffraction problems, the potential influence matrix is $[G]$=$[\bar{G}]$, and the normal velocity influence matrix is $[G_n]$=$[\bar{G}_n]$. Here we should note that each influence matrix contains four submatrices :

$$\begin{pmatrix} G^{aa} & G^{ab} \\ G^{ba} & G^{bb} \end{pmatrix} \qquad \begin{pmatrix} {G_n}^{aa} & {G_n}^{ab} \\ {G_n}^{ba} & {G_n}^{bb} \end{pmatrix} \tag{4.25}$$

The submatrices represent interaction between the two ships. This will be defined in detail in the following sections.

4.3 Source Densities

Applying the body surface conditions of ϕ to Equation(4.7), we have the following integral equations:

$$\begin{cases} 2\pi\sigma_a(p) + \int\int_{S_a} \sigma_a(q)\frac{\partial G(p,q)}{\partial n}|_{S_a} dS(q) + \int\int_{S_b} \sigma_b(q)\frac{\partial G(p,q)}{\partial n}|_{S_a} dS(q) &= \frac{\partial \phi(p)}{\partial n}|_{S_a} = B^a(p) \\ 2\pi\sigma_b(p) + \int\int_{S_a} \sigma_a(q)\frac{\partial G(p,q)}{\partial n}|_{S_b} dS(q) + \int\int_{S_b} \sigma_b(q)\frac{\partial G(p,q)}{\partial n}|_{S_b} dS(q) &= \frac{\partial \phi(p)}{\partial n}|_{S_b} = B^b(p) \end{cases} \tag{4.26}$$

The source densities $\sigma_a(q)$, $\sigma_b(q)$ can be obtained by solving the linear equation system

formed by producing a discretized on the from of Equation(4.26):

$$2\pi\sigma_a(p_i) + \sum_{j=1}^{npa}[\int\int_{S_a^j} \frac{\partial G(p_i,q_j)}{\partial n}|s_a^j dS(q_j)]\sigma_a{}^j(q_j) + \sum_{j=1}^{npb}[\int\int_{S_b^j} \frac{\partial G(p_i,q_j)}{\partial n}|s_a^j dS(q_j)]\sigma_b{}^j(q_j) = B^a(p_i) \quad (4.27)$$

$$2\pi\sigma_b(p_i) + \sum_{j=1}^{npa}[\int\int_{S_a^j} \frac{\partial G(p_i,q_j)}{\partial n}|s_b^j dS(q_j)]\sigma_a{}^j(q_j) + \sum_{j=1}^{npb}[\int\int_{S_b^j} \frac{\partial G(p_i,q_j)}{\partial n}|s_b^j dS(q_j)]\sigma_b{}^j(q_j) = B^b(p_i) \quad (4.28)$$

By defining:

$$G_{n_{ij}}^{aa} = \int\int_{S_a^j} \frac{\partial G(p_i,q_j)}{\partial n}|s_a^j dS(q_j) \quad (4.29)$$

$$G_{n_{ij}}^{ab} = \int\int_{S_b^j} \frac{\partial G(p_i,q_j)}{\partial n}|s_a^j dS(q_j) \quad (4.30)$$

$$G_{n_{ij}}^{ba} = \int\int_{S_a^j} \frac{\partial G(p_i,q_j)}{\partial n}|s_b^j dS(q_j) \quad (4.31)$$

$$G_{n_{ij}}^{bb} = \int\int_{S_b^j} \frac{\partial G(p_i,q_j)}{\partial n}|s_b^j dS(q_j) \quad (4.32)$$

$$B_i^a = B^a(p_i) \qquad B_i^b = B^b(p_i) \quad (4.33)$$

$$\sigma_a^j = \sigma_a^j(q_j) \qquad \sigma_b^j = \sigma_b^j(q_j) \quad (4.34)$$

Equations(4.27) and (4.28) can be reduced to:

$$\sum_{j=1}^{npa} G_{n_{ij}}^{aa}\sigma_a{}^j + \sum_{j=1}^{npb} G_{n_{ij}}^{ab}\sigma_b{}^j = B_i^a, \qquad i = 1,2,...,npa \quad (4.35)$$

$$\sum_{j=1}^{npa} G_{n_{ij}}^{ba}\sigma_a{}^j + \sum_{j=1}^{npb} G_{n_{ij}}^{bb}\sigma_b{}^j = B_i^b, \qquad i = 1,2,...,npb \quad (4.36)$$

If we further define:

$$G_n{}^{aa} = \begin{pmatrix} G_{n11}^{aa} & G_{n12}^{aa} & \ldots\ldots & G_{n1,npa}^{aa} \\ G_{n21}^{aa} & G_{n22}^{ac} & \ldots\ldots & G_{n2,npa}^{aa} \\ & & \ldots\ldots & \\ G_{nnpa,1}^{aa} & G_{nnpa,2}^{aa} & \ldots\ldots & G_{nnpa,npa}^{aa} \end{pmatrix} \quad G_n{}^{ab} = \begin{pmatrix} G_{n11}^{ab} & G_{n12}^{ab} & \ldots\ldots & G_{n1,npb}^{ab} \\ G_{n21}^{ab} & G_{n22}^{ab} & \ldots\ldots & G_{n2,npb}^{ab} \\ & & \ldots\ldots & \\ G_{nnpa,1}^{ab} & G_{nnpa,2}^{ab} & \ldots\ldots & G_{nnpa,npb}^{ab} \end{pmatrix} \tag{4.37}$$

$$G_n{}^{ba} = \begin{pmatrix} G_{n11}^{ba} & G_{n12}^{ba} & \ldots\ldots & G_{n1,npa}^{ba} \\ G_{n21}^{ba} & G_{n22}^{ba} & \ldots\ldots & G_{n2,npa}^{ba} \\ & & \ldots\ldots & \\ G_{nnpb,1}^{ba} & G_{nnpb,2}^{ba} & \ldots\ldots & G_{nnpb,npa}^{ba} \end{pmatrix} \quad G_n{}^{bb} = \begin{pmatrix} G_{n11}^{bb} & G_{n12}^{bb} & \ldots\ldots & G_{n1,npb}^{bb} \\ G_{n21}^{bb} & G_{n22}^{bb} & \ldots\ldots & G_{n2,npb}^{bb} \\ & & \ldots\ldots & \\ G_{nnpb,1}^{bb} & G_{nnpb,2}^{bb} & \ldots\ldots & G_{nnpb,npb}^{bb} \end{pmatrix} \tag{4.38}$$

$$\sigma_a = \begin{pmatrix} \sigma_a^1 \\ \sigma_a^2 \\ \ldots \\ \sigma_a^{npa} \end{pmatrix} \qquad \sigma_b = \begin{pmatrix} \sigma_b^1 \\ \sigma_b^2 \\ \ldots \\ \sigma_b^{npb} \end{pmatrix} \tag{4.39}$$

$$B^a = \begin{pmatrix} B_1^a \\ B_2^a \\ \ldots \\ B_{npa}^a \end{pmatrix} \qquad B^b = \begin{pmatrix} B_1^b \\ B_2^b \\ \ldots \\ B_{npb}^b \end{pmatrix} \tag{4.40}$$

we obtain the linear equation system for the source densities in matrix form as:

$$\begin{pmatrix} G_n{}^{aa} & G_n{}^{ab} \\ G_n{}^{ba} & G_n{}^{bb} \end{pmatrix} \begin{pmatrix} \sigma_a \\ \sigma_b \end{pmatrix} = \begin{pmatrix} B^a \\ B^b \end{pmatrix} \tag{4.41}$$

This is the linear algebra equation system for numerical determination of the source densities. This represents the basis of the numerical implementation. $G_n{}^{aa}$, $G_n{}^{ab}$, $G_n{}^{ba}$, $G_n{}^{bb}$ are influence submatrices and their elements can be obtained from Green's function computation for each ship hull panel. B^a and B^b are the body surface conditions on ship_a and ship_b which depend on the problem considered. By substituting the known body surface conditions into Equation(4.41), we can obtain the source densities for the steady flow, as well as radiated and diffracted wave problems. In the numerical implementation, we solve the wave radiation and diffraction problems together by assuming diffraction source densities as the seventh component of the radiation source strength σ_k. Therefore, we can solve just one set of linear equations for each σ_k, $k = 1, 2, ..., 7$.

Once the source strength σ_a and σ_b are known, Equation(4.21) can be solved for velocity potentials, and then the hydrodynamic coefficients and forces can be determined. The latter are required for solving the equations of motion.

4.4 Ship Motions

As discussed in Section 2.7, the coupled motion equations for two-ship interaction are given as follows:

$$\sum_{k=1}^{6}[-\omega_e^2(m_{jk}^a + \mu_{jk}^{aa}) - i\omega_e\lambda_{jk}^{aa} + C_{jk}^a]\bar{x}_k^a + \sum_{k=1}^{6}[-\omega_e^2\mu_{jk}^{ab} - i\omega_e\lambda_{jk}^{ab}]\bar{x}_k^b = f_j^{Wa}, \quad j = 1, 2, ..., 6 \tag{4.42}$$

$$\sum_{k=1}^{6}[-\omega_e^2\mu_{jk}^{ba} - i\omega_e\lambda_{jk}^{ba}]\bar{x}_k^a + \sum_{k=1}^{6}[-\omega_e^2(m_{jk}^b + \mu_{jk}^{bb}) - i\omega_e\lambda_{jk}^{bb} + C_{jk}^b]\bar{x}_k^b = f_j^{Wb}, \quad j = 1, 2, ..., 6 \tag{4.43}$$

If we define:

$$M_{jk}^{aa} = -\omega_e^2(m_{jk}^a + \mu_{jk}^{aa}) - i\omega_e\lambda_{jk}^{aa} + C_{jk}^a \tag{4.44}$$

$$M_{jk}^{ab} = -\omega_e^2\mu_{jk}^{ab} - i\omega_e\lambda_{jk}^{ab} \tag{4.45}$$

$$M_{jk}^{ba} = -\omega_e^2\mu_{jk}^{ba} - i\omega_e\lambda_{jk}^{ba} \tag{4.46}$$

$$M_{jk}^{bb} = -\omega_e^2(m_{jk}^b + \mu_{jk}^{bb}) - i\omega_e\lambda_{jk}^{bb} + C_{jk}^b \tag{4.47}$$

we have:

$$\sum_{k=1}^{6} M_{jk}^{aa}\bar{x}_k^a + \sum_{k=1}^{6} M_{jk}^{ab}\bar{x}_k^b = f_j^{Wa}, \quad j = 1, ..., 6 \tag{4.48}$$

$$\sum_{k=1}^{6} M_{jk}^{ba}\bar{x}_k^a + \sum_{k=1}^{6} M_{jk}^{bb}\bar{x}_k^b = f_j^{Wb}, \quad j = 1, ..., 6 \tag{4.49}$$

Further more, if we define:

$$M^{aa} = \begin{pmatrix} M_{11}^{aa} & M_{12}^{aa} & ..... & M_{16}^{aa} \\ M_{21}^{aa} & M_{22}^{aa} & ..... & M_{26}^{aa} \\ & & ..... & \\ M_{61}^{aa} & M_{62}^{aa} & ..... & M_{66}^{aa} \end{pmatrix} \qquad M^{ab} = \begin{pmatrix} M_{11}^{ab} & M_{12}^{ab} & ..... & M_{16}^{ab} \\ M_{21}^{ab} & M_{22}^{ab} & ..... & M_{26}^{ab} \\ & & ..... & \\ M_{61}^{ab} & M_{62}^{ab} & ..... & M_{66}^{ab} \end{pmatrix} \tag{4.50}$$

$$M^{ba} = \begin{pmatrix} M_{11}^{ba} & M_{12}^{ba} & ..... & M_{16}^{ba} \\ M_{21}^{ba} & M_{22}^{ba} & ..... & M_{26}^{ba} \\ & & ..... & \\ M_{61}^{ba} & M_{62}^{ba} & ..... & M_{66}^{ba} \end{pmatrix} \qquad M^{bb} = \begin{pmatrix} M_{11}^{bb} & M_{12}^{bb} & ..... & M_{16}^{bb} \\ M_{21}^{bb} & M_{22}^{bb} & ..... & M_{26}^{bb} \\ & & ..... & \\ M_{61}^{bb} & M_{62}^{bb} & ..... & M_{66}^{bb} \end{pmatrix} \tag{4.51}$$

$$\bar{x}^a = \begin{pmatrix} \bar{x}_1^a \\ \bar{x}_2^a \\ \cdots \\ \bar{x}_6^a \end{pmatrix} \qquad \bar{x}^b = \begin{pmatrix} \bar{x}_1^b \\ \bar{x}_2^b \\ \cdots \\ \bar{x}_6^b \end{pmatrix} \tag{4.52}$$

$$f^{Wa} = \begin{pmatrix} f_1^{Wa} \\ f_2^{Wa} \\ \cdots \\ f_6^{Wa} \end{pmatrix} \qquad f^{Wb} = \begin{pmatrix} f_1^{Wb} \\ f_2^{Wb} \\ \cdots \\ f_6^{Wb} \end{pmatrix} \tag{4.53}$$

the discretized equations of motion in the matrix form can be written as follows:

$$\begin{pmatrix} M^{aa} & M^{ab} \\ M^{ba} & M^{bb} \end{pmatrix} \begin{pmatrix} \bar{x}^a \\ \bar{x}^b \end{pmatrix} = \begin{pmatrix} f^{Wa} \\ f^{Wb} \end{pmatrix} \tag{4.54}$$

This is a complex linear algebraic equation system with 12 unknown complex variables for the motion displacements. Finally, the motions resulting from ship interaction can be numerically determined from this system.

4.5 m-terms

The integral equations in Equation(2.34) can be discretized as follows:

$$\frac{\partial \phi_s(p_i)}{\partial x}|_{p \epsilon S_a} = \frac{1}{4\pi} \sum_j \phi_{s\xi}(q_j) \int\int_{S_a^j} \frac{\partial \hat{G}(p,q)}{\partial n(q_j)}|_{p \epsilon S_a} dS \tag{4.55}$$

$$
\begin{aligned}
&- \frac{1}{4\pi}\sum_j m_1^a(q_j)\int\int_{S_a^j}\hat{G}(p,q)|_{p\epsilon S_a}dS \\
&+ \frac{1}{4\pi}\sum_j \phi_{s\xi}(q_j)\int\int_{S_b^j}\frac{\partial\hat{G}(p,q)}{\partial n(q_j)}|_{p\epsilon S_a}dS_j^b \\
&- \frac{1}{4\pi}\sum_j m_1^b(q_j)\int\int_{S_b^j}\hat{G}(p,q)|_{p\epsilon S_a}dS
\end{aligned}
$$

$$
\begin{aligned}
\frac{\partial\phi_s(p_i)}{\partial x}|_{p\epsilon S_b} &= \frac{1}{4\pi}\sum_j \phi_{s\xi}(q_j)\int\int_{S_a^j}\frac{\partial\hat{G}(p,q)}{\partial n(q_j)}|_{p\epsilon S_b}dS \\
&- \frac{1}{4\pi}\sum_j m_1^a(q_j)\int\int_{S_a^j}\hat{G}(p,q)|_{p\epsilon S_b}dS \\
&+ \frac{1}{4\pi}\sum_j \phi_{s\xi}(q_j)\int\int_{S_b^j}\frac{\partial\hat{G}(p,q)}{\partial n(q_j)}|_{p\epsilon S_b}dS \\
&- \frac{1}{4\pi}\sum_j m_1^b(q_j)\int\int_{S_b^j}\hat{G}(p,q)|_{p\epsilon S_a}dS
\end{aligned}
\tag{4.56}
$$

Equations(4.56) and (4.57) can be rewritten as :

$$
\sum_j(\int\int_{S_a^j}\hat{G}(p,q)|_{p\epsilon S_a}dS)m_1^a(q_j)+\sum_j(\int\int_{S_b^j}\hat{G}(p,q)|_{p\epsilon S_a}dS)m_1^b(q_j) =
$$

$$
\sum_j(\int\int_{S_a^j}\frac{\partial\hat{G}(p,q)}{\partial n(q_j)}|_{p\epsilon S_a}dS)\phi_{s\xi}(q_j)+\sum_j(\int\int_{S_b^j}\frac{\partial\hat{G}(p,q)}{\partial n(q_j)}|_{p\epsilon S_a}dS_j^b)\phi_{s\xi}(q_j)-4\pi\frac{\partial\phi_s(p_i)}{\partial x}|_{p\epsilon S_a}
\tag{4.57}
$$

$$
\sum_j(\int\int_{S_a^j}\hat{G}(p,q)|_{p\epsilon S_b}dS)m_1^a(q_j)+\sum_j(\int\int_{S_b^j}\hat{G}(p,q)|_{p\epsilon S_b}dS)m_1^b(q_j) =
$$

$$
\sum_j(\int\int_{S_a^j}\frac{\partial\hat{G}(p,q)}{\partial n(q_j)}|_{p\epsilon S_b}dS)\phi_{s\xi}(q_j)+\sum_j(\int\int_{S_b^j}\frac{\partial\hat{G}(p,q)}{\partial n(q_j)}|_{p\epsilon S_b}dS_j^b)\phi_{s\xi}(q_j)-4\pi\frac{\partial\phi_s(p_i)}{\partial x}|_{p\epsilon S_b}
\tag{4.58}
$$

If we define:

$$
\hat{G}_{ij}^{aa} = \int\int_{S_a^j}\hat{G}(p,q)|_{p\epsilon S_a}dS, \qquad \hat{G}_{ij}^{ba} = \int\int_{S_a^j}\hat{G}(p,q)|_{p\epsilon S_b}dS
\tag{4.59}
$$

$$\hat{G}_{ij}^{ab} = \int\int_{S_b^j} \hat{G}(p,q)|_{p\epsilon S_a} dS, \qquad \hat{G}_{ij}^{bb} = \int\int_{S_b^j} \hat{G}(p,q)|_{p\epsilon S_b} dS \tag{4.60}$$

$$\hat{G}_{n_{ij}}^{\ aa} = \int\int_{S_a^j} \frac{\partial \hat{G}(p,q)}{\partial n(q_j)}|_{p\epsilon S_a} dS, \qquad \hat{G}_{n_{ij}}^{\ ba} = \int\int_{S_a^j} \frac{\partial \hat{G}(p,q)}{\partial n(q_j)}|_{p\epsilon S_b} dS \tag{4.61}$$

$$\hat{G}_{n_{ij}}^{\ ab} = \int\int_{S_b^j} \frac{\partial \hat{G}(p,q)}{\partial n(q_j)}|_{p\epsilon S_a} dS. \qquad \hat{G}_{n_{ij}}^{\ bb} = \int\int_{S_b^j} \frac{\partial \hat{G}(p,q)}{\partial n(q_j)}|_{p\epsilon S_b} dS \tag{4.62}$$

$$\phi_{s_x}^{\ a}(p_i) = \frac{\partial \phi_s(p_i)}{\partial x}|_{p\epsilon S_a}, \qquad \phi_{s_x}^{\ b}(p_i) = \frac{\partial \phi_s(p_i)}{\partial x}|_{p\epsilon S_b} \tag{4.63}$$

we obtain:

$$\sum_{j_a=1}^{npa} \hat{G}_{ij_a}^{aa} m_{1j_a}^{a} + \sum_{j_b=1}^{npb} \hat{G}_{ij_b}^{ab} m_{1j_b}^{b} = \sum_{j_a=1}^{npa} \hat{G}_{n_{ij_a}}^{\ aa} \phi_{s\xi_{j_a}}^{\ a} + \sum_{j_b=1}^{npb} \hat{G}_{n_{ij_b}}^{\ ab} \phi_{s\xi_{j_b}}^{\ b} - 4\pi\phi_{sxi}^{a}, i = 1, ..., npa \tag{4.64}$$

$$\sum_{j_a=1}^{npa} \hat{G}_{kj_a}^{ba} m_{1j_a}^{a} + \sum_{j_b=1}^{npb} \hat{G}_{kj_b}^{bb} m_{1j_b}^{b} = \sum_{j_a=1}^{npa} \hat{G}_{nkj_a}^{\ ba} \phi_{s\xi_{j_a}}^{\ a} + \sum_{j_b=1}^{npb} \hat{G}_{nkj_b}^{\ bb} \phi_{s\xi_{j_b}}^{\ b} - 4\pi\phi_{sxk}^{b}, \ k = 1, ..., npb \tag{4.65}$$

This is a linear equation system with unknowns $m_{1j_a}^{a}$ and $m_{1j_b}^{a}$. If we define:

$$\hat{G}^{aa} = \begin{pmatrix} \hat{G}_{11}^{aa} & \hat{G}_{12}^{aa} & ..... & \hat{G}_{1,npa}^{aa} \\ \hat{G}_{21}^{aa} & \hat{G}_{22}^{aa} & ..... & \hat{G}_{2,npa}^{aa} \\ ... & ... & ..... & ... \\ \hat{G}_{npa,1}^{aa} & \hat{G}_{npa,2}^{aa} & ..... & \hat{G}_{npa,npa}^{aa} \end{pmatrix} \quad \hat{G}^{ab} = \begin{pmatrix} \hat{G}_{11}^{ab} & \hat{G}_{12}^{ab} & ..... & \hat{G}_{1,npb}^{ab} \\ \hat{G}_{21}^{ab} & \hat{G}_{22}^{ab} & ..... & \hat{G}_{2,npb}^{ab} \\ ... & ... & ..... & ... \\ \hat{G}_{npa,1}^{ab} & \hat{G}_{npa,2}^{ab} & ..... & \hat{G}_{npa,npb}^{ab} \end{pmatrix} \tag{4.66}$$

$$\hat{G}^{ba} = \begin{pmatrix} \hat{G}^{ba}_{11} & \hat{G}^{ba}_{12} & \ldots\ldots & \hat{G}^{ba}_{1,npa} \\ \hat{G}^{ba}_{21} & \hat{G}^{ba}_{22} & \ldots\ldots & \hat{G}^{ba}_{2,npa} \\ \ldots & \ldots & \ldots\ldots & \ldots \\ \hat{G}^{ba}_{npb,1} & \hat{G}^{ba}_{npb,2} & \ldots\ldots & \hat{G}^{ba}_{npb,npa} \end{pmatrix} \quad \hat{G}^{bb} = \begin{pmatrix} \hat{G}^{bb}_{11} & \hat{G}^{bb}_{12} & \ldots\ldots & \hat{G}^{bb}_{1,npb} \\ \hat{G}^{bb}_{21} & \hat{G}^{bb}_{22} & \ldots\ldots & \hat{G}^{bb}_{2,npb} \\ \ldots & \ldots & \ldots\ldots & \ldots \\ \hat{G}^{bb}_{npb,1} & \hat{G}^{bb}_{npb,2} & \ldots\ldots & \hat{G}^{bb}_{npb,npb} \end{pmatrix} \tag{4.67}$$

$$\hat{G}_n{}^{aa} = \begin{pmatrix} \hat{G}^{aa}_{n11} & \hat{G}^{aa}_{n12} & \ldots\ldots & \hat{G}^{aa}_{n1,npa} \\ \hat{G}^{aa}_{n21} & \hat{G}^{aa}_{n22} & \ldots\ldots & \hat{G}^{aa}_{n2,npa} \\ \ldots & \ldots & \ldots\ldots & \ldots \\ \hat{G}^{aa}_{nnpa,1} & \hat{G}^{aa}_{nnpa,2} & \ldots\ldots & \hat{G}^{aa}_{nnpa,npa} \end{pmatrix} \quad \hat{G}_n{}^{ab} = \begin{pmatrix} \hat{G}^{ab}_{n11} & \hat{G}^{ab}_{n12} & \ldots\ldots & \hat{G}^{ab}_{n1,npb} \\ \hat{G}^{ab}_{n21} & \hat{G}^{ab}_{n22} & \ldots\ldots & \hat{G}^{ab}_{n2,npb} \\ \ldots & \ldots & \ldots\ldots & \ldots \\ \hat{G}^{ab}_{nnpa,1} & \hat{G}^{ab}_{nnpa,2} & \ldots\ldots & \hat{G}^{ab}_{nnpa,npb} \end{pmatrix} \tag{4.68}$$

$$\hat{G}_n{}^{ba} = \begin{pmatrix} \hat{G}^{ba}_{n11} & \hat{G}^{ba}_{n12} & \ldots\ldots & \hat{G}^{ba}_{n1,npa} \\ \hat{G}^{ba}_{n21} & \hat{G}^{ba}_{n22} & \ldots\ldots & \hat{G}^{ba}_{n2,npa} \\ \ldots & \ldots & \ldots\ldots & \ldots \\ \hat{G}^{ba}_{nnpb,1} & \hat{G}^{ba}_{nnpb,2} & \ldots\ldots & \hat{G}^{ba}_{nnpb,npa} \end{pmatrix} \quad \hat{G}_n{}^{bb} = \begin{pmatrix} \hat{G}^{bb}_{n11} & \hat{G}^{bb}_{n12} & \ldots\ldots & \hat{G}^{bb}_{n1,npb} \\ \hat{G}^{bb}_{n21} & \hat{G}^{bb}_{n22} & \ldots\ldots & \hat{G}^{bb}_{n2,npb} \\ \ldots & \ldots & \ldots\ldots & \ldots \\ \hat{G}^{bb}_{nnpb,1} & \hat{G}^{bb}_{nnpb,2} & \ldots\ldots & \hat{G}^{bb}_{nnpb,npb} \end{pmatrix} \tag{4.69}$$

$$M^a_1 = \begin{pmatrix} m^a_{11} \\ m^a_{12} \\ \ldots \\ m^a_{1npa} \end{pmatrix} \quad M^b_1 = \begin{pmatrix} m^b_{11} \\ m^b_{12} \\ \ldots \\ m^b_{1npb} \end{pmatrix} \tag{4.70}$$

$$\Phi^a_{s\xi} = \begin{pmatrix} \phi^a_{s\xi_1} \\ \phi^a_{s\xi_2} \\ \cdots \\ \phi^a_{s\xi_{npa}} \end{pmatrix} \quad \Phi^b_{s\xi} = \begin{pmatrix} \phi^b_{s\xi_1} \\ \phi^b_{s\xi_2} \\ \cdots \\ \phi^b_{s\xi_{npb}} \end{pmatrix} \quad \Phi^a_{sx} = \begin{pmatrix} \phi^a_{sx1} \\ \phi^a_{sx2} \\ \cdots \\ \phi^a_{sxnpa} \end{pmatrix} \quad \Phi^b_{sx} = \begin{pmatrix} \phi^b_{sx1} \\ \phi^b_{sx2} \\ \cdots \\ \phi^b_{sxnpb} \end{pmatrix} \tag{4.71}$$

Equation(4.64) and (4.65) can be rewritten in the matrix form as:

$$\begin{pmatrix} \hat{G}^{aa} & \hat{G}^{ab} \\ \hat{G}^{ba} & \hat{G}^{bb} \end{pmatrix} \begin{pmatrix} M^a_1 \\ M^b_1 \end{pmatrix} = \begin{pmatrix} \hat{G_n}^{aa} & \hat{G_n}^{ab} \\ \hat{G_n}^{ba} & \hat{G_n}^{bb} \end{pmatrix} \begin{pmatrix} \Phi_{s\xi}{}^a \\ \Phi_{s\xi}{}^b \end{pmatrix} - \begin{pmatrix} \Phi^a_{sx} \\ \Phi^b_{sx} \end{pmatrix} \tag{4.72}$$

Similarly, we can derive the linear algebraic equations for m_2 and m_3

$$\begin{pmatrix} \hat{G}^{aa} & \hat{G}^{ab} \\ \hat{G}^{ba} & \hat{G}^{bb} \end{pmatrix} \begin{pmatrix} M^a_2 \\ M^b_2 \end{pmatrix} = \begin{pmatrix} \hat{G_n}^{aa} & \hat{G_n}^{ab} \\ \hat{G_n}^{ba} & \hat{G_n}^{bb} \end{pmatrix} \begin{pmatrix} \Phi_{s\eta}{}^a \\ \Phi_{s\eta}{}^b \end{pmatrix} - \begin{pmatrix} \Phi^a_{sy} \\ \Phi^b_{sy} \end{pmatrix} \tag{4.73}$$

$$\begin{pmatrix} \hat{G}^{aa} & \hat{G}^{ab} \\ \hat{G}^{ba} & \hat{G}^{bb} \end{pmatrix} \begin{pmatrix} M^a_3 \\ M^b_3 \end{pmatrix} = \begin{pmatrix} \hat{G_n}^{aa} & \hat{G_n}^{ab} \\ \hat{G_n}^{ba} & \hat{G_n}^{bb} \end{pmatrix} \begin{pmatrix} \Phi_{s\zeta}{}^a \\ \Phi_{s\zeta}{}^b \end{pmatrix} - \begin{pmatrix} \Phi^a_{sz} \\ \Phi^b_{sz} \end{pmatrix} \tag{4.74}$$

where:

$$M^a_2 = \begin{pmatrix} m^a_{21} \\ m^a_{22} \\ \cdots \\ m^a_{2npa} \end{pmatrix} \quad M^b_2 = \begin{pmatrix} m^b_{21} \\ m^b_{22} \\ \cdots \\ m^b_{2npb} \end{pmatrix} \tag{4.75}$$

$$\Phi^a_{s\eta} = \begin{pmatrix} \phi^a_{s\eta_1} \\ \phi^a_{s\eta_2} \\ \cdots \\ \phi^a_{s\eta_{npa}} \end{pmatrix} \quad \Phi^b_{s\eta} = \begin{pmatrix} \phi^b_{s\eta_1} \\ \phi^b_{s\eta_2} \\ \cdots \\ \phi^b_{s\eta_{npb}} \end{pmatrix} \quad \Phi^a_{sy} = \begin{pmatrix} \phi^a_{sy_1} \\ \phi^a_{sy_2} \\ \cdots \\ \phi^a_{sy_{npa}} \end{pmatrix} \quad \Phi^b_{sy} = \begin{pmatrix} \phi^b_{sy_1} \\ \phi^b_{sy_2} \\ \cdots \\ \phi^b_{sy_{npb}} \end{pmatrix} \tag{4.76}$$

$$M^a_3 = \begin{pmatrix} m^a_{31} \\ m^a_{32} \\ \cdots \\ m^a_{3npa} \end{pmatrix} \quad M^b_3 = \begin{pmatrix} m^b_{31} \\ m^b_{32} \\ \cdots \\ m^b_{3npb} \end{pmatrix} \tag{4.77}$$

$$\Phi^a_{s\zeta} = \begin{pmatrix} \phi^a_{s\zeta_1} \\ \phi^a_{s\zeta_2} \\ \cdots \\ \phi^a_{s\zeta_{npa}} \end{pmatrix} \quad \Phi^b_{s\zeta} = \begin{pmatrix} \phi^b_{s\zeta_1} \\ \phi^b_{s\zeta_2} \\ \cdots \\ \phi^b_{s\zeta_{npb}} \end{pmatrix} \quad \Phi^a_{sz} = \begin{pmatrix} \phi^a_{sz1} \\ \phi^a_{sz2} \\ \cdots \\ \phi^a_{sznpa} \end{pmatrix} \quad \Phi^b_{sz} = \begin{pmatrix} \phi^b_{sz1} \\ \phi^b_{sz2} \\ \cdots \\ \phi^b_{sznpb} \end{pmatrix} \tag{4.78}$$

Equations(4.72), (4.73) and (4.74) are the linear algebraic equation systems used for numerically solving the m_j-terms, $j = 1, 2, 3$, of two-ship interaction. m_j-terms, $j = 4, 5, 6$, can be obtained from Equations(2.39) to (2.44).

Chapter 5

Results and Discussions

In order to demonstrate the proposed Green's function algorithm, interaction theory and shallow water theory, numerical computations were carried out by performing two test cases, and then numerical results of two ship interactions in 11 cases are presented and discussed in this chapter.

5.1 Code Validation:

Due to the scarcity of experimental data and published numerical results in the open literature for seakeeping of two ship interactions in close proximity in the shallow water region, two identical simple geometric structures (i.e. circular cylinders) for which data are available were chosen to verify the computer code. In Section 5.1.1, two circular cylinder interactions in finite depth of water were considered and results obtained with our code were compared with published results by Matsui & Tamaki(1981). In Section 5.1.2, two circular cylinder interactions in a shallow water region

were considered and results were compared with published results by Williams(1988, 1989).

5.1.1 Two Identical Circular Cylinder Interactions in Finite Depth of Water

In this test case, the radius of each cylinder $r = a$; the draft of each cylinder $T = 0.5a$; each cylinder has been discretized by 98 panels which are shown in Figure 5.1, for water depth $h = 10a$; the ratio of water depth to cylinder draft $\delta = h/T = 10$; the longitudinal separation distance $dx = 0.0$; the lateral separation distance $dy = 5a$; lateral gap $Gy = 3a$; wave heading $\beta = 90^o$. The details are shown in Figure 5.2 and Figure 5.3. The mass of body is $0.5\rho\pi a^3$, mass moment of inertia is $0.75\rho\pi a^5$.

In Figure 5.4, results are presented for non-dimensional vertical and lateral hydrodynamic interaction wave exciting forces and non-dimensional lateral dynamic responses with varying frequency parameter ka for cylinder_a and cylinder_b, where k is the wave number. The wave exciting forces are non-dimensionalized by the factor $\rho g\zeta_a a^3$; ρ is the water density; g is the acceleration of gravity; and ζ_a is the wave amplitude. For cylinder_a, the vertical wave exciting force and the lateral motion provide very good agreement with Matsui & Tamaki's results; but the lateral wave exciting forces around $ka = 0.8$ and $ka = 1.2$ are slightly larger than Matsui & Tamaki's results. For cylinder_b, the lateral wave exciting forces and the vertical motion are in reasonable agreement with those obtained by Matsui & Tamaki. However, the present result of lateral motion is smaller at $ka = 1.0$. Figure 5.4 demonstrates that the present algorithm and theories can provide accurate prediction of the interaction wave exciting

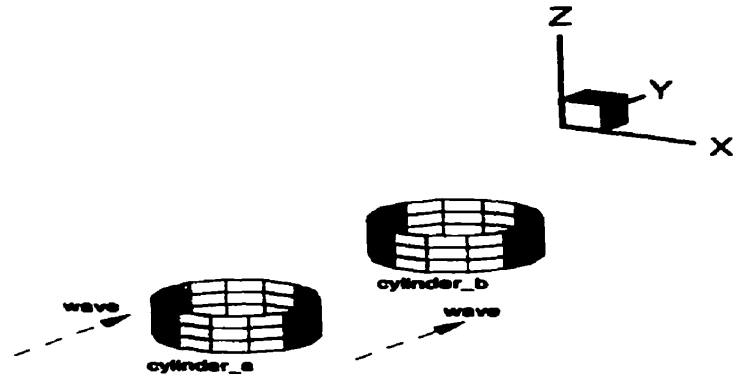

Figure 5.1: Panelized cylinder_a and cylinder_b for test case 1

forces and motions.

In Figure 5.5, the comparisons of wave radiation forces are presented in terms of dimensionless added mass and damping coefficients which are non-dimensionalized by dividing $0.5\rho\pi a^3$ and $0.5\rho\omega\pi a^3$, respectively. Where ω is the wave frequency, good agreements were found. However, for added mass, $a_{33}^{a,b}$, and damping coefficient, $b_{33}^{a,b}$, of interaction terms, a little discrepancy can be seen when $ka > 1.0$. For the surge added mass and damping coefficients $a_{11}^{a,a}$ and $b_{11}^{a,a}$, a small deviation can be found when $ka > 0.8$. The heave added mass and damping coefficients $a_{33}^{a,a}$ and $b_{33}^{a,a}$, agree well. This test case can show that the numerical method and algorithm for finite depth water interaction problem are encouraging.

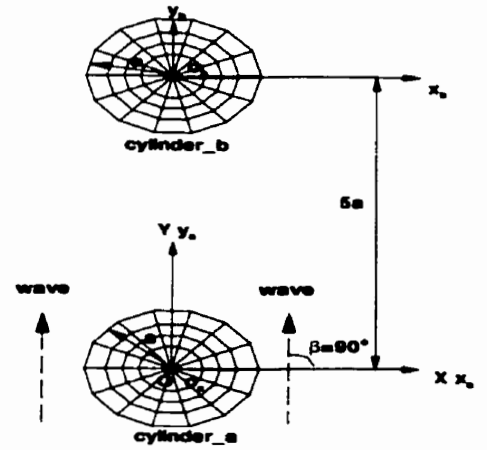

Figure 5.2: Relative position of two cylinders: $dx = 0.0$, $dy = 5a$ for test case 1

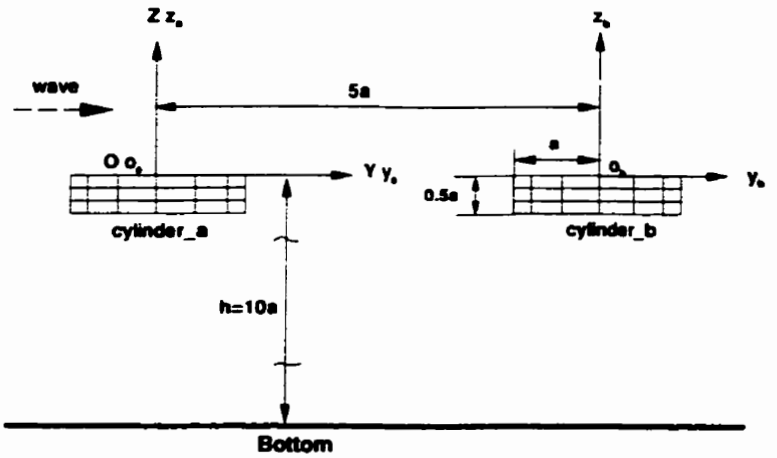

Figure 5.3: Water depth h=10a for test case 1

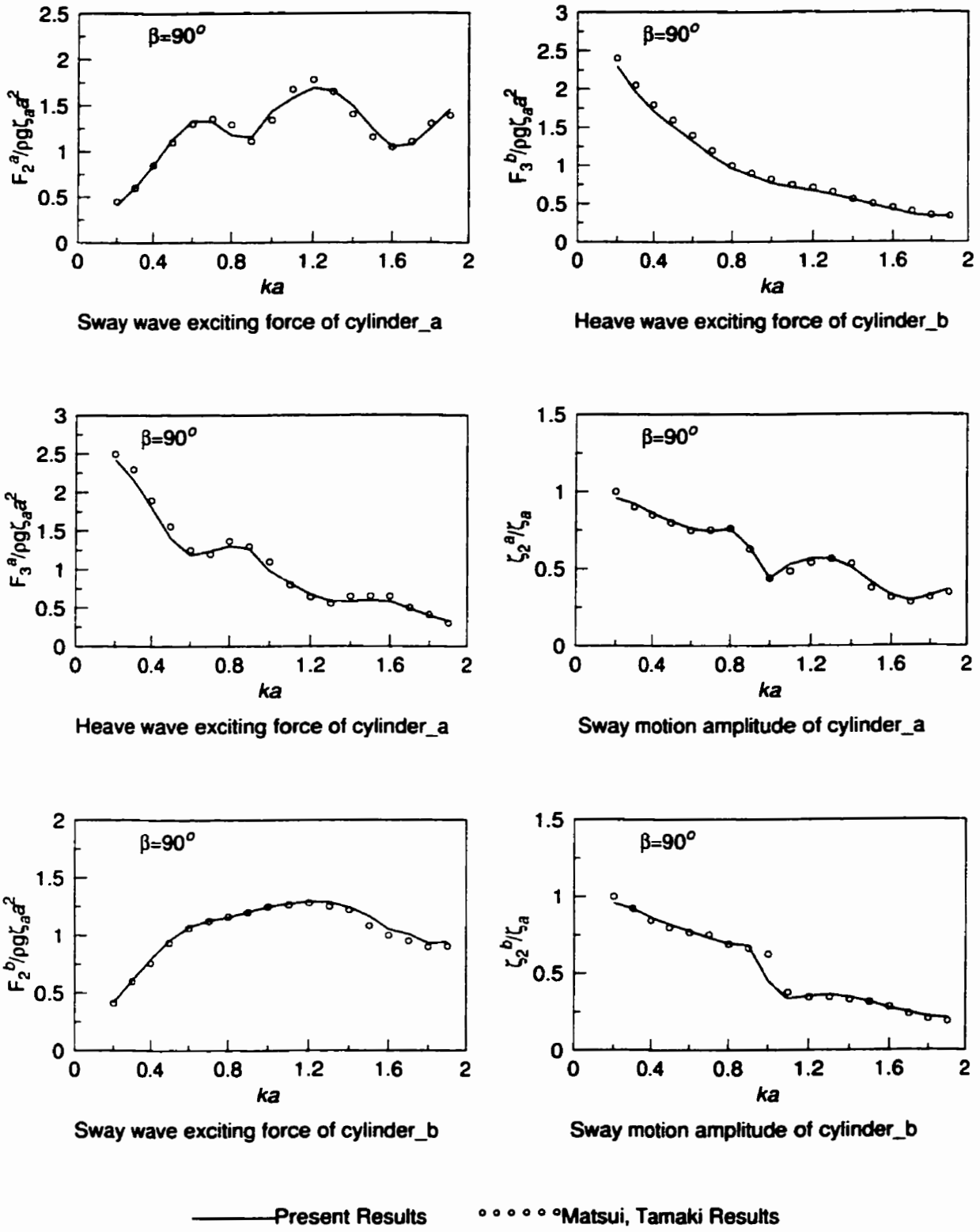

Figure 5.4: Non-dimensional wave exciting forces and motions in test case 1

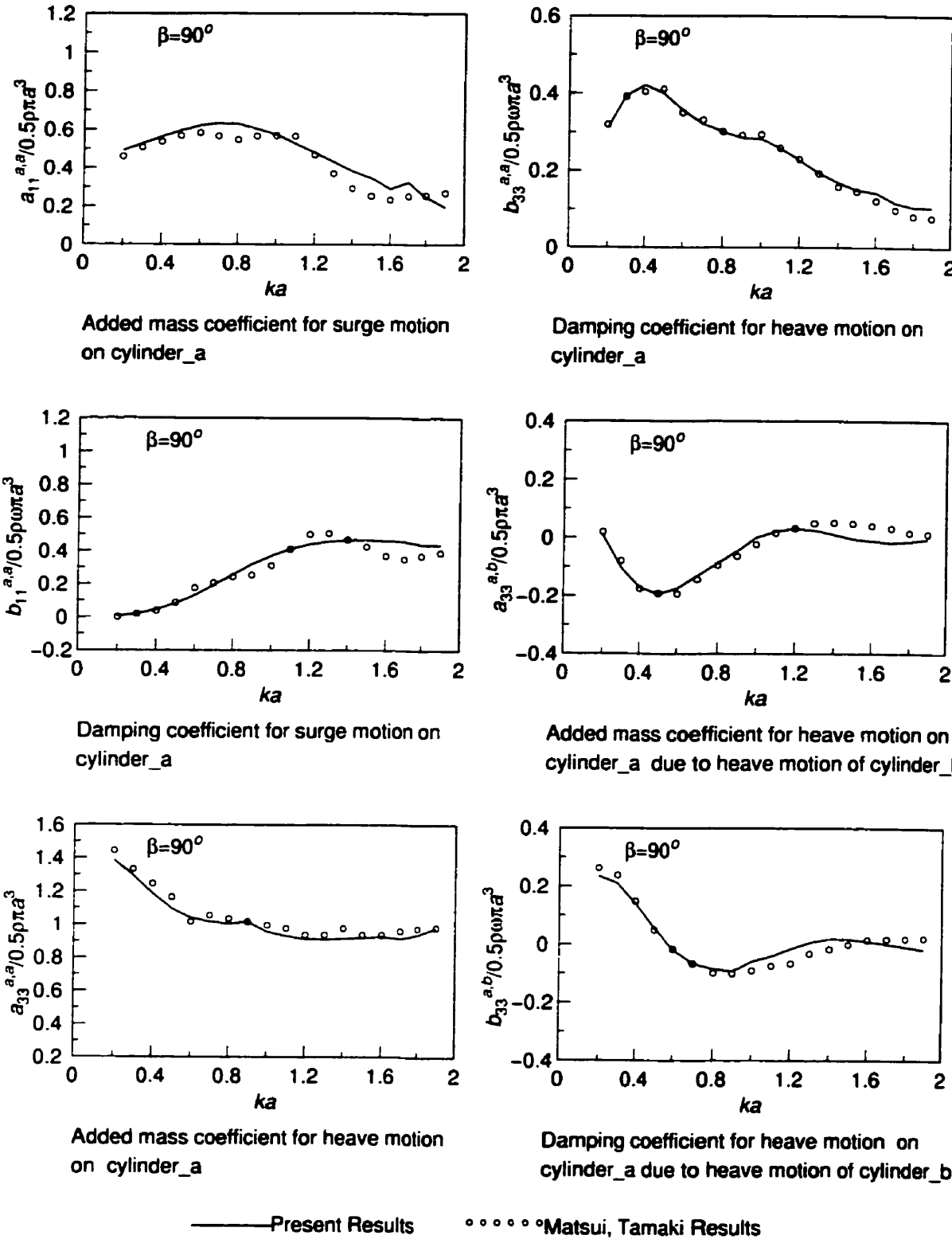

Figure 5.5: Non-dimensional added mass and damping coefficients in test case 1

5.1.2 Two Identical Circular Cylinder Interactions in Shallow Water

A further validation is made for two cylinder interactions in waves in shallow water, and the results were compared with those of Williams (1988, 1989). In this case, the radius of each cylinder $r = a$; the draft of each cylinder $T = 3a$; and, each cylinder has been discretized by 168 panels as shown in Figure 5.6. Water depth $h = 10a$; the ratio of water depth of each cylinder to draft: $\delta = h/T = 3.33 < 4.0$ which identified in the shallow water region by Van Oortmerssen(1976); the longitudinal separation distance $dx = 0.0$; the lateral separation distance $dy = 5a$; the lateral gap $Gy = 3a$; the wave heading $\beta = 90^0$. The details are shown in Figure 5.7 and Figure 5.8.

In Figure 5.9, the wave exciting force results are presented in the dimensionless form with forces normalized by the corresponding force component on an isolated cylinder (denoted by F_x^a and F_z^a for the isolated cylinder_a; and F_x^b and F_z^b for the isolated cylinder_b). The lateral interaction wave exciting forces for cylinder_a and cylinder_b. are found to be in good agreement with Williams' results. The vertical interaction wave exciting forces on cylinder_a are slightly smaller around $ka = 0.8$ and slightly greater at $ka = 1.2$. On cylinder_b. the vertical wave exciting forces are in acceptable agreement. In the longitudinal direction, the interaction forces are zero because of the heading angle of $\beta = 90.0^o$. This figure has shown that the numerical method and algorithm are acceptable for computing the interaction wave exciting forces in the shallow water region.

In Figure 5.10, the added mass is non-dimensionalized by dividing $0.5\rho\pi a^3$ and the

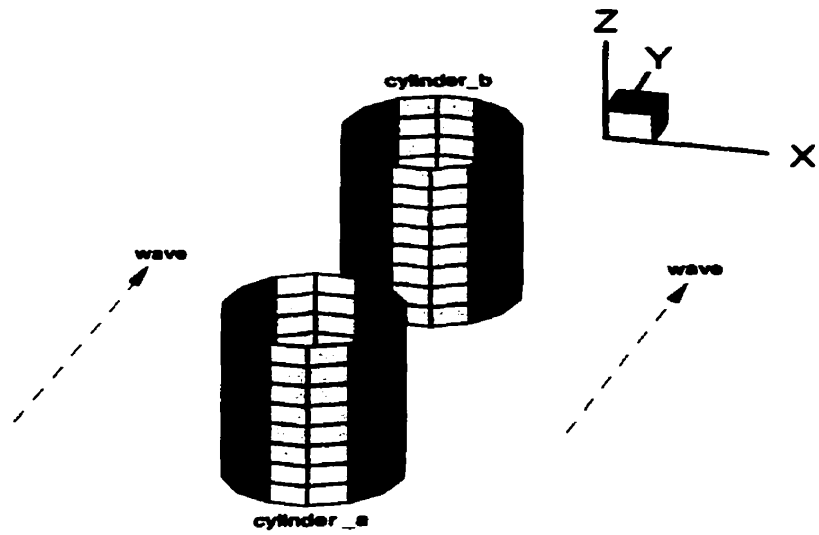

Figure 5.6: Panelized cylinder_a and cylinder_b for test case 2

damping coefficient is non-dimensionalized by $0.5\rho\omega\pi a^3$. The added mass, $a_{11}^{a,b}$, and damping coefficients $b_{11}^{a,b}$ and $b_{22}^{a,b}$, of interaction terms are in good agreement with results of Williams. The surge added mass on cylinder_a, $a_{11}^{a,a}$, is found to be a slightly larger around $ka = 0.5$. The added mass, $a_{22}^{a,a}$, and damping coefficient, $b_{22}^{a,a}$, for sway motion on cylinder_a are found to be in reasonable agreement. Through two testing cases. the computer code has demonstrated that it is very effective for solving the shallow water interaction problems as well.

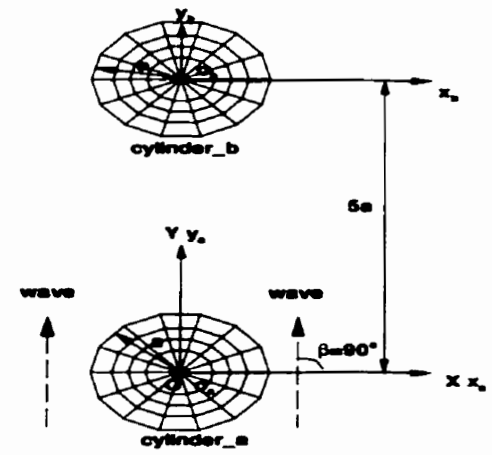

Figure 5.7: Relative position of two cylinders: $dx = 0.0$, $dy = 5a$ for test case 2

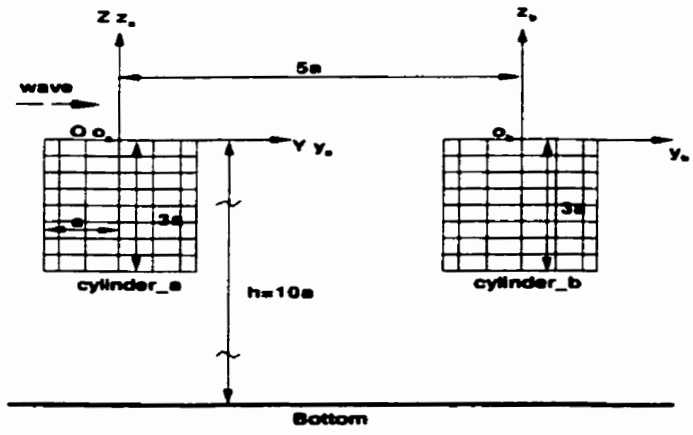

Figure 5.8: Water depth h=10a for test case 2

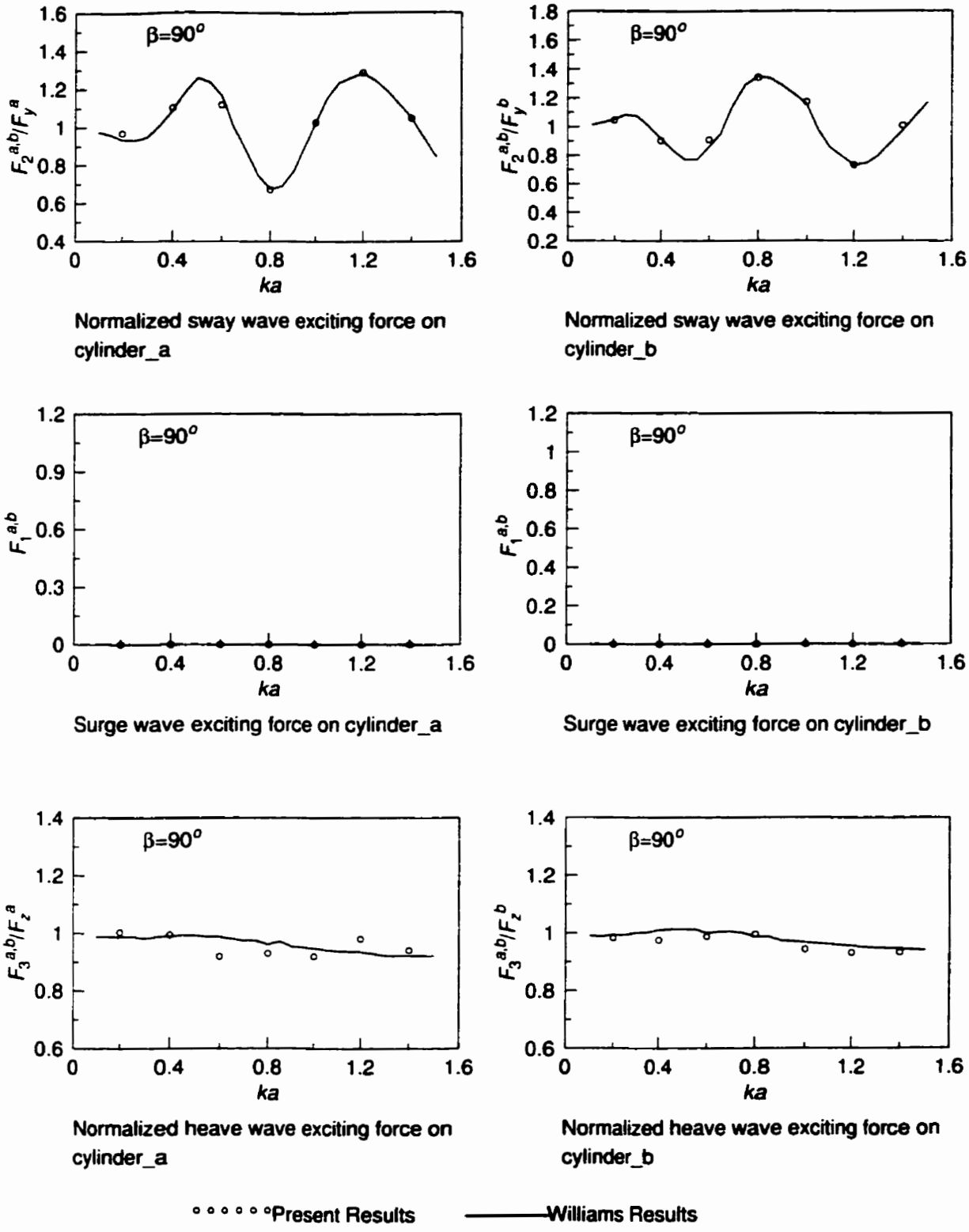

Figure 5.9: Non-dimensional wave exciting forces in test case 2

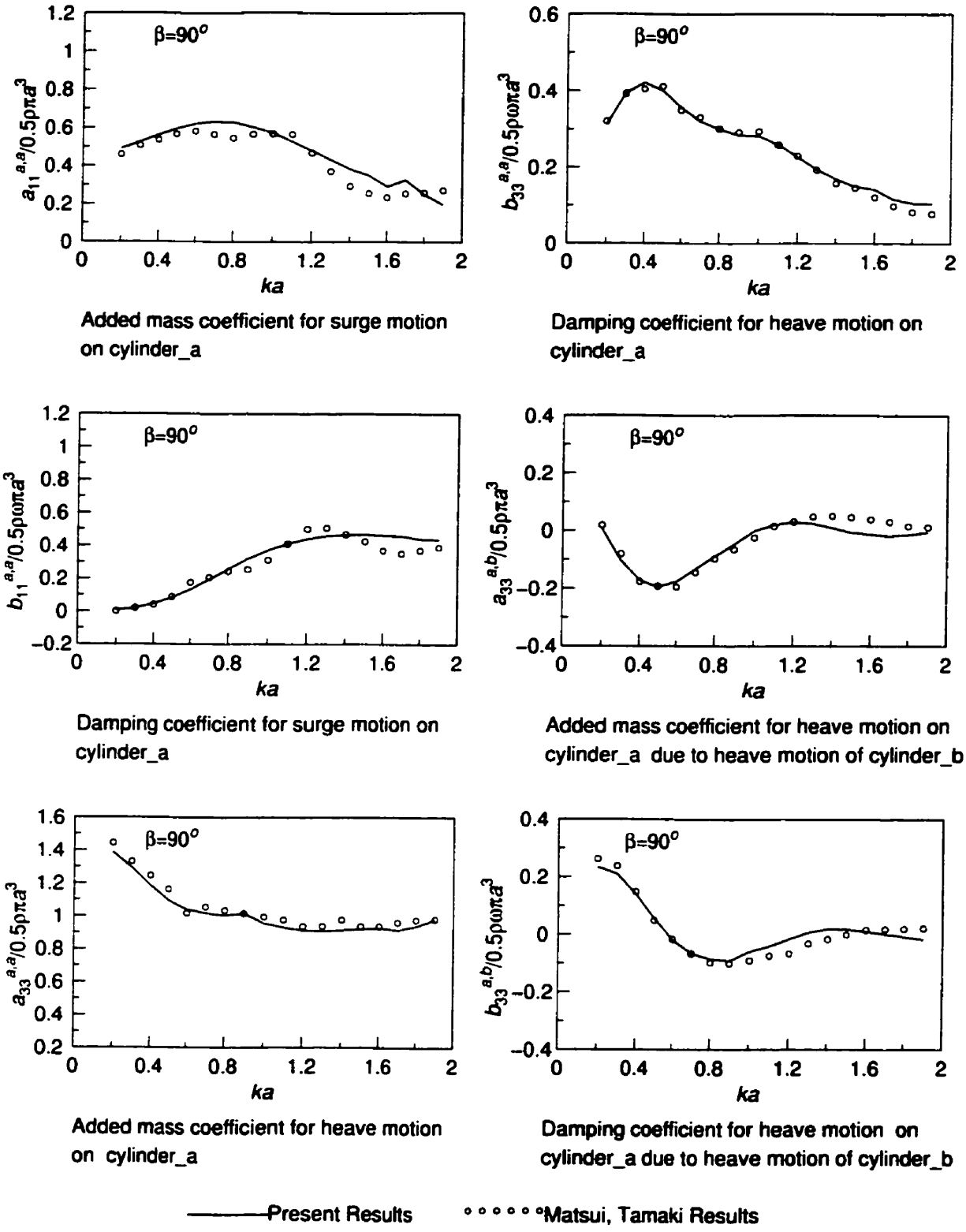

Figure 5.10: Non-dimensional added mass and damping coefficient in test case 2

5.1.3 The Effect of Panel Resolution

In order to investigate the panel resolution effect, computations were carried out for the two cylinders (given in Section 5.1.1) with 30 panels, 56 panels, 98 panels, respectively. The numerical results for cylinder_a sway motion and cylinder_b sway motion on different panels in water of finite depth are shown in Figure 5.11 and Figure 5.12. As we can see, with 98 panels on cylinder_a and cylinder_b surface, the converged numerical results have been obtained. Therefore, cylinders with 98 panels were chosen to perform as two cylinders interacting in water of finite depth in Section 5.1.1.

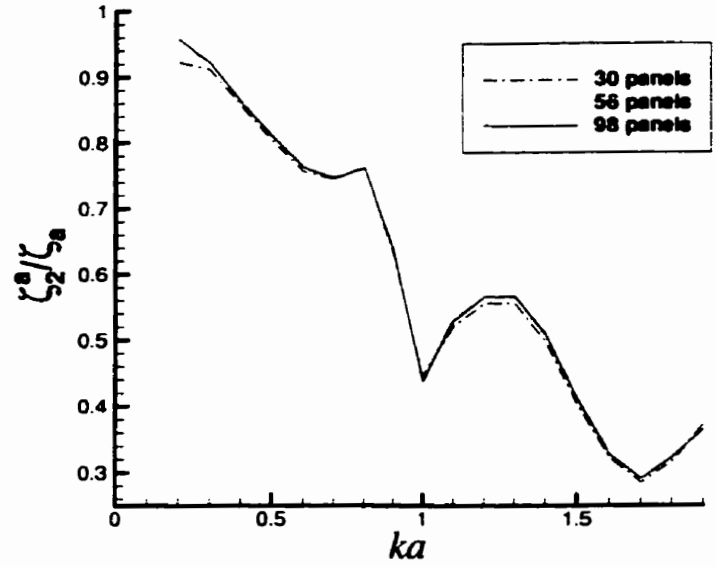

Figure 5.11: Sway motion amplitude for cylinder_a

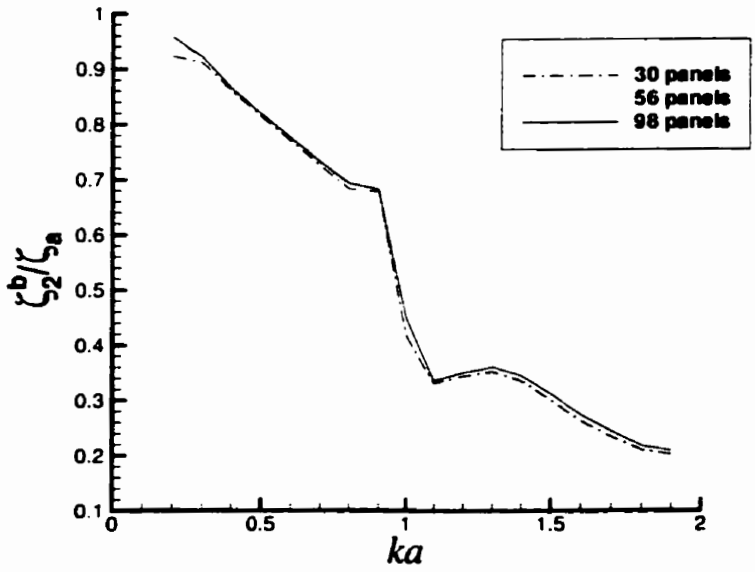

Figure 5.12: Sway motion amplitude for cylinder_b

5.2 Results for Interactions of Two Ships in Shallow Water, Finite Depth of Water and Deep Water

The ships denoted as ship_a (a supply ship) and ship_b (a frigate), as given by McTaggart *et al* (2001), were chosen to perform interactions in waves.

5.2.1 Panelization of Two Ships

According to Hsiung & Huang (1991), the hull surface at one side of the ship with 21 stations is suggested to be discretized into a minimum of 5 panels between every two stations. Further increasing the panel resolution would not improve the numerical results for a mono-hull ship. Normally, with 200 panels on a ship hull surface, the converged numerical results can be obtained. The personal computer memory also presented the limitation for the ship panel number which should not exceed 300 panels for each ship. Therefore, ship_a and ship_b were panelized as follows:

Ship_a:

The ship_a hull was panelized directly from the given regular 21 station offset table by using the computer program *PANELGEN*(Hsiung *et al*, 1996). The 210 panels were produced by using 21 stations, 6 waterlines and 264 nodes. The principal dimensions are as shown in Table 5.1. The panelized ship_a and body plan are shown in Figure 5.13 and Figure 5.16, respectively.

Table 5.1: The principal dimensions for ship_a and ship_b

ship_a	ship_b
$L_a = 180.0m$	$L_b = 122.0m$
$B_a = 30.633m$	$B_b = 14.78m$
$T_a = 8.5m$	$T_b = 4.5m$
$\nabla_a = 28223.3tonnes$	$\nabla_b = 4023.7tonnes$
$C_b^a = 0.588$	$C_b^b = 0.484$
$X_g^a = -1.688m$ (aft midships)	$X_g^b = 3.284m$ (forward midships)
$Z_g^a = 3.925m$ (relative to the calm waterline)	$Z_g^b = 2.049m$ (relative to the calm waterline)
$R_{xx}^a = 8.047m$	$R_{xx}^b = 4.921m$
$R_{yy}^a = 45.0m$	$R_{yy}^b = 30.5m$
$R_{zz}^a = 45.0m$	$R_{zz}^b = 30.5m$

Ship_b:

The ship_b hull was panelized directly from the given 26 station offset table (from the software *fastship* output) by using the computer program *PANELGEN*. 240 panels were produced by using 26 stations, 6 waterlines and 300 nodes. The principal dimensions are also shown in Table 5.1. The panelized ship_b and body plan are shown in Figure 5.15 and Figure 5.16, respectively. And the table 5.1 shows that ship_a is larger than ship_b. Then, the interaction problem would focus on the large-small ship interactions in shallow water, finite depth of water and deep water.

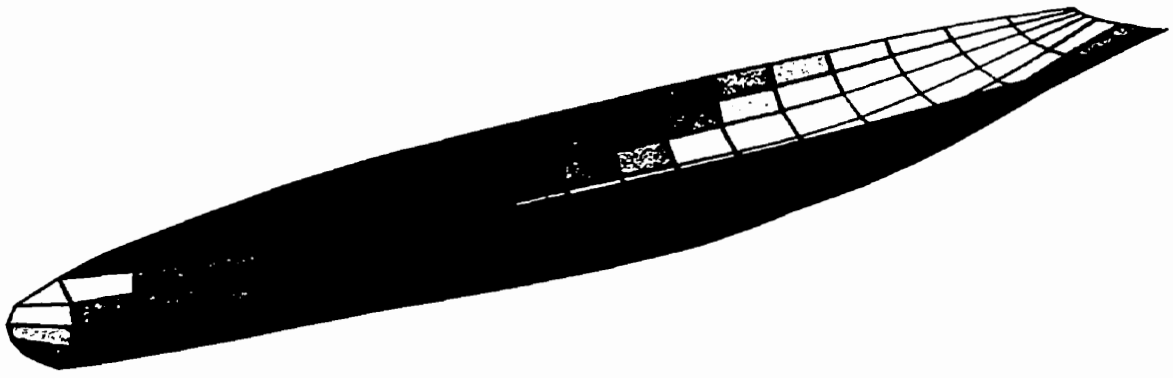

Figure 5.13: Panelized ship_a hull (supply ship)

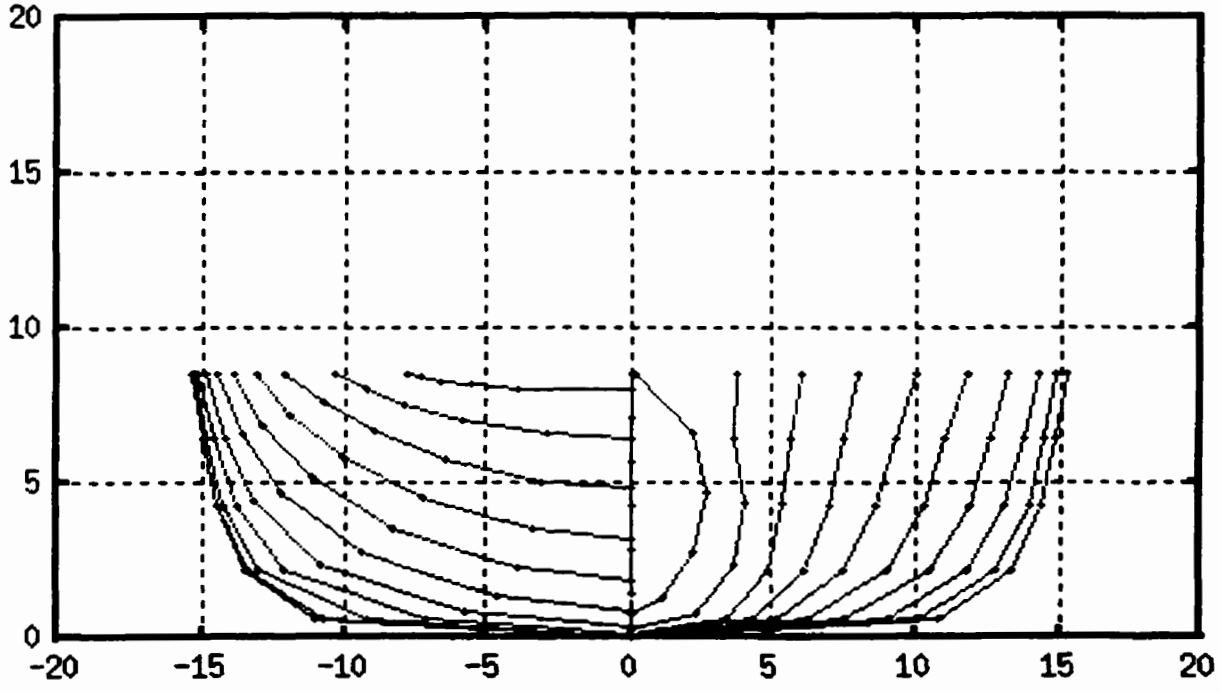

Figure 5.14: Body plan of ship_a hull (supply ship)

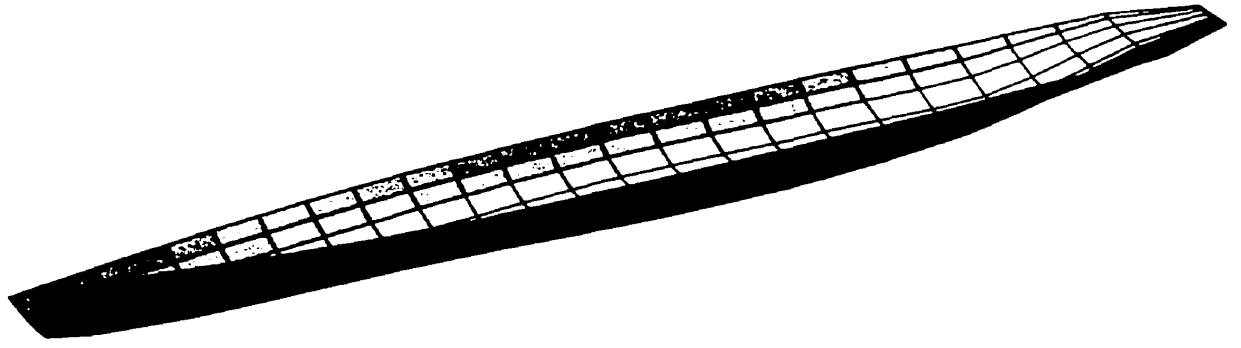

Figure 5.15: Panelized ship_b hull (frigate)

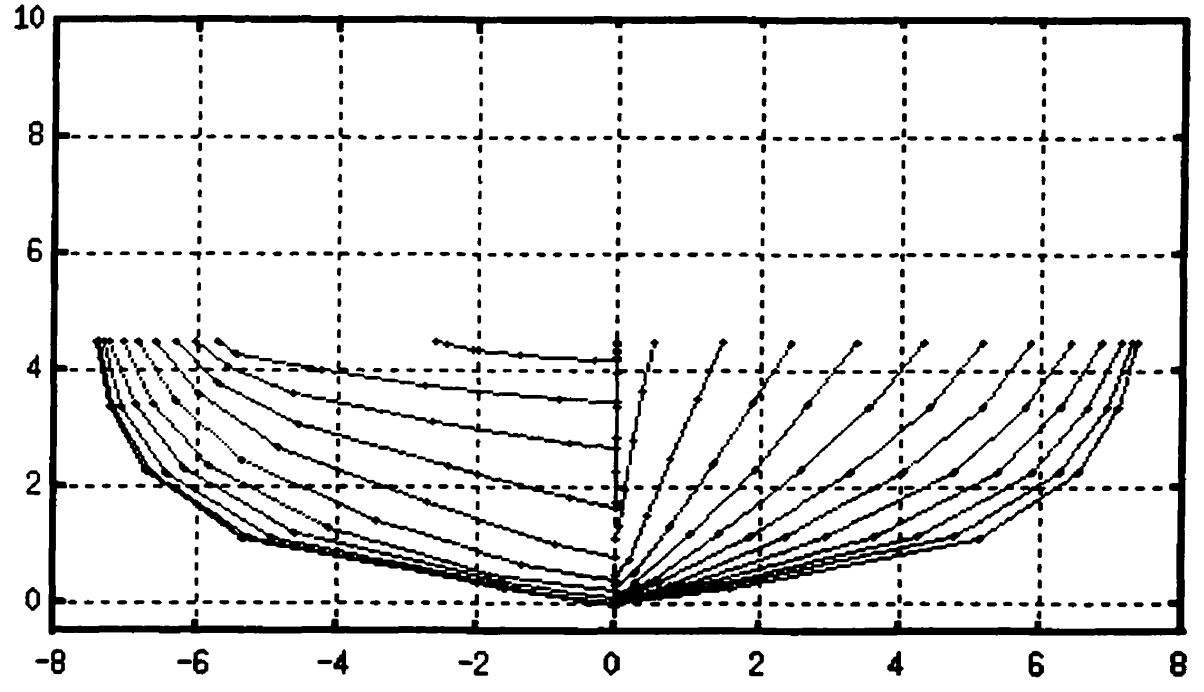

Figure 5.16: Body plan of the ship_b hull (frigate)

5.2.2 The Validation of Two Ship Interactions in Deep Water

The computational results for two ship interactions in deep water case have been validated by McTaggart *et al*(2001) with a wealth of experimental data by conducting semi-captive model tests in the towing tank at the Institute for Marine Dynamics(IMD) in St.John's. Newfoundland. With the control of speed and heading of ship_a (a supply ship) and ship_b (a frigate) model tests were performed by restraining the models in surge, sway and yaw. In order to make comparisons with semi-captive model tests, in the computer program an input restraint flag was set to indicate that a restraining force or moment was applied at the centre of gravity of ship_a or ship_b. Two typical cases were chosen here: head seas for a forward speed of 6.18m/s, with the ship_b alongside the ship_a (Figure 5.17) and 45m ahead of ship_a (Figure 5.18). The figures also show the walls of the towing tank. The lateral gap $Gy = 30.0m$ was set to present the close proximity interactions and $Gy = 2000.0m$ was set to present that two ships perform individually and no interaction effect is involved. These cases are presented here because they are the most representative of operational conditions and likely free of water interference effect.

Figure 5.19 and Figure 5.20 show that the numerical predictions give generally good agreement with the experiments. The existence of the smaller ship_b has very little influence on the motions of the larger ship_b. But the larger ship_a has a prominent influence on the motion of the smaller ship_b, particularly for heave and roll at longer wavelengths. For the ship_b ahead of the ship_a (Figure 5.20) the experiments could not be completed for the highest two wavelengths due to excessive motions of the ship_b (roll amplitude exceeding 30^0). The discrepancies between experiments and

predictions in Figure 5.19 and Figure 5.20 occur for motions of the ship_b in longer wavelengths due to the limitation of linear assumptions for the large amplitude motions of ship_b. For zero speed test, the interference effect induced from the existence of the towing tank wall on both head seas and oblique seas were significant during the experiments. The interference presence might be solved numerically by distributing the sources on the tank walls as stationary panels in the future.

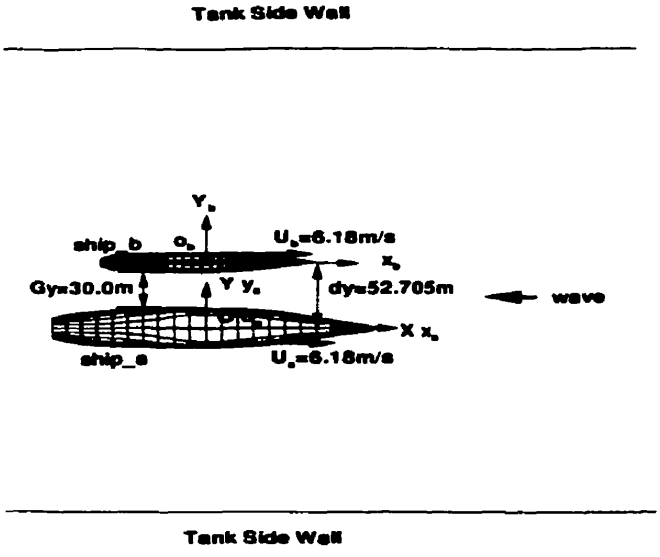

Figure 5.17: Ship_b alongside ship_a, head seas

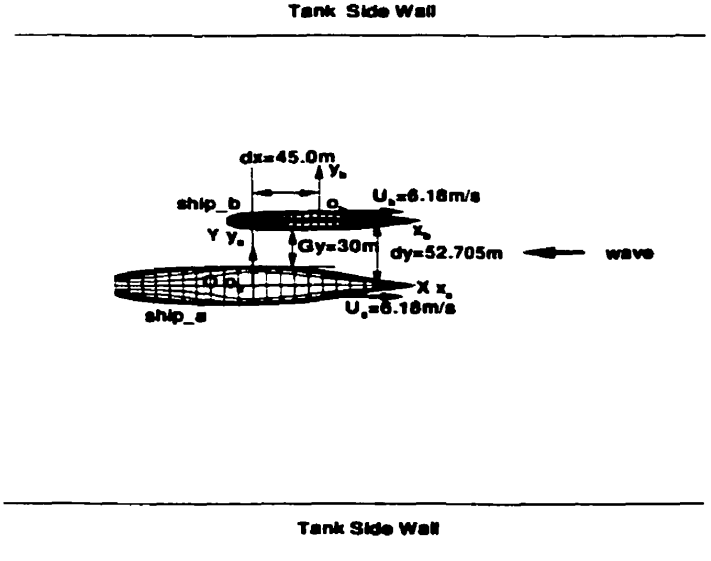

Figure 5.18: Ship_b ahead of ship_a $45m$, head seas

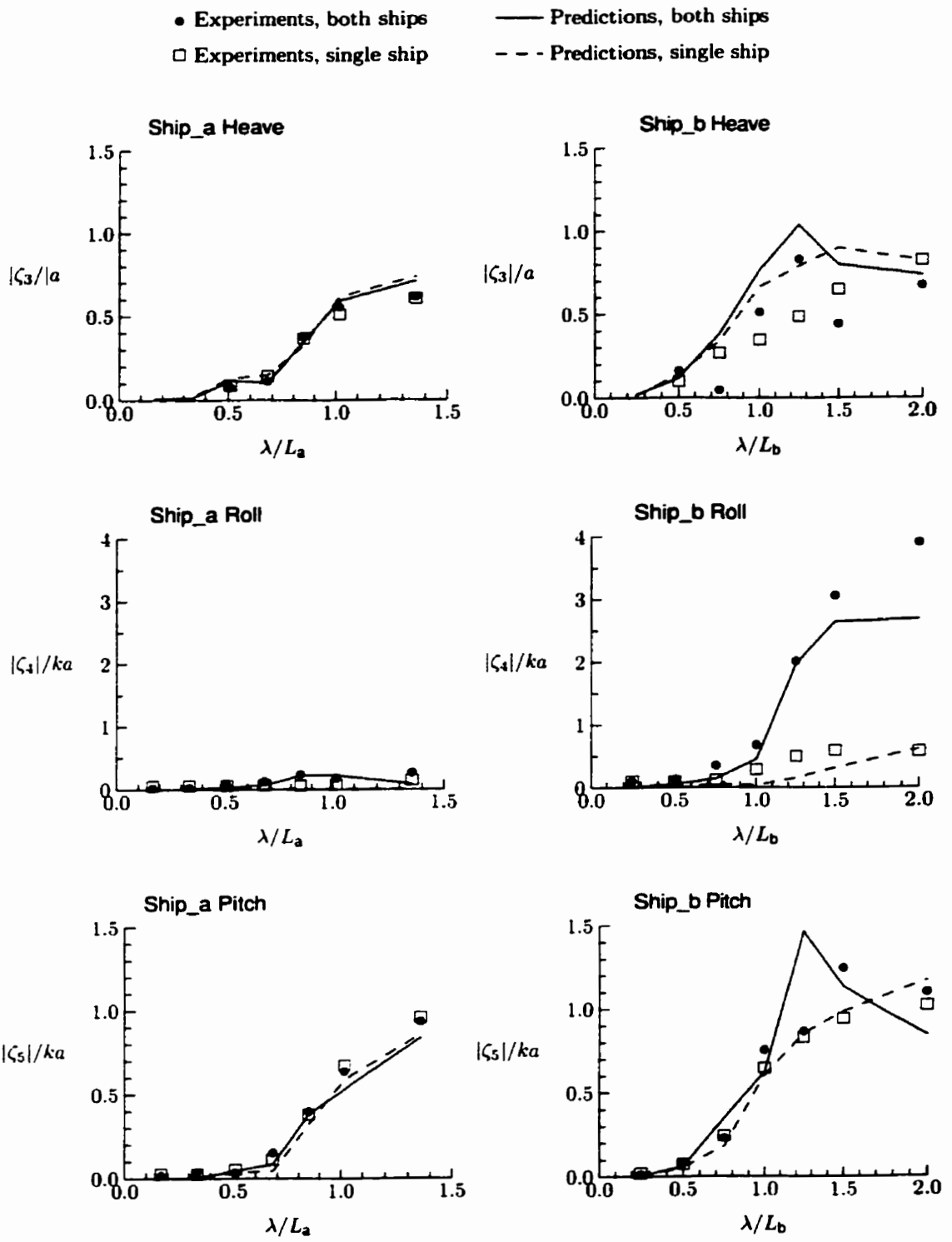

Figure 5.19: Ship motions with ship_b alongside ship_a, 6.18m/s, head seas, (McTaggart, Cumming, Hsiung & Li, 2001)

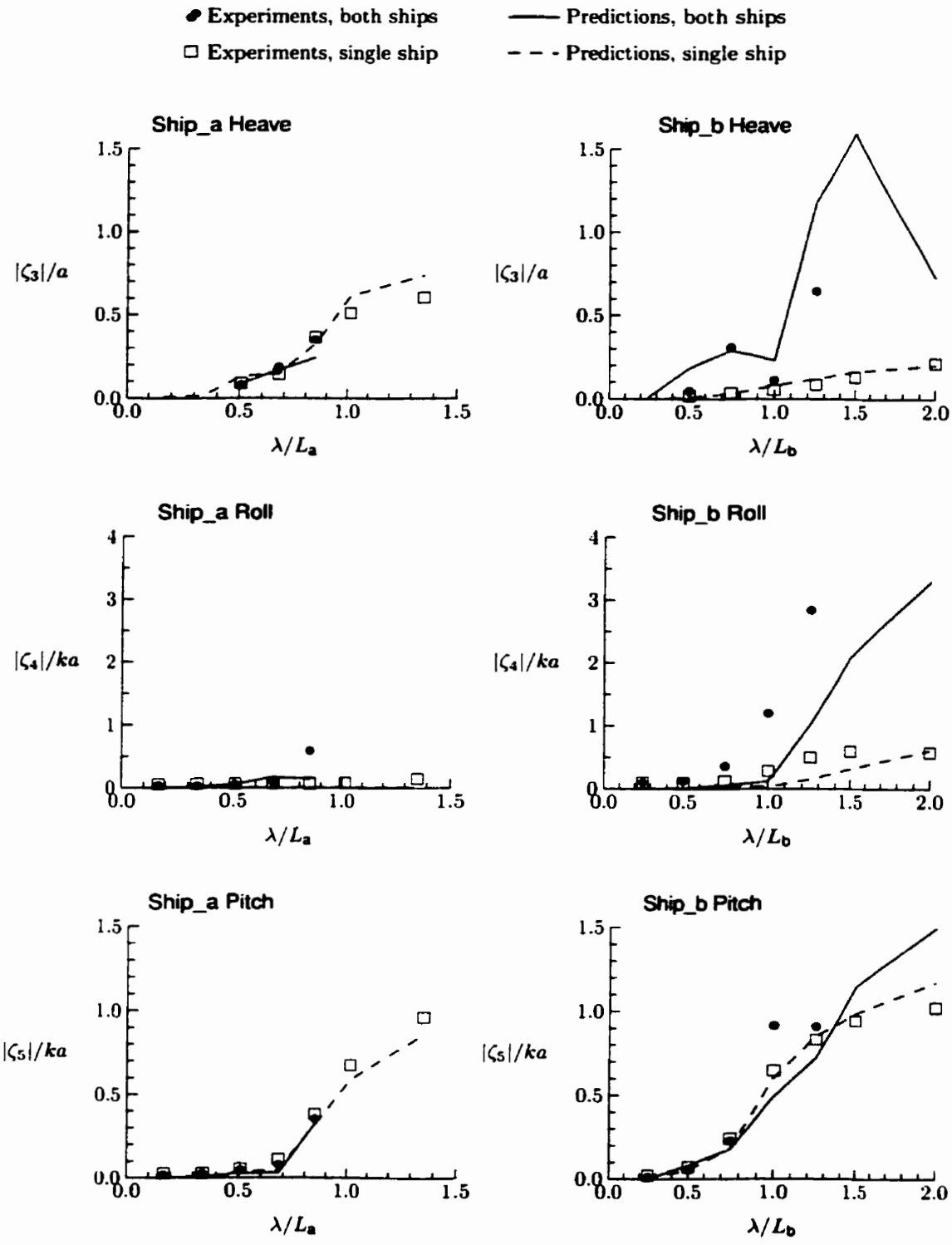

Figure 5.20: Ship motions with ship_b $45m$ ahead of ship_a, 6.18m/s, head seas, (McTaggart, Cumming, Hsiung & Li, 2001)

5.2.3 The Comparisons of Two Ship Interactions in Shallow Water, Water of Finite Depth and Deep Water

Different from Section 5.2.2, ship_a and ship_b were regards as the unrestrained rigid bodies for present computations. Four typical water depths were chosen to present the shallow water, water of finite depth and deep water which are $h = 10.2m$, $h = 16.0m$, h=90.0m and $h = \infty$. Usually, the ratio of water depth to the ship draft, δ, was used to judge the water depth condition according to Van Oortmerssen(1976). When $1.0 < \delta = h/T \leq 4.0$, it was regarded as in the shallow water region; when $4.0 < \delta = h/T \leq 10.0$ it was regarded as in the finite depth of water region; when $\delta = h/T > 10.0$, it would be considered as in the deep water condition. The δ value details for ship_a and ship_b are shown in Tab 5.2.

In order to observe the effect of wave heading $\beta = 180^0, 150^0, 120^0$, longitudinal separation distance $dx = 0.0m, 45.0m$, lateral separation distance $dy = 52.705m, 2022.705m$ or gap $Gy = 30.0m, 2000.0m$ and forward speed $U = 0.0m/s, 6.18m/s$ on the interactions in the shallow water, finite depth of water and deep water regions, eleven cases were designed as shown in Table 5.3. For each case, four different water depths were computed and studied. For ship_a , the ratio of wave length to ship_a length, λ/L_a, was chosen between 0.495 and 2.03. For ship_b, the ratio of wave length to ship_b length ,λ/L_b, was chosen between 0.75 and 3.0. The viscous roll damping was computed for each case, the details of hull parameters for computing the viscous roll damping for ship_a and ship_b were reported by Li *et al* (2000).

The results of wave exciting force and motion are all presented in non-dimensional

Table 5.2: δ values for ship_a and ship_b

$\delta = h/T$	ship_a ($\delta_a = h/T_a$)	ship_b ($\delta_b = h/T_b$)
$h = 10.2m$	1.2	2.27
$h = 16.0m$	1.88	3.56
$h = 90.0m$	10.59	20.0
$h = \infty$	∞	∞

forms. The details are as follows:

For ship_a:

- $F_i/\rho g\zeta_a L_a B_a$: non-dimensional wave exciting force amplitude in the ith mode, $i = 1, 2, 3$.
- $M_j/\rho g\zeta_a L_a^2 B_a$: non-dimensional wave exciting moment amplitude in the jth mode, $j = 4, 5, 6$.
- ζ_i/ζ_a: non-dimensional motion amplitude in the ith mode, $i = 1, 2, 3$.
- $\zeta_j/\zeta_a k$: non-dimensional motion amplitude in the jth mode, $j = 4, 5, 6$.

For ship_b:

- $F_i/\rho g\zeta_a L_b B_b$: non-dimensional wave exciting force amplitude in the ith mode, $i = 1, 2, 3$.
- $M_j/\rho g\zeta_a L_b^2 B_b$: non-dimensional wave exciting moment amplitude in the jth mode, $j = 4, 5, 6$.
- ζ_i/ζ_a: non-dimensional motion amplitude in the ith mode, $i = 1, 2, 3$.
- $\zeta_j/\zeta_a k$: non-dimensional motion amplitude in the jth mode, $j = 4, 5, 6$.

Table 5.3: Cases for study

Case No.	dy (m)	Gy (m)	dx (m)	wave heading β	speed U (m/s)	water depth (m)
Case 1	52.705	30.0	0.0	180°	0.0	10.2,16,90,∞
Case 2	52.705	30.0	45.0	180°	0.0	10.2,16,90,∞
Case 3	2022.705	2000.0	0.0	180°	0.0	10.2,16,90,∞
Case 4	52.705	30.0	0.0	150°	0.0	10.2,16,90,∞
Case 5	52.705	30.0	45.0	150°	0.0	10.2,16,90,∞
Case 6	2022.705	2000.0	0.0	150°	0.0	10.2,16,90,∞
Case 7	52.705	30.0	0.0	120°	0.0	10.2,16,90,∞
Case 8	52.705	30.0	45.0	120°	0.0	10.2,16,90,∞
Case 9	2022.705	2000.0	0.0	120°	0.0	10.2,16,90,∞
Case 10	52.705	30.0	45.0	180°	6.18	10.2,16,90,∞
Case 11	2022.705	2000.0	0.0	180°	6.18	10.2,16,90,∞

5.2.4 Case 1

In this case, the arrangement of the panelized ship_a and ship_b is shown in Figure 5.21. Wave heading $\beta = 180°$: lateral separation $dy = 52.705m$ and gap $Gy = 30.0m$; longitudinal separation dx=0.0m; and forward speed $U = 0.0m/s$ are all shown in Figure 5.22. Figure 5.23 and Figure 5.24 show the positions of ship_a and ship_b relative to the sea bottom for water depths of $h = 10.2m$ and $h = 16.0m$, respectively.

Discussions on Case 1

In Figure 5.25, the non-dimensional wave exciting forces versus λ/L_a are given for ship_a. For head sea, the surge and heave forces and pitch moment are very sensitive to the water depth and increasing with λ/L_a. The sway force and roll moment were affected slightly. The water depth does not seem to affect the yaw moment for head

sea. When the water depth $h = 90.0m$, the effect of water depth on wave exciting forces approaches zero. This phenomenon was found by Kim(1969) as well. When $h = \infty$, the results were obtained by solving the deep water Green's function. When $h = 90.0m$, the results were based on the Green function of the finite depth of water. Very good agreement was found between these two methods and proved that the algorithm we used for solving the Green function in the finite depth of water was very successful.

In Figure 5.26, the non-dimensional wave exciting forces versus λ/L_b are given for ship_b. The surge and heave forces and the pitch moment were found more sensitive to the water depth than the sway force and the roll yaw moments. However, when $\lambda/L_b > 1.0$, a decreasing trend is found with increasing λ/L_b and less effect is found than with ship_a. Since $\delta_a < \delta_b$, ship_a forces could have more the shallow water effect than on ship_b.

In Figure 5.27, the non-dimensional motions of ship_a are presented. Only the surge motion is increasing with λ/L_a. The surge motion of the larger ship is also affected by shallow water for head sea. In Figure 5.28, the non-dimensional motions of ship_b are presented. Comparing with ship_a, the water depth effect on motions of ship_b is more significant. The prominent water depth effect on the surge motion for higher λ/L_b values. The shallower water depth made the roll resonance peak to move to a lower λ/L_b value area. The sway motion is affected for $\lambda/L_b > 1.50$ and the effect on the yaw motion starts from $\lambda/L_b > 1.25$. This is because the presence of a larger ship (ship_a) can significantly influence on the motions of a smaller ship (ship_b) in waves. Therefore, the motions of the smaller ship (ship_b) in the shallow water region will be affected not only by the water depth but also by the interaction influence from the larger ship (ship_a).

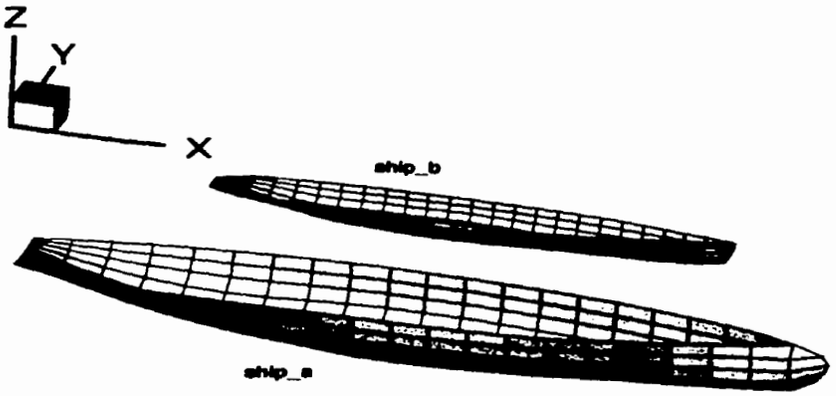

Figure 5.21: Panelized ship_a and ship_b for Case 1

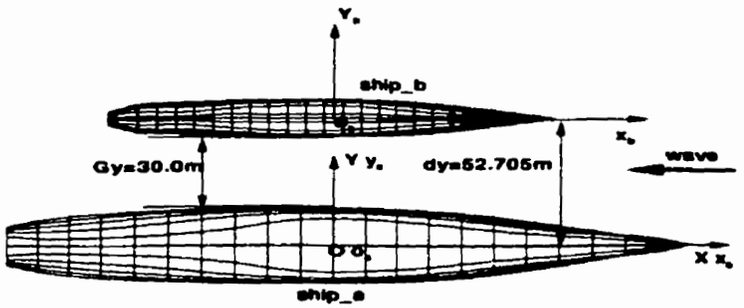

Figure 5.22: Relative position of two ships: $dx = 0.0m$, $Gy = 30.0m$ for Case 1

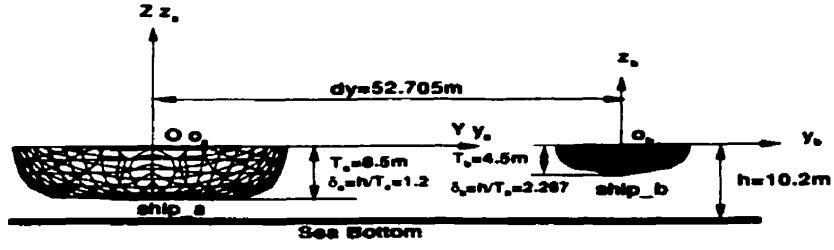

Figure 5.23: Water depth h=10.2m for Case 1

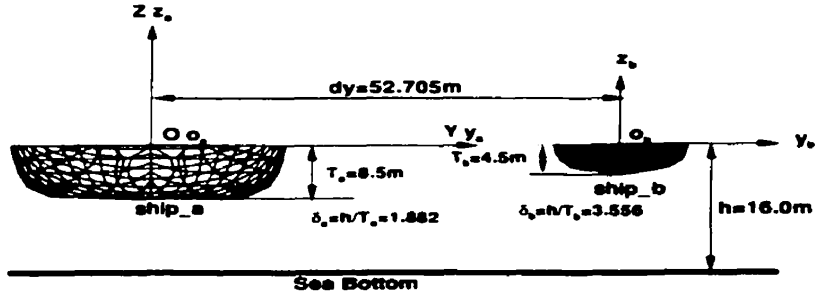

Figure 5.24: Water depth h=16.0m for Case 1

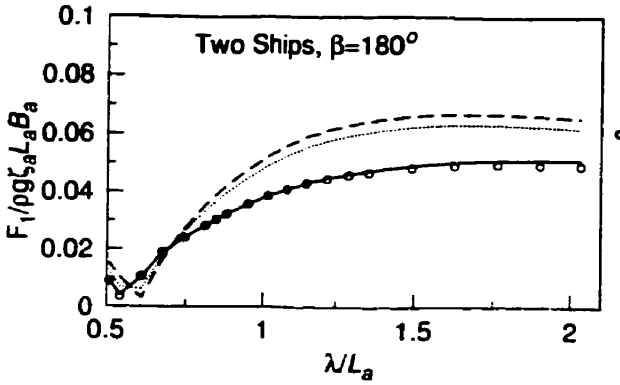

Surge force on ship_a at a separation
Gy=30.0m, dx=0.0m, U=0.0m/s

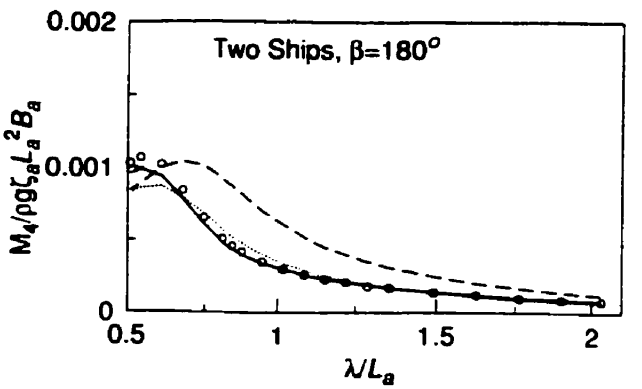

Roll moment on ship_a at a separation
Gy=30.0m, dx=0.0m, U=0.0m/s

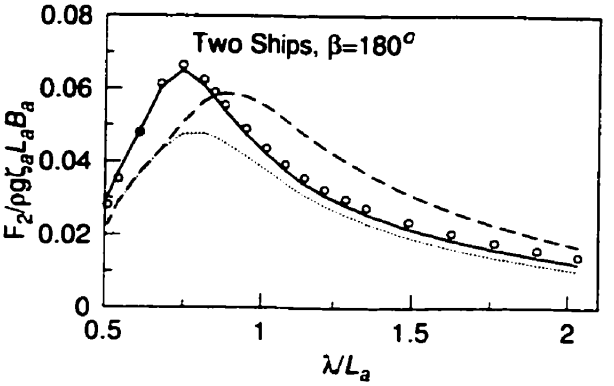

Sway force on ship_a at a separation
Gy=30.0m, dx=0.0m, U=0.0m/s

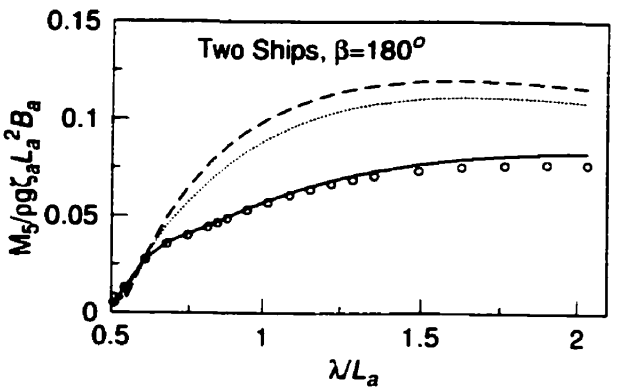

Pitch moment on ship_a at a separation
Gy=30.0m, dx=0.0m, U=0.0m/s

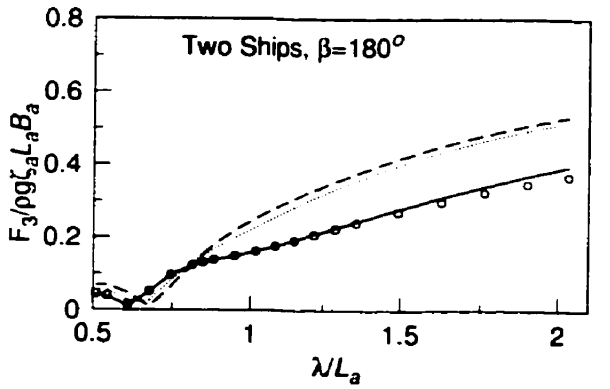

Heave force on ship_a at a separation
Gy=30.0m, dx=0.0m, U=0.0m/s

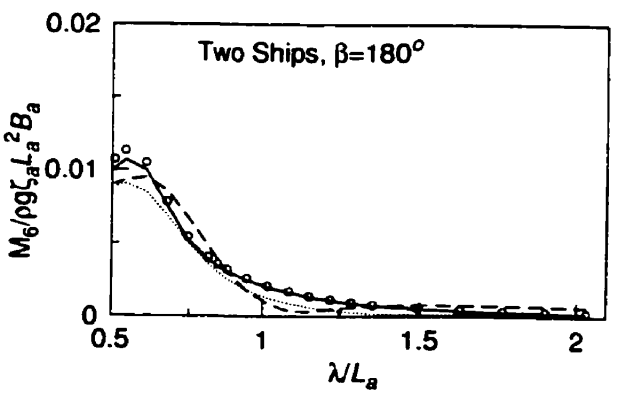

Yaw moment on ship_a at a separation
Gy=30.0m, dx=0.0m, U=0.0m/s

– – – –h=10.2m(δ=1.20), ...h=16.0m(δ=1.88), ———h=90m(δ=10.59), ° ° ° °h=∞(δ=∞)

Figure 5.25: Non-dimensional wave exciting force amplitudes on ship_a in Case 1

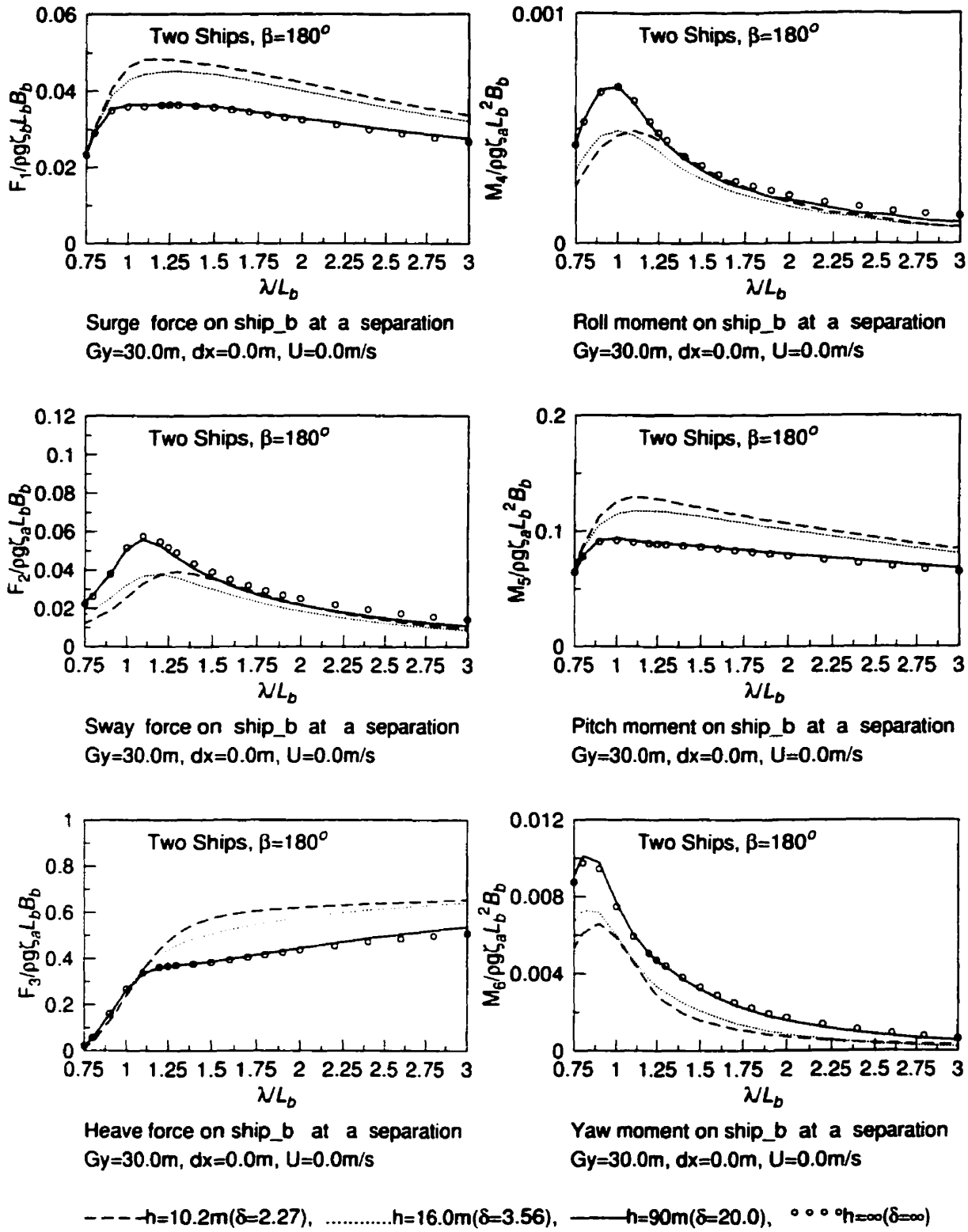

Figure 5.26: Non-dimensional wave exciting force amplitudes on ship_b in Case 1

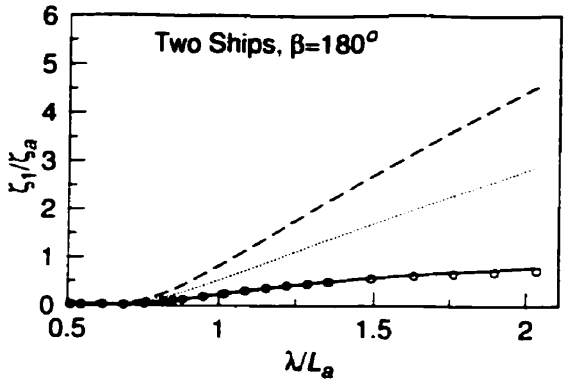

Surge motion of ship_a at a separation
Gy=30.0m, dx=0.0m, U=0.0m/s

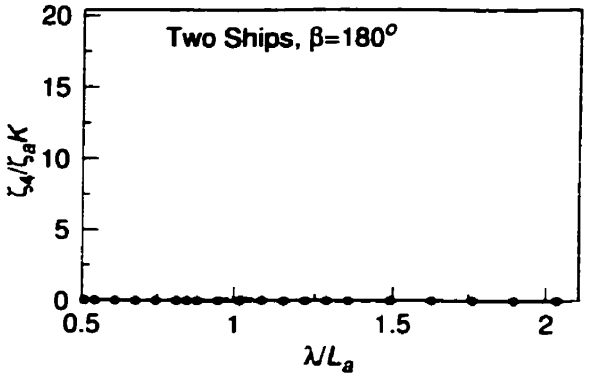

Roll motion of ship_a at a separation
Gy=30.0m, dx=0.0m, U=0.0m/s

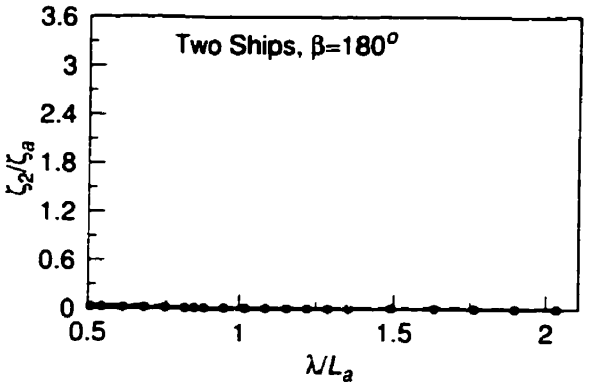

Sway motion of ship_a at a separation
Gy=30.0m, dx=0.0m, U=0.0m/s

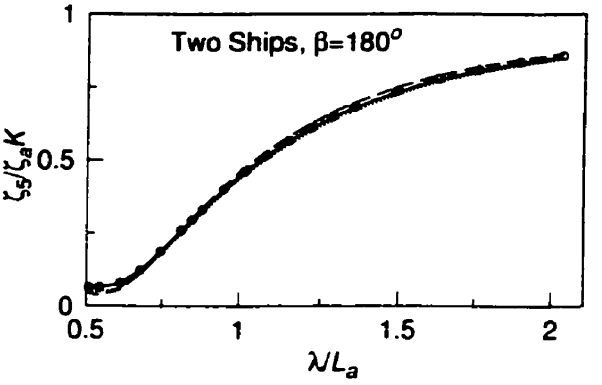

Pitch motion of ship_a at a separation
Gy=30.0m, dx=0.0m, U=0.0m/s

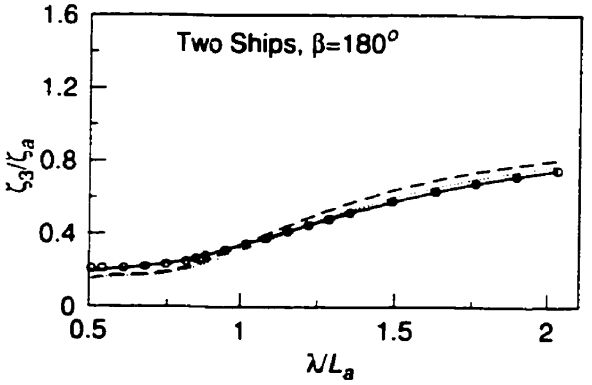

Heave motion of ship_a at a separation
Gy=30.0m, dx=0.0m, U=0.0m/s

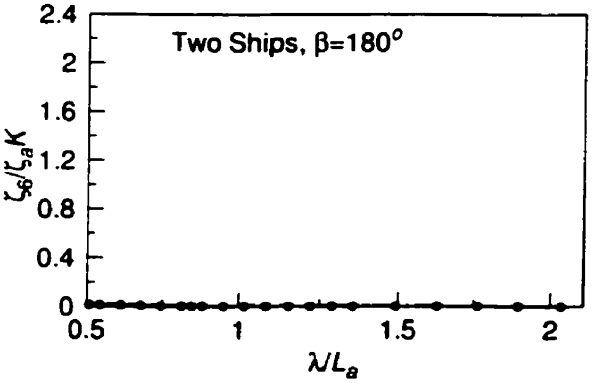

Yaw motion of ship_a at a separation
Gy=30.0m, dx=0.0m, U=0.0m/s

----h=10.2m(δ=1.20), ...h=16.0m(δ=1.88), ——h=90m(δ=10.59), ° ° ° °h=∞(δ=∞)

Figure 5.27: Non-dimensional motion displacement amplitudes on ship_a in Case 1

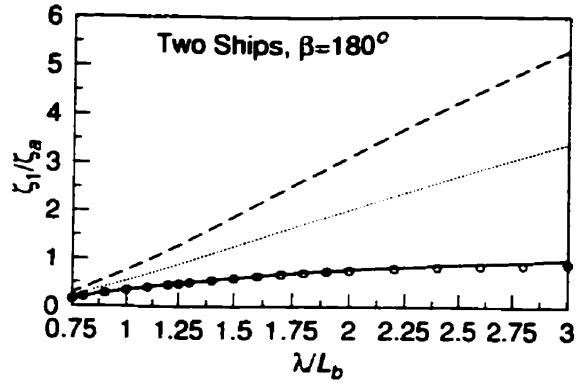

Surge motion of ship_b at a separation
Gy=30.0m, dx=0.0m, U=0.0m/s

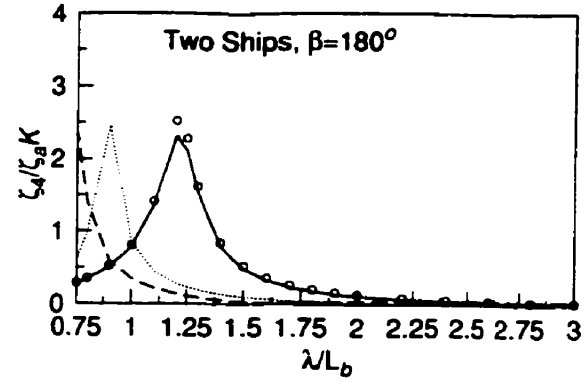

Roll motion of ship_b at a separation
Gy=30.0m, dx=0.0m, U=0.0m/s

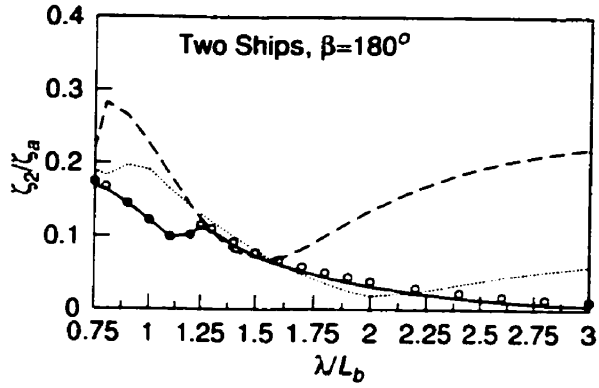

Sway motion of ship_b at a separation
Gy=30.0m, dx=0.0m, U=0.0m/s

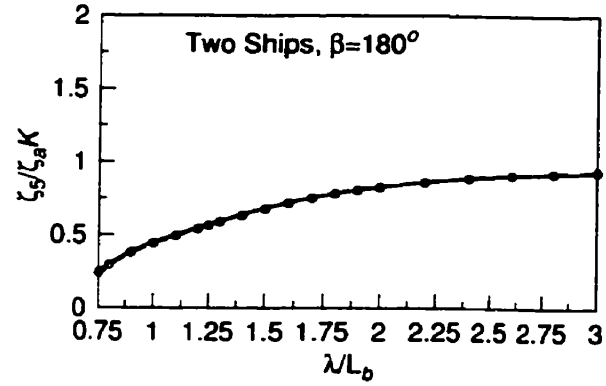

Pitch motion of ship_b at a separation
Gy=30.0m, dx=0.0m, U=0.0m/s

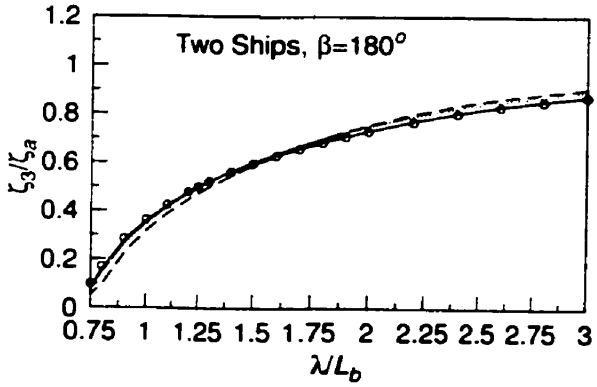

Heave motion of ship_b at a separation
Gy=30.0m, dx=0.0m, U=0.0m/s

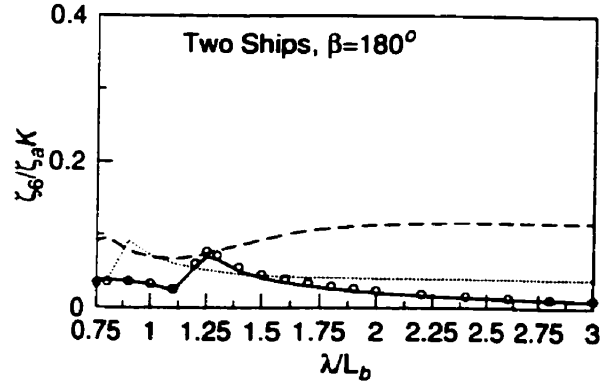

Yaw motion of ship_b at a separation
Gy=30.0m, dx=0.0m, U=0.0m/s

----h=10.2m(δ=2.27), ...h=16.0m(δ=3.56), ——h=90m(δ=20.0), ° ° ° °h=∞(δ=∞)

Figure 5.28: Non-dimensional motion displacement amplitudes on ship_b in Case 1

5.2.5 Case 2

The arrangement of the panelized ship_a and ship_b is shown in Figure 5.29. Wave heading $\beta = 180^o$; lateral separation $dy = 52.705m$ and gap $Gy = 30.0m$: longitudinal separation dx=45.0m; and forward speed $U = 0.0m/s$ are all shown in Figure 5.30. Figure 5.31 and Figure 5.32 show the positions of ship_a and ship_b relative to the sea bottom for water depths of $h = 10.2m$ and $h = 16.0m$, respectively.

Discussions on Case 2

In Case 2, the effect of longitudinal separation distance, $dx = 45.0m$, on the ship interactions in head seas has been observed. In Figure 5.33, the non-dimensional wave exciting interaction forces are given for ship_a. Comparing with Case 1, the roll and yaw moments of ship_a were affected slightly by dx. In Figure 5.34, the non-dimensional wave exciting interaction forces on ship_b are given. Comparing with Case 1, only the peak force value of surge becomes less, and the yaw moment gets smaller. This means that when the smaller ship moves toward the bow of the larger ship, the interaction forces is getting less. In Figure 5.35, the non-dimensional motions are given for ship_a. Comparing with Case 1, there is no effect of dx on ship_a motion. This means that the effect from dx is not enough to change the motion of ship_a. In Figure 5.36, the non-dimensional motions are given for ship_b. Comparing with Case 1, the motions of sway, roll and yaw become less. This means that dx can affect only the smaller ship's behavior.

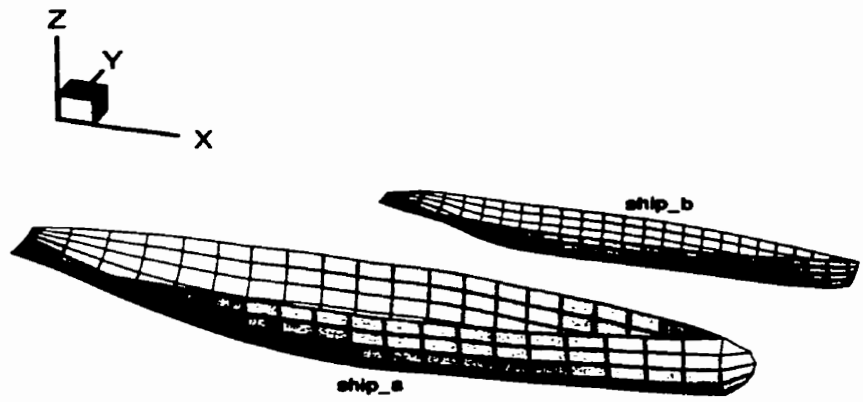

Figure 5.29: Panelized ship_a and ship_b for case 2

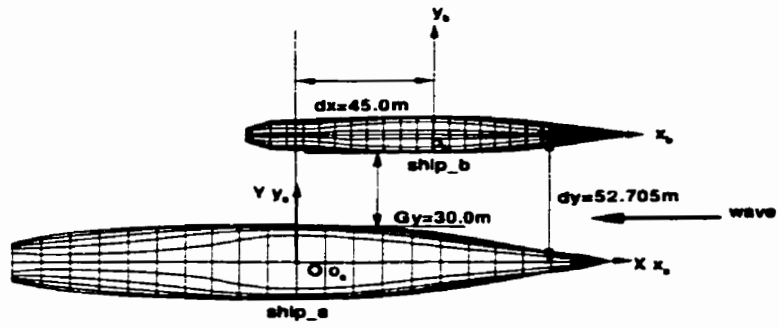

Figure 5.30: Relative position of two ships: $dx = 45.0m$, $Gy = 30.0m$ for Case 2

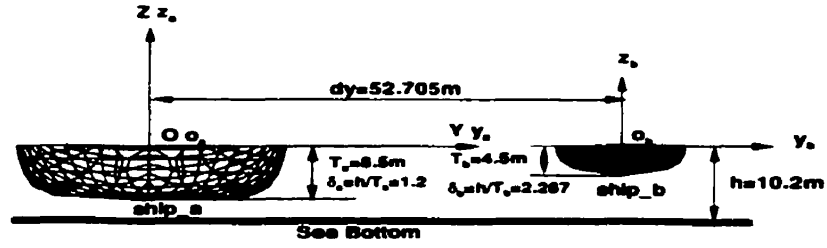

Figure 5.31: Water depth h=10.2m for Case 2

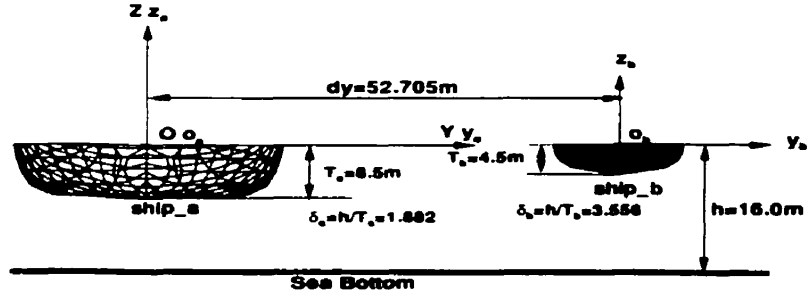

Figure 5.32: Water depth h=16.0m for Case 2

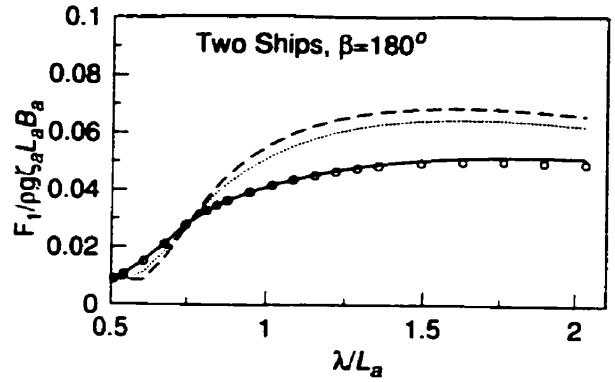

Surge force on ship_a at a separation
Gy=30.0m, dx=45.0m, U=0.0m/s

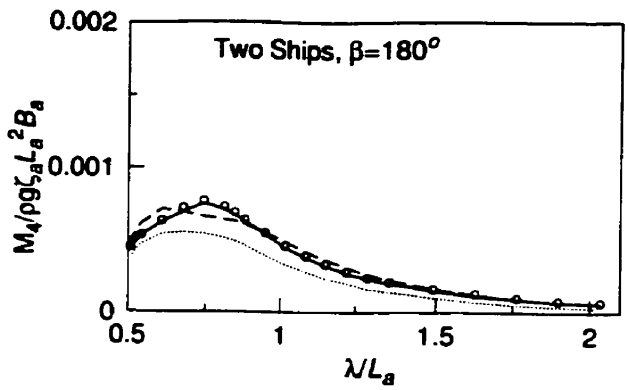

Roll moment on ship_a at a separation
Gy=30.0m, dx=45.0m, U=0.0m/s

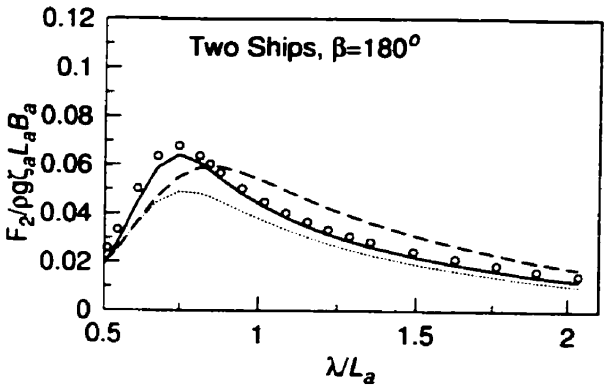

Sway force on ship_a at a separation
Gy=30.0m, dx=45.0m, U=0.0m/s

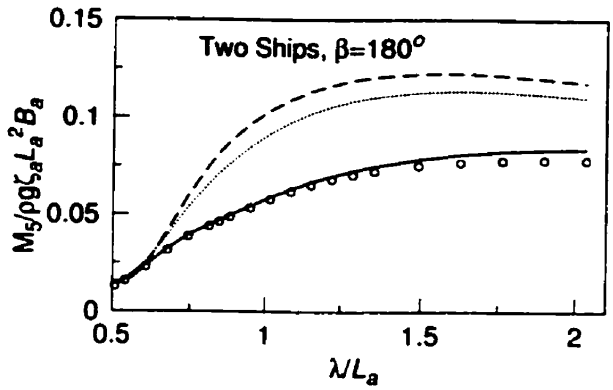

Pitch moment on ship_a at a separation
Gy=30.0m, dx=45.0m, U=0.0m/s

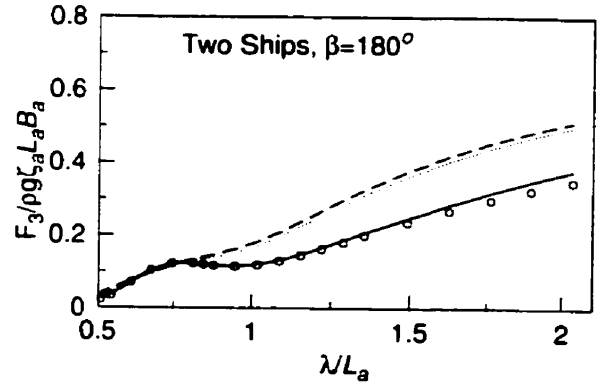

Heave force on ship_a at a separation
Gy=30.0m, dx=45.0m, U=0.0m/s

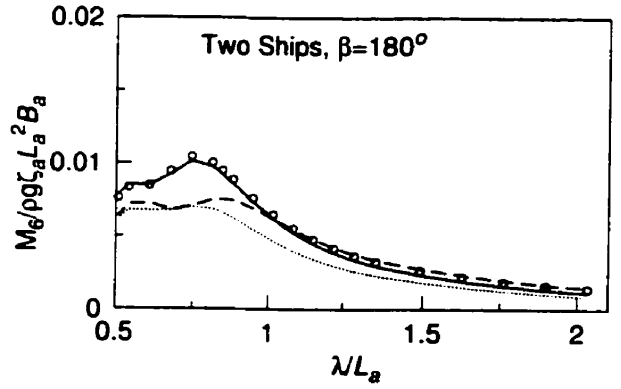

Yaw moment on ship_a at a separation
Gy=30.0m, dx=45.0m, U=0.0m/s

----h=10.2m(δ=1.20), ...h=16.0m(δ=1.88), ——h=90m(δ=10.59), ° ° ° °h=∞(δ=∞)

Figure 5.33: Non-dimensional wave exciting force amplitudes on ship_a in Case 2

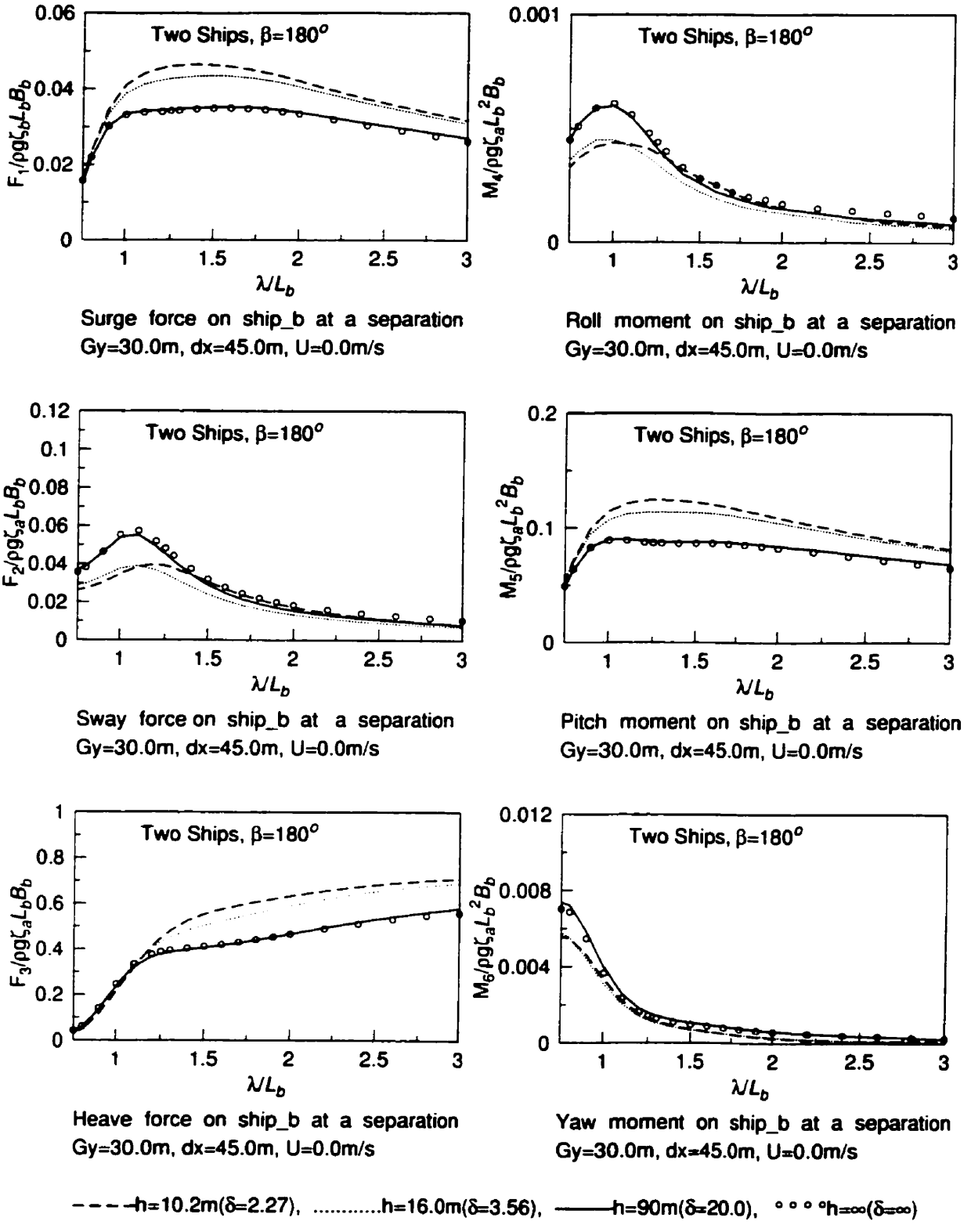

Figure 5.34: Non-dimensional wave exciting force amplitudes on ship_b in Case 2

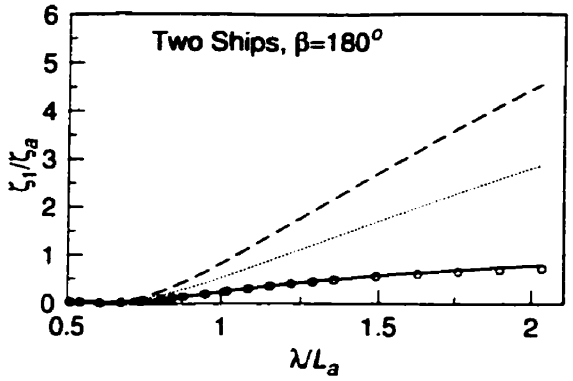

Surge motion of ship_a at a separation
Gy=30.0m, dx=45.0m, U=0.0m/s

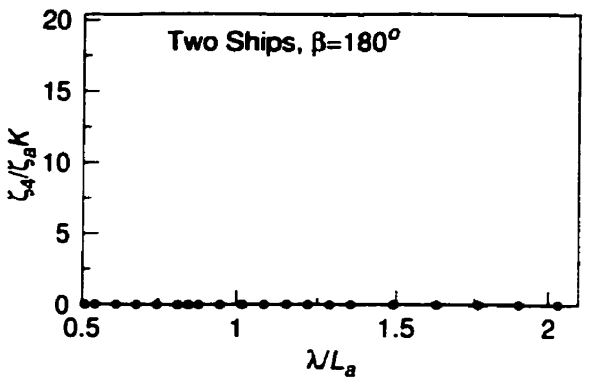

Roll motion of ship_a at a separation
Gy=30.0m, dx=45.0m, U=0.0m/s

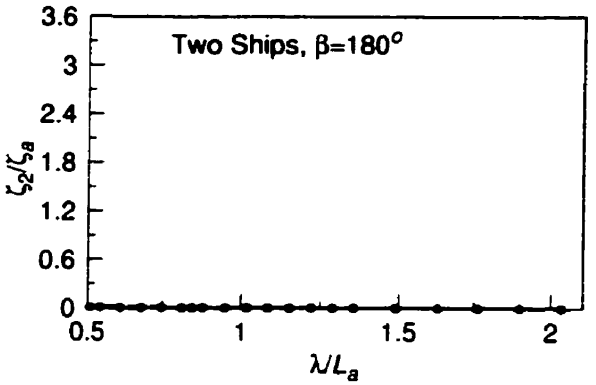

Sway motion of ship_a at a separation
Gy=30.0m, dx=45.0m, U=0.0m/s

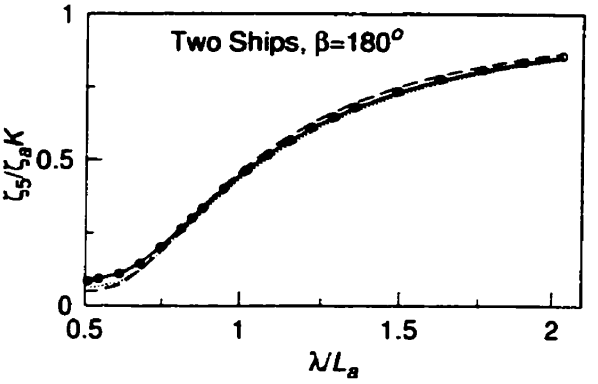

Pitch motion of ship_a at a separation
Gy=30.0m, dx=45.0m, U=0.0m/s

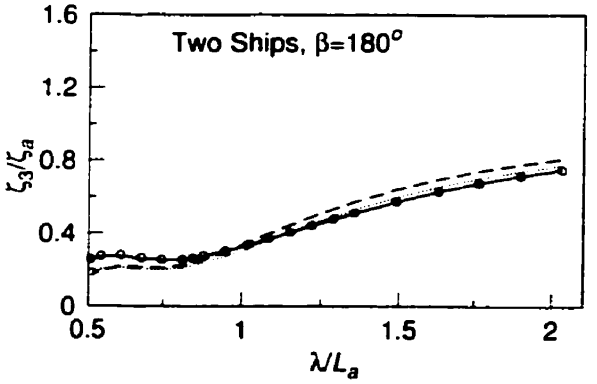

Heave motion of ship_a at a separation
Gy=30.0m, dx=45.0m, U=0.0m/s

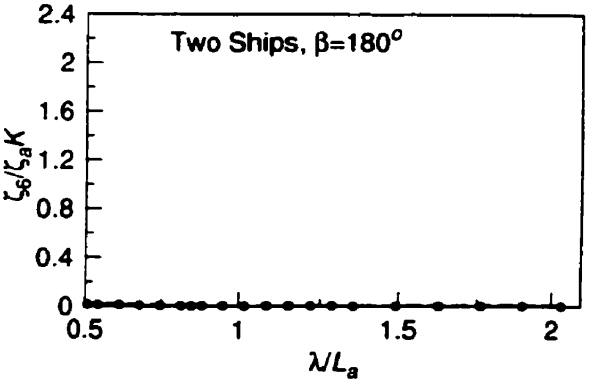

Yaw motion of ship_a at a separation
Gy=30.0m, dx=45.0m, U=0.0m/s

– – – –h=10.2m(δ=1.20), ...h=16.0m(δ=1.88), ——h=90m(δ=10.59), ° ° ° °h=∞(δ=∞)

Figure 5.35: Non-dimensional motion displacement amplitudes on ship_a in Case 2

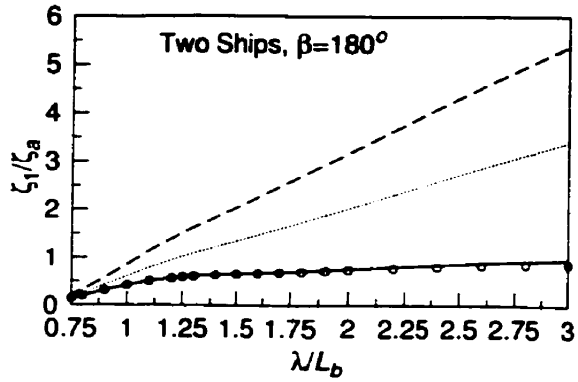

Surge motion of ship_b at a separation
Gy=30.0m, dx=45.0m, U=0.0m/s

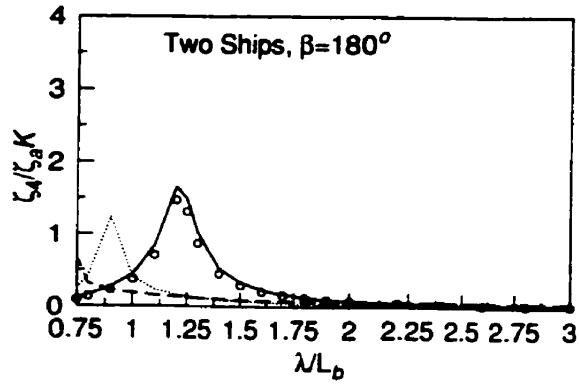

Roll motion of ship_b at a separation
Gy=30.0m, dx=45.0m, U=0.0m/s

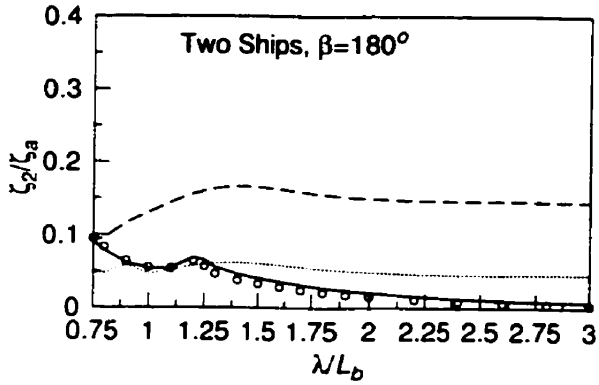

Sway motion of ship_b at a separation
Gy=30.0m, dx=45.0m, U=0.0m/s

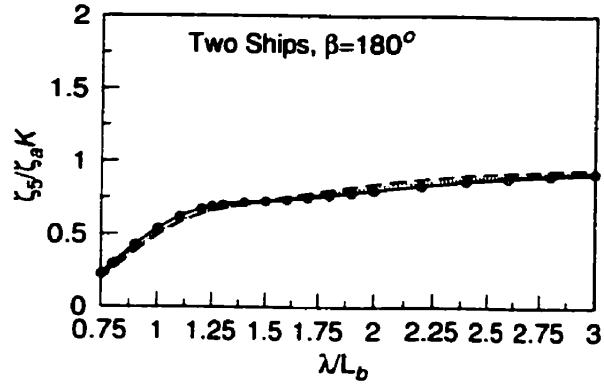

Pitch motion of ship_b at a separation
Gy=30.0m, dx=45.0m, U=0.0m/s

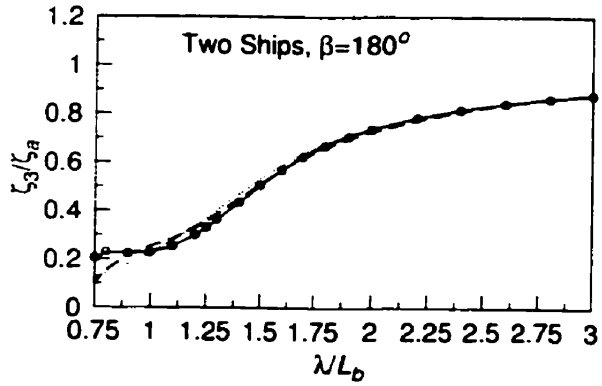

Heave motion of ship_b at a separation
Gy=30.0m, dx=45.0m, U=0.0m/s

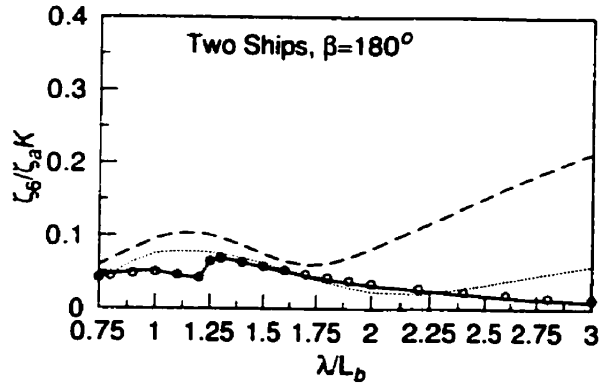

Yaw motion of ship_b at a separation
Gy=30.0m, dx=45.0m, U=0.0m/s

– – – h=10.2m(δ=2.27), ... h=16.0m(δ=3.56), ——— h=90m(δ=20.0), ° ° ° h=∞(δ=∞)

Figure 5.36: Non-dimensional motion displacement amplitudes on ship_b in Case 2

5.2.6 Case 3

The arrangement of the panelized ship_a and ship_b is shown in Figure 5.37. Wave heading $\beta = 180^o$; lateral separation $dy = 2022.705m$ and gap $Gy = 2000.0m$; longitudinal separation dx=0.0m; and forward speed $U = 0.0m/s$ are all shown in Figure 5.38. Figure 5.39 and Figure 5.40 show the positions of ship_a and ship_b relative to the sea bottom for water depths of $h = 10.2m$ and $h = 16.0m$, respectively.

Discussions on Case 3

The lateral separation was set far enough to consider ship_a and ship_b performing individually. The wave exciting forces and ship motions solely come from the water depth effect. There is no interaction effect involved in this case. In Figure 5.41, wave exciting forces are given for ship_a. Based on the results of this case, we may say that the surge, heave and pitch forces in shallow water as in Case 1 was found mainly coming from the water depth effect, and the moments for sway, roll and yaw mainly coming from the interaction effect. Very similar phenomena have been shown in Figure 5.42 for ship_b. In Figure 5.43, comparing with Case 1, the ship_a motions were not changed by the interaction forces, only the surge motion is sensitive to both the water depth and λ/L_a. In Figure 5.44, only the surge motion of ship_b itself affected by the water depth. Also, comparing with Case 1, we may say that, for head sea, the smaller ship motion would be affected by the larger ship's existence and would take more risk in shallow water than in deep water.

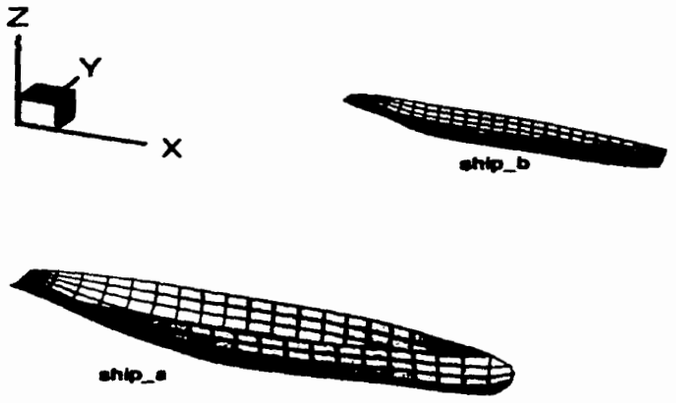

Figure 5.37: Panelized ship_a and ship_b for Case 3

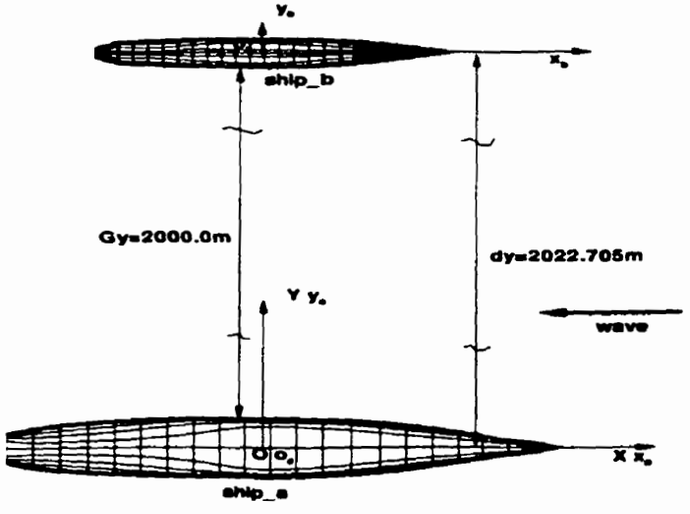

Figure 5.38: Relative position of two ships: $dx = 0.0m$, $Gy = 2000.0m$ for Case 3

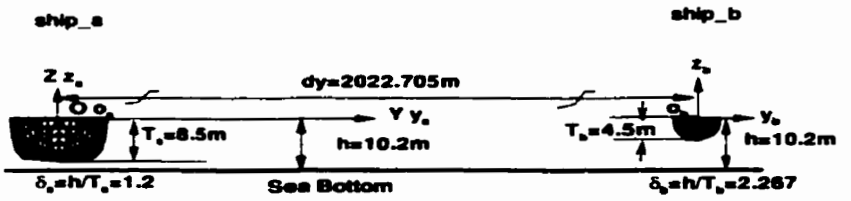

Figure 5.39: Water depth h=10.2m for Case 3

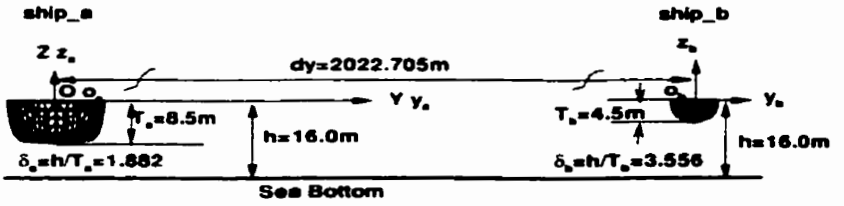

Figure 5.40: Water depth h=16.0m for Case 3

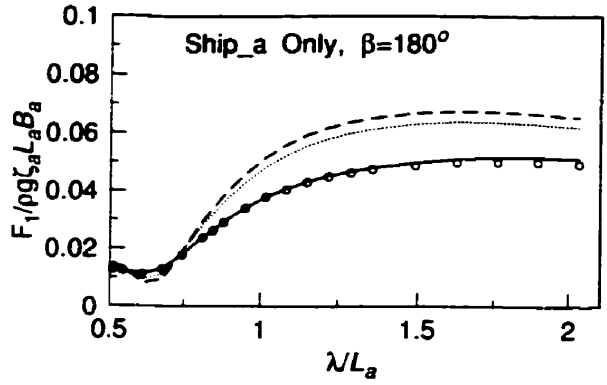

Surge force on ship_a at a separation
Gy=2000.0m, dx=0.0m, U=0.0m/s

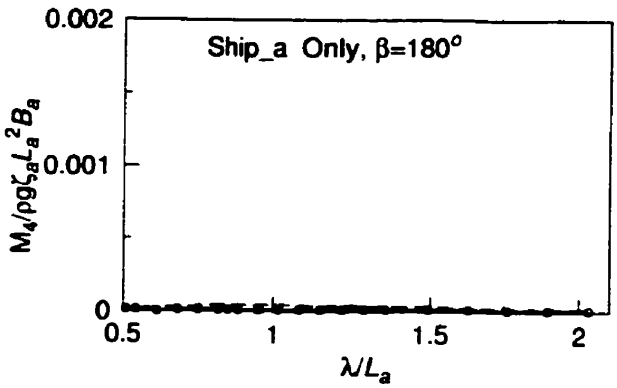

Roll moment on ship_a at a separation
Gy=2000.0m, dx=0.0m, U=0.0m/s

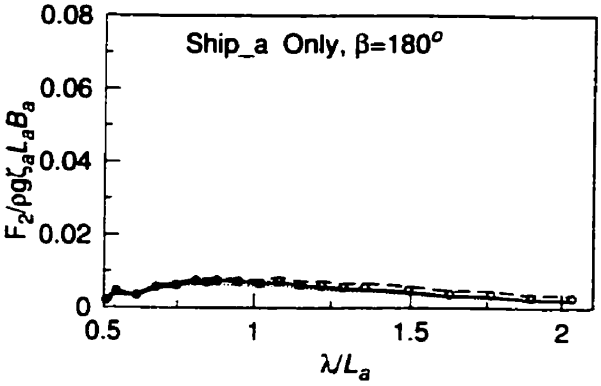

Sway force on ship_a at a separation
Gy=2000.0m, dx=0.0m, U=0.0m/s

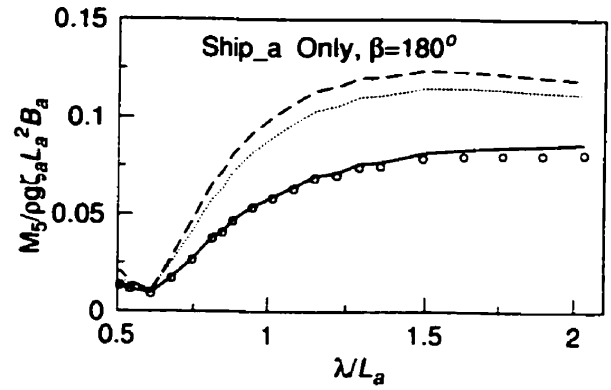

Pitch moment on ship_a at a separation
Gy=2000.0m, dx=0.0m, U=0.0m/s

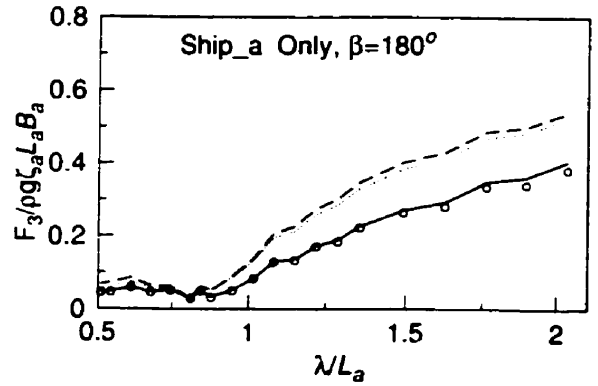

Heave force on ship_a at a separation
Gy=2000.0m, dx=0.0m, U=0.0m/s

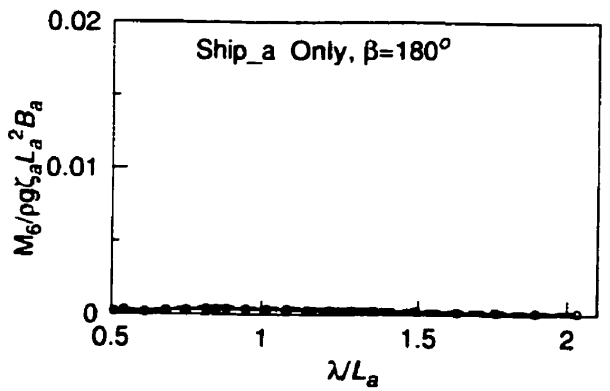

Yaw moment on ship_a at a separation
Gy=2000.0m, dx=0.0m, U=0.0m/s

----h=10.2m(δ=1.20), ...h=16.0m(δ=1.88), ——h=90m(δ=10.59), ° ° ° °h=∞(δ=∞)

Figure 5.41: Non-dimensional wave exciting force amplitudes on ship_a in case 3

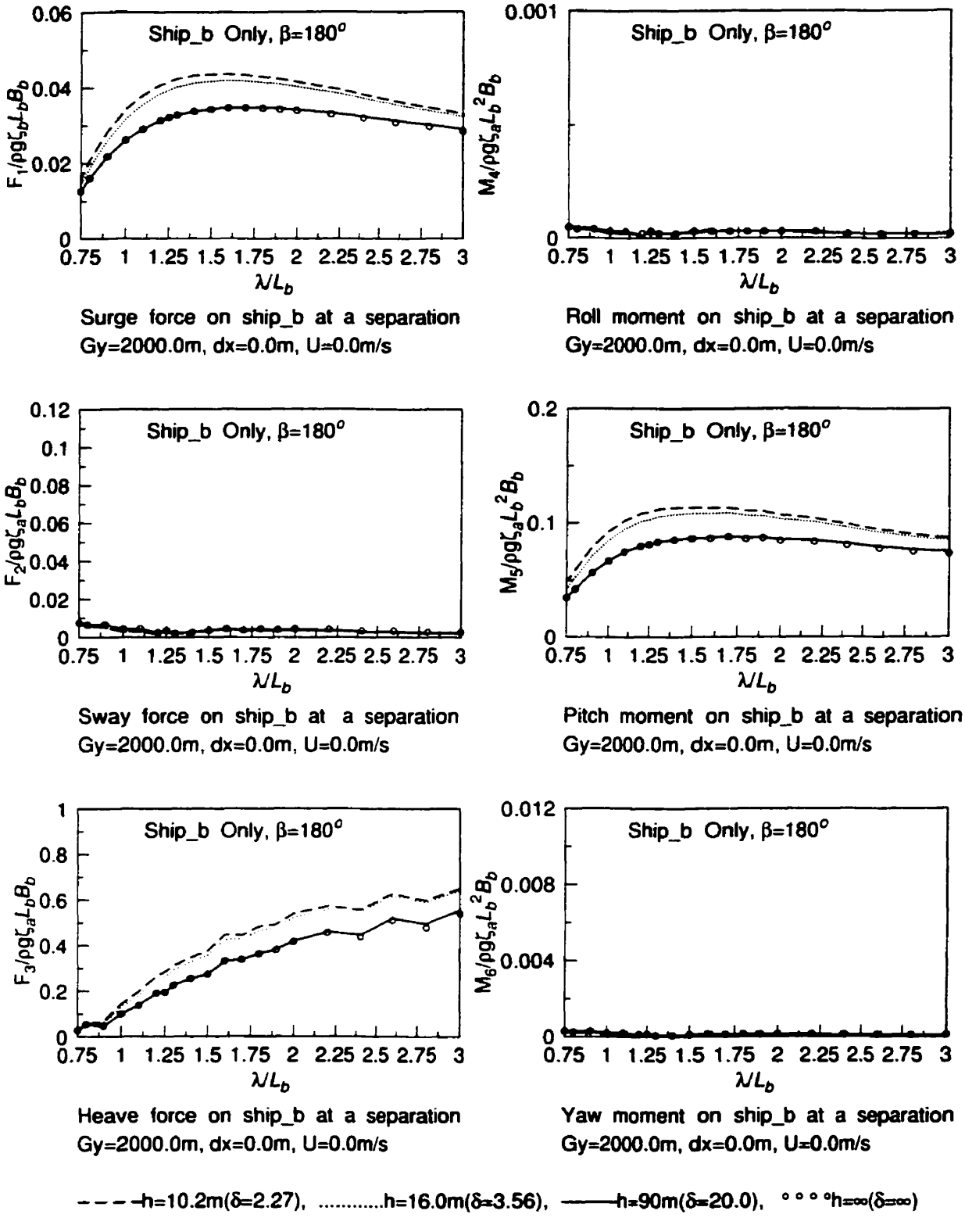

Figure 5.42: Non-dimensional wave exciting force amplitudes on ship_b in Case 3

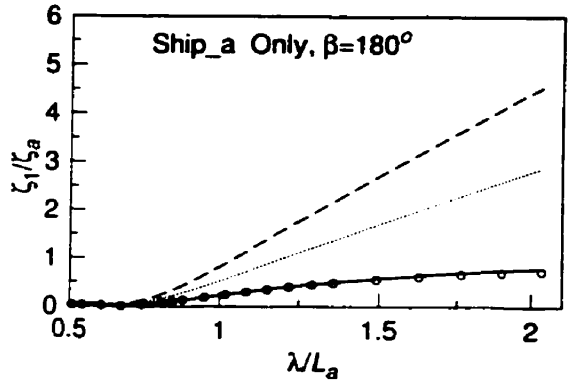

Surge motion of ship_a at a separation
Gy=2000.0m, dx=0.0m, U=0.0m/s

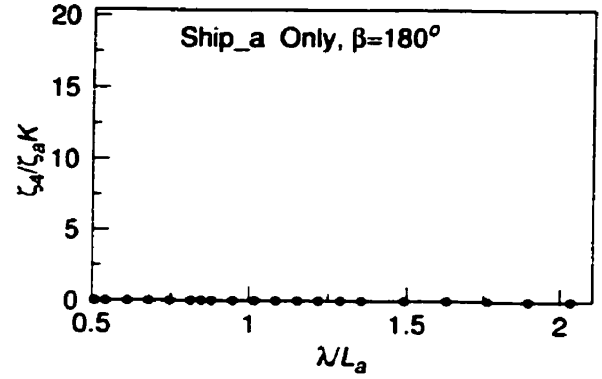

Roll motion of ship_a at a separation
Gy=2000.0m, dx=0.0m, U=0.0m/s

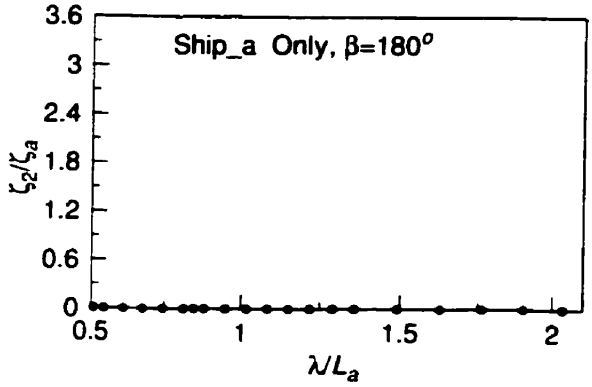

Sway motion of ship_a at a separation
Gy=2000.0m, dx=0.0m, U=0.0m/s

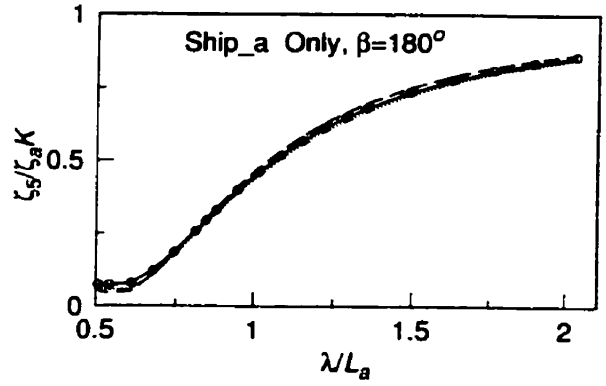

Pitch motion of ship_a at a separation
Gy=2000.0m, dx=0.0m, U=0.0m/s

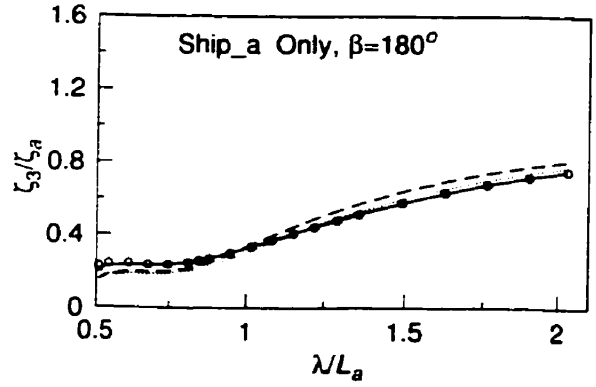

Heave motion of ship_a at a separation
Gy=2000.0m, dx=0.0m, U=0.0m/s

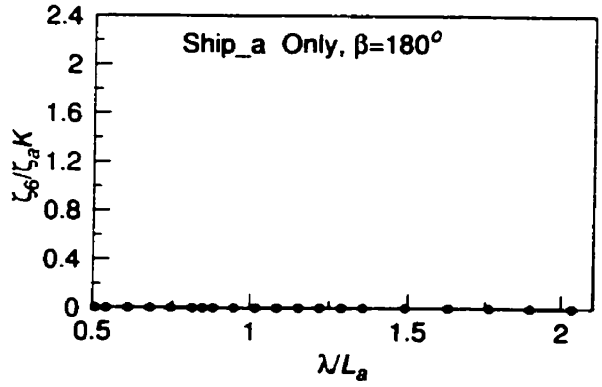

Yaw motion of ship_a at a separation
Gy=2000.0m, dx=0.0m, U=0.0m/s

----h=10.2m(δ=1.20), ...h=16.0m(δ=1.88), ——h=90m(δ=10.59), ° ° ° °h=∞(δ=∞)

Figure 5.43: Non-dimensional motion displacement amplitudes on ship_a in Case 3

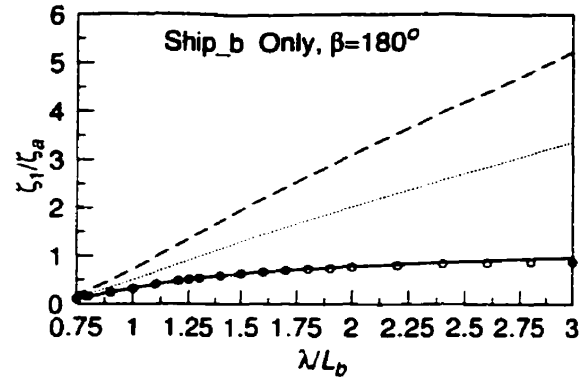

Surge motion of ship_b at a separation
Gy=2000.0m, dx=0.0m, U=0.0m/s

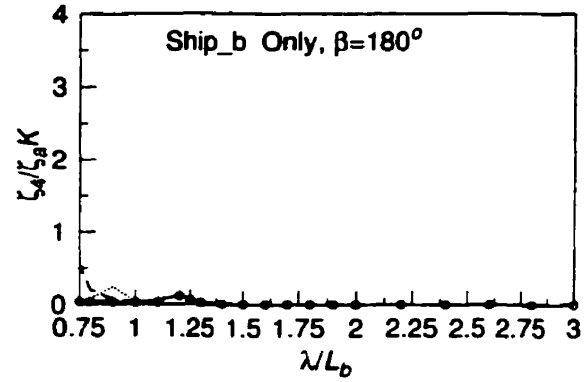

Roll motion of ship_b at a separation
Gy=2000.0m, dx=0.0m, U=0.0m/s

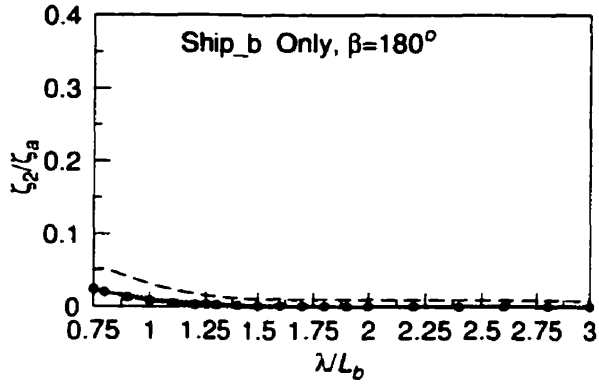

Sway motion of ship_b at a separation
Gy=2000.0m, dx=0.0m, U=0.0m/s

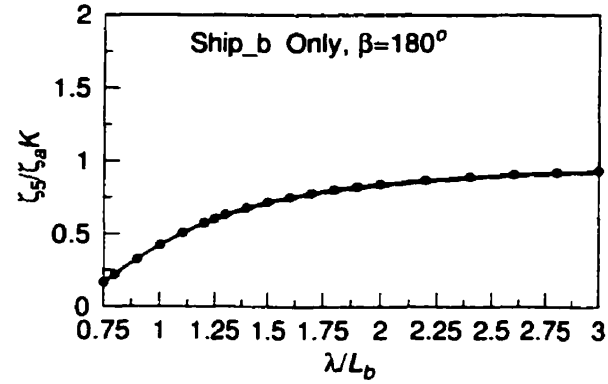

Pitch motion of ship_b at a separation
Gy=2000.0m, dx=0.0m, U=0.0m/s

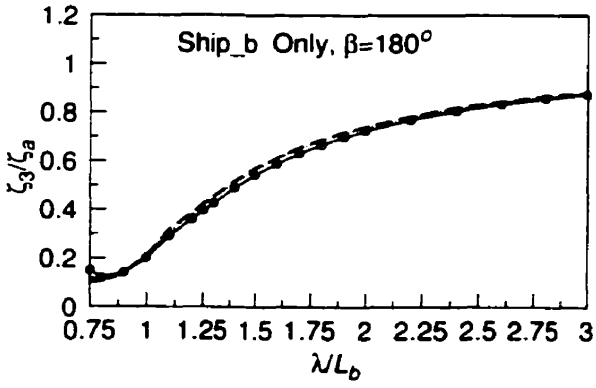

Heave motion of ship_b at a separation
Gy=2000.0m, dx=0.0m, U=0.0m/s

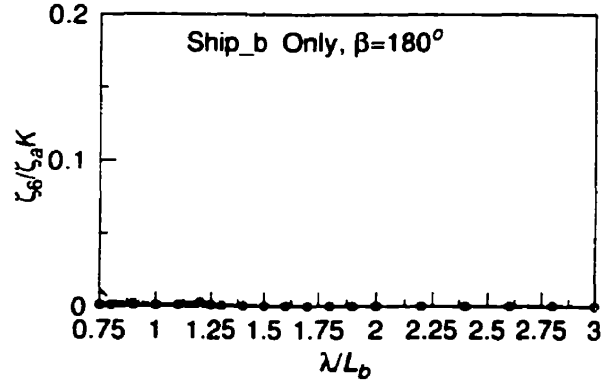

Yaw motion of ship_b at a separation
Gy=2000.0m, dx=0.0m, U=0.0m/s

– – – –h=10.2m(δ=2.27), ...h=16.0m(δ=3.56), ———h=90m(δ=20.0), ° ° ° °h=∞(δ=∞)

Figure 5.44: Non-dimensional motion displacement amplitudes on ship_b in Case 3

5.2.7 Case 4

The arrangement of the panelized ship_a and ship_b is shown in Figure 5.45. Wave heading $\beta = 150^o$; lateral separation $dy = 52.705m$ and gap $Gy = 30.0m$: longitudinal separation dx=0.0m: and forward speed $U = 0.0m/s$ are all shown in Figure 5.46. Figure 5.47 and Figure 5.48 give the positions of ship_a and ship_b relative to the sea bottom for water depths of $h = 10.2m$ and $h = 16.0m$, respectively.

Discussions on Case 4

In this case, the effects of oblique wave, $\beta = 150^o$, on the interaction wave exciting forces and motions were examined. In Figure 5.49, the wave exciting forces are given for ship_a. Comparing with the head sea case (Case 1), there is a prominent water depth effect on forces for sway, roll and yaw. But forces for surge, heave and pitch are less affected. In Figure 5.50, the wave exciting forces of ship_b are given. Comparing with Case 1, the water depth has more effects on sway, heave, roll and yaw. However, the wave exciting forces for ship_b are less affected by oblique wave than that of ship_a. This is because $\delta_a < \delta_b$, ship_a is more sensitive to the shallower water effect than ship_b. In Figure 5.51, the motions of ship_a are shown. Comparing with head sea case (Case 1), the sway, roll and yaw motions are affected by the water depth. The motion amplitudes of sway and yaw are proportional to the ratio of λ/L_a. The motion resonance peak starts to appear for the roll motion in the shallow water region. The surge motion is close to the head sea case (Case 1). Therefore, the oblique wave has a considerable effect on the motion behavior of the larger ship motion.

The motions of ship_b are given in Figure 5.52. Comparing with corresponding case in Case 1, the surge motion is almost 12 times greater than that of Case 1 when $\lambda/L_b = 3.0$ and water depth $h = 10.2m$. This effect is remarkable. In the roll motion, the resonance peak shifts toward the lower value of λ/L_b when the water depth gets shallower. The yaw motion is about 17 times greater than that of Case 1. The surge motion is not changed much compared with Case 1. Based on above observation, it has been found that the oblique wave affects the smaller ship's seakeeping and manoeuvring characteristics, particularly when it couples with the larger ship's motion.

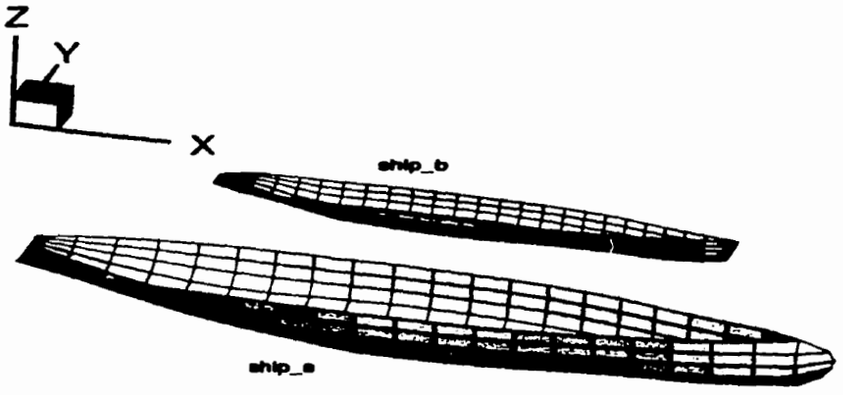

Figure 5.45: Panelized ship_a and ship_b for Case 4

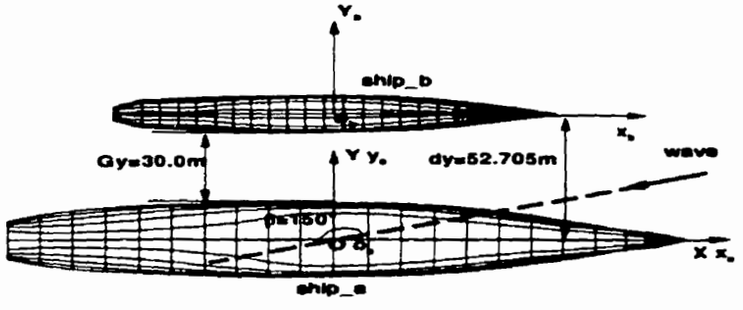

Figure 5.46: Relative position of two ships: $dx = 0.0m$, $Gy = 30.0m$ for Case 4

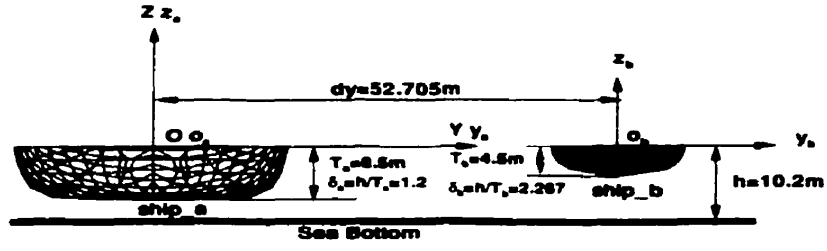

Figure 5.47: Water depth h=10.2m for Case 4

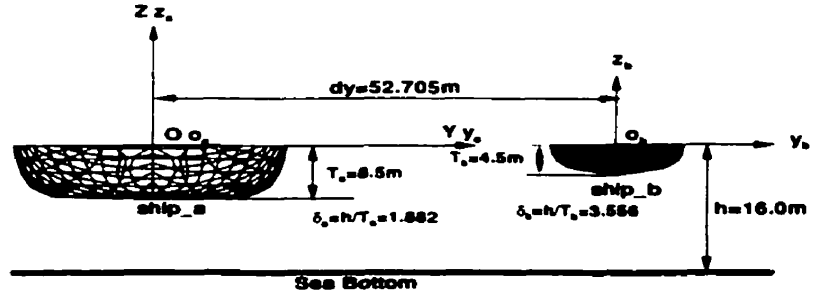

Figure 5.48: Water depth h=16.0m for Case 4

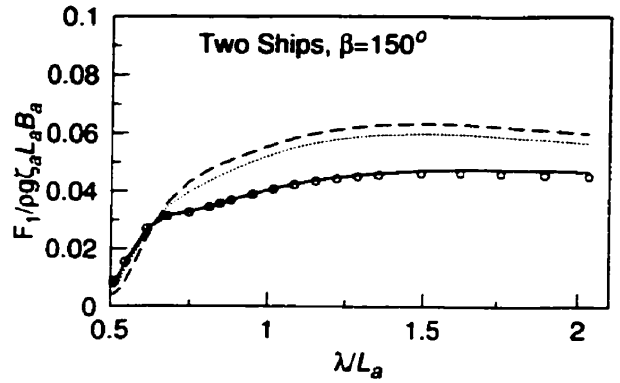

Surge force on ship_a at a separation
Gy=30.0m, dx=0.0m, U=0.0m/s

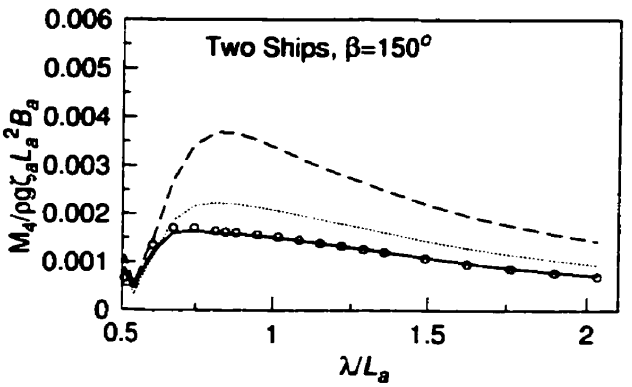

Roll moment on ship_a at a separation
Gy=30.0m, dx=0.0m, U=0.0m/s

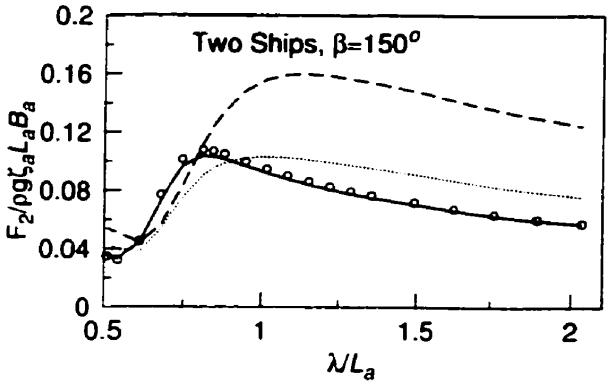

Sway force on ship_a at a separation
Gy=30.0m, dx=0.0m, U=0.0m/s

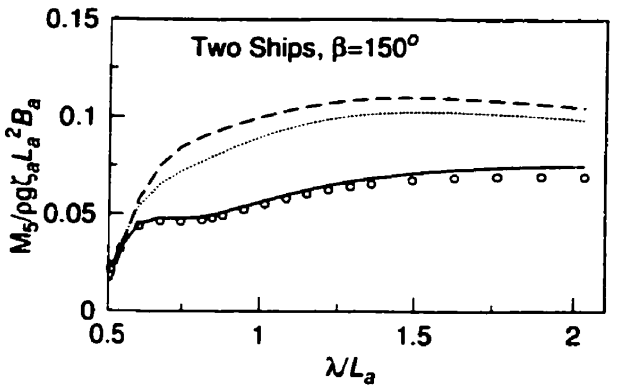

Pitch moment on ship_a at a separation
Gy=30.0m, dx=0.0m, U=0.0m/s

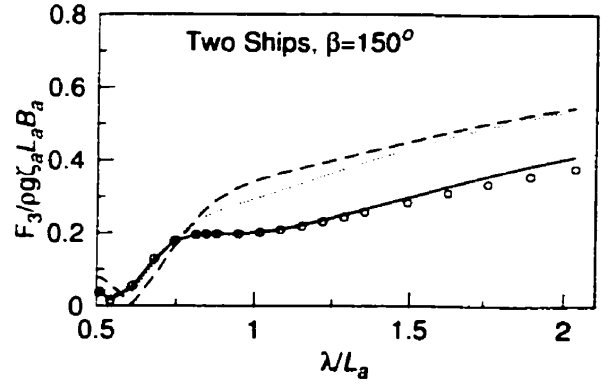

Heave force on ship_a at a separation
Gy=30.0m, dx=0.0m, U=0.0m/s

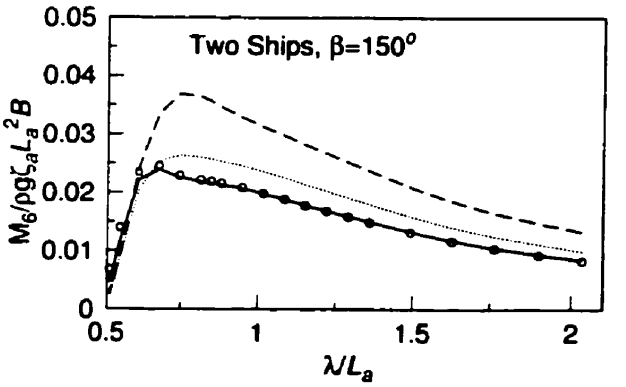

Yaw moment on ship_a at a separation
Gy=30.0m, dx=0.0m, U=0.0m/s

– – – –h=10.2m(δ=1.20), ...h=16.0m(δ=1.88), ——h=90m(δ=10.59), ° ° ° °h=∞(δ=∞)

Figure 5.49: Non-dimensional wave exciting force amplitudes on ship_a in Case 4

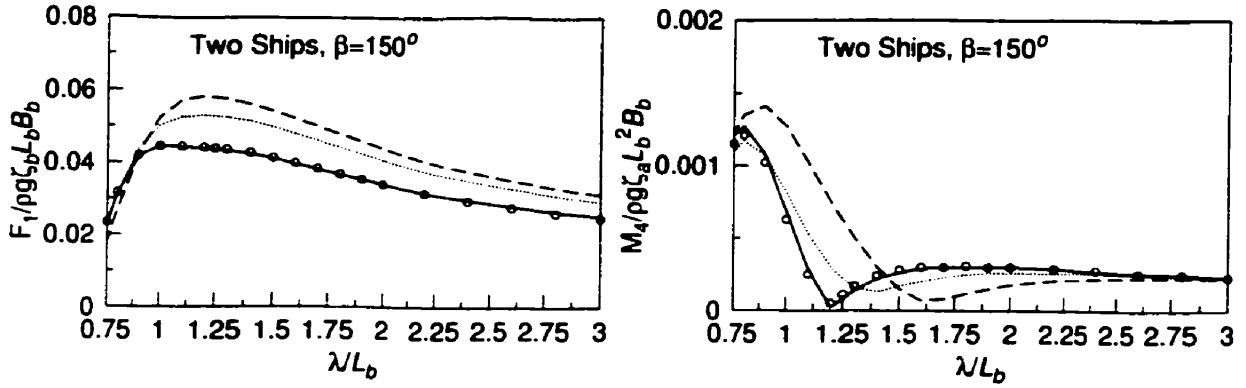

Surge force on ship_b at a separation
Gy=30.0m, dx=0.0m, U=0.0m/s

Roll moment on ship_b at a separation
Gy=30.0m, dx=0.0m, U=0.0m/s

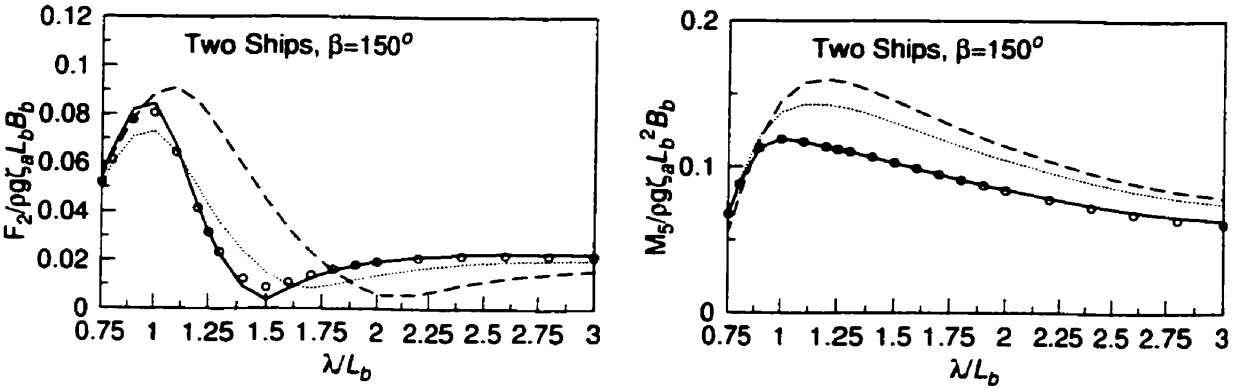

Sway force on ship_b at a separation
Gy=30.0m, dx=0.0m, U=0.0m/s

Pitch moment on ship_b at a separation
Gy=30.0m, dx=0.0m, U=0.0m/s

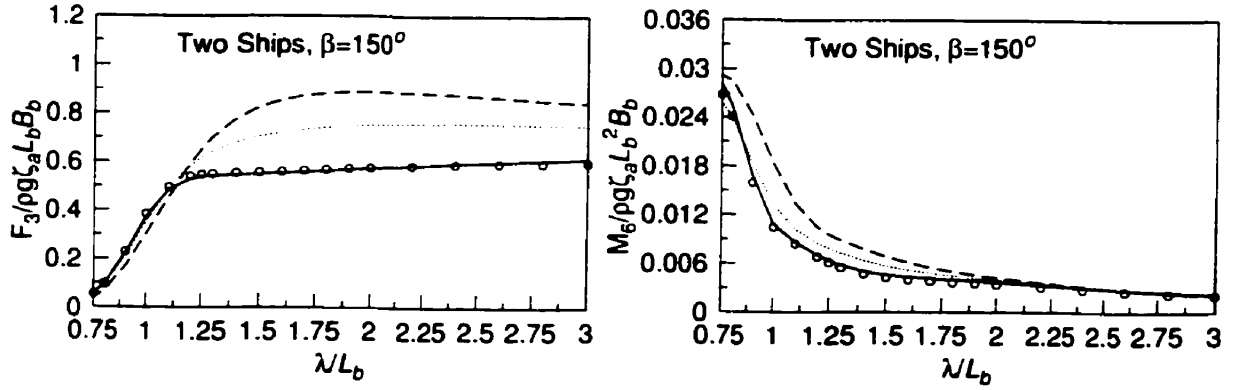

Heave force on ship_b at a separation
Gy=30.0m, dx=0.0m, U=0.0m/s

Yaw moment on ship_b at a separation
Gy=30.0m, dx=0.0m, U=0.0m/s

----h=10.2m(δ=2.27), ...h=16.0m(δ=3.56), ——h=90m(δ=20.0), ° ° ° °h=∞(δ=∞)

Figure 5.50: Non-dimensional wave exciting force amplitudes on ship_b in Case 4

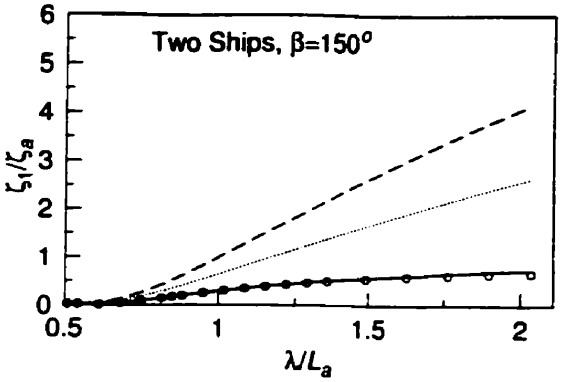

Surge motion of ship_a at a separation
Gy=30.0m, dx=0.0m, U=0.0m/s

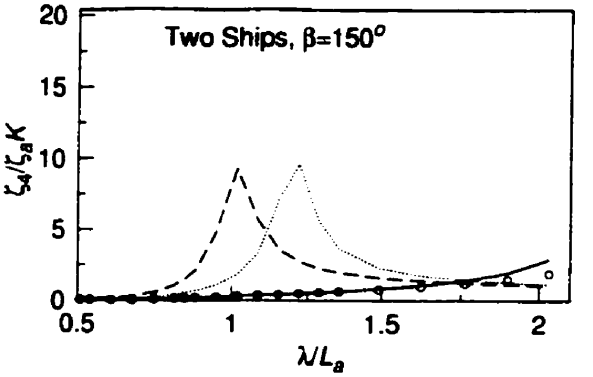

Roll motion of ship_a at a separation
Gy=30.0m, dx=0.0m, U=0.0m/s

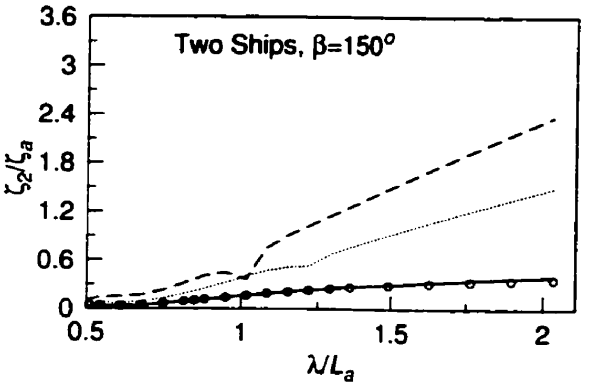

Sway motion of ship_a at a separation
Gy=30.0m, dx=0.0m, U=0.0m/s

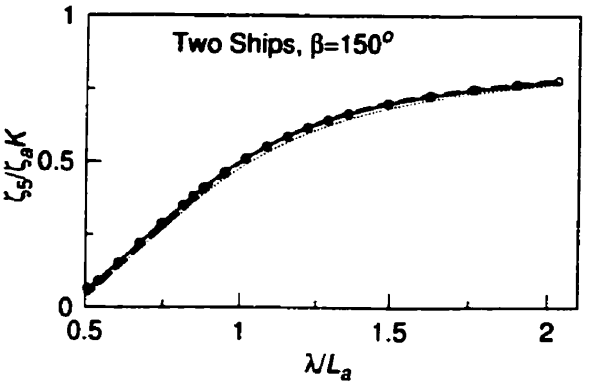

Pitch motion of ship_a at a separation
Gy=30.0m, dx=0.0m, U=0.0m/s

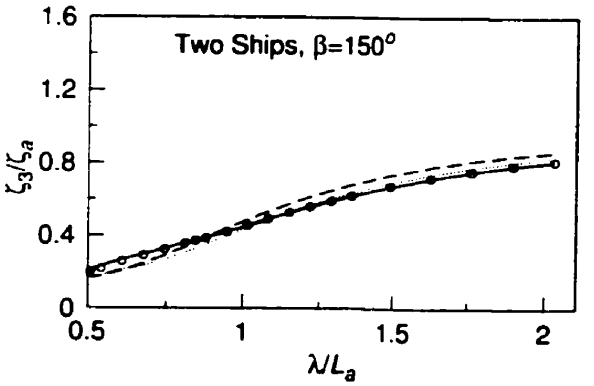

Heave motion of s hip_a at a separation
Gy=30.0m, dx=0.0m, U=0.0m/s

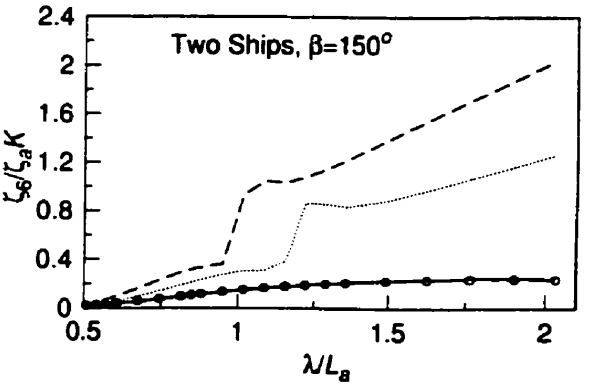

Yaw motion of ship_a at a separation
Gy=30.0m, dx=0.0m, U=0.0m/s

----h=10.2m(δ=1.20), ...h=16.0m(δ=1.88), ——h=90m(δ=10.59), ° ° ° °h=∞(δ=∞)

Figure 5.51: Non-dimensional motion displacement amplitudes on ship_a in Case 4

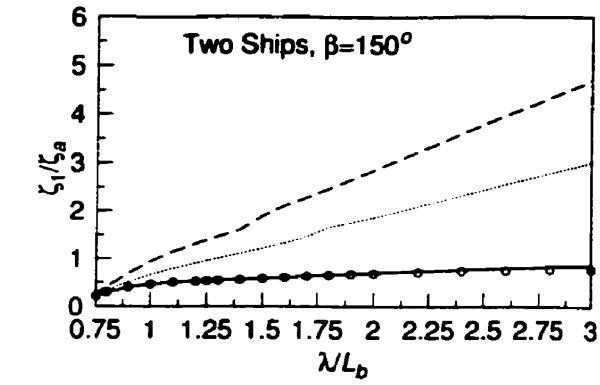

Surge motion of ship_b at a separation
Gy=30.0m, dx=0.0m, U=0.0m/s

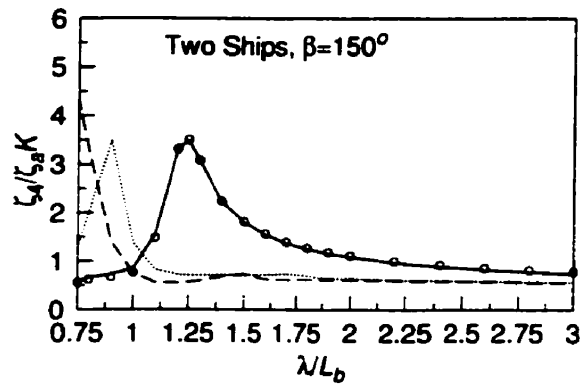

Roll motion of ship_b at a separation
Gy=30.0m, dx=0.0m, U=0.0m/s

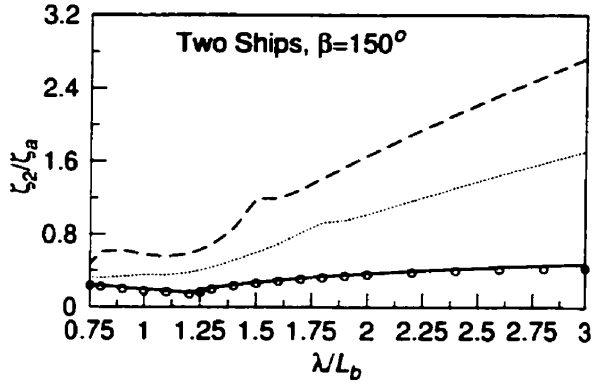

Sway motion of ship_b at a separation
Gy=30.0m, dx=0.0m, U=0.0m/s

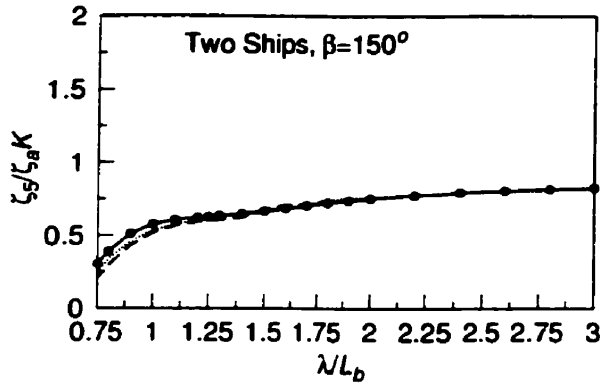

Pitch motion of ship_b at a separation
Gy=30.0m, dx=0.0m, U=0.0m/s

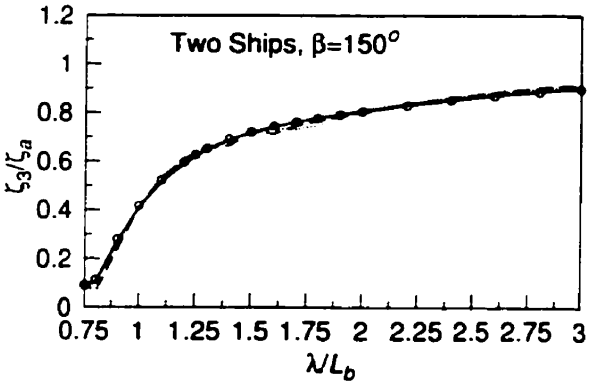

Heave motion of ship_b at a separation
Gy=30.0m, dx=0.0m, U=0.0m/s

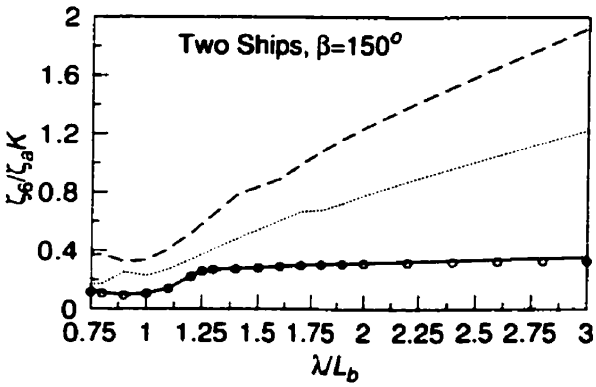

Yaw motion of ship_b at a separation
Gy=30.0m, dx=0.0m, U=0.0m/s

– – – –h=10.2m(δ=2.27), ...h=16.0m(δ=3.56), ———h=90m(δ=20.0), ° ° ° °h=∞(δ=∞)

Figure 5.52: Non-dimensional motion displacement amplitudes on ship_b in Case 4

5.2.8 Case 5

Figure 5.53 shows the panelized ship_a and ship_b. Wave heading $\beta = 150°$: lateral separation $dy = 52.705m$ and gap $Gy = 30.0m$; longitudinal separation dx=45.0m: and forward speed $U = 0.0m/s$ are all shown in Figure 5.54. Figure 5.55 and Figure 5.56 give the positions of ship_a and ship_b relative to the sea bottom for water depths of $h = 10.2m$ and $h = 16.0m$, respectively.

Discussions on Case 5

This case was set to observe the effect of longitudinal separation distance dx in a oblique wave with heading $\beta = 150°$. From Figure 5.57, comparing with Case 4, dx only affects slightly on the sway wave exciting force for ship_a. From Figure 5.58, comparing with Case 4, the effect of dx is only shown on the surge and pitch wave exciting forces for ship_b. In Figure 5.59, the roll motion resonance peak is increased and shifted toward the higher λ/L_a value. In Figure 5.60, we have observed that only the ship_b's roll motion is affected by dx.

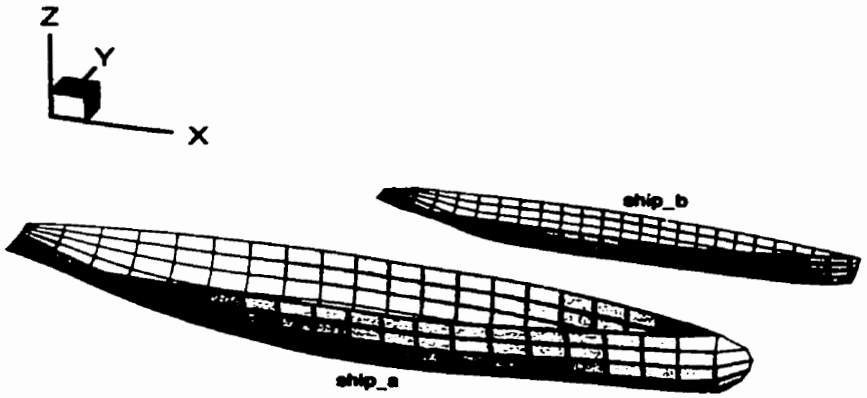

Figure 5.53: Panelized ship_a and ship_b for Case 5

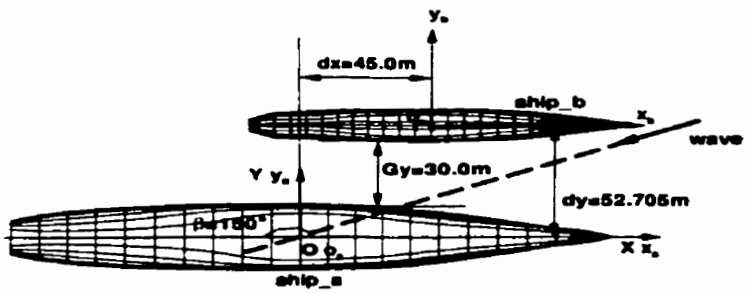

Figure 5.54: Relative position of two ships: $dx = 45.0m$, $Gy = 30.0m$ for Case 5

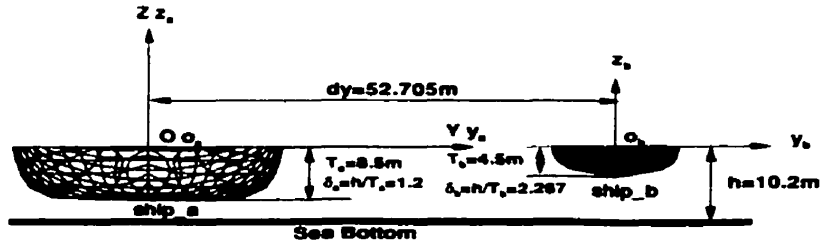

Figure 5.55: Water depth h=10.2m for Case 5

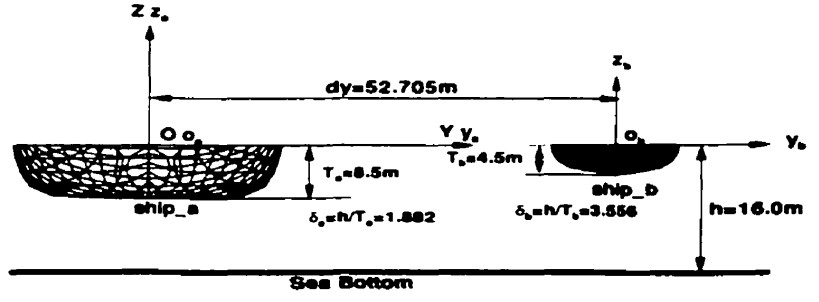

Figure 5.56: Water depth h=16.0m for Case 5

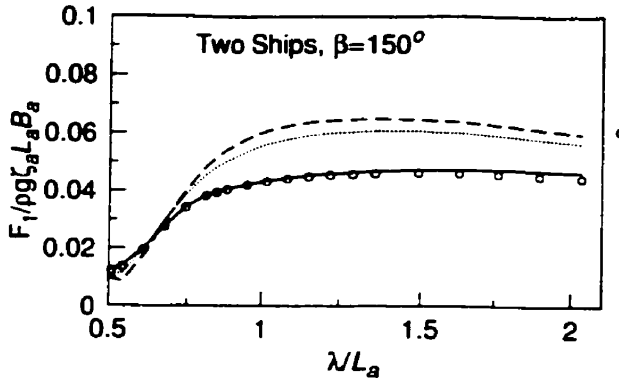

Surge force on ship_a at a separation
Gy=30.0m, dx=0.0m, U=0.0m/s

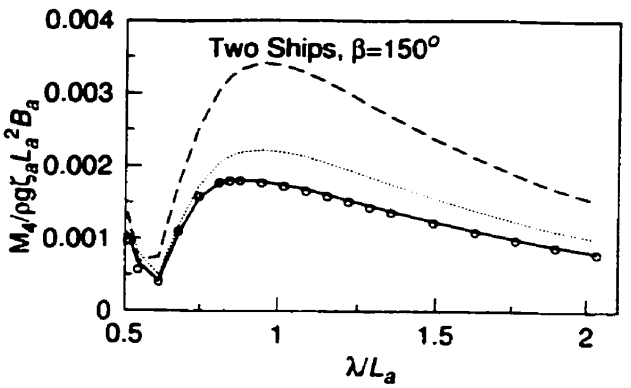

Roll moment on ship_a at a separation
Gy=30.0m, dx=0.0m, U=0.0m/s

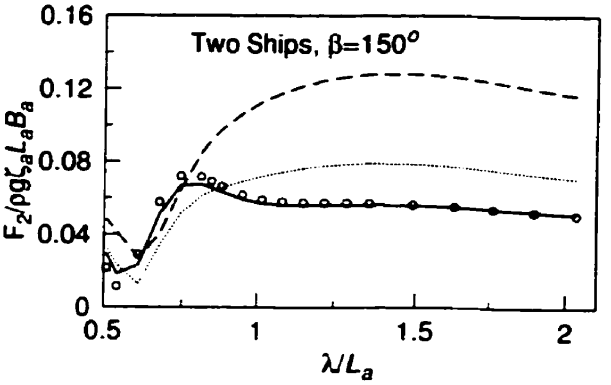

Sway force on ship_a at a separation
Gy=30.0m, dx=0.0m, U=0.0m/s

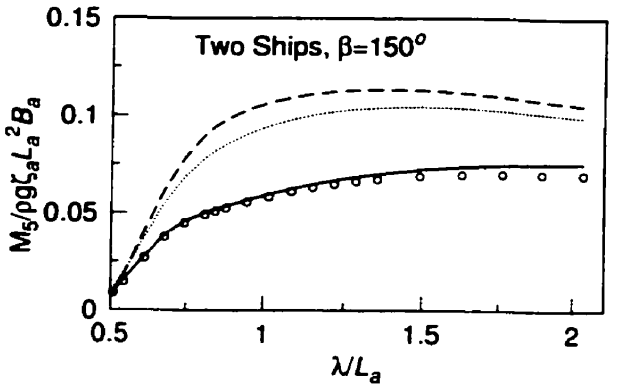

Pitch moment on ship_a at a separation
Gy=30.0m, dx=0.0m, U=0.0m/s

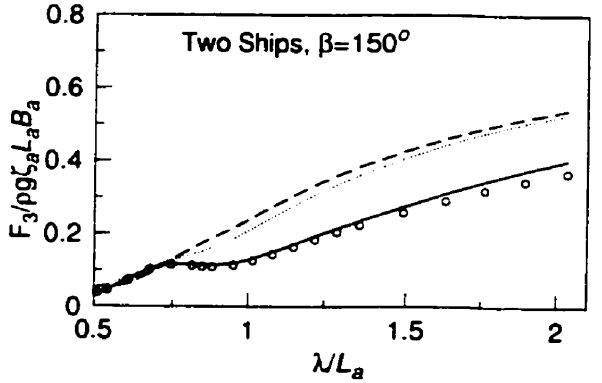

Heave force on ship_a at a separation
Gy=30.0m, dx=0.0m, U=0.0m/s

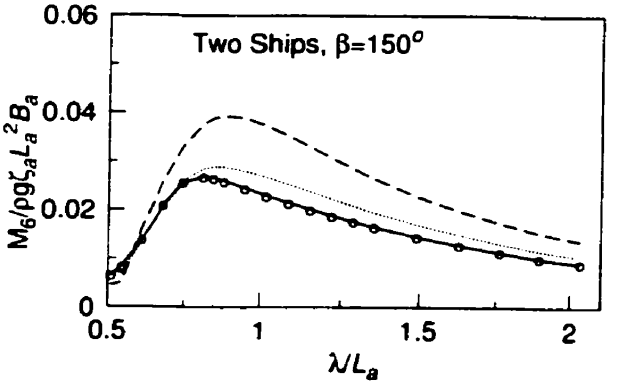

Yaw moment on ship_a at a separation
Gy=30.0m, dx=0.0m, U=0.0m/s

----h=10.2m(δ=1.20), ...h=16.0m(δ=1.88), ——h=90m(δ=10.59), ° ° ° °h=∞(δ=∞)

Figure 5.57: Non-dimensional wave exciting force amplitudes on ship_a in Case 5

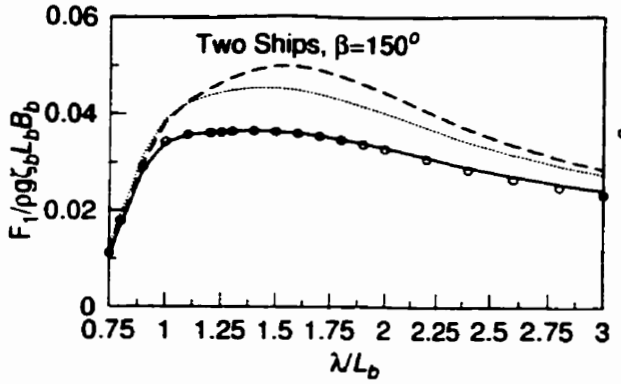

Surge force on ship_b at a separation
Gy=30.0m, dx=0.0m, U=0.0m/s

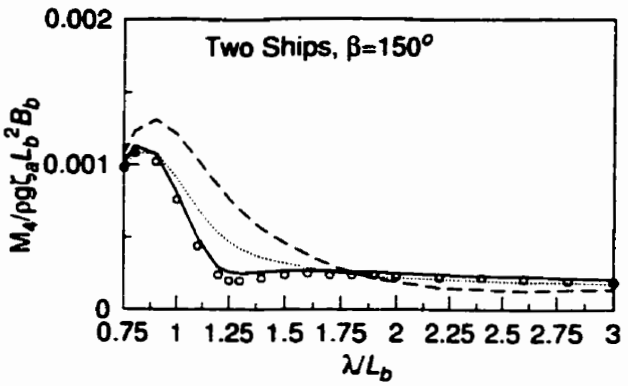

Roll moment on ship_b at a separation
Gy=30.0m, dx=0.0m, U=0.0m/s

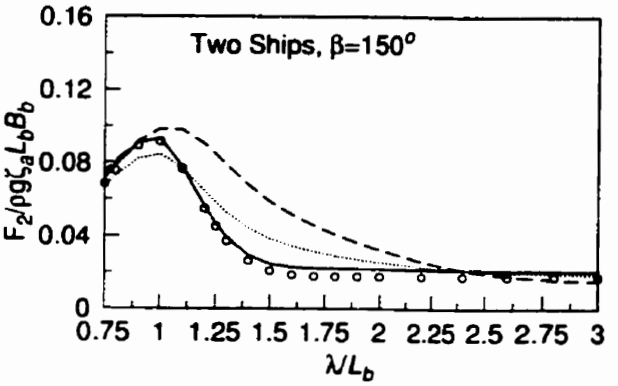

Sway force on ship_b at a separation
Gy=30.0m, dx=0.0m, U=0.0m/s

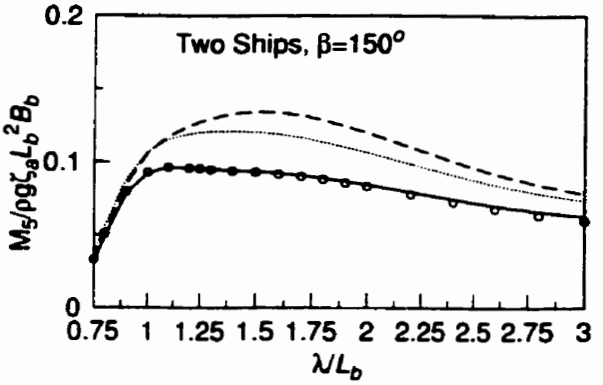

Pitch moment on ship_b at a separation
Gy=30.0m, dx=0.0m, U=0.0m/s

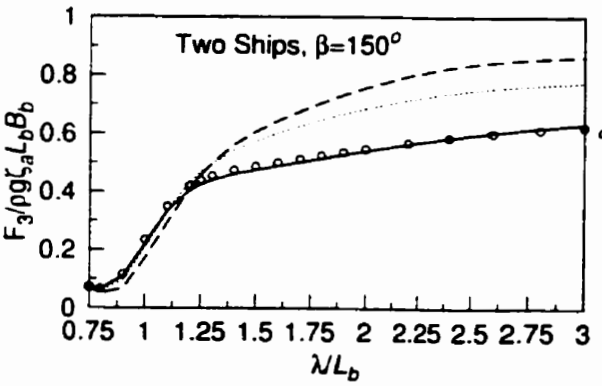

Heave force on ship_b at a separation
Gy=30.0m, dx=0.0m, U=0.0m/s

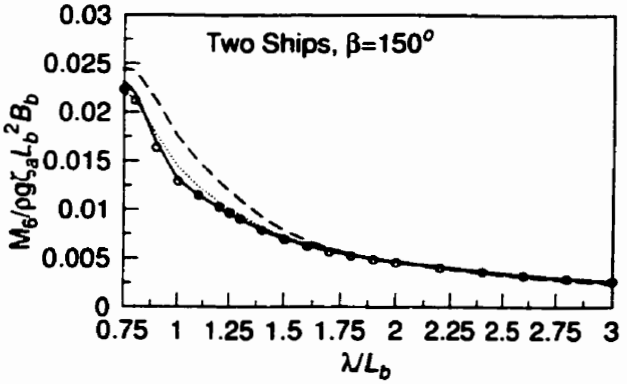

Yaw moment on ship_b at a separation
Gy=30.0m, dx=0.0m, U=0.0m/s

– – – –h=10.2m(δ=2.27), ...h=16.0m(δ=3.56), ——h=90m(δ=20.0), ° ° ° °h=∞(δ=∞)

Figure 5.58: Non-dimensional wave exciting force amplitudes on ship_b in Case 5

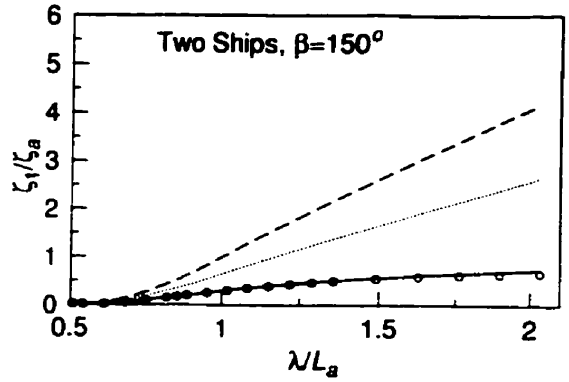

Surge motion of ship_a at a separation
Gy=30.0m, dx=0.0m, U=0.0m/s

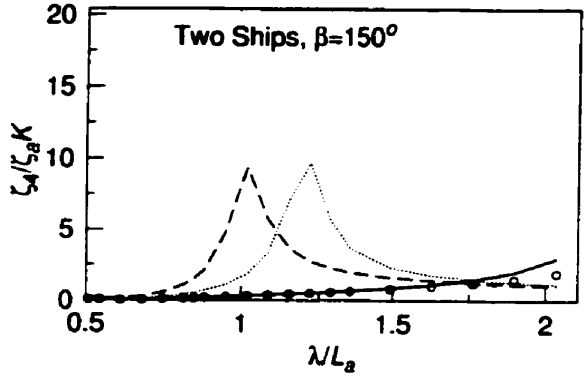

Roll motion of ship_a at a separation
Gy=30.0m, dx=0.0m, U=0.0m/s

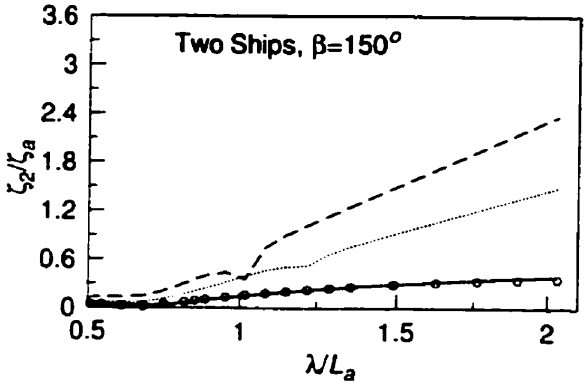

Sway motion of ship_a at a separation
Gy=30.0m, dx=0.0m, U=0.0m/s

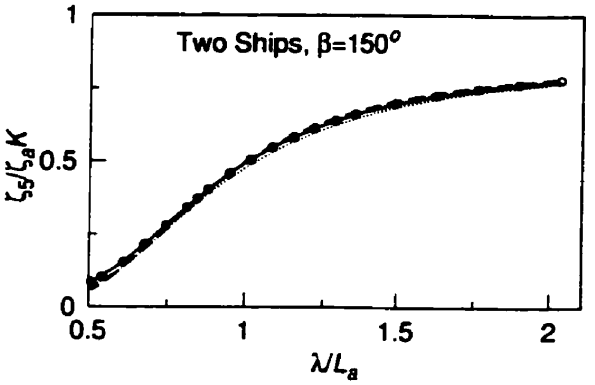

Pitch motion of ship_a at a separation
Gy=30.0m, dx=0.0m, U=0.0m/s

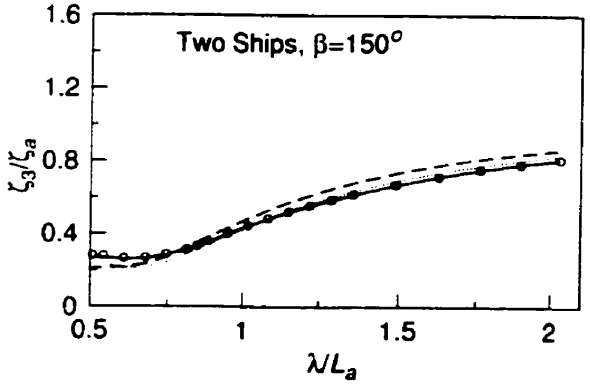

Heave motion of ship_a at a separation
Gy=30.0m, dx=0.0m, U=0.0m/s

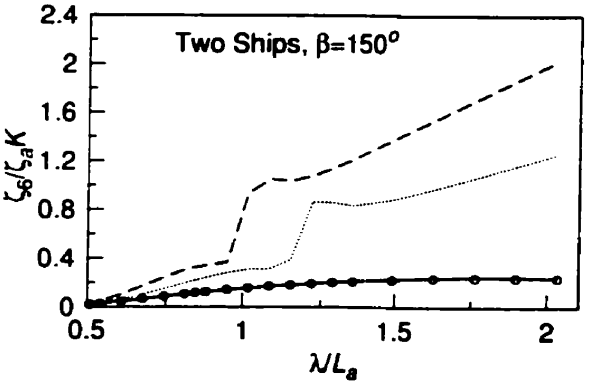

Yaw motion of ship_a at a separation
Gy=30.0m, dx=0.0m, U=0.0m/s

– – – –h=10.2m(δ=1.20), ...h=16.0m(δ=1.88), ——h=90m(δ=10.59), ° ° ° °h=∞(δ=∞)

Figure 5.59: Non-dimensional motion displacement amplitudes on ship_a in Case 5

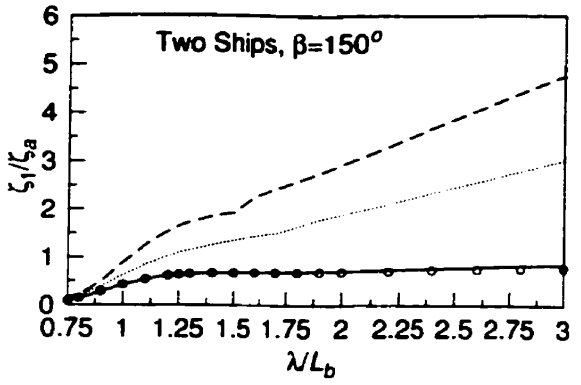

Surge motion of ship_b at a separation
Gy=30.0m, dx=0.0m, U=0.0m/s

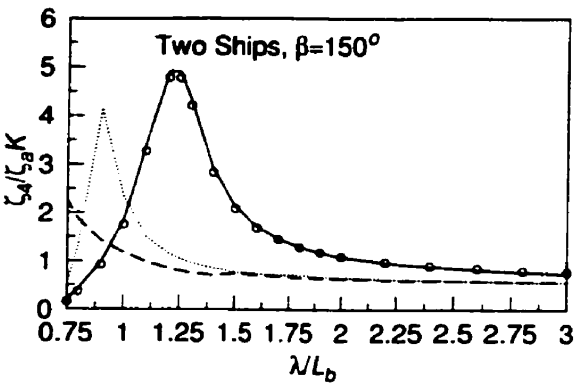

Roll motion of ship_b at a separation
Gy=30.0m, dx=0.0m, U=0.0m/s

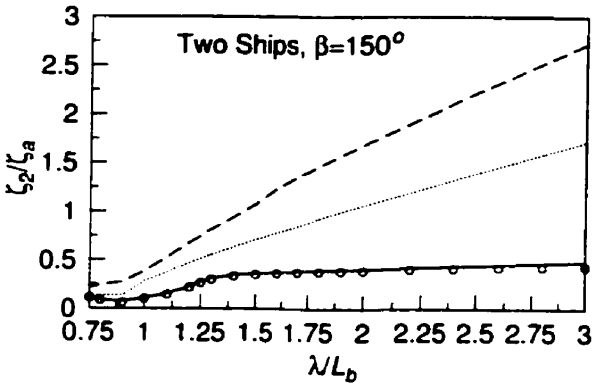

Sway motion of ship_b at a separation
Gy=30.0m, dx=0.0m, U=0.0m/s

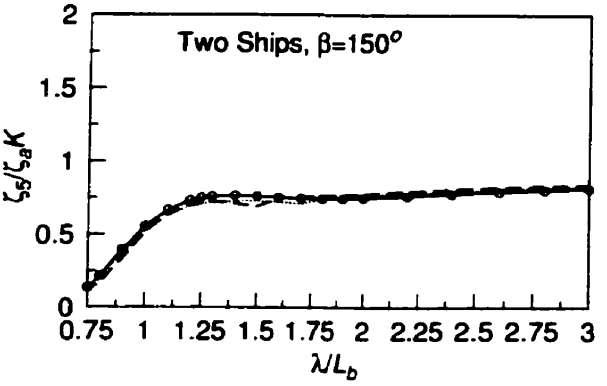

Pitch motion of ship_b at a separation
Gy=30.0m, dx=0.0m, U=0.0m/s

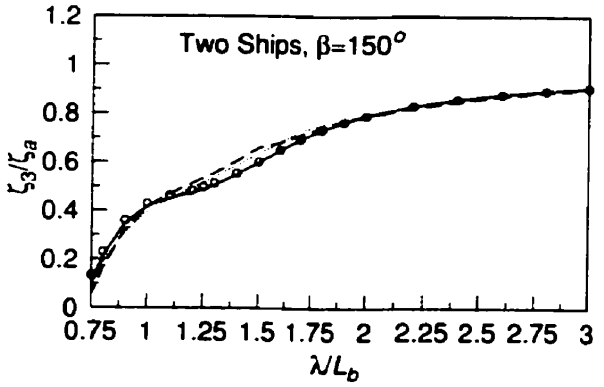

Heave motion of ship_b at a separation
Gy=30.0m, dx=0.0m, U=0.0m/s

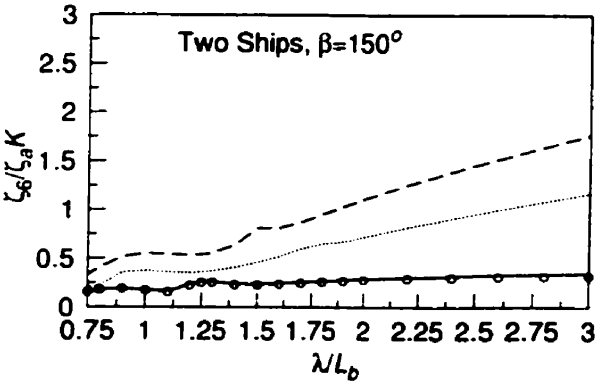

Yaw motion of ship_b at a separation
Gy=30.0m, dx=0.0m, U=0.0m/s

– – – h=10.2m(δ=2.27), ... h=16.0m(δ=3.56), ——— h=90m(δ=20.0), ° ° ° h=∞(δ=∞)

Figure 5.60: Non-dimensional motion displacement amplitudes on ship_b in Case 5

5.2.9 Case 6

The panelized ship_a and ship_b are shown in Figure 5.61. Wave heading $\beta = 150^o$; lateral separation $dy = 2022.705m$ and gap $Gy = 2000.0m$; longitudinal separation dx=0.0m; and forward speed $U = 0.0m/s$ are all shown in Figure 5.62. Figure 5.63 and Figure 5.64 give the positions of ship_a and ship_b relative to the sea bottom for water depths of $h = 10.2m$ and $h = 16.0m$, respectively.

Discussions on Case 6

In order to investigate the effect of water depth on a single ship, the the distance between two ships is set very far with $dy = 2022.705m$. In this case, ship_a and ship_b perform under wave heading $\beta = 150^o$, individually. The wave exciting forces and motions do not include the interaction effect between two ships for this case. In Figure 5.65, comparing this case with case 4, the surge force of ship_a mainly comes from the effect of water depth. and the wave exciting forces in the other modes of motion all have the interaction effect. In Figure 5.66, comparing with this case, the wave exciting forces of ship_b in Case 4 involve a considerable interaction forces in all modes of motion. Therefore, the interaction forces cannot be neglected in the shallow water region. In Figure 5.67, the ship_a motions are not affected much by the interaction forces. In Figure 5.68, the ship_b's roll motion resonance peak value is decreased and shifted in shallow water compared with that in deep water.

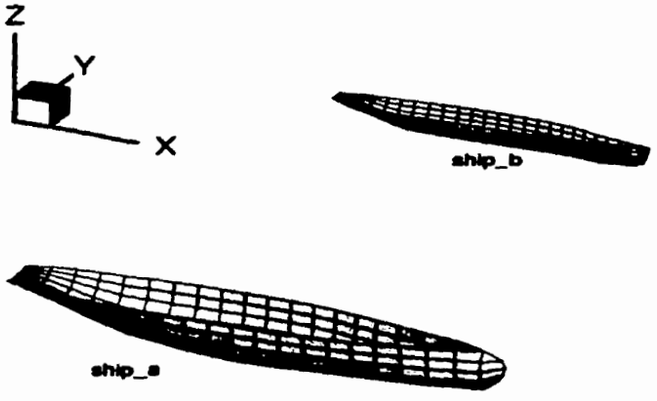

Figure 5.61: Panelized ship_a and ship_b for Case 6

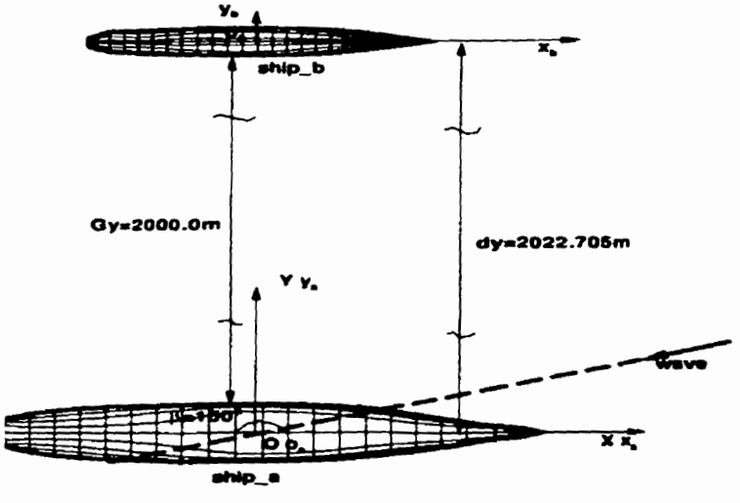

Figure 5.62: Relative position of two ships: $dx = 0.0m$, $Gy = 2000.0m$ for Case 6

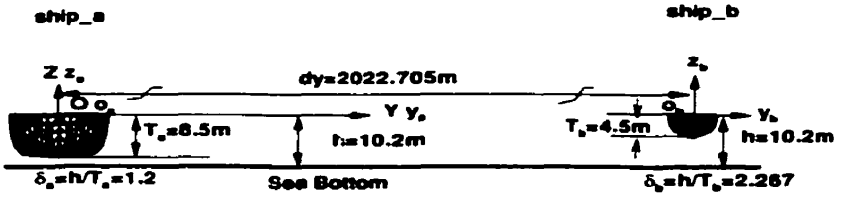

Figure 5.63: Water depth h=10.2m for Case 6

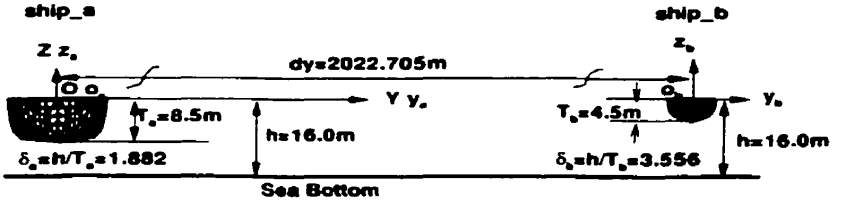

Figure 5.64: Water depth h=16.0m for Case 6

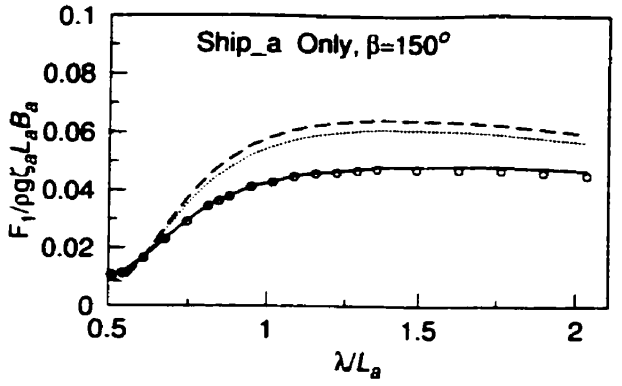

Surge force on ship_a at a separation
Gy=2000.0m, dx=0.0m, U=0.0m/s

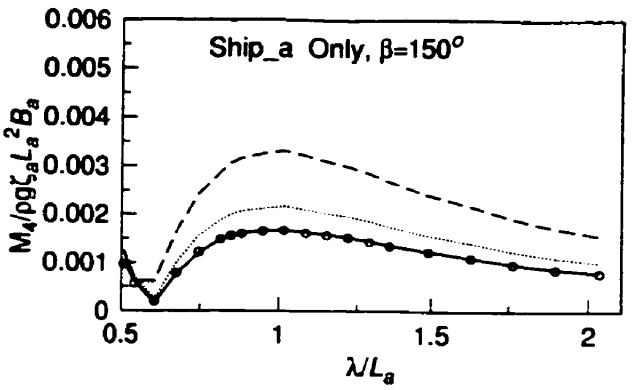

Roll moment on ship_a at a separation
Gy=2000.0m, dx=0.0m, U=0.0m/s

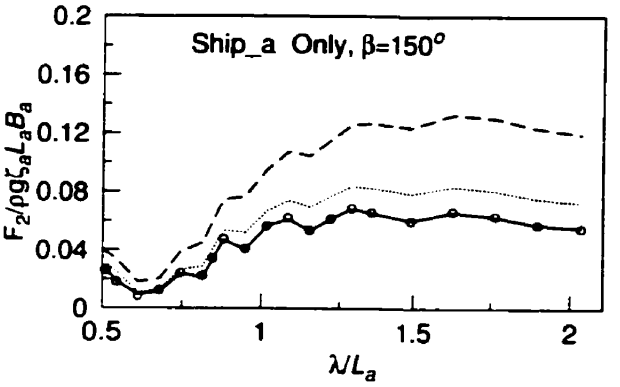

Sway force on ship_a at a separation
Gy=2000.0m, dx=0.0m, U=0.0m/s

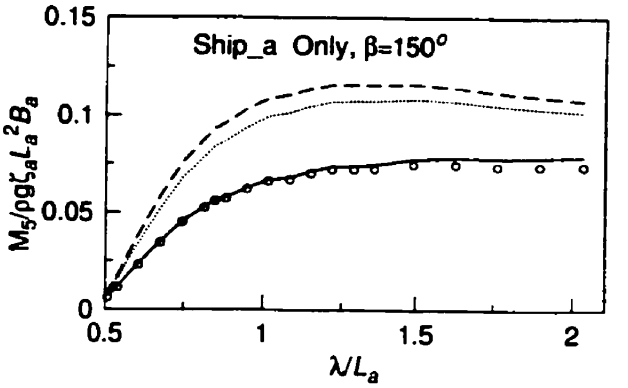

Pitch moment on ship_a at a separation
Gy=2000.0m, dx=0.0m, U=0.0m/s

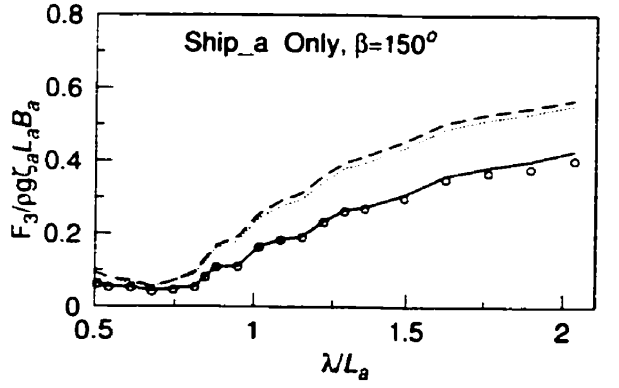

Heave force on ship_a at a separation
Gy=2000.0m, dx=0.0m, U=0.0m/s

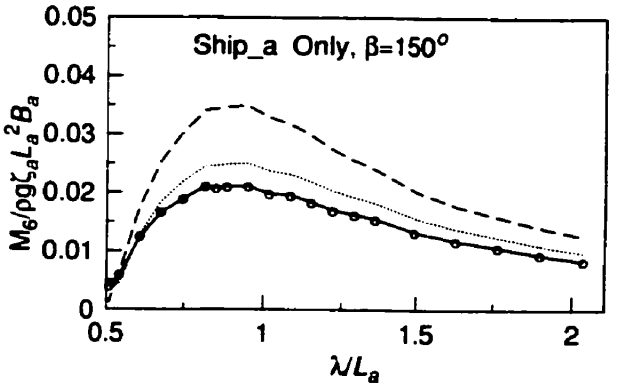

Yaw moment on ship_a at a separation
Gy=2000.0m, dx=0.0m, U=0.0m/s

– – – –h=10.2m(δ=1.20), ...h=16.0m(δ=1.88), ———h=90m(δ=10.59), ° ° ° °h=∞(δ=∞)

Figure 5.65: Non-dimensional wave exciting force amplitudes on ship_a in Case 6

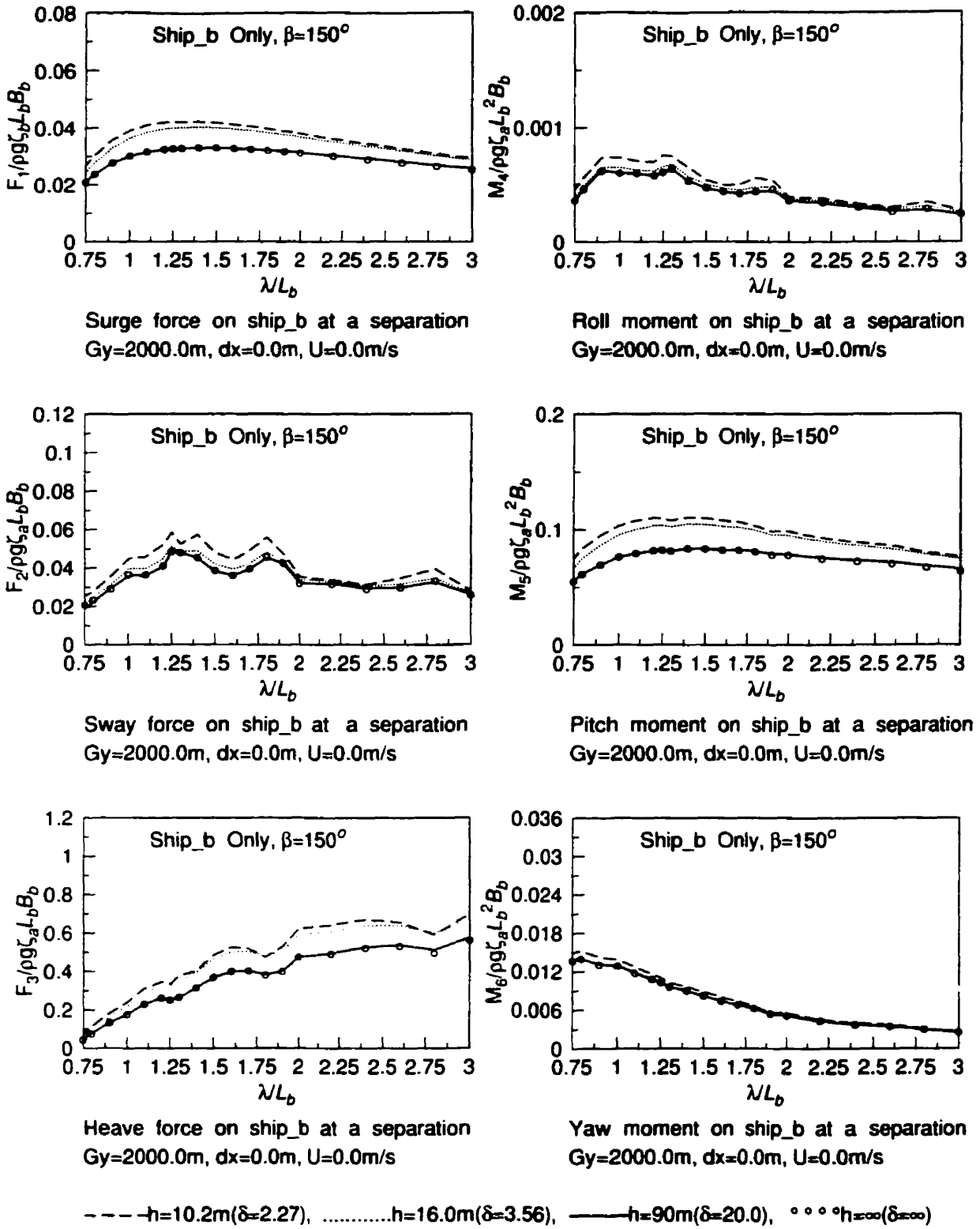

Figure 5.66: Non-dimensional wave exciting force amplitudes on ship_b in Case 6

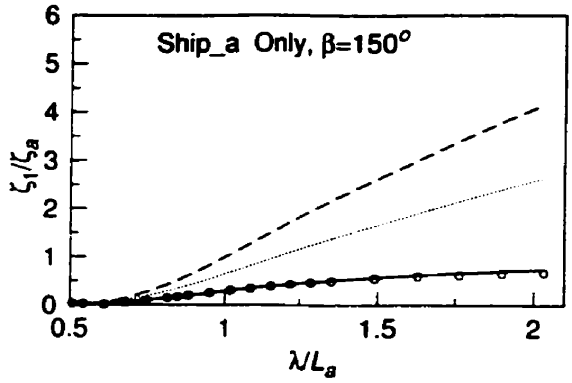

Surge motion of ship_a at a separation
Gy=2000.0m, dx=0.0m, U=0.0m/s

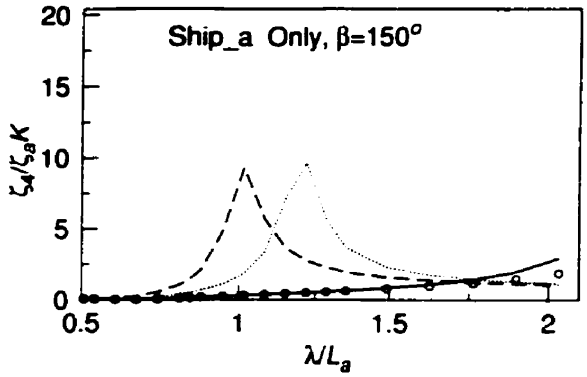

Roll motion of ship_a at a separation
Gy=2000.0m, dx=0.0m, U=0.0m/s

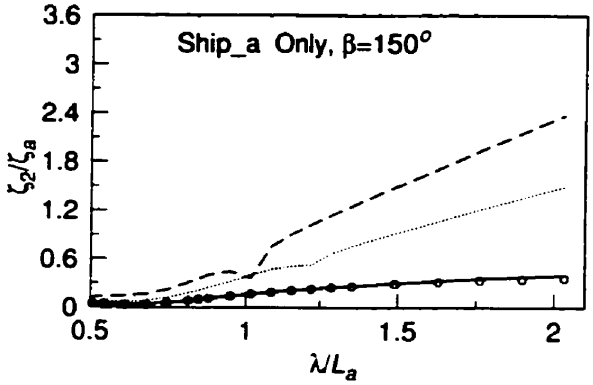

Sway motion of ship_a at a separation
Gy=2000.0m, dx=0.0m, U=0.0m/s

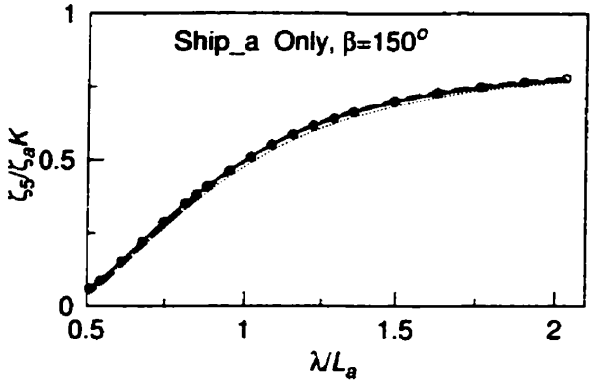

Pitch motion of ship_a at a separation
Gy=2000.0m, dx=0.0m, U=0.0m/s

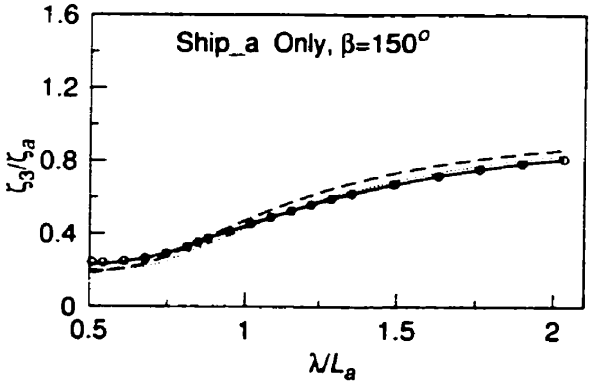

Heave motion of ship_a at a separation
Gy=2000.0m, dx=0.0m, U=0.0m/s

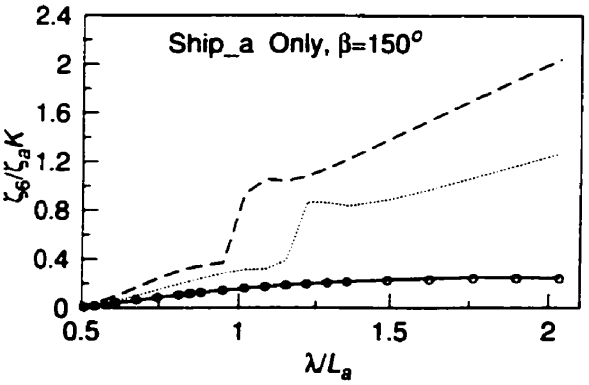

Yaw motion of ship_a at a separation
Gy=2000.0m, dx=0.0m, U=0.0m/s

– – – –h=10.2m(δ=1.20), ...h=16.0m(δ=1.88), ———h=90m(δ=10.59), ° ° ° °h=∞(δ=∞)

Figure 5.67: Non-dimensional motion displacement amplitudes on ship_a in Case 6

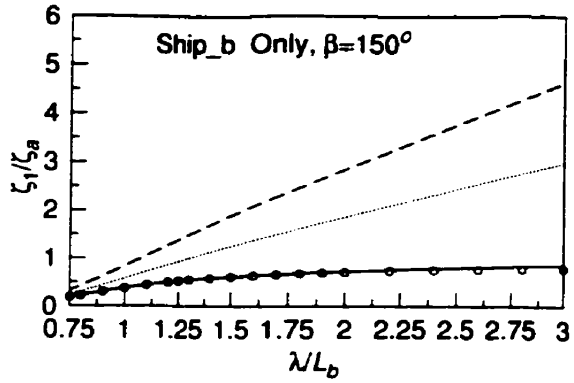

Surge motion of ship_b at a separation
Gy=2000.0m, dx=0.0m, U=0.0m/s

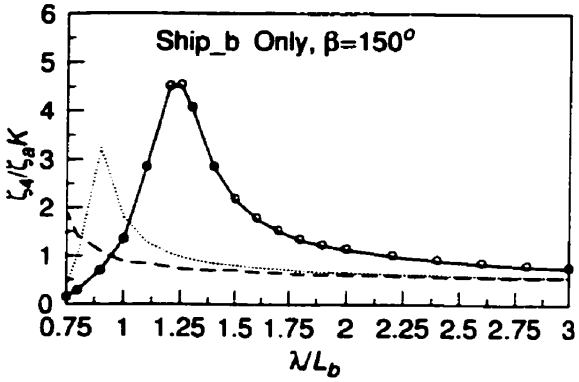

Roll motion of ship_b at a separation
Gy=2000.0m, dx=0.0m, U=0.0m/s

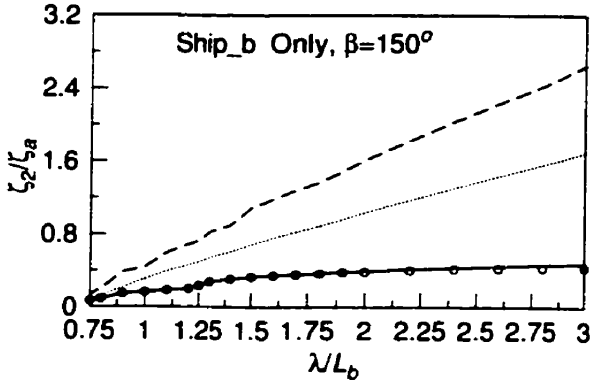

Sway motion of ship_b at a separation
Gy=2000.0m, dx=0.0m, U=0.0m/s

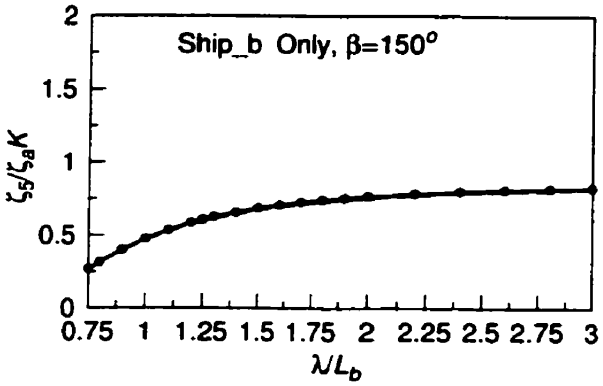

Pitch motion of ship_b at a separation
Gy=2000.0m, dx=0.0m, U=0.0m/s

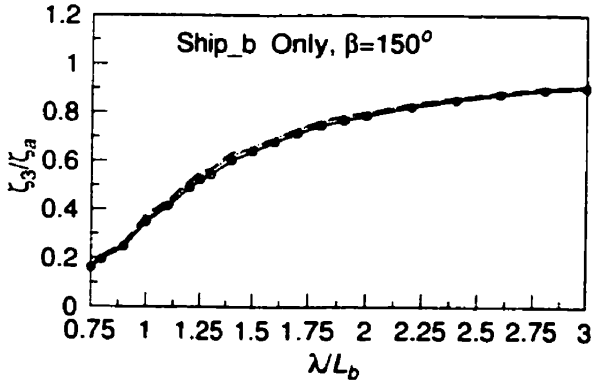

Heave motion of ship_b at a separation
Gy=2000.0m, dx=0.0m, U=0.0m/s

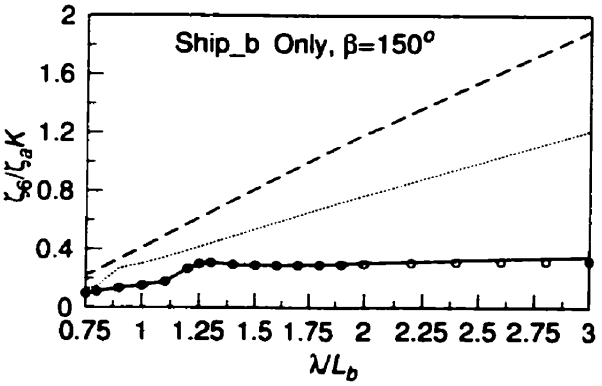

Yaw motion of ship_b at a separation
Gy=2000.0m, dx=0.0m, U=0.0m/s

----h=10.2m(δ=1.20), ...h=16.0m(δ=1.88), ——h=90m(δ=10.59), ° ° ° °h=∞(δ=∞)

Figure 5.68: Non-dimensional motion displacement amplitudes on ship_b in Case 6

5.2.10 Case 7

Figure 5.69 shows the panelized ship_a and ship_b. Wave heading $\beta = 120^o$; lateral separation $dy = 52.705m$ and gap $Gy = 30.0m$; longitudinal separation dx=0.0m: and forward speed $U = 0.0m/s$ are all shown in Figure 5.70. Figure 5.71 and Figure 5.72 give the positions of ship_a and ship_b relative to the sea bottom for water depths of $h = 10.2m$ and $h = 16.0m$, respectively.

Discussions on Case 7

This is another oblique wave case for wave heading $\beta = 120^o$. In Figure 5.73, the wave exciting forces are given for ship_a. By comparing with Case 1 ($\beta = 180^o$) and Case 4 ($\beta = 150^o$), we have found that the surge wave exciting force has a decreasing trend which is different from Case 1 and Case 4; the peak value for the sway force is about 2 times greater than that of Case 4 and 5 times than Case 1, and the heave force is greater in the lower λ/L_a value. The decreasing trend is also found in the pitch motion. Roll and yaw forces are similar to the Case 1 and Case 4. In Figure 5.74, for ship_b, the forces in surge and pitch are generally reduced comparing with Case 1 and Case 4, and the forces in sway, roll, heave and yaw are generally increased. In Figure 5.75, for ship_a , the sway and roll motions are generally increased, the surge motion is reduced, and there is no change in the yaw motion in comparison with Case 1 and Case 4. In Figure 5.76, for ship_b, the motion trends are very similar to ship_a. They are getting greater in sway and roll, less in surge, and no changes in the yaw motion.

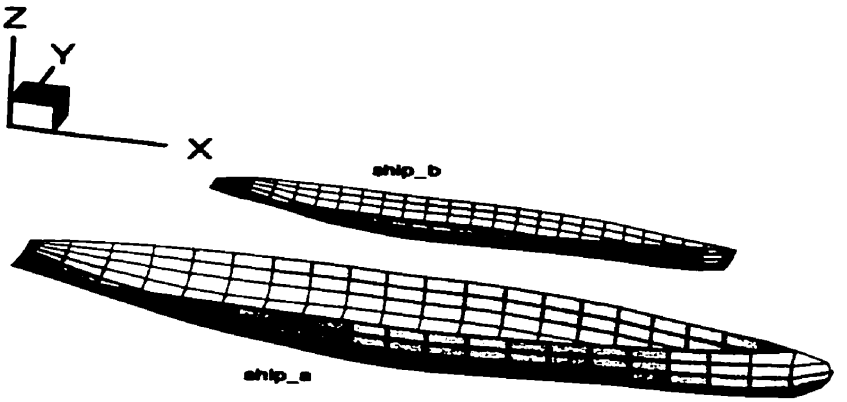

Figure 5.69: Panelized ship_a and ship_b for Case 7

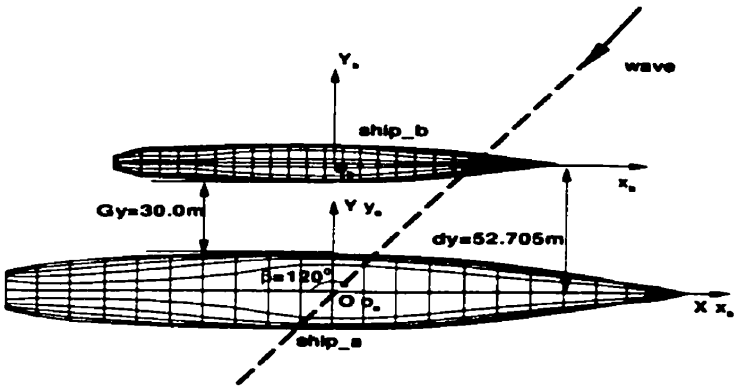

Figure 5.70: Relative position of two ships: $dx = 0.0m$, $Gy = 30.0m$ for Case 7

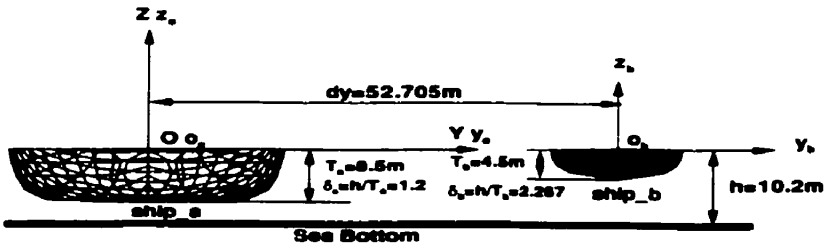

Figure 5.71: Water depth h=10.2m for Case 7

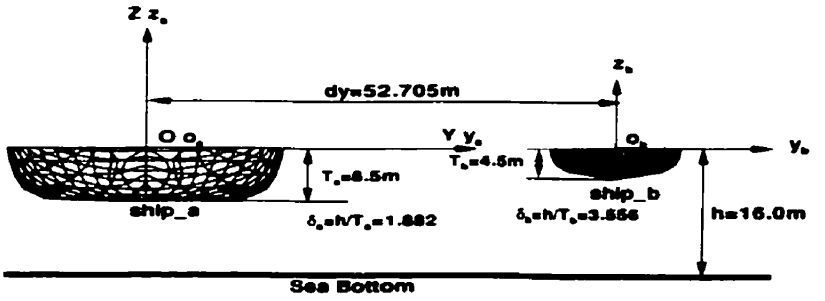

Figure 5.72: Water depth h=16.0 for Case 7

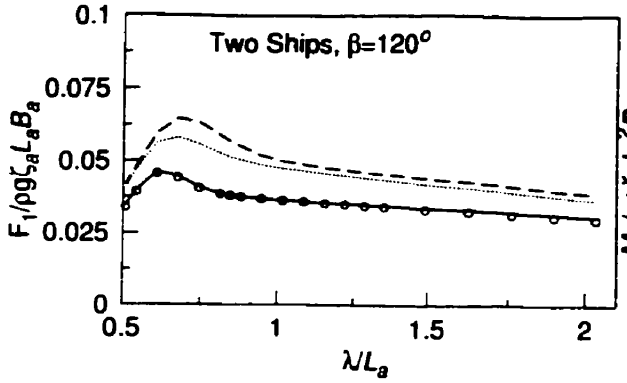

Surge force on ship_a at a separation
Gy=30.0m, dx=0.0m, U=0.0m/s

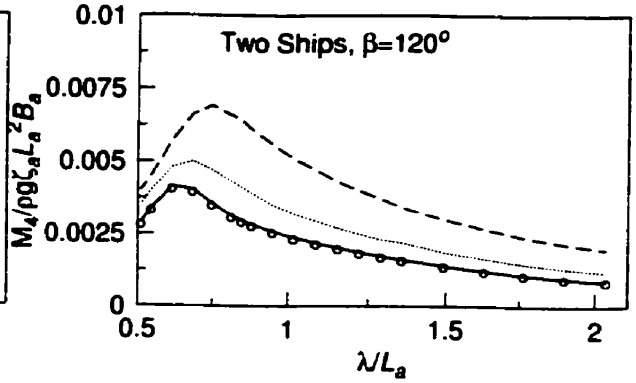

Roll moment on ship_a at a separation
Gy=30.0m, dx=0.0m, U=0.0m/s

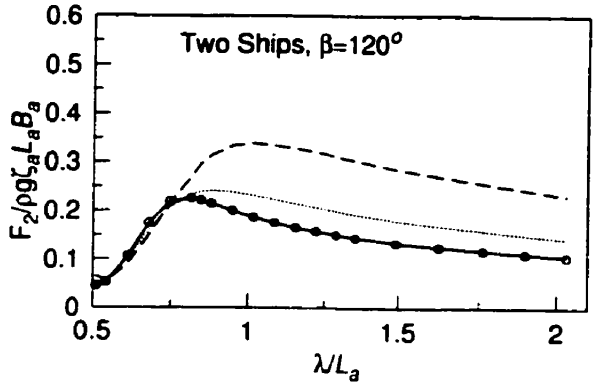

Sway force on ship_a at a separation
Gy=30.0m, dx=0.0m, U=0.0m/s

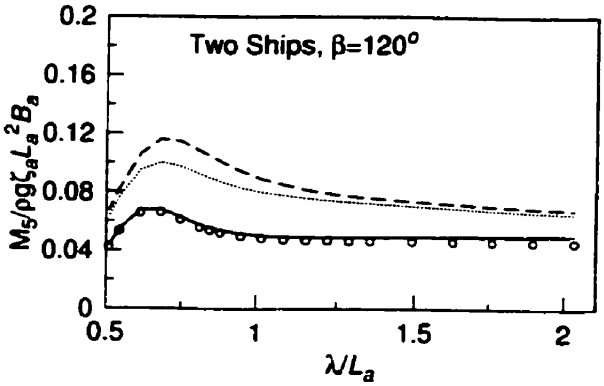

Pitch moment on ship_a at a separation
Gy=30.0m, dx=0.0m, U=0.0m/s

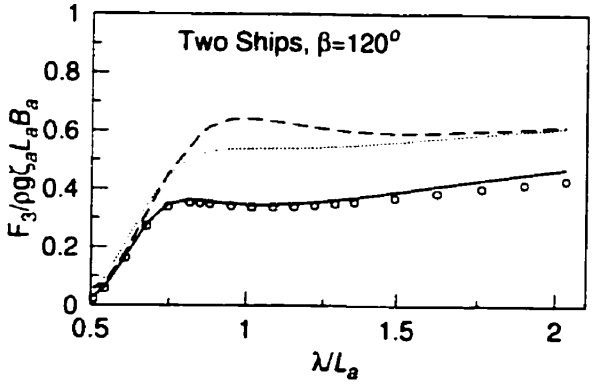

Heave force on ship_a at a separation
Gy=30.0m, dx=0.0m, U=0.0m/s

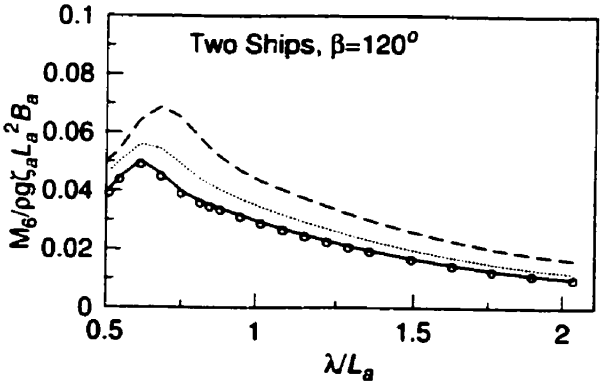

Yaw moment on ship_a at a separation
Gy=30.0m, dx=0.0m, U=0.0m/s

----h=10.2m(δ=1.20), ...h=16.0m(δ=1.88), ——h=90m(δ=10.59), ° ° ° °h=∞(δ=∞)

Figure 5.73: Non-dimensional wave exciting force amplitudes on ship_a in Case 7

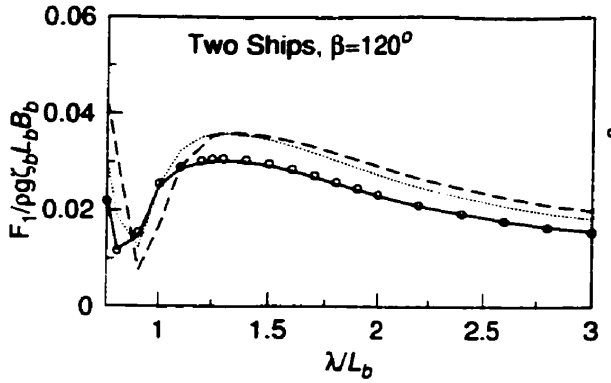

Surge force on ship_b at a separation
Gy=30.0m, dx=0.0m, U=0.0m/s

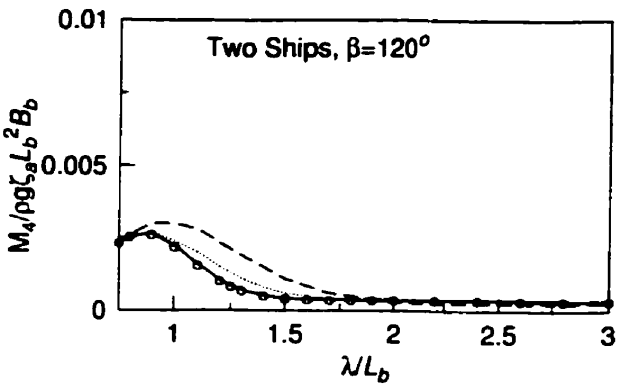

Roll moment on ship_b at a separation
Gy=30.0m, dx=0.0m, U=0.0m/s

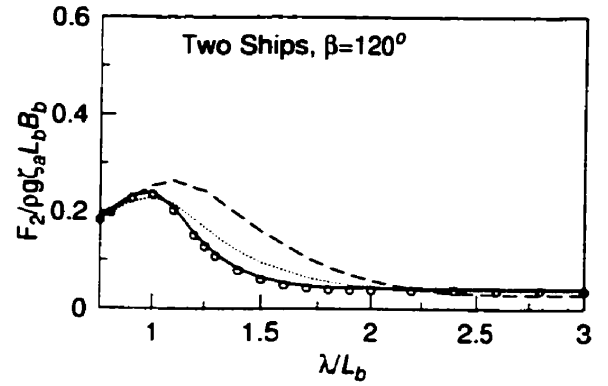

Sway force on ship_b at a separation
Gy=30.0m, dx=0.0m, U=0.0m/s

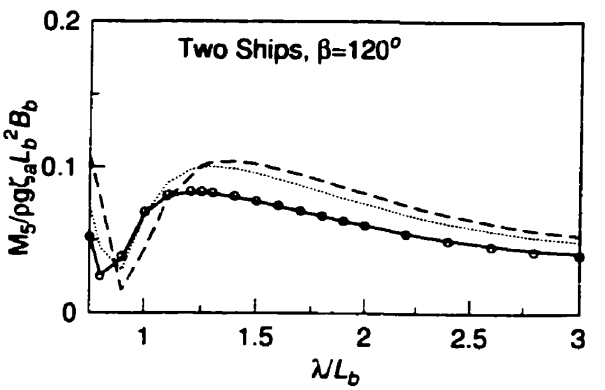

Pitch moment on ship_b at a separation
Gy=30.0m, dx=0.0m, U=0.0m/s

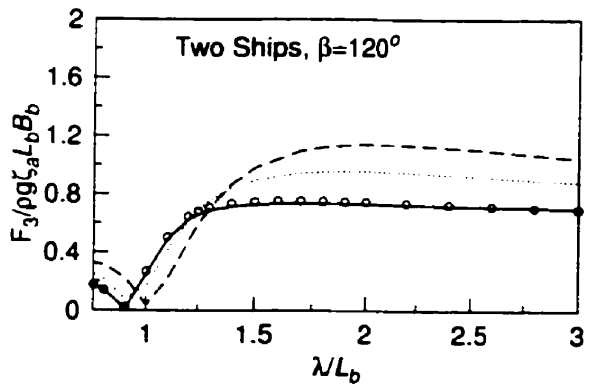

Heave force on ship_b at a separation
Gy=30.0m, dx=0.0m, U=0.0m/s

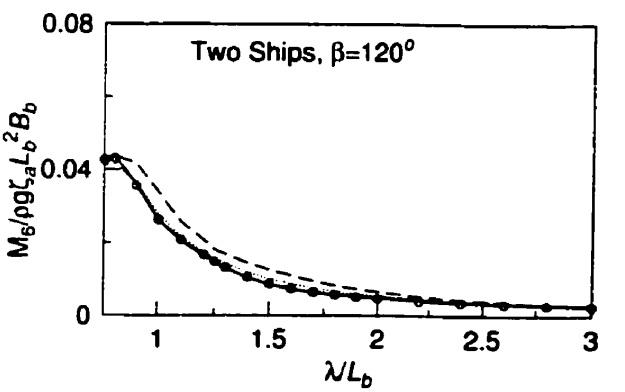

Yaw moment on ship_b at a separation
Gy=30.0m, dx=0.0m, U=0.0m/s

----h=10.2m(δ=2.27), ...h=16.0m(δ=3.56), ——h=90m(δ=20.0), ° ° ° °h=∞(δ=∞)

Figure 5.74: Non-dimensional wave exciting force amplitudes on ship_b in Case 7

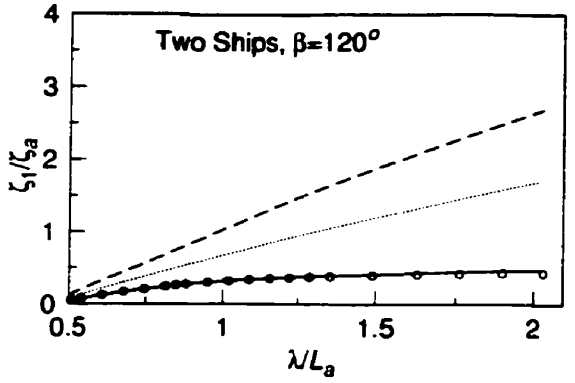

Surge motion of ship_a at a separation
Gy=30.0m, dx=0.0m, U=0.0m/s

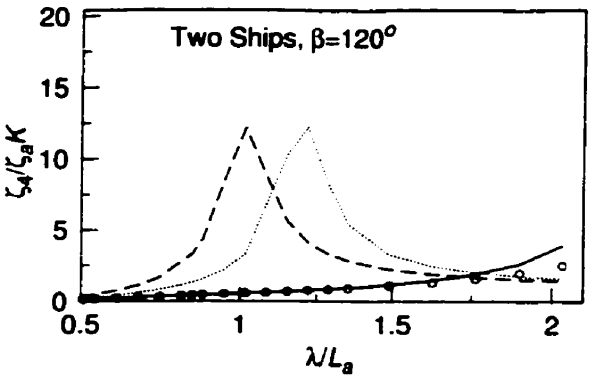

Roll motion of ship_a at a separation
Gy=30.0m, dx=0.0m, U=0.0m/s

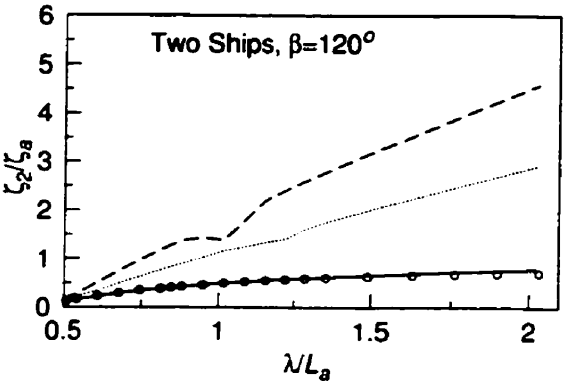

Sway motion of ship_a at a separation
Gy=30.0m, dx=0.0m, U=0.0m/s

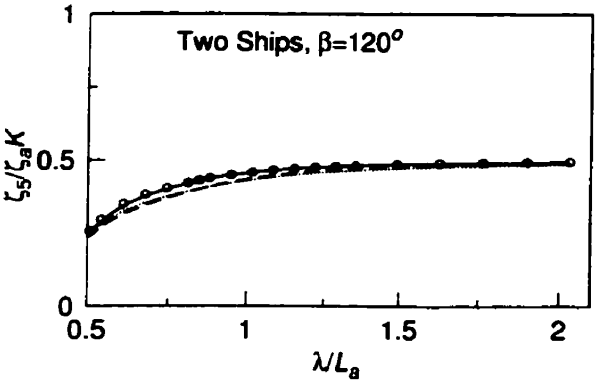

Pitch motion of ship_a at a separation
Gy=30.0m, dx=0.0m, U=0.0m/s

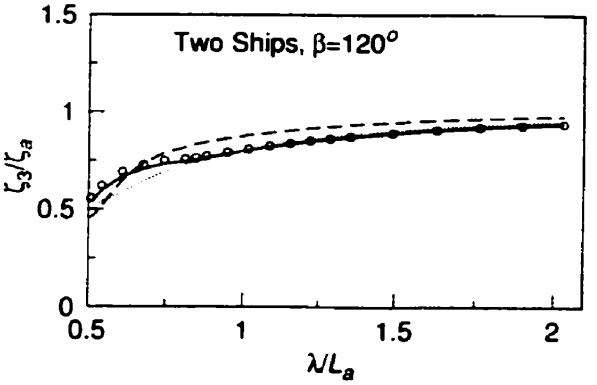

Heave motion of ship_a at a separation
Gy=30.0m, dx=0.0m, U=0.0m/s

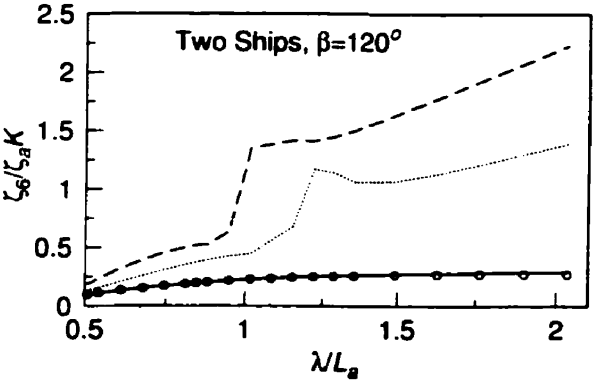

Yaw motion of ship_a at a separation
Gy=30.0m, dx=0.0m, U=0.0m/s

– – – –h=10.2m(δ=1.20), ...h=16.0m(δ=1.88), ———h=90m(δ=10.59), ° ° ° °h=∞(δ=∞)

Figure 5.75: Non-dimensional motion displacement amplitudes on ship_a in Case 7

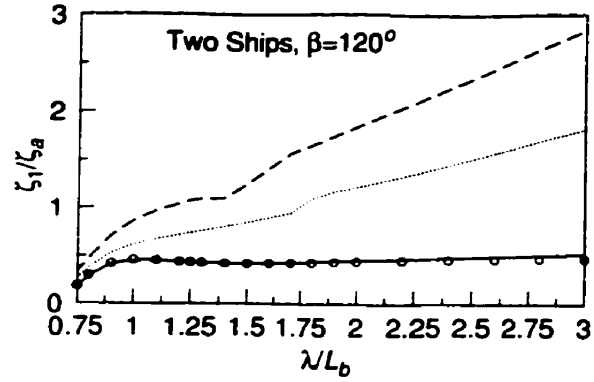

Surge motion of ship_b at a separation
Gy=30.0m, dx=0.0m, U=0.0m/s

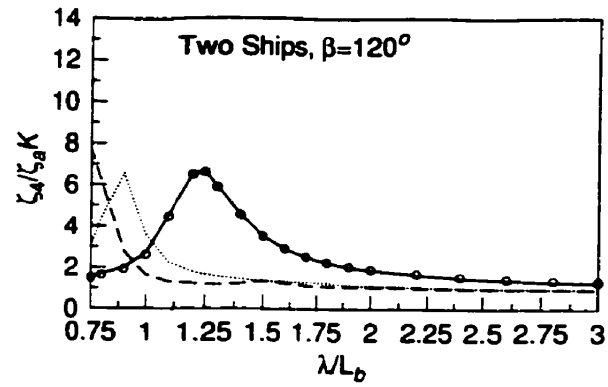

Roll motion of ship_b at a separation
Gy=30.0m, dx=0.0m, U=0.0m/s

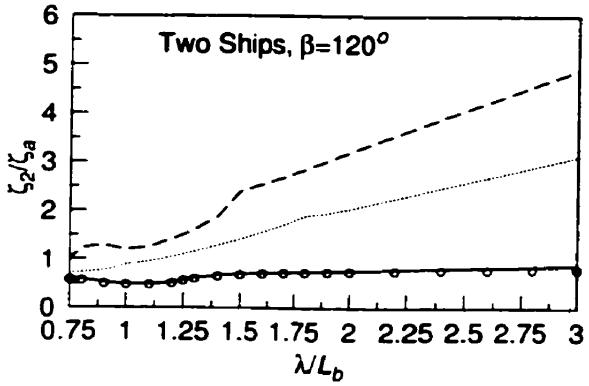

Sway motion of ship_b at a separation
Gy=30.0m, dx=0.0m, U=0.0m/s

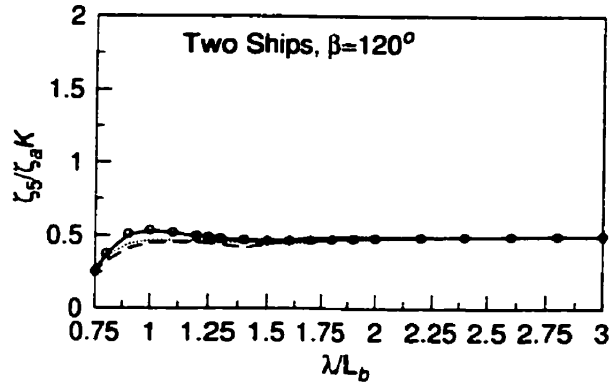

Pitch motion of ship_b at a separation
Gy=30.0m, dx=0.0m, U=0.0m/s

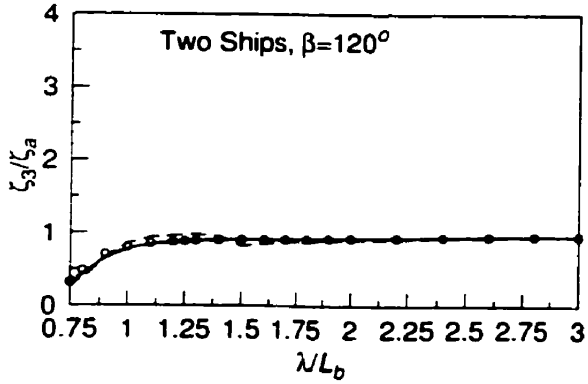

Heave motion of ship_b at a separation
Gy=30.0m, dx=0.0m, U=0.0m/s

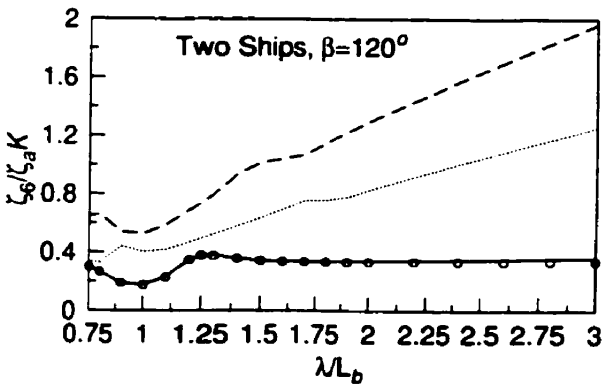

Yaw motion of ship_b at a separation
Gy=30.0m, dx=0.0m, U=0.0m/s

– – – –h=10.2m(δ=2.27), ...h=16.0m(δ=3.56), ——h=90m(δ=20.0), ° ° ° °h=∞(δ=∞)

Figure 5.76: Non-dimensional motion displacement amplitudes on ship_b in Case 7

5.2.11 Case 8

Figure 5.77 shows the panelized ship_a and ship_b. Wave heading $\beta = 120^o$; lateral separation $dy = 52.705m$ and gap $Gy = 30.0m$: longitudinal separation dx=45.0m; and forward speed $U = 0.0m/s$ are all shown in Figure 5.78. Figure 5.79 and Figure 5.80 give the positions of ship_a and ship_b relative to the sea bottom for water depths of $h = 10.2m$ and $h = 16.0m$, respectively.

Discussions on Case 8

This case is very similar to Case 2 ($\beta = 180^o$) and Case 5 ($\beta = 150^o$). $dx = 45.0m$ is set to study the effect of the longitudinal separation distance under the wave heading $\beta = 120^o$. The trends of force and motion are very similar to that of the Case 2 and Case 5. Here, the computed results for ship_a and ship_b wave exciting forces and motions would be a great help for the experimental verification in the future.

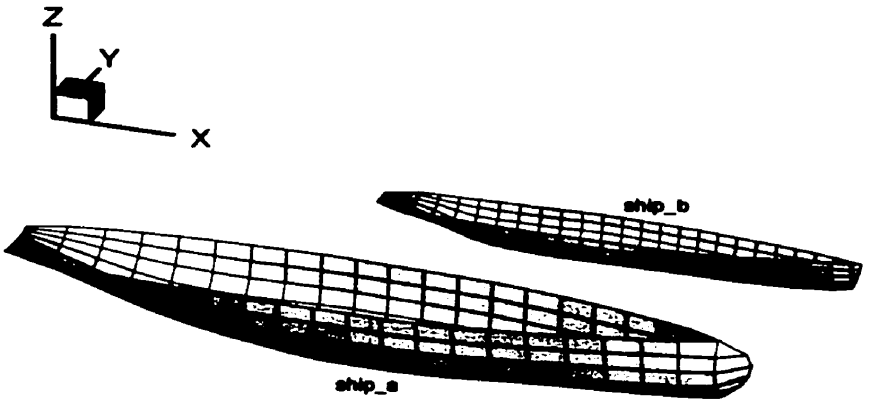

Figure 5.77: Panelized ship_a and ship_b for Case 8

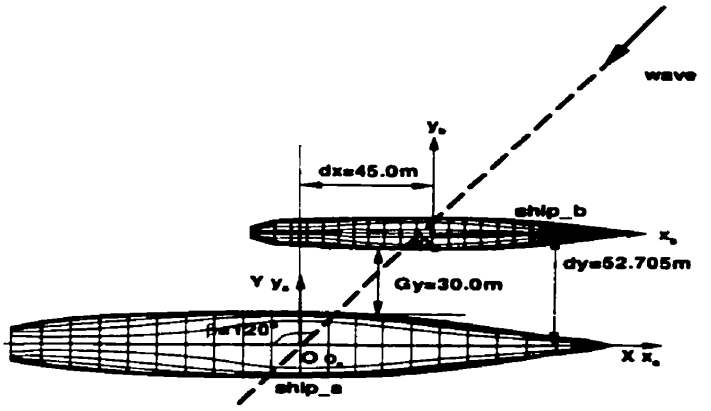

Figure 5.78: Relative position of two ships: $dx = 45.0m$, $Gy = 30.0m$ for Case 8

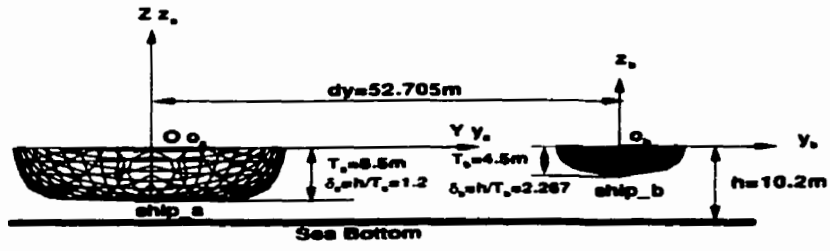

Figure 5.79: Water depth h=10.2m for Case 8

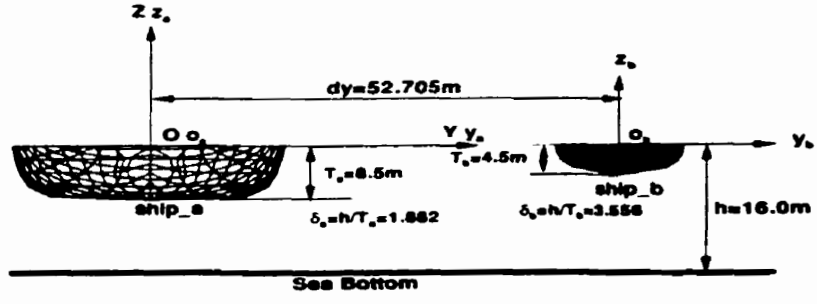

Figure 5.80: Water depth h=16.0m Case 8

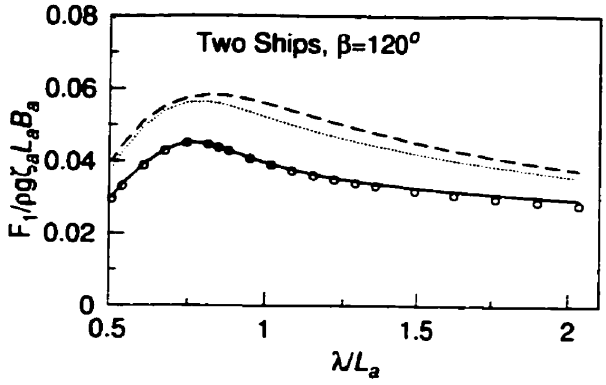

Surge force on ship_a at a separation
Gy=30.0m, dx=45.0m, U=0.0m/s

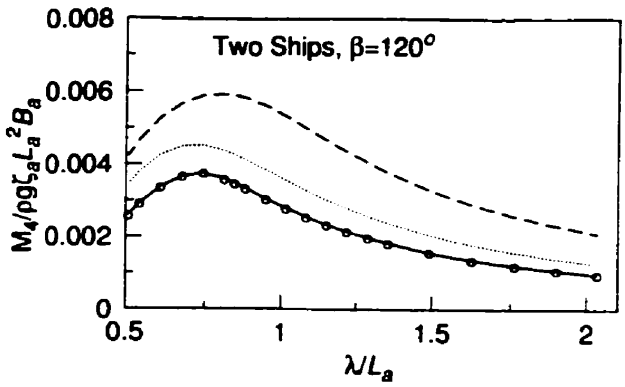

Roll moment on ship_a at a separation
Gy=30.0m, dx=45.0m, U=0.0m/s

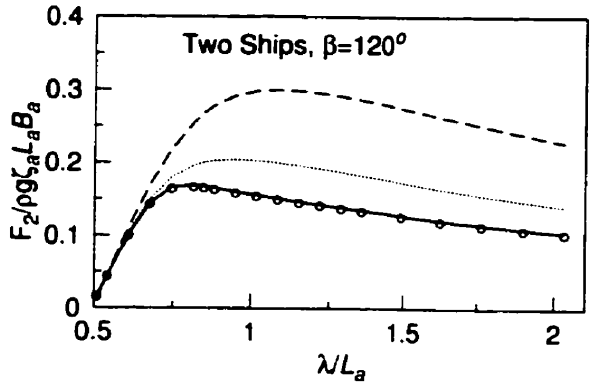

Sway force on ship_a at a separation
Gy=30.0m, dx=45.0m, U=0.0m/s

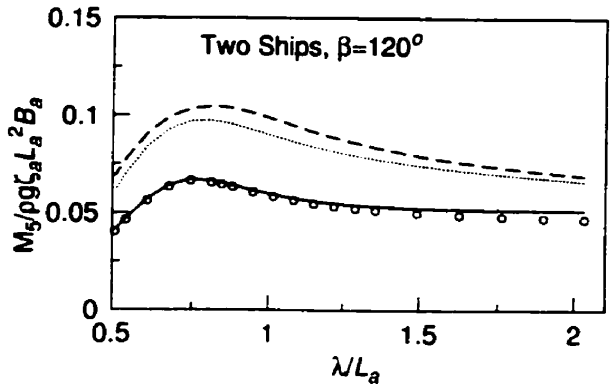

Pitch moment on ship_a at a separation
Gy=30.0m, dx=45.0m, U=0.0m/s

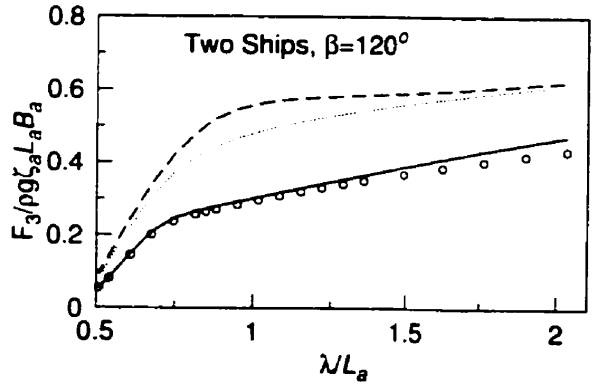

Heave force on ship_a at a separation
Gy=30.0m, dx=45.0m, U=0.0m/s

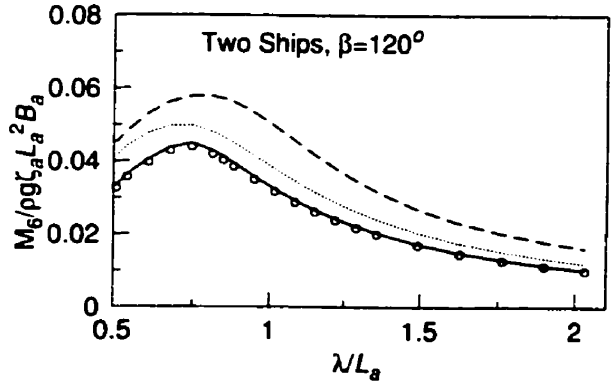

Yaw moment on ship_a at a separation
Gy=30.0m, dx=45.0m, U=0.0m/s

----h=10.2m(δ=1.20), ...h=16.0m(δ=1.88), ——h=90m(δ=10.59), ° ° ° °h=∞(δ=∞)

Figure 5.81: Non-dimensional wave exciting force amplitudes on ship_a in Case 8

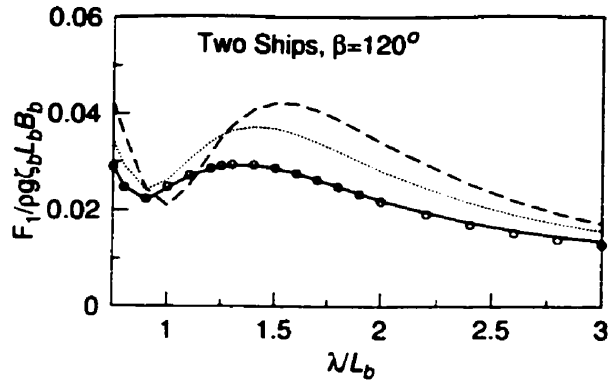

Surge force on ship_b at a separation
Gy=30.0m, dx=45.0m, U=0.0m/s

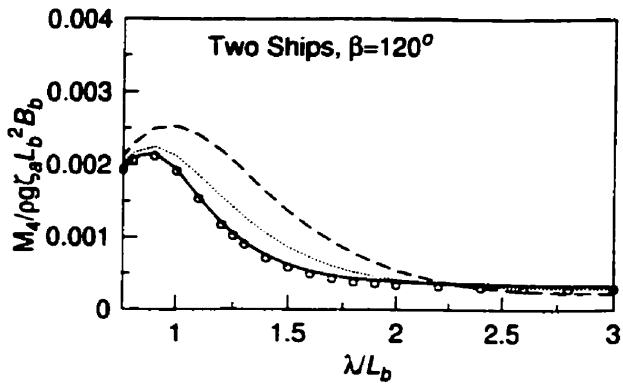

Roll moment on ship_b at a separation
Gy=30.0m, dx=45.0m, U=0.0m/s

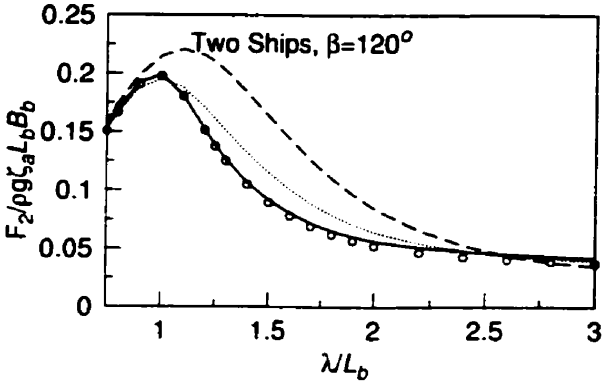

Sway force on ship_b at a separation
Gy=30.0m, dx=45.0m, U=0.0m/s

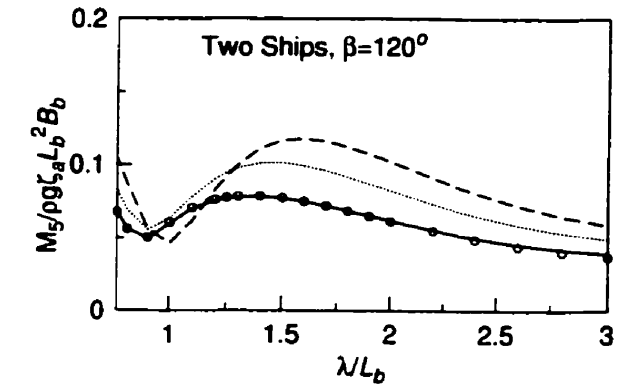

Pitch moment on ship_b at a separation
Gy=30.0m, dx=45.0m, U=0.0m/s

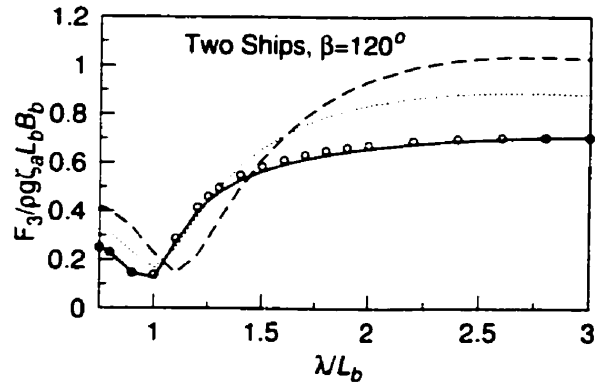

Heave force on ship_b at a separation
Gy=30.0m, dx=45.0m, U=0.0m/s

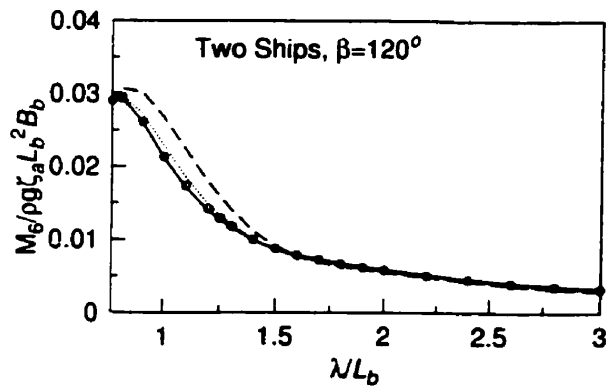

Yaw moment on ship_b at a separation
Gy=30.0m, dx=45.0m, U=0.0m/s

– – – –h=10.2m(δ=2.27), ...h=16.0m(δ=3.56), ——h=90m(δ=20.0), ° ° ° °h=∞(δ=∞)

Figure 5.82: Non-dimensional wave exciting force amplitudes on ship_b in Case 8

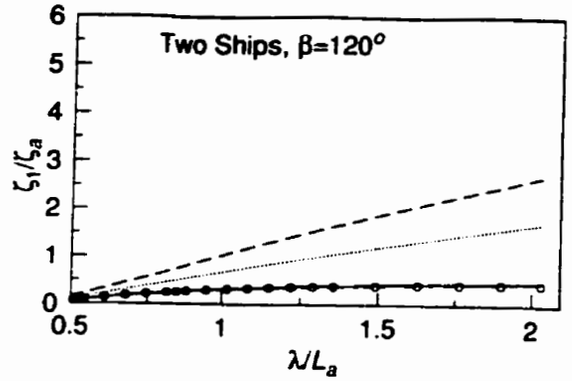

Surge motion of ship_a at a separation
Gy=30.0m, dx=45.0m, U=0.0m/s

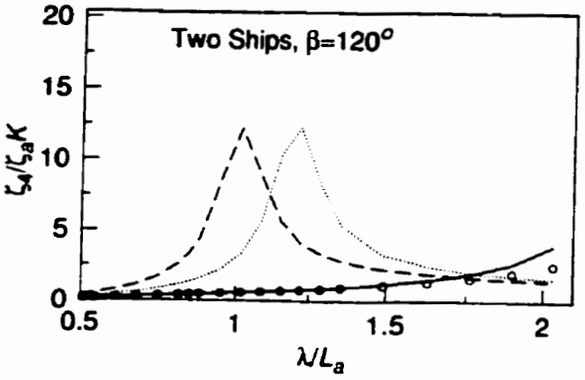

Roll motion of ship_a at a separation
Gy=30.0m, dx=45.0m, U=0.0m/s

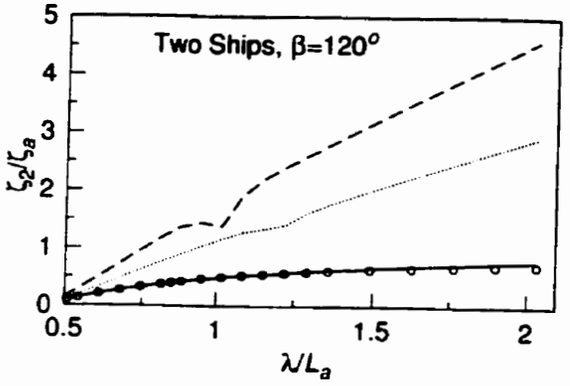

Sway motion of ship_a at a separation
Gy=30.0m, dx=45.0m, U=0.0m/s

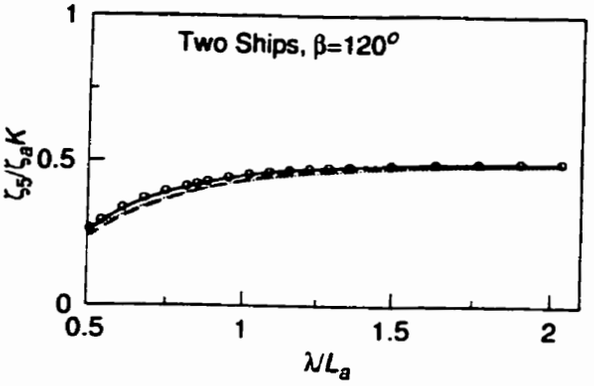

Pitch motion of ship_a at a separation
Gy=30.0m, dx=45.0m, U=0.0m/s

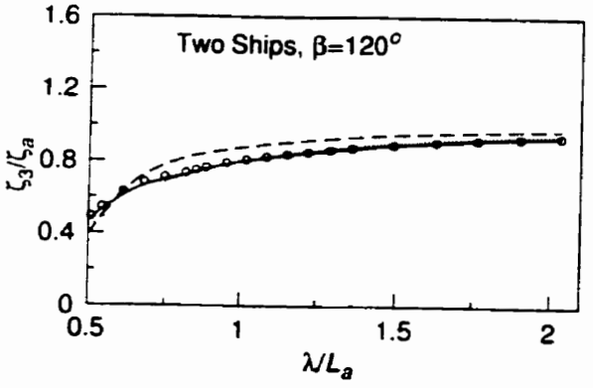

Heave motion of ship_a at a separation
Gy=30.0m, dx=45.0m, U=0.0m/s

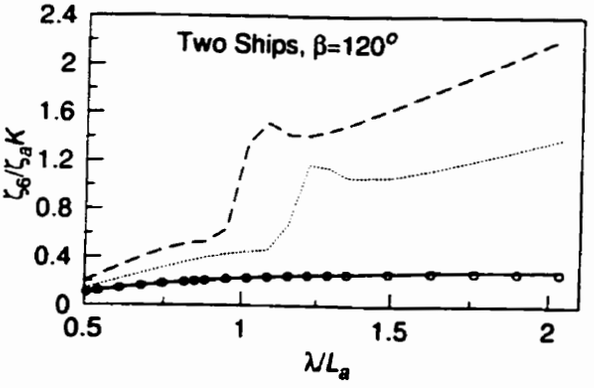

Yaw motion of ship_a at a separation
Gy=30.0m, dx=45.0m, U=0.0m/s

– – – –h=10.2m(δ=1.20), ...h=16.0m(δ=1.88), ———h=90m(δ=10.59), ° ° ° °h=∞(δ=∞)

Figure 5.83: Non-dimensional motion displacement amplitudes on ship_a in Case 8

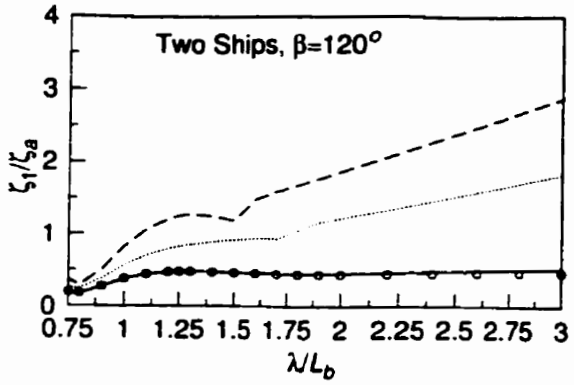

Surge motion of ship_b at a separation
Gy=30.0m, dx=45.0m, U=0.0m/s

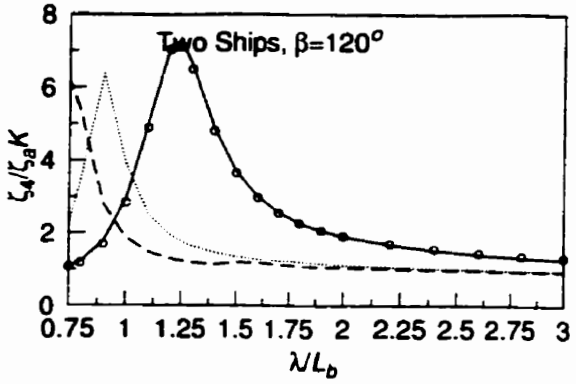

Roll motion of ship_b at a separation
Gy=30.0m, dx=45.0m, U=0.0m/s

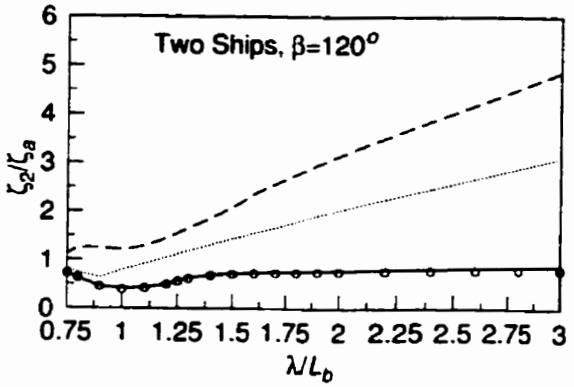

Sway motion of ship_b at a separation
Gy=30.0m, dx=45.0m, U=0.0m/s

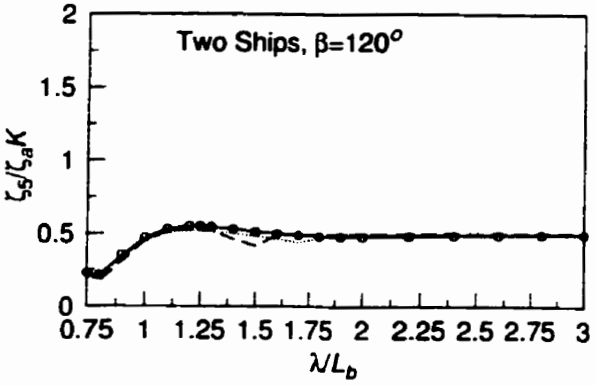

Pitch motion of ship_b at a separation
Gy=30.0m, dx=45.0m, U=0.0m/s

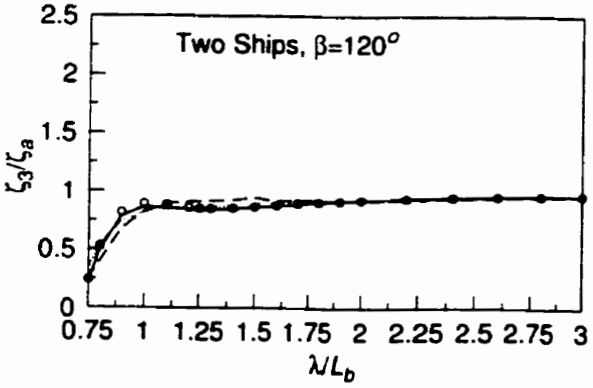

Heave motion of ship_b at a separation
Gy=30.0m, dx=45.0m, U=0.0m/s

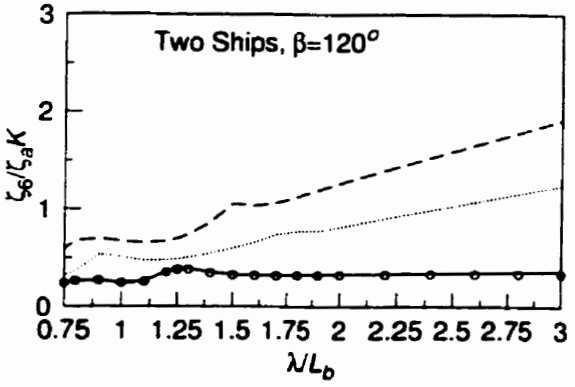

Yaw motion of ship_b at a separation
Gy=30.0m, dx=45.0m, U=0.0m/s

– – – –h=10.2m(δ=2.27), ...h=16.0m(δ=3.56), ———h=90m(δ=20.0), ° ° ° °h=∞(δ=∞)

Figure 5.84: Non-dimensional motion displacement amplitudes on ship_b in Case 8

5.2.12 Case 9

The panelized ship_a and ship_b are shown in Figure 5.85. Wave heading $\beta = 120^o$; lateral separation $dy = 2022.705m$ and gap $Gy = 2000.0m$; longitudinal separation dx=0.0m; and forward speed $U = 0.0m/s$ are all shown in Figure 5.86. Figure 5.87 and Figure 5.88 give the positions of ship_a and ship_b relative to the sea bottom for water depths of $h = 10.2m$ and $h = 16.0m$, respectively.

Discussions on Case 9

In this case, ship_a and ship_b were isolated to perform individually at $\beta = 120^o$. The effect of wave heading on the wave exciting forces and motions of ship_a and ship_b is very similar to those of Case 6. This case gives the further proof of the existence of interaction effect in shallow water, finite depth of water and deep water. The oblique wave will affect not only the single ship but also the two ship interactions.

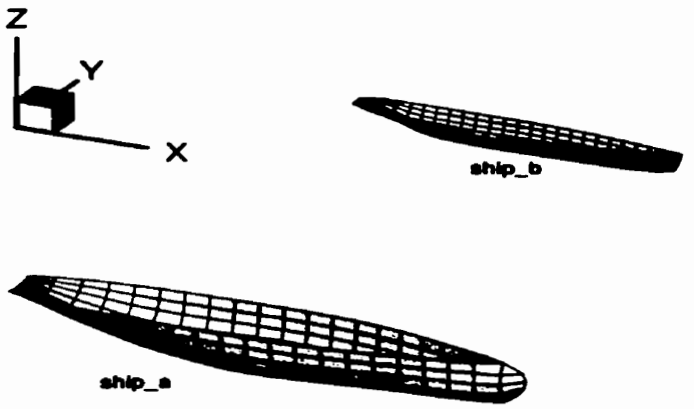

Figure 5.85: Panelized ship_a and ship_b for Case 9

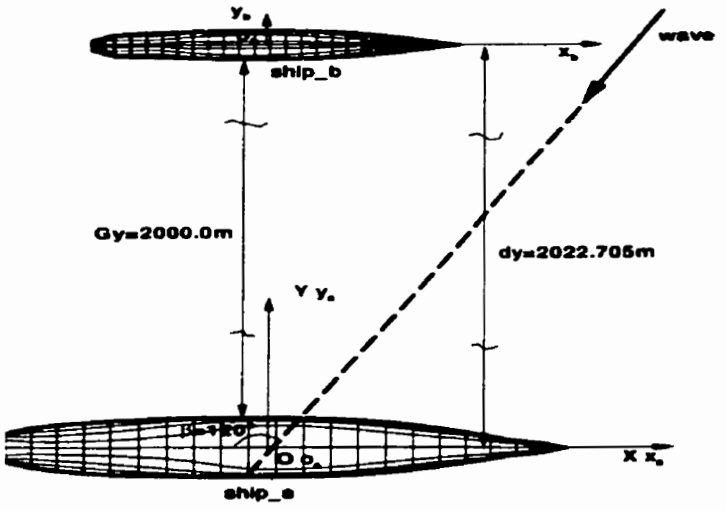

Figure 5.86: Relative position of two ships: $dx = 0.0m$, $Gy = 2000.0m$ for Case 9

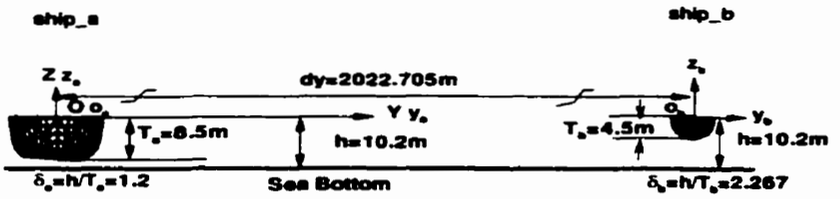

Figure 5.87: Water depth h=10.2m for Case 9

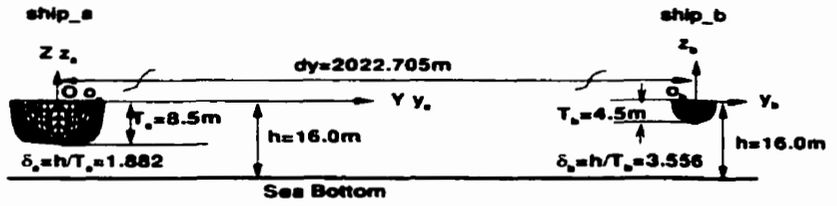

Figure 5.88: Water depth h=16.0m for Case 9

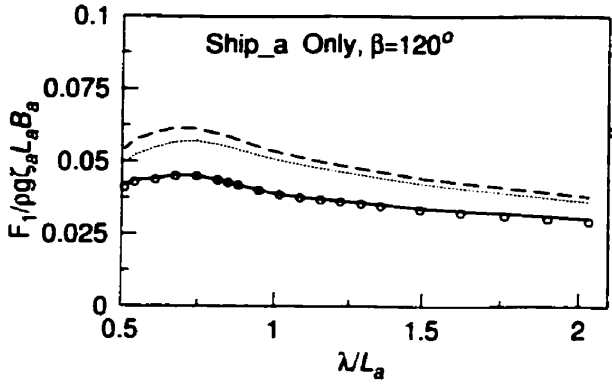

Surge force on ship_a at a separation
Gy=2000.0m, dx=0.0m, U=0.0m/s

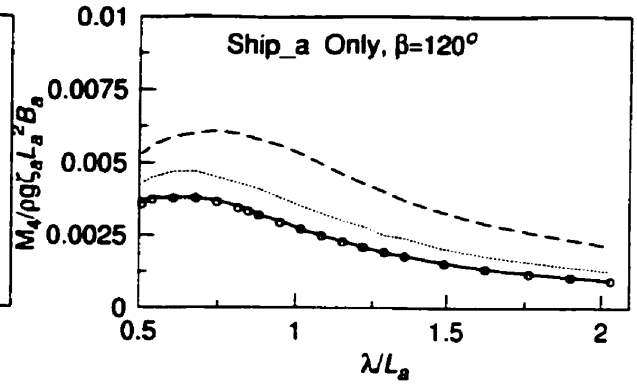

Roll moment on ship_a at a separation
Gy=2000.0m, dx=0.0m, U=0.0m/s

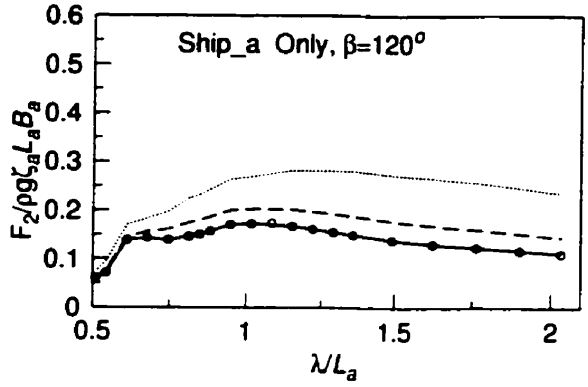

Sway force on ship_a at a separation
Gy=2000.0m, dx=0.0m, U=0.0m/s

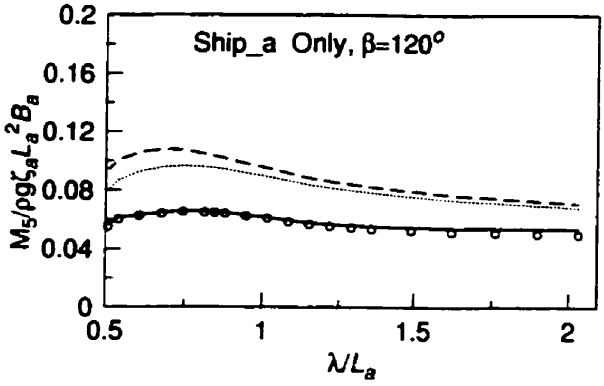

Pitch moment on ship_a at a separation
Gy=2000.0m, dx=0.0m, U=0.0m/s

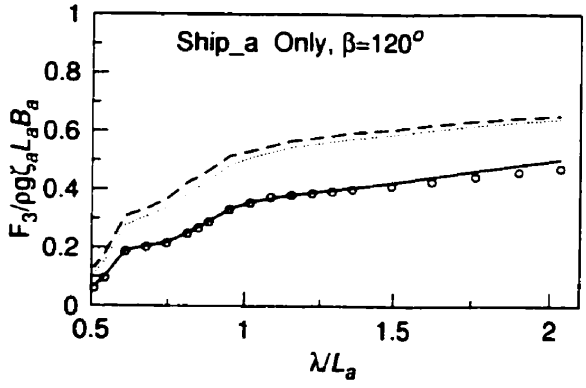

Heave force on ship_a at a separation
Gy=2000.0m, dx=0.0m, U=0.0m/s

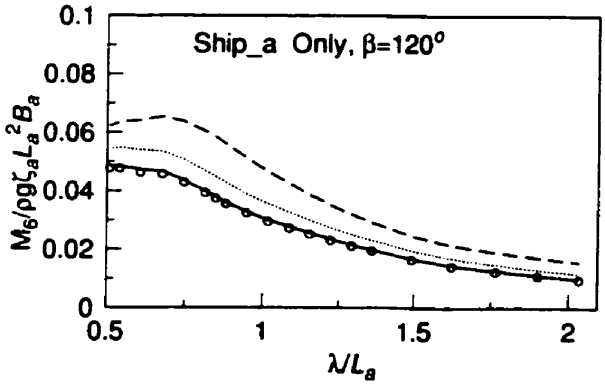

Yaw moment on ship_a at a separation
Gy=2000.0m, dx=0.0m, U=0.0m/s

– – – –h=10.2m(δ=1.20), ...h=16.0m(δ=1.88), ———h=90m(δ=10.59), ° ° ° °h=∞(δ=∞)

Figure 5.89: Non-dimensional wave exciting force amplitudes on ship_a in Case 9

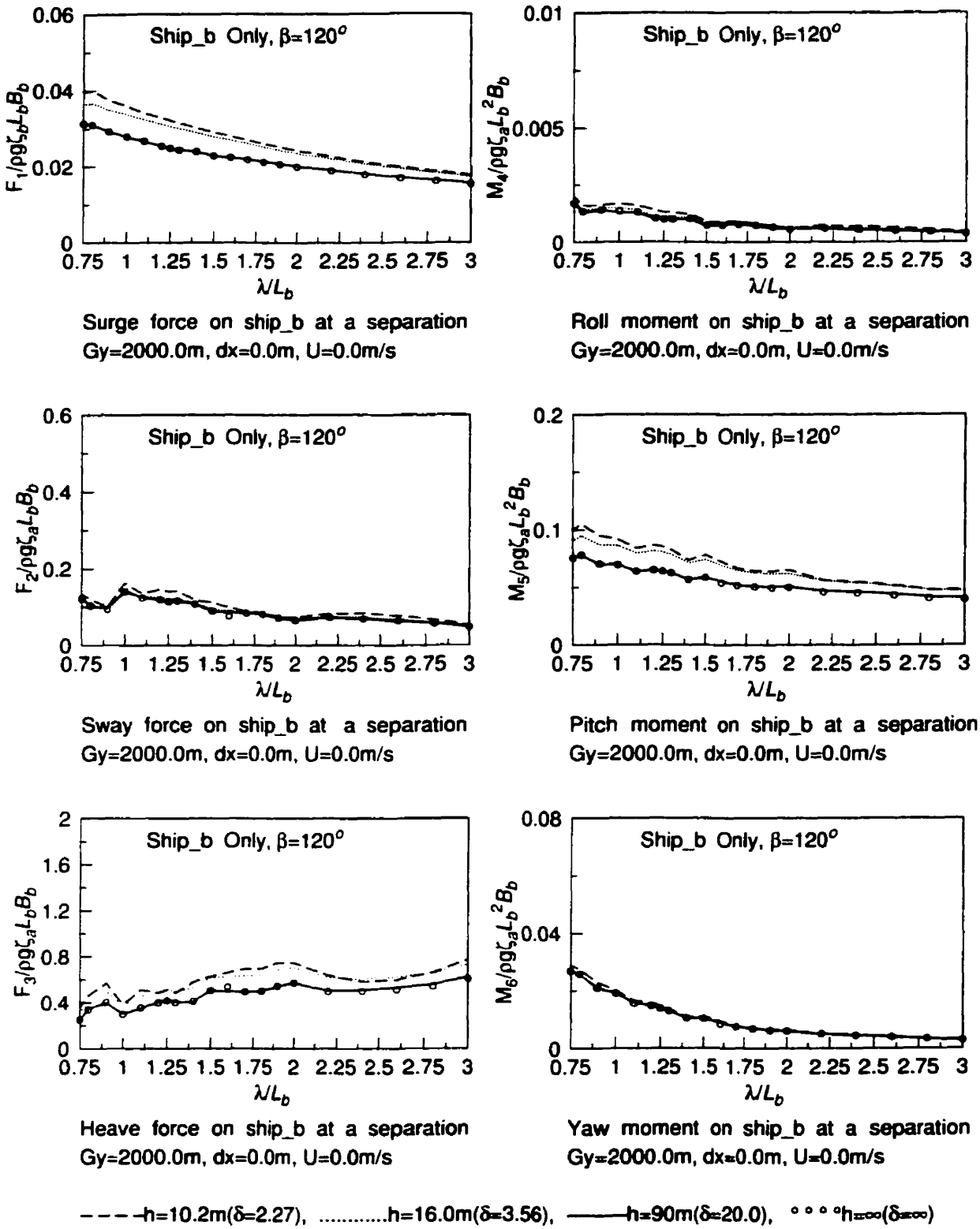

Figure 5.90: Non-dimensional wave exciting force amplitudes on ship_b in Case 9

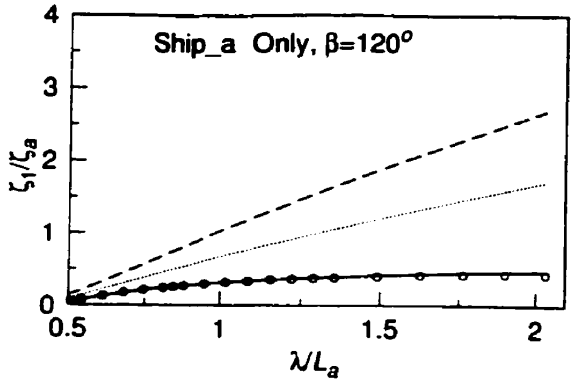

Surge motion of ship_a at a separation
Gy=2000.0m, dx=0.0m, U=0.0m/s

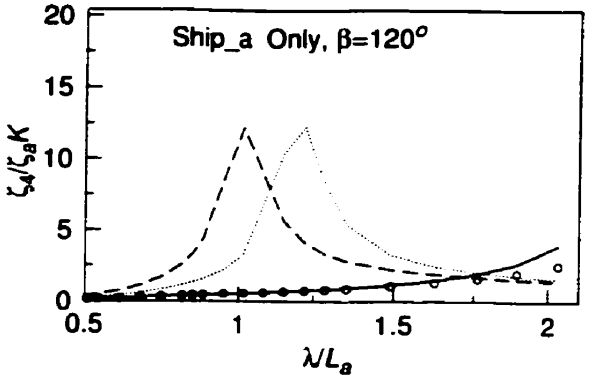

Roll motion of ship_a at a separation
Gy=2000.0m, dx=0.0m, U=0.0m/s

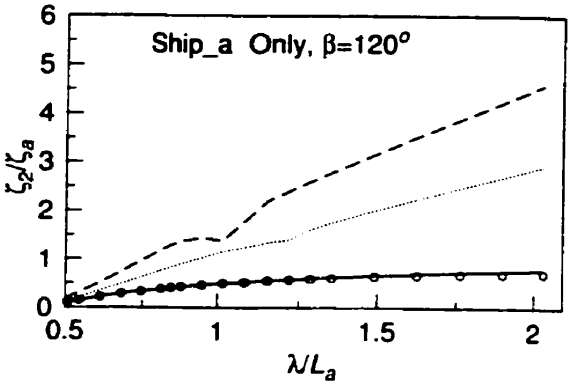

Sway motion of ship_a at a separation
Gy=2000.0m, dx=0.0m, U=0.0m/s

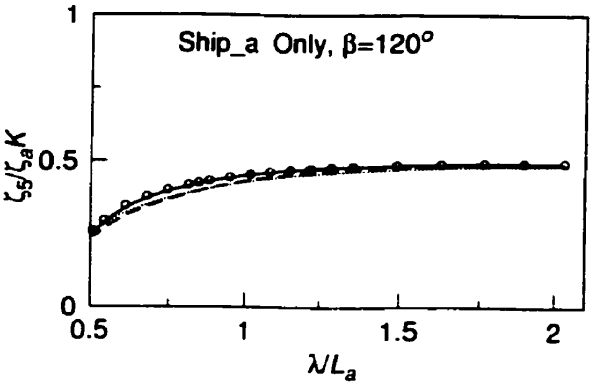

Pitch motion of ship_a at a separation
Gy=2000.0m, dx=0.0m, U=0.0m/s

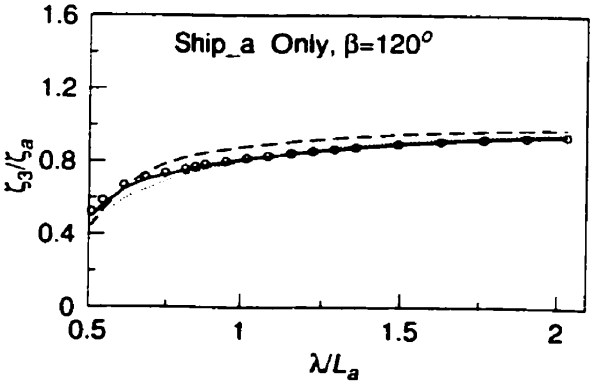

Heave motion of ship_a at a separation
Gy=2000.0m, dx=0.0m, U=0.0m/s

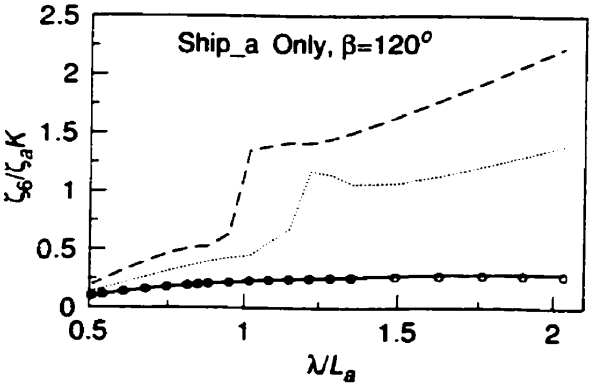

Yaw motion of ship_a at a separation
Gy=2000.0m, dx=0.0m, U=0.0m/s

----h=10.2m(δ=1.20), ...h=16.0m(δ=1.88), ——h=90m(δ=10.59), ° ° ° °h=∞(δ=∞)

Figure 5.91: Non-dimensional motion displacement amplitudes on ship_a in Case 9

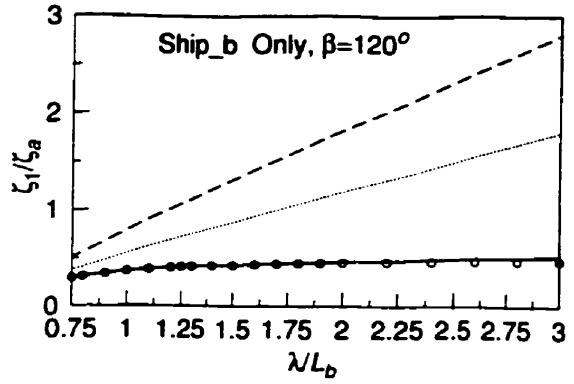

Surge motion of ship_b at a separation
Gy=2000.0m, dx=0.0m, U=0.0m/s

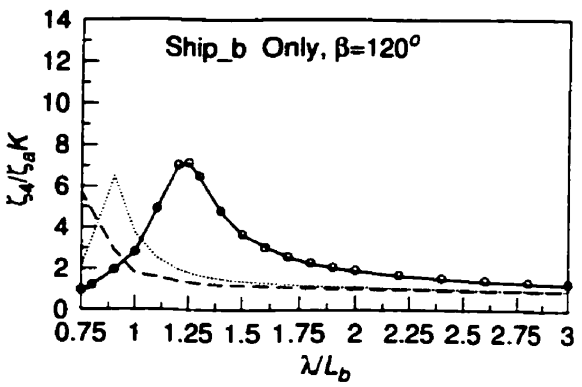

Roll motion of ship_b at a separation
Gy=2000.0m, dx=0.0m, U=0.0m/s

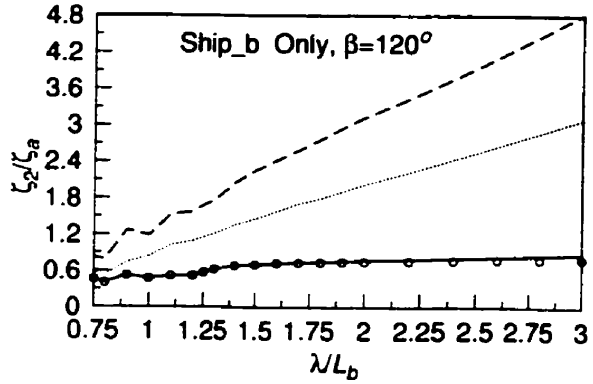

Sway motion of ship_b at a separation
Gy=2000.0m, dx=0.0m, U=0.0m/s

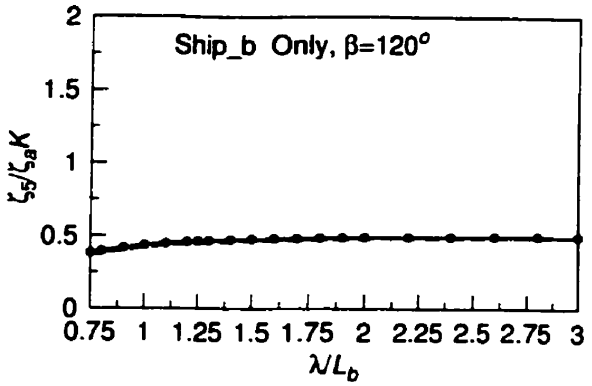

Pitch motion of ship_b at a separation
Gy=2000.0m, dx=0.0m, U=0.0m/s

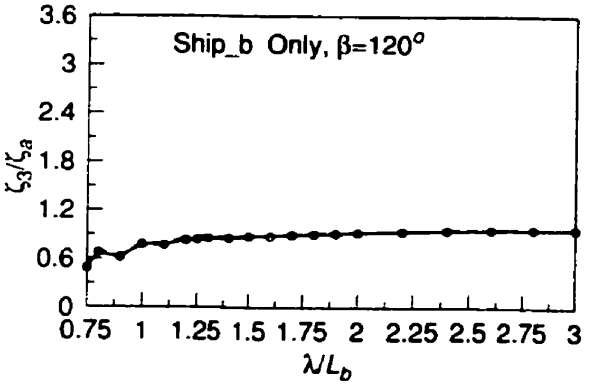

Heave motion of ship_b at a separation
Gy=2000.0m, dx=0.0m, U=0.0m/s

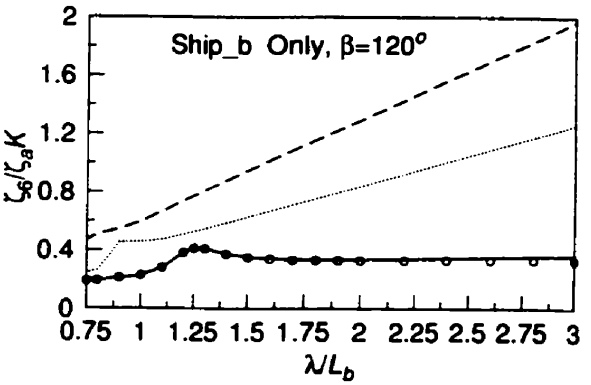

Yaw motion of ship_b at a separation
Gy=2000.0m, dx=0.0m, U=0.0m/s

– – – –h=10.2m(δ=2.27), ...h=16.0m(δ=3.56), ———h=90m(δ=20.0), ° ° ° °h=∞(δ=∞)

Figure 5.92: Non-dimensional motion displacement amplitudes on ship_b in Case 9

5.2.13 Case 10

The panelized ship_a and ship_b are shown in Figure 5.93. Wave heading $\beta = 180^o$; lateral separation $dy = 52.705m$ and gap $Gy = 30.0m$; longitudinal separation dx=45.0m; and forward speed $U = 6.18m/s$ are all shown in Figure 5.94. Figure 5.95 and Figure 5.96 give the positions of ship_a and ship_b relative to the sea bottom for water depths of $h = 10.2m$ and $h = 16.0m$, respectively.

Discussions on Case 10

A forward speed $U = 6.18m/s$ and a longitudinal separation distance $dx = 45.0m$ are considered at the same time. In Figure 5.97, for ship_a, the surge motion is reduced by the forward speed in head seas compared with Case 2 where the speed is zero. In Figure 5.98, the surge motion of ship_b is also reduced and the yaw motion is increased around $\lambda/L_b > 1.75$ by the forward speed in comparison with the surge motion and yaw motion of ship_b in Case 2.

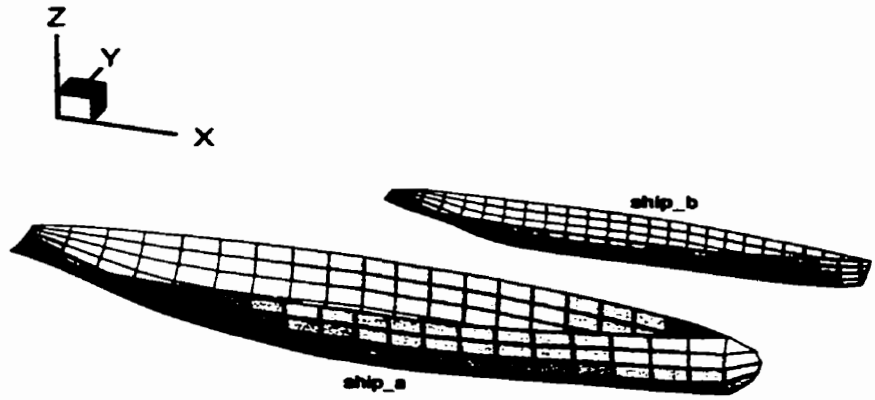

Figure 5.93: Panelized Ship_a and Ship_b for Case 10

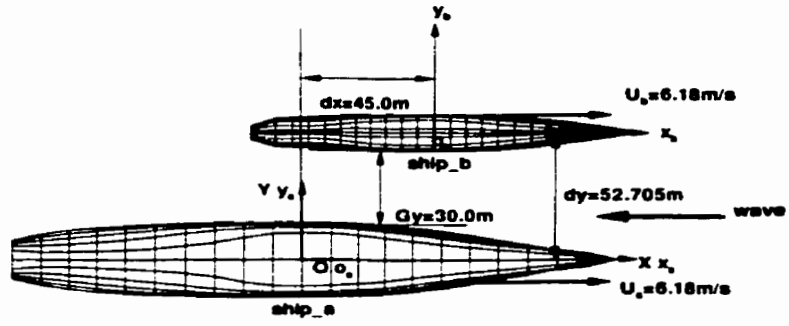

Figure 5.94: Relative position of two ships: $dx = 45.0m$, $Gy = 30.0m$ for Case 10

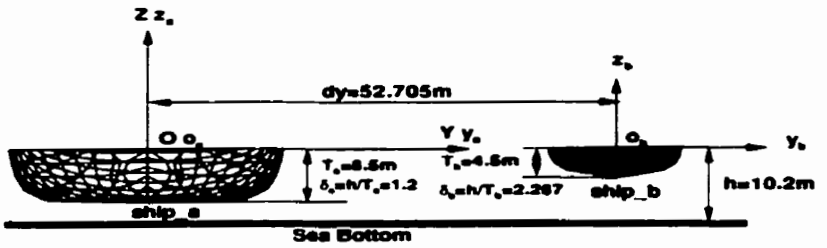

Figure 5.95: Water depth h=10.2m for Case 10

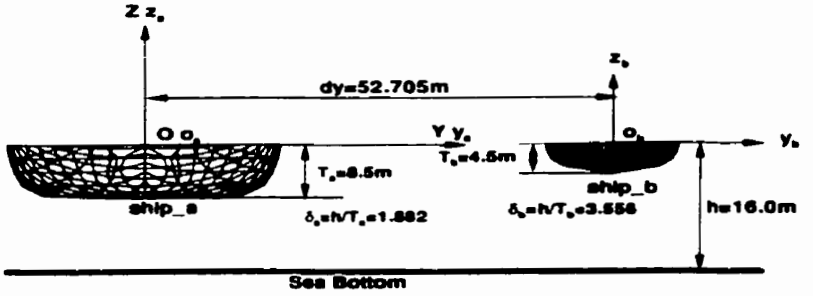

Figure 5.96: Water depth h=16.0m for Case 10

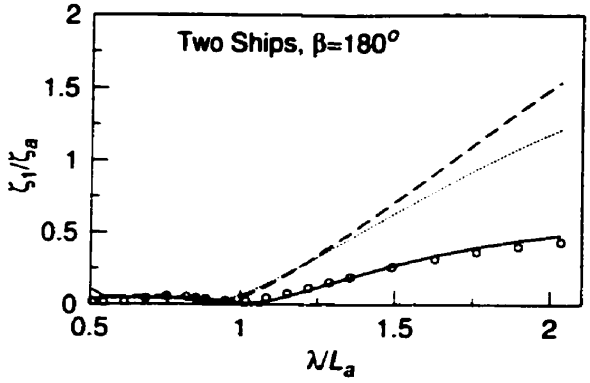

Surge motion of ship_a at a separation
Gy=30.0m, dx=45.0m, U=6.18m/s

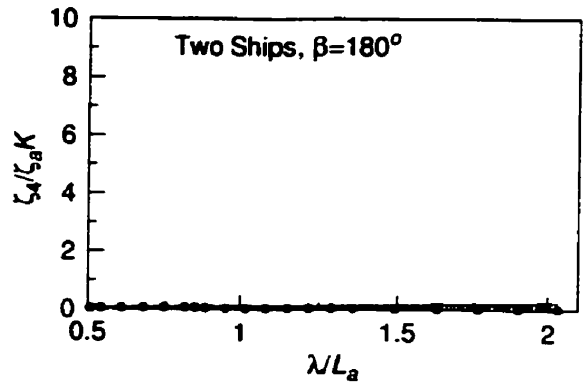

Roll motion of ship_a at a separation
Gy=30.0m, dx=45.0m, U=6.18m/s

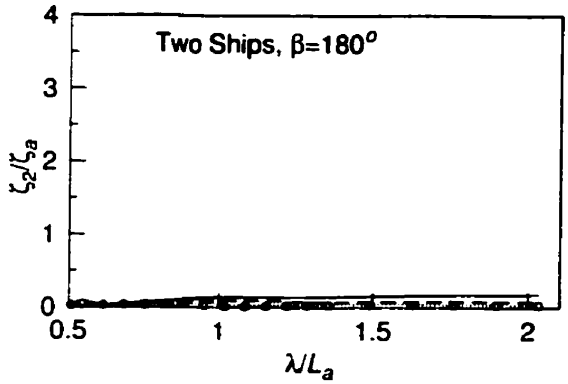

Sway motion of ship_a at a separation
Gy=30.0m, dx=45.0m, U=6.18m/s

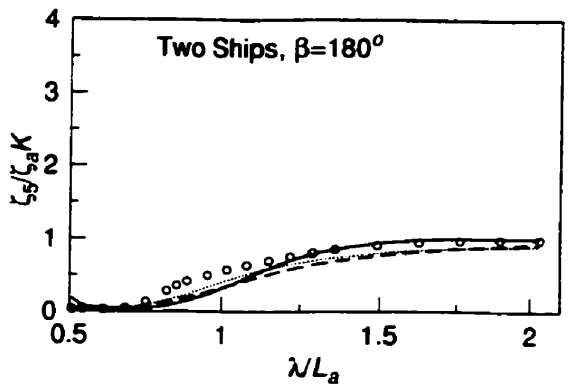

Pitch motion of ship_a at a separation
Gy=30.0m, dx=45.0m, U=6.18m/s

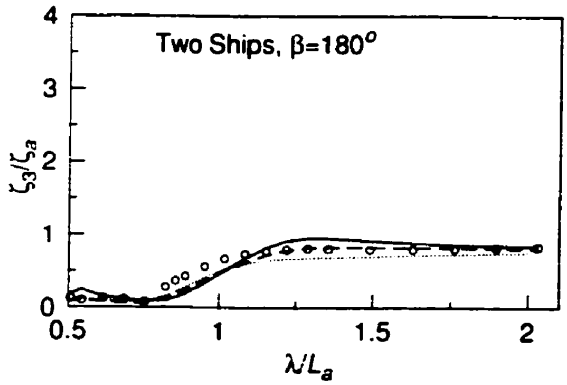

Heave motion of ship_a at a separation
Gy=30.0m, dx=45.0m, U=6.18m/s

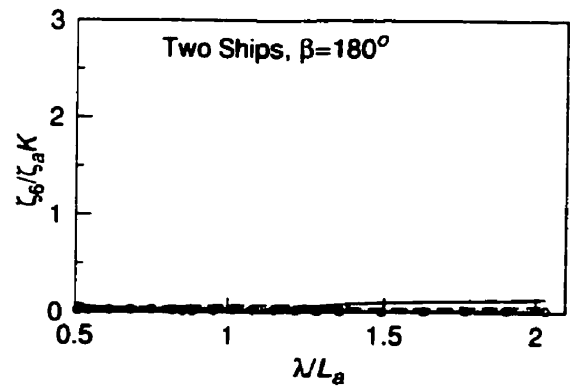

Yaw motion of ship_a at a separation
Gy=30.0m, dx=45.0m, U=6.18m/s

– – – h=10.2m(δ=1.20), ... h=16.0m(δ=1.88), ——— h=90m(δ=10.59), ° ° ° °h=∞(δ=∞)

Figure 5.97: Non-dimensional motion displacement amplitudes on Ship_a in Case 10

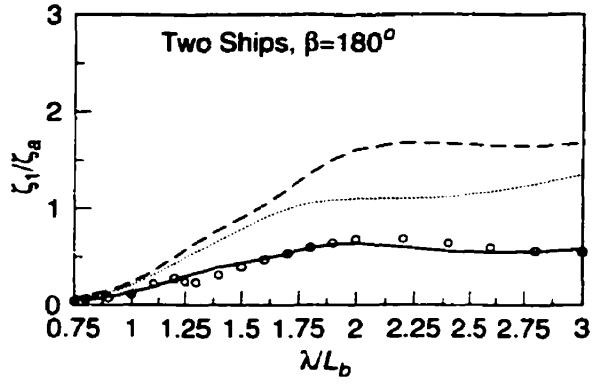

Surge motion of ship_b at a separation
Gy=30.0m, dx=45.0m, U=6.18m/s

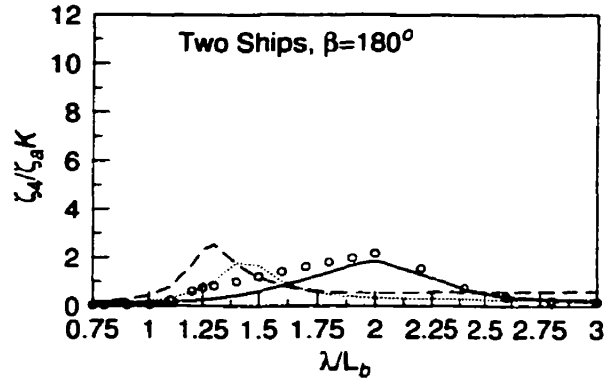

Roll motion of ship_b at a separation
Gy=30.0m, dx=45.0m, U=6.18m/s

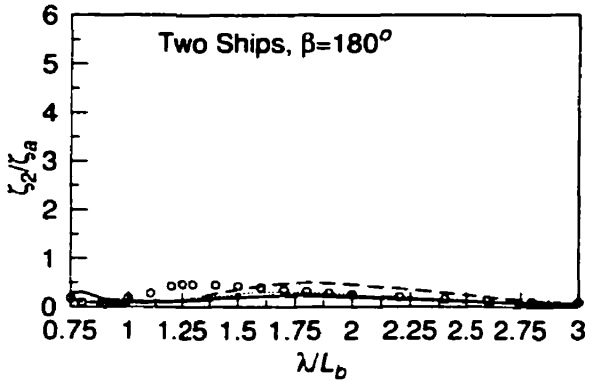

Sway motion of ship_b at a separation
Gy=30.0m, dx=45.0m, U=6.18m/s

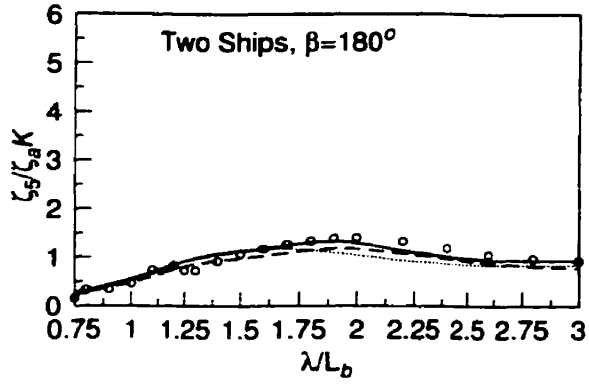

Pitch motion of ship_b at a separation
Gy=30.0m, dx=45.0m, U=6.18m/s

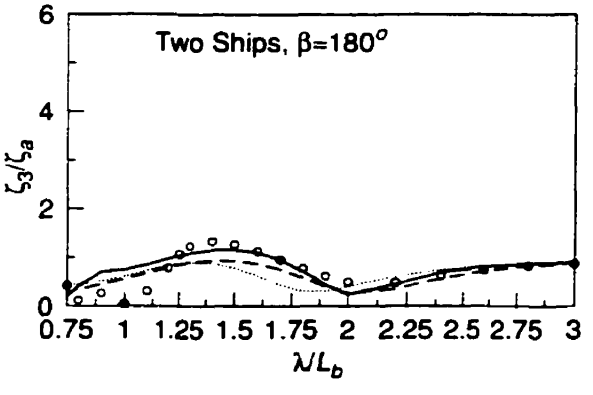

Heave motion of ship_b at a separation
Gy=30.0m, dx=45.0m, U=6.18m/s

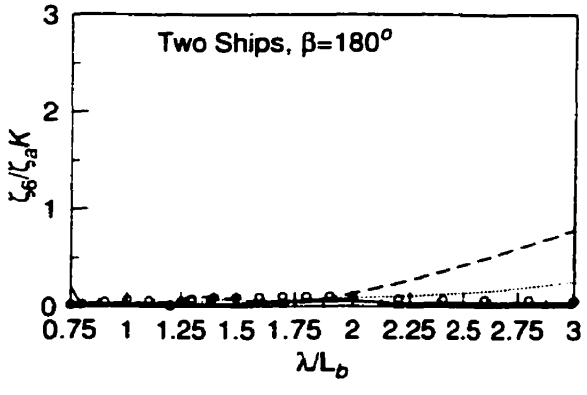

Yaw motion of ship_b at a separation
Gy=30.0m, dx=45.0m, U=6.18m/s

– – – –h=10.2m(δ=2.27), ...h=16.0m(δ=3.56), ———h=90m(δ=20.0), ° ° ° °h=∞(δ=∞)

Figure 5.98: Non-dimensional motion displacement amplitudes on Ship_b in Case 10

5.2.14 Case 11

The panelized ship_a and ship_b are shown in Figure 5.99. Wave heading $\beta = 180^o$; lateral separation $dy = 2022.705m$ and gap $Gy = 2000.0m$; longitudinal separation dx=0.0m; and forward speed $U = 6.18m/s$ are all shown in Figure 5.100. Figure 5.101 and Figure 5.102 give the positions of ship_a and ship_b relative to the sea bottom for water depths of $h = 10.2m$ and $h = 16.0m$, respectively.

Discussions on Case 11

Both ship_a and ship_b are with a forward speed in four water depths in head seas. In Figure 5.103, the surge motion is reduced about 2.5 times for $\lambda/L_a = 2.03$ and water depth $h = 10.2m$, compared with Case 3, the motions in other modes are not changed too much. In Figure 5.104, for ship_b, the surge motion is drastically reduced by forward speed compared with Case 3 where the speed is zero.

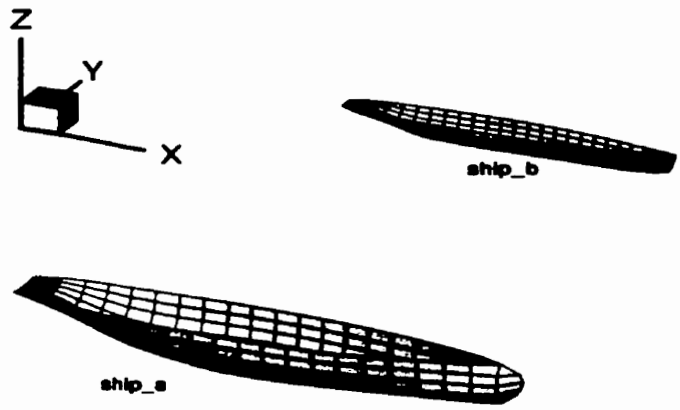

Figure 5.99: Panelized Ship_a and Ship_b for Case 11

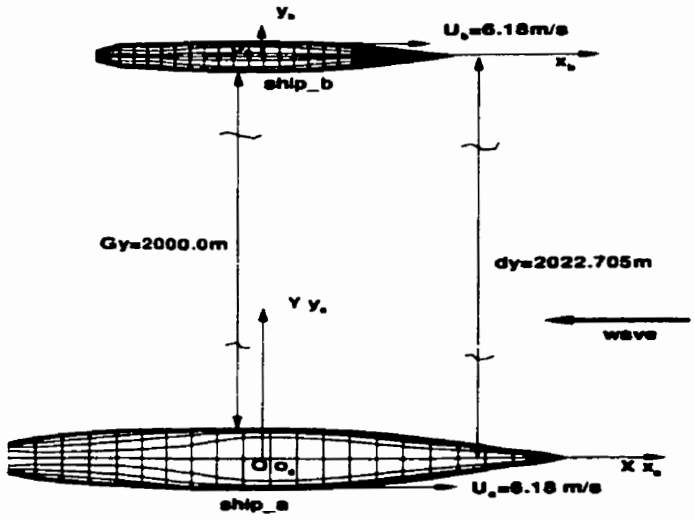

Figure 5.100: Relative position of two ships: $dx = 0.0m$, $Gy = 2000.0m$ for Case 11

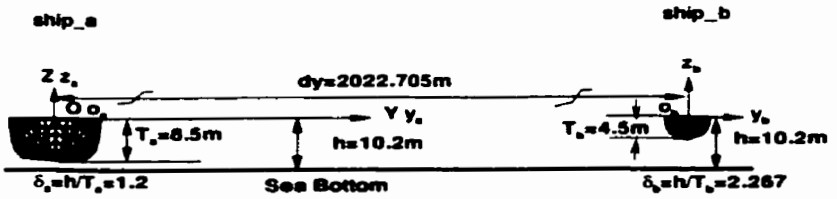

Figure 5.101: Water depth h=10.2m for Case 11

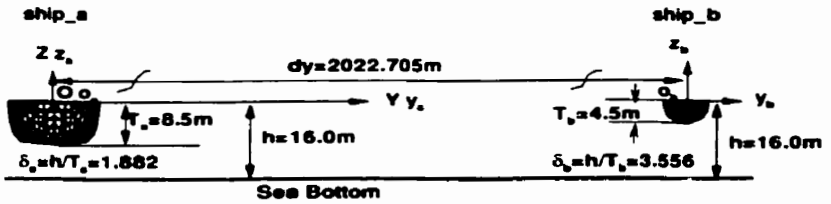

Figure 5.102: Water depth h=16.0m for Case 11

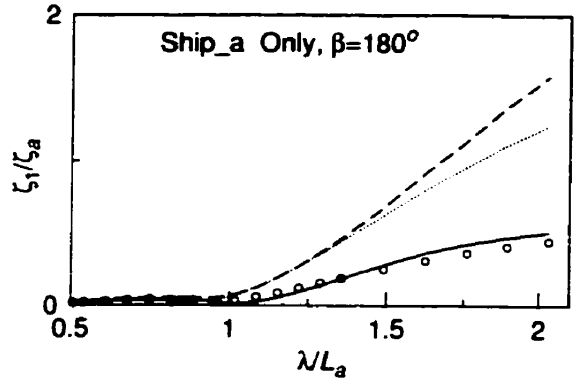

Surge motion of ship_a at a separation
Gy=2000.0m, dx=0.0m, U=6.18m/s

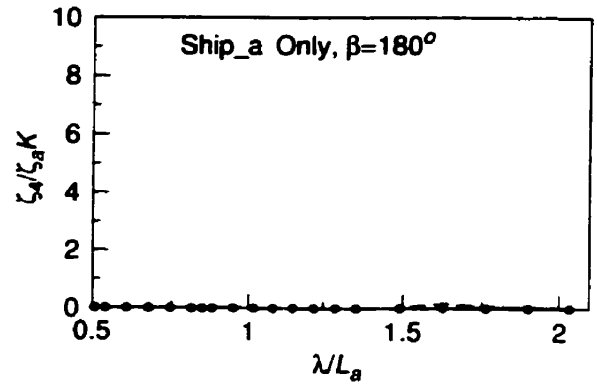

Roll motion of ship_a at a separation
Gy=2000.0m, dx=0.0m, U=6.18m/s

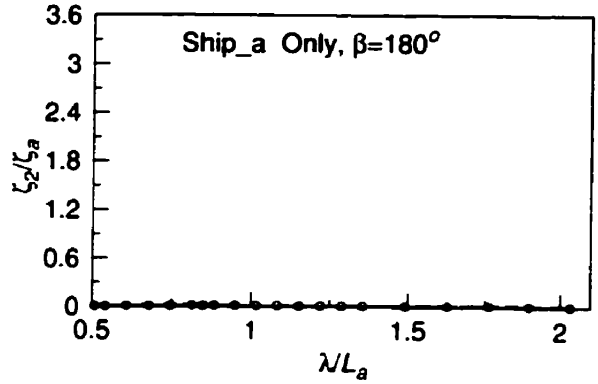

Sway motion of ship_a at a separation
Gy=2000.0m, dx=0.0m, U=6.18m/s

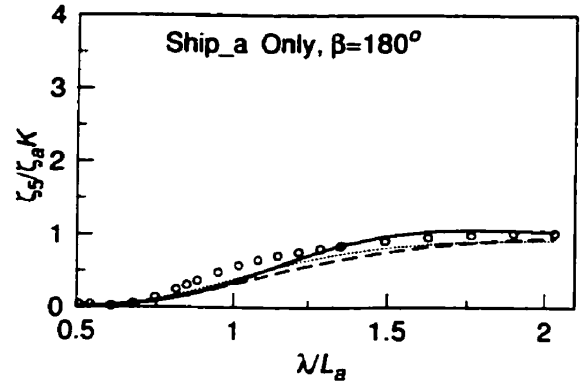

Pitch motion of ship_a at a separation
Gy=2000.0m, dx=0.0m, U=6.18m/s

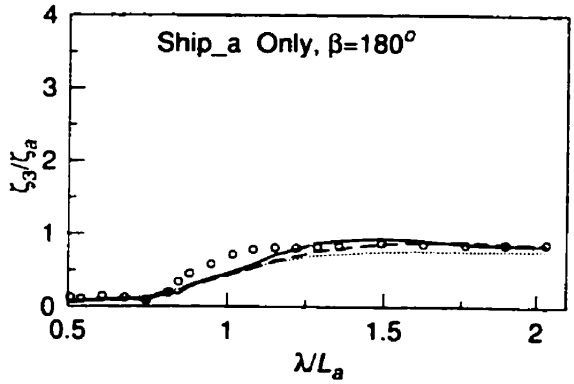

Heave motion of ship_a at a separation
Gy=2000.0m, dx=0.0m, U=6.18m/s

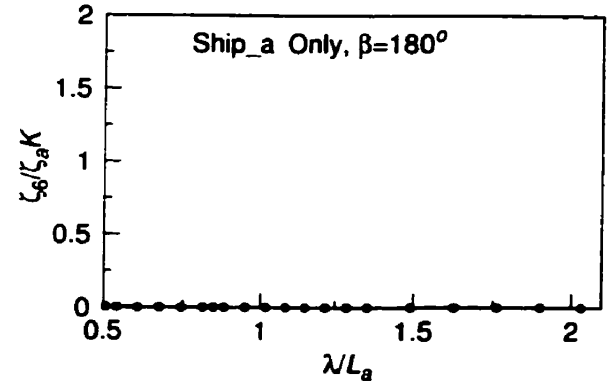

Yaw motion of ship_a at a separation
Gy=2000.0m, dx=0.0m, U=6.18m/s

– – – –h=10.2m(δ=1.20), ...h=16.0m(δ=1.88), ———h=90m(δ=10.59), ° ° ° °h=∞(δ=∞)

Figure 5.103: Non-dimensional motion displacement amplitudes on Ship_a in Case 11

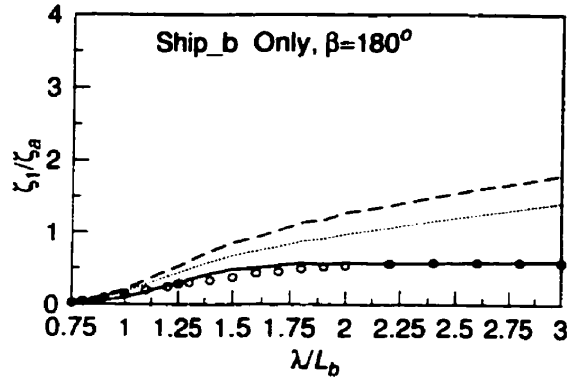

Surge motion of ship_b at a separation
Gy=2000.0m, dx=0.0m, U=6.18m/s

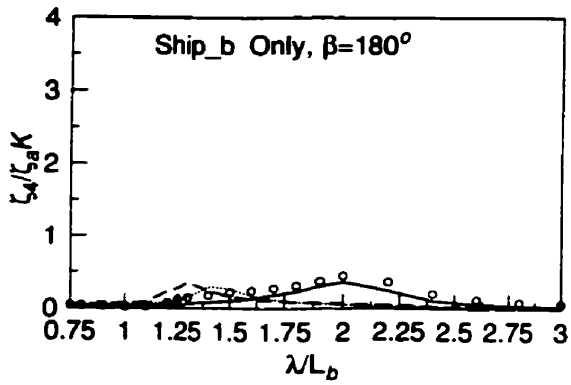

Roll motion of ship_b at a separation
Gy=2000.0m, dx=0.0m, U=6.18m/s

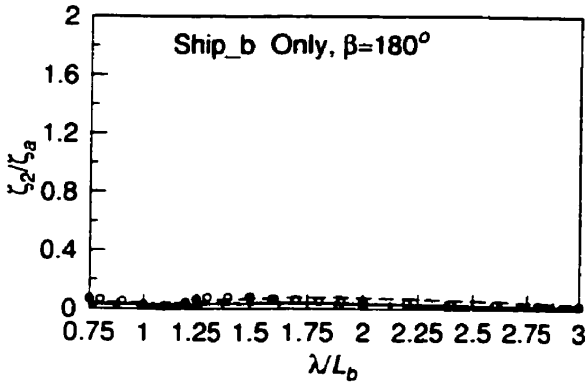

Sway motion of ship_b at a separation
Gy=2000.0m, dx=0.0m, U=6.18m/s

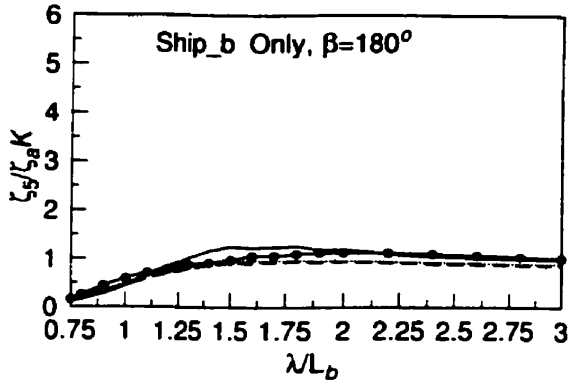

Pitch motion of ship_b at a separation
Gy=2000.0m, dx=0.0m, U=6.18m/s

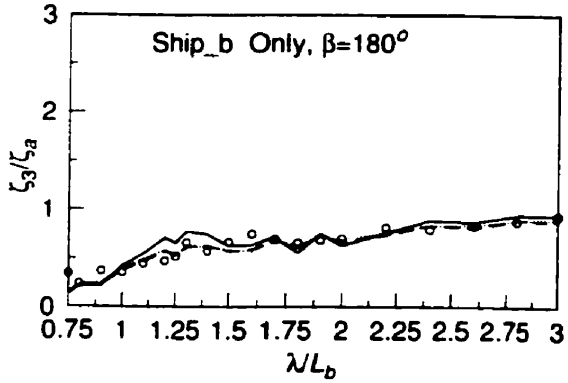

Heave motion of ship_b at a separation
Gy=2000.0m, dx=0.0m, U=6.18m/s

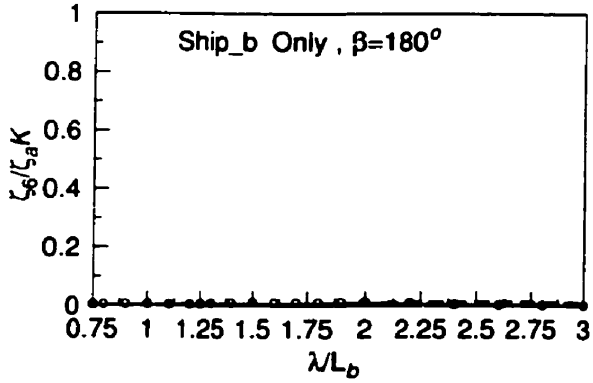

Yaw motion of ship_b at a separation
Gy=2000.0m, dx=0.0m, U=6.18m/s

– – – –h=10.2m(δ=2.27), ...h=16.0m(δ=3.56), ——h=90m(δ=20.0), ° ° ° °h=∞(δ=∞)

Figure 5.104: Non-dimensional motion displacement amplitudes on Ship_b in Case 11

5.2.15 Discussions on the Implication of Irregular Frequencies

The integral equations which are used to analyse wave-body interaction suffer from the presence of irregular frequencies. The irregular frequencies are caused by numerical solutions which satisfy prescribed boundary conditions but initiate sloshing within the body. The detrimental effects on the numerical solution are manifested over the high frequency range owing to the high density of the irregular frequency. At the irregular frequencies the integral equations either posses no solutions, or if solutions exist they are not unique. The discrete approximation of these equations generates ill-conditioned linear systems for the unknown function on the body boundary and leads to appreciable errors which can present significant practical problems for numerical hydrodynamic prediction. Irregular frequencies are common among source distribution methods at the higher frequency range, and will directly affect the prediction hydrodynamics forces, moments and coupled motions for two ship interactions in shallow water, water of finite depth and deep water. In this study, the irregular frequencies were not encountered. The current computations did not get into the high frequency region, but irregular frequencies might occur in the higher frequency range. Therefore, the occurrence and removal of irregular frequencies in the high frequency region should be studied in the future work. Irregular frequency effects have been investigated extensively for the two-dimensional strip theory method by McTaggart (1996) and for the three-dimensional panel method by Lee, Newman & Zhu (1996).

5.2.16 Discussions on Asymptotic Behavior of Ship Motions at High and Low Frequencies

The analysis of asymptotic behavior of ship motions at high and low wave frequencies is useful to check the numerical prediction results (Newman, 1977). At high frequency as $\omega \to \infty$, the boundary condition on the free surface is the potential function $\phi = 0$, and the horizontal motions: surge, sway or yaw approach zero. At low frequency as $\omega \to 0$, the boundary condition on the free surface is $\frac{\partial \phi}{\partial y} = 0$, and the horizontal motions become predominant. For a water particle near the free surface in waves, the trajectory is circular in deep water, and elliptical in finite depth and shallow water. The degree of elongation increases as water depth decreases. Therefore, at low frequency and in water of finite depth, the ship's motion will be strongly affected by the wave particle motion which may cause large horizontal motions such as surge, sway and yaw.

Chapter 6

Conclusions and Recommendations

6.1 Concluding Remarks

The main objective of this thesis is to numerically predict the shallow water effect on the seakeeping of two ship interactions in waves. A computer program has been devised to solve the free-surface Green's function in finite depth and shallow water, and it involves combining both the integral form and the series form of free-surface Green's function. The application of the three-dimensional panel method has been proven very reliable and effective. The zero speed free-surface Green function with the forward speed correction has been adopted. The numerical investigation of the shallow water effect on interactions has shown good agreement with published literature. The shallow water effect on double body flow or m-terms has been proven to be very important. The $1/r$ term was treated by the Hess and Smith method. It has been found that the water depth has a strong influence on the incident wave, diffracted wave, added mass and damping coefficients, double body flow, and coupled

motions.

The following conclusions have been drawn based on the studies of eleven cases in Chapter 5:

- In general, the influence of the shallow-water effect on the coupled motions and interaction hydrodynamic forces is prominent. Through analysis of eleven cases, the surge wave exciting force and motion were sensitive to both the water depth and the ratio of wave length to ship length. Particularly in the oblique wave, the wave exciting forces would be much higher than the deep water case in all modes of motion; the motions of surge, sway, roll and yaw were significantly affected by the water depth.

- Through Case 4 to Case 9, the oblique wave would induce more interaction hydrodynamic forces and coupled motions than those in head seas in the shallow water region as shown in Case 1 through Case 3, and would make the seakeeping and manoeuvring behaviour of both ships more different, particularly for the smaller ship.

- The presence of a larger ship in the vicinity of a smaller ship can significantly influence the motion of a smaller ship, particularly in the shallow water region. This phenomenon could be observed through all eleven cases. Therefore, the smaller ship would take more risks of collision and even capsizing in shallow water than in deep water.

- Through discussions and analyses in Cases 2,5,8 and 10, we have found that the effect of the horizonal separation distance, dx, on the motion of the smaller

ship would be more than that of larger ship.

- Comparing Cases 3,6,9 and 11 with Cases 1,4,7 and 10, the interaction forces and coupled motions could be reduced with increasing the lateral separation distance *dy*. The two ships would act as a single ship's behaviour at a far lateral separation, individually.

- Based on the computed results of eleven cases, the shallow water effect on the heave and pitch motions was not significant.

- From Case 10 and Case 11, the effect of forward speed could be prominent, and in head seas, the surge motion would be less than that of cases without forward speed.

- When two ships interact in shallow water, the hydrodynamic forces and dynamic responses would be affected by not only the water depth but also by the interactions.

- Overall, the coupling motions of two advancing ships in the shallow water region mainly depend on the wave heading, separation distance, speed and water depth.

6.2 Contributions

The contributions of this thesis are summarized as follows:

- The algorithms for solving the free-surface Green's function in water of finite depth were developed, which combined both the integral form and the series form.

- The three-dimensional panel method has been employed in numerical computations and has overcome the strip theory limitation on ship geometries and wave frequencies. It has been observed that the shallow water effect is very sensitive to the ship forms, particularly around the areas of stern and bow. Therefore, the method to describe the ship geometry is very important. The three-dimensional panel method has been proven to be very effective in this respect.

- The free-surface Green's function in water of finite depth has been applied to solve the seakeeping problem of two ship interactions in shallow water or water of finite depth. Two ship interactions have rarely been studied by the three-dimensional free-surface Green's function method. Most of them were based on strip theory and slender body theory or using the rigid free-surface assumption with a two-dimensional problem or even no incident wave.

- The water depth effect on m-terms has been computed. The double-body Green function has been modified for the application of water of finite depth and shallow water.

- As a by-product, the shallow water effect on a single ship's seakeeping characteristics has also been covered in this study.

6.3 Recommendations for the Future Research

The following research work can be achievable in the near future and is recommended to be carried out:

- Studies can be extended to two ship interactions in a restricted waterway, in

which the wall effect is considered.

- Two ship interactions in nonlinear shallow water waves should be considered in the future. The incident wave could be extended to the nonlinear wave in shallow water, such as solitary wave, cnoidal wave and even Stokes wave in water of finite depth.

- The changeable bottom topography could be considered in the future.

- The boundary layer effect on the bow or stern of two ships should be considered. In the shallow water region, the flow around the bow and stern is very sensitive to the hull shape. The accurate description of the shape of stern and bow would give more accurate prediction of the shallow water effect. Even the three-dimensional panel method made it possible; but, at the same time, viscous effect should not be ignored.

- If a ship is moving in a very shallow region, the thickness of the boundary layer could be of the same order as the clearance between the bottom of the ship and the bottom of the sea. The effect of the bottom could be complicated. Studies for this aspect should be carried out in the future. Particularly, the viscous roll damping should be also modified by considering the clearance effect.

- The second-order wave force, such as the drift force should be considered in the future. Particularly, when a large vessel is mooring in the shallow water region, the effect of drift force should not be neglected.

- The two ship interaction research should be extended to cover studies of hydrodynamic forces and motions in irregular waves in the shallow water region. Spectral analysis should be carried out to obtain statistical characteristics on ship's interaction behaviour in a shallow random sea.

References

[1] Andersen, P.(1979) Ship Motions and Sea Loads in Restricted Water Depth, Ocean Engineering, Vol. 6, pp. 557-569.

[2] Beck, R.F. and Tuck, E.O.(1972) Computation of Shallow Water Ship Motions, 9th ONR Naval Hydrodynamics Symposium, pp. 1543-1586.

[3] Bertram, V. and Söding,H.(1991) A Panel Method for Ship Motions, Proceedings of the Sixth International Workshop on Water Waves and Floating Bodies, Woods Hole, Massachusetts.

[4] Chang, M.S.(1977) Computations of Three-Dimensional Ship-Motions with Forward Speed, Second International Conference on Numerical Ship Hydrodynamics, pp. 124-135.

[5] Dand, I.W.(1975) Some Aspects of Tug-Ship Interaction, Fourth International Tug Convention, New Orleans, pp. 61-80.

[6] Davis, A.M.J. and Geer, J.F.(1982) The Application of Uniform-slender-body Theory to the Motion of Two ships in Shallow Water, Journal Fluid Mechanics, Vol.114, pp. 419-441.

[7] Endo, H.(1983) Numerical Evaluation of Principal Value Integral by Gauss-Laguerre Quadrature, AIAA Journal, American Institute of Aeromautics and Astronautics, Vol. 21, pp. 149-151.

[8] Endo, H.(1987) Shallow-Water Effect on the Motions of Three-Dimensional Bodies in Waves, Journal of Ship Research, Vol. 31, No. 1 , pp. 34-40.

[9] Faltinsen, O.M. and Michelsen, F.C.(1975) Motions of Large Structures in Waves at Zero Foude Number, In Proceedings, Symposium on The Dynamics of Marine Vehicle and Structures in Waves, Paper 11, The Institution of Mechanical Engineers, pp. 91-106.

[10] Fang, M.C. and Kim, C.H.(1986) Hydrodynamically Coupled Motions of Two Ships Advancing in Oblique Waves, Journal of Ship Research, Vol. 30, No. 3, pp. 159-171.

[11] Fujino, M.(1976) Maneuverability in Restricted Waters: State of the Art, University of Michigan, Department of Naval Architecture, Marine Engineering Report, No.184.

[12] Hess, J.L. and Smith, A.M.O.(1964) Calculation of Nonlifting Potential Flow About Arbitrary Three-Dimensional Bodies, Journal of Ship Research, Vol. 8, No. 3, pp. 22-44.

[13] Hsiung, C.C. and Gui, Q.Y.(1988) Computing Interaction Forces and Moments on a Ship in Restricted Waterway, International Shipbuilding Progress, Vol.35, No.403, pp. 219-254

[14] Hsiung, C.C. and Huang, Z.J.(1990) A New Approach to Computational Seakeeping Prediction, DREA Contractor Report, Technical Report CMVDR-1990-10.

[15] Hsiung, C.C. and Huang, Z.J.(1991) Comparison of the Strip Theory and the Panel Method in Computing Ship Motion with Forward Speed, Proceedings of Symposium on Selected Topics of Marine Hydrodynamics, St. John's, Nfld.

[16] Hsiung, C.C., He, Y.J. and Lu X.G. (1996) User's Guide for an Automatic Panelization Program PANELGEN, DREA Contractor Report 96/419.

[17] Inglis, R.B. and Price, W.G.(1981) A Three Dimensional Ship Motion Theory-Comparisons Between Theoretical Predictions and Experimental Data of the Hydrodynamic Coefficient with Forward Speed Transactions. Royal Institution of Naval Architects, Vol. 124, pp. 141-157.

[18] John, F.(1950) On The Motion of Floating Bodies, Communication of Pure Applied Mathematics, No. 3, pp. 45-101.

[19] Kagemoto, H. and Yue, D.K.P.(1986) Interactions Among Multiple Three-Dimensional Bodies in Water Waves: An Exact Algebraic

[20] Kashiwagi, M.(1993) Interaction Forces Between Twin Hulls of Catamaran Advancing in Waves (Part 1: Radiation Problem), Journal of the Society of Naval Architecture of Japan, Vol. 173, No. 173, pp. 119-131.

[21] Kim, C. H.(1969) Hydrodynamic Forces and Moments for Heaving Swaying, and Rolling Cylinders on Water of Finite Depth, Journal of Ship Research, Vol. 13. No. 2, pp. 137-154.

[22] King, G.W.(1977) Unsteady hydrodynamic interactions between ships, Journal of Ship Research. Vol. 21, pp.157-164.

[23] Lee, C. H., Newman, J.N. and Zhu, X (1996) An Extended Boundary Integral Equation Mehtod for the Removal of Irregular Frequency Effect, International Journal for Numerical Method in Fluid, Vol. 23, pp. 637-660.

[24] Li, L., He, Y.J. and Hsiung, C.C.(2000) Final Report on Numerical Seakeeping Predictions Including Interaction Effects between Two Ships, DREA Contractor Report, Technical Report CMVDR-2000-1, DalTech, Dalhousie University, Halifax, Nova Scotia.

[25] Li, L., He, Y.J. and Hsiung, C.C.(1999) Initial Report on Numerical Seakeeping Predictions, DREA Contractor Report, Technical Report CMVDR-1999-5, DalTech, Dalhousie University, Halifax, Nova Scotia.

[26] Lin W.C.(1974) The Force and Moment on a Twin-Hull Ship in a Steady Potential Flow, The 10th Symposium on Naval Hydrodynamics, M.I.T., Cambridge, Mass, U.S.A., June 24-28r, pp. 493-516.

[27] Liu, Y.Z. and Miao, G.P.(1986) *Ship Motion in Waves*, Shanghai Jiaotong University Press, Shanghai, China.(in Chinese)

[28] Matsui,T. and Tamaki,T.(1981) Hydrodynamic Interaction Between Groups of Vertical Axisymmetric Bodies Floating in Waves, International Symposium on Hydrodynamics in Ocean Engineering, Trondheim, pp. 817-836.

[29] McTaggart, K. A.(1996) Improved Boundary Element Methods for Predictiong Sectional Hydrodynamic Coefficients for Strip Theory Ship Motion Programs, DREA Technical Memorandum 96/212.

[30] McTaggart, K. A., Cumming, D., Hsiung, C.C. and Li, L.(2001) Hydrodynamic Interactions Between Ships During Underway Replenishment, 6th Canadian Marine Hydrodynamics & Structures Conference, Vancouver, 23-26 May.

[31] Monacella, V.J.(1966) The Disturbance Due to a Slender Ship Oscillating in a Fluid of Finite Depth, Journal of Ship Research, Vol. 10, pp. 242-252.

[32] Newman, J.N.(1992) The Approximation of Free-Surface Green Functions, Wave Asymptotics, The Proceedings of the Meeting to Mark the Retirement of Professor Fritz Useel from the Beyer Chair of Applied Mathematics in University of Manchester, Edited by Martin, P.A. and Wickham, G.R., Cambridge University Press.

[33] Newman, J.N.(1985) Algorithms for the Free-Surface Green Function, Journal of Engineering Mathematics, Vol. 19, pp. 57-67.

[34] Newman, J.N.(1984) Double-Precision Evaluation of the Oscillatory Source Potential, Journal of Ship Research, Vol. 28, No. 3, pp. 151-154.

[35] Newman, J.N. (1977) *Marine Hydrodynamics*, MIT Press, Cambridge, Massachusetts.

[36] Newman, J.N.(1969) Lateral Motion of Slender Body Between Two Parallel Walls, Journal of Fluid Mechanics, Vol. 39, pp. 97-115.

[37] Newman, J.N.(1961) The Damping of an Oscillating Ellipsoid Near a free surface, Journal of Ship Research, Vol. 5, pp. 44-58.

[38] Schmitke, R.T.(1978) Ship Sway, Roll, and Yaw Motions in Oblique Seas, S-NAME Transactions, Vol. 86, pp. 24-46.

[39] Susbielles, G. and Bratu, C.(1981) Vagues et Ouvrages Petroliers en Mer, Editions Technip, Paris.

[40] Thorne, R.C.(1953) Multipole Expansions in the Theory of Surface Waves, Proceedings. Cambridge Philosophical Society, Vol. 49, pp. 707-716.

[41] Tuck, E.O.(1978) Hydrodynamic Problems of Ships in Restricted Waters, Annual Review of Fluid Mechanics, Vol. 10, pp. 33-46.

[42] Tuck, E.O.(1974) Hydrodynamic Interactions Between Ships, 10th ONR Naval Hydrodynamics Symposium, MIT, pp. 35-70.

[43] Tuck, E.O. and Newman, J.N.(1974) Hydrodynamic interactions Between Ships, 10th ONR Naval Hydrodynamics Symposium, MIT, Office Naval Research, Report No. ACR-204, pp. 35-58.

[44] Tuck, E.O.(1970) Ship Motions in Shallow Water, Journal of Ship Research, Vol. 14, pp. 317-328.

[45] Ursell, F.(1949) On the Heave Motion of Circular Cylinder in the Surface of Fluid, Quarterly Journal of Mechanics and Applied Mathematics, Vol. 2, pp. 335-353.

[46] Van Oortmerssen, G.(1976) The Motions of A Ship in Shallow Water, Ocean Engineering, Vol. 3, pp. 221-225.

[47] Wehausen, J.V. and Laitone, E.V.(1960) Surface Waves. Handbuch der Physik, 9, Springer-Verlag, Berlin

[48] Williams, A.N. and Abul-Azm, A.G.(1989) Hydrodynamic Interactions in Floating Cylinder Arrarys-II Wave Radiation, Ocean Engineering, Vol. 16, No. 3, pp. 217-263.

[49] Williams, A.N. and Demirbilek, Z.(1988) Hydrodynamic Interactions in Floating Cylinder Arrays-I. Wave Scattering, Ocean Engineering, Vol. 15, No. 6, pp. 549-583.

[50] Wu, G.X.(1991) Hydrodynamic Forces on a Submerged cylinder Advancing in Water of Finite Depth, Journal of Fluid Mechanics, No. 224, pp. 645-659.

[51] Wu, G.X.(1991) A Numerical Scheme for Calculating the m_j Terms in Wave-current-body Interaction Problem, Applied Ocean Research, Vol. 13, No. 6, pp. 317-319.

[52] Wu, G.X. and Eatock-Taylor, R.(1988) Radiation and Diffraction of Water Waves by a Submerged Sphere at Forward Speed, Proceedings, Royal Society of London, Series A. Mathematical and Physical Sciences, A417, pp. 433-461.

[53] Yeung, R.W.(1978) On the Interactions of Slender Ships in Shallow Water, Journal of Fluid Mechanics, Vol. 85, Part 1, pp. 143-159.

[54] Yeung, R.W. and Hwang, W.Y.(1977) Nearfield Hydrodynamic Interactions of Ships in Shallow Water, Journal of Hydronautics, Vol. 11, No. 4, pp. 128-135.